CLEAN WATER WATER POLLUTION CONTROL RESEARCH SERIES ● 16130 DPU 02/71

RESEARCH ON THE PHYSICAL ASPECTS OF THERMAL POLLUTION

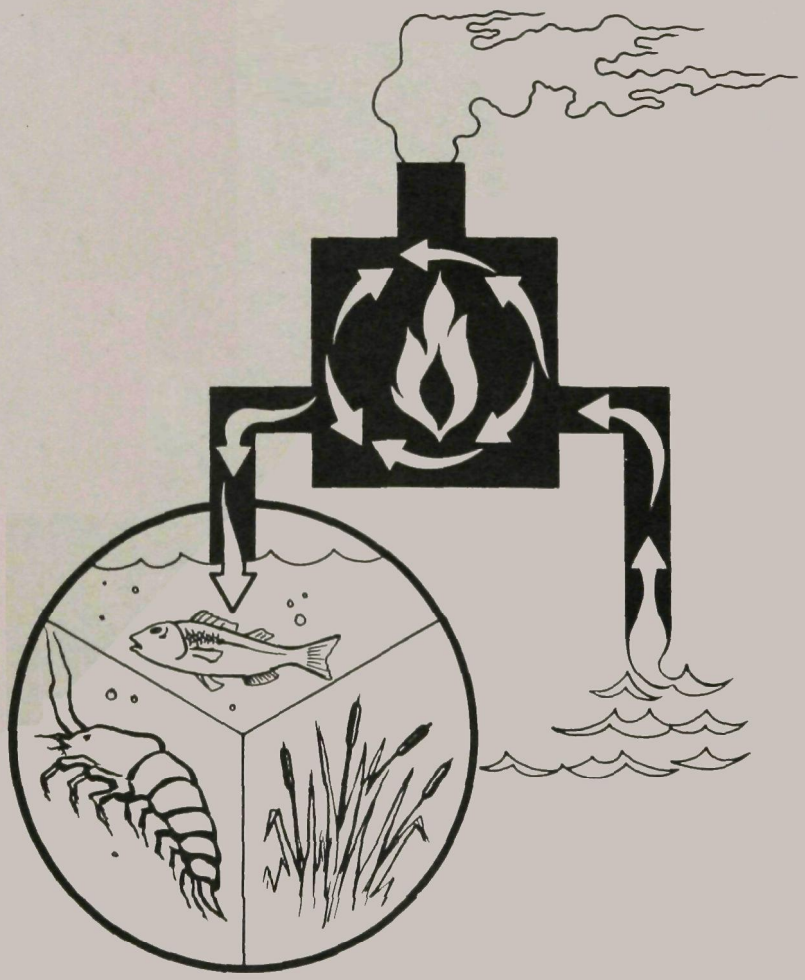

ENVIRONMENTAL PROTECTION AGENCY ● WATER QUALITY OFFICE

WATER POLLUTION CONTROL RESEARCH SERIES

The Water Pollution Control Research Series describes the results and progress in the control and abatement of pollution in our Nation's waters. They provide a central source of information on the research , development, and demonstration activities in the Water Quality Office, Environmental Protection Agency, through inhouse research and grants and contracts with Federal, State, and local agencies, research institutions, and industrial organizations.

Inquiries pertaining to Water Pollution Control Research Reports should be directed to the Head, Project Reports System, Office of Research and Development, Water Quality Office, Environmental Protection Agency, Room 1108, Washington, D. C. 20242.

RESEARCH ON THE PHYSICAL ASPECTS OF THERMAL POLLUTION

By

Cornell Aeronautical Laboratory, Inc.
Buffalo, New York 14221

for the

WATER QUALITY OFFICE
ENVIRONMENTAL PROTECTION AGENCY

Project #16130 DPU
Contract #14-12-526

February 1971

For sale by the Superintendent of Documents, U.S. Government Printing Office, Washington, D.C. 20402 - Price $1.75
Stock Number 5501-0143

EPA Review Notice

This report has been reviewed by the Water Quality Office, EPA, and approved for publication Approval does not signify that the contents necessarily reflect the views and policies of the Environmental Protection Agency, nor does mention of trade names or commercial products constitute endorsement or recommendation for use.

ABSTRACT

The mechanisms of formation and maintenance of the characteristic thermal structure of deep, temperate lakes are investigated along with the effects on the thermal structure of discharges of waste heat from electric generating plants. It is shown that a thermocline is formed by the nonlinear interaction between the wind-induced turbulence and stable buoyancy gradients due to surface heating.

A theoretical description of the stratification cycle of temperate lakes is given in which the interaction between wind-induced turbulence and buoyancy gradients is included explicitly. The theoretical model predicts all the observed features of stratification accurately. It is shown that thermal discharges increase the temperature of the epilimnion and also the temperature during spring homothermy. A lengthening of the stratification period also occurs. In addition, the attendant transfer of large quantities of water from one level to another has a significant effect.

An exploratory experimental study is described on the nature of the interfacial mixing between a flowing layer of warm water and an underlying cooler pool of water. It is shown that the downward transfer of both momentum and heat are severely inhibited at the interface by the stable buoyancy gradients; momentum to a lesser degree.

This report was submitted in fulfillment of Contract Number 14-12-526 under the sponsorship of the Federal Water Quality Administration.

TABLE OF CONTENTS

LIST OF ILLUSTRATIONS

LIST OF TABLES

NOMENCLATURE

A_o	Surface area of the waterbody
A_z	Cross-sectional area of the waterbody at depth
C_p	Constant-pressure specific heat
d	Depth
g	Acceleration due to gravity
H	Depth of the interface
h	Depth of the upper layer of water
k	von Karman's constant ≈ 0.4
K_H	Eddy diffusivity for heat
K_M	Eddy diffusivity for momentum
K	Heat exchange coefficient
L	Monin-Obukhov length
P	Potential energy of stratification of a lake
q	Heat flux
Q_p	Volumetric flow rate through power plant
R_e	Reynolds number
R_i	Richardson number
S	Dilution factor
$S(z)$	Heat source term
T	Temperature
t	Time
T_E	Equilibrium temperature

u, v, w	Velocity components
w^*	Friction velocity
z	Vertical coordinate
z_d	Effective depth of discharge
z_i	Depth of the intake
z_m	Depth of lake
z_g	Depth of center of gravity of the lake
α_v	Coefficient of volumetric expansion for water
ρ	Density
μ	Viscosity
ν	Kinematic viscosity
τ	Shear stress
κ	Molecular thermal diffusity
σ	Normal stress
σ_1, σ_2	Empirical constants used in form of eddy diffusivity
ϕ, ψ	Phase angles
ω	An angular frequency = $2\pi/365$ day^{-1}

Subscripts

s	Surface values
o	Initial values
l	Local values

FOREWORD

This report describes the results of a study, on some problems on the physical aspects of thermal pollution, that was carried out by Cornell Aeronautical Laboratory under Contract No. 14-12-526 with the Department of Interior, Federal Water Quality Administration. Technical monitoring for the program was provided by Dr. Bruce A. Tichenor, National Thermal Pollution Research Program, Pacific Northwest Water Laboratory, Corvallis, Oregon.

The experimental part of the study, reported in Section VI was conducted by Drs. G. Rudinger and G. E. Merritt, while the remaining parts of the study were conducted by Drs. T. R. Sundaram and R. G. Rehm. The authors would like to express their thanks to Mr. John Moselle for his very capable programming of the numerical computations. The authors also wish to express their appreciation for the valuable help given by A. F. Gretch who built the flow system and assisted with the running of the experiments, R. Hiemenz who designed and constructed the electronic bridge circuit and relay for the temperature measurements and N. Kay who prepared the thermistor probes.

The computer program developed during the project is not contained in this report. Individuals interested in obtaining program documentation should contact National Thermal Pollution Research Program, EPA-WQO, Pacific Northwest Water Laboratory, Corvallis, Oregon 97330.

I. INTRODUCTION

One of the problems that has gained increasing importance in recent years is the thermal pollution problem which is caused by the discharge of waste heat from electric generating plants into various bodies of water and the subsequent degradation of the quality of these waters. The degradation of the body of water may occur either through the direct influence of the increased temperature on aquatic life or through the lowering of the amount of dissolved oxygen. In the last few years a number of investigations on the effects of elevated temperature on various aquatic life have been carried out, and a fairly extensive amount of literature on the subject exists.[1-5] These studies have also resulted in some criteria for judging water quality requirements of aquatic life.[6]

On the other hand, corresponding physical studies on how the heat from a discharge is dispersed and distributed within a receiving body of water are relatively few in number, and the state of the art has been summarized recently by several authors.[7-9] It should be emphasized that an understanding of the changes in the thermal and current structure of the body of water due to the effluent discharge is a necessary first step in assessing the possible adverse effects of the discharge on the aquatic life in the receiving waters. Only when these physical changes caused by the discharge are known can the attendant ecological effects be predicted.

The present report describes the results of a study on two specific problem areas connected with the physical aspects of thermal pollution. The first problem area is concerned with the mechanisms of formation and maintenance of the characteristic thermal structure of temperate lakes and reservoirs, and the effects on this structure of thermal discharges at or below the level of the thermocline. The second problem area is concerned with the manner and rate of spreading of a warm-water wedge overlying a body of colder water with specific reference to the behavior of the interfacial mixing between the two. The latter problem is of importance in determining the extent of the mixing zone in river discharges and the possibility of recirculation of the warm water through the condensers

of the electric generating plants. The choice of these two specific problems from the myriad of problems in the broad area of thermal pollution was dictated, in part, by the priorities for research set forth in a recent paper.[10]

A critical review of the existing knowledge on the above two problem areas is given in Section II of the present report. Specific emphasis is placed not so much on giving detail descriptions of related work, but rather, on pointing out those aspects of existing theories that are unsatisfactory. A theory for the formation and maintenance of thermoclines in stratified lakes and reservoirs is put forth in Section III. The theoretical model is also used in Section IV to study the stratification cycle of temperate lakes and reservoirs. The effects of thermal discharges, at or below the level of the thermocline, on the stratification cycle are discussed in Section V. The results of an experimental study to investigate the nature of the interfacial mixing between a flowing, warm layer of water and an underlying cooler pool of water are given in Section VI. Finally some concluding remarks and recommendations for further study are given in Section VII.

Most of the detailed mathematical discussions are given in the appendices at the end of the report. In Appendices A and B detailed discussions are given, respectively, of a perturbation-expansion technique and of an integral technique for the analysis of the thermal structure of temperate bodies of water. In Appendix C a discussion of the numerical procedure used in the analyses is given, while Appendix D consists of a discussion of the adequacy of the basic equations used. Finally, a discussion of a semi-empirical parameter used in the analyses is given in Appendix E.

II. A CRITICAL REVIEW OF THE STATE OF THE ART

In the present section a brief review will be given of existing knowledge on the specific problems mentioned above. General reviews of the state of the art of thermal pollution research can be found in Refs. 7-9. It should be emphasized that the brief review given below is not meant to be an exhaustive one, but rather, it represents a selection of some of the more important studies that are directly relevant to the present study.

II. 1 General Remarks

When considering the dispersion of thermal discharges from a power plant into an aquatic environment it should be recognized that almost all geophysical fluid-dynamic phenomena are dominated by turbulent transport processes. A number of years ago, Jeffreys[11] demonstrated that in a channel much wider than deep, transition from laminar to turbulent flow occurs at a Reynolds number of only 310, where the Reynolds number is defined as

$$Re = \frac{\rho u d}{\mu}$$

Here ρ is the density of the fluid, u is the velocity, d is the depth and μ is the viscosity of the fluid. In other words, in a lake about ten meters deep, transition to turbulent flow will occur at a velocity of about 3×10^{-3} cms/sec. Thus as Hutchinson[12] points out in his monumental treatise, almost all limnological flows are turbulent, the only exceptions being flows close to a smooth bottom or cases in which turbulence is inhibited by a stable density stratification.

When a heated effluent is discharged into the top layers of a body of water, part of the heat is lost to the atmosphere directly and part of the heat is transferred to the lower, colder layers of water by turbulent diffusion. The downward transfer of heat influences, and is in turn influenced by, the prevalent circulation patterns in the body of water. Moreover, the turbulence that causes the downward diffusion is the result of wind-generated waves and is influenced strongly by various factors such as the

prevalent thermal stratification in the body of water and the ambient meterological conditions. In some cases the turbulence may also be caused by hydraulic factors such as those due to inflow. When the body of water of concern is an estuary, the density stratifications resulting from varying salinity also influence the turbulence (and hence the downward diffusion). Thus, the effect of discharge of a heated effluent into the top layers of a body of water is felt over the entire body of water through a series of complicated, and coupled, processes.

Because of the complexity of the problem, most of the analyses that have dealt with the physical aspects of thermal pollution are based on grossly simplifying assumptions. For example, in some of the analyses[13, 14] complete vertical and lateral mixing of the effluent with the receiving waters is assumed. The former of the above assumptions is invalid in a lake or reservoir with a well-defined thermocline or in an estuary with significant stratification. Estimates based on such assumptions on the effect of the thermal discharge from the Marchwood power station[15] into the Southampton bay (which is an estuary with significant stratification) proved to be completely incorrect. It should be emphasized that approximations such as that of complete vertical mixing cannot be uniformly valid in all cases. Thus, the assumption of complete vertical mixing may be a realistic one if the receiving water is a relatively shallow river. On the other hand, this assumption is likely to lead to erroneous results if the receiving water is an estuary, a reservoir or a deep lake with a well-developed thermocline.

Recently, several[16-19] mathematical models have been developed specifically for predicting thermal discharges into lakes and streams. While some of these models have been able to predict fairly accurately the thermal patterns in specific water bodies for which they were developed, they are in general not applicable to other environments since these models include empirical coefficients unique to the given environment for which they were formulated. When developing methodologies and techniques for predicting the effects of thermal discharges, it is desirable that they have as general a validity as possible and not be confined to specific situations. Therefore the use of empirical coefficients should be avoided whenever

possible. However, because of the inherent turbulent nature of the transport processes involved, a certain degree of empiricism would become unavoidable. In this context, as pointed out by Brooks,[20] it is necessary to differentiate between empirical coefficients and physical coefficients. Thus while empirical coefficients which are unique to given bodies of water are to be avoided, the use of experimentally determined relations between environmental conditions and the resulting turbulent transport properties would become unavoidable. It should be emphasized that, if properly executed, the latter step will in no way limit the general validity of the results.

It has been pointed out in the literature that generalized three-dimensional models need to be developed. While the inclusion of spatial variation in all three coordinate directions is certainly desirable when such variations are important, it should be emphasized that this step has to be in addition to, not instead of, the inclusion of the essential variable nature of the eddy diffusivities. The primary difficulty in predicting the physical effects of thermal discharges into a body of water is indeed that the turbulent transport properties are complicated functions of the environmental conditions above the body of water as well as the prevalent thermal and current structures in the body of water. In our view, it is of utmost importance to consider the complex interactions between the thermal discharges and the turbulent transport properties if a satisfactory prediction of the effects of thermal discharges is to be obtained. On the other hand, as Sundaram et al[16] point out, if the turbulent transport properties are assumed to be constant (as has been done often in the literature), then there is no basic <u>conceptual</u> difficulty in solving even the full three-dimensional equations. However the limited usefulness of the results would hardly justify the effort and expense that would be involved in such a procedure.

We interpret three-dimensional models as meaning models in which transport in all three spatial directions are considered (when important), and in which transport in a given direction is <u>not</u> neglected purely for mathe matical convenience. However, in many practical problems diffusion in all three directions do not become important simultaneously, and indeed over significant regions of the flow diffusion in only one or two directions

predominates. For example, when there is a thermal discharge to the top of the epilimnion of a stratified body of water, the stable three-dimensional plume can be treated as being essentially two dimensional.[16] Conversely, when considering the effects of the discharges on the entire body of water, conditions are essentially quasi-homogeneous in the horizontal directions and vertical diffusion predominates.[16] Problems of this type can be analyzed in terms of suitably chosen combinations of two- and quasi-one-dimensional problems.

With the above general remarks in mind, we will now critically review the literature relevant to the specific problems being considered in the present study. Again, it should be emphasized that the review given here is by no means exhaustive, the purpose here being mainly to discuss those aspects of existing literature that are essential for placing the present study in the proper perspective.

II. 2 Theories of the Thermocline

The term 'thermocline' was first proposed by Birge in 1897 (see Fairbridge[21]) to describe the layer of intense temperature gradient that separates the almost homogeneous upper layer from the colder bottom waters of deep, stratified lakes. Because of its obvious importance in limnology and oceanography, several studies on the physical mechanism of the formation of the thermocline have been carried out since the time of Birge. However, it is fair to state that a satisfactory quantitative theory of the thermocline has not yet been found.

Before considering the salient aspects of various thermocline theories, it is first relevant to review the actually observed characteristics of stratification. During early spring, most temperate lakes exhibit a nearly homothermal temperature distribution with a temperature of about 4°C (which is the temperature of maximum density for water) extending all the way to the bottom. As the weather above the lake begins to warm, the lake receives heat, mainly by solar radiation, at an increasingly rapid rate. During the early part of the warming season the lake continues to remain nearly homothermal, since the heat that is received at the surface layers

by solar radiation is transported to the deeper layers by wind-induced currents and turbulence. As the rate of heating of the lake continues to increase, the rate at which heat is received at the surface layers soon exceeds the rate of heat removal to the deeper layers, and the temperature of surface layers begins to increase. During this early period the temperature decreases monotonically with increasing depth, with the bottom temperature remaining close to that at the end of vernal circulation.

Figure 1 shows some typical plots of the vertical distributions of temperature in Cayuga Lake, New York, during various parts of the stratification cycle. The plots given in Fig. 1 have been constructed using the monthly averages of the temperatures measured by Henson, Bradshaw and Chandler.[22] The initial isothermal distribution and the later monotonically decreasing distribution can be seen in (a) and (b) of Fig. 1.

As the heating continues, a point of inflection develops in the temperature profile and a well-mixed upper layer, with relatively intense temperature gradients at its bottom boundary, is formed (as shown in (c) of Fig. 1). The plane of the maximum temperature gradient is, of course, the thermocline. During the remainder of the heating period, the thermocline slowly descends into the deeper, colder layers of the lake. It should be noted that once a thermocline forms, the deeper regions of the lake are relatively uninfluenced by changes in surface conditions. In fact, the temperature structure of the deeper layers below the thermocline changes very little with time, so that the deeper layers often serve as records of the processes, during the early parts of the heating period, which created the prevalent thermal structure.[61]

As the lake attains its maximum heat content and subsequently begins to cool, the thermocline moves down rapidly into the deeper layers of the lake as wind mixing is now augmented by convective mixing due to surface cooling. The thermocline continues to move down rapidly as the well-mixed upper layers cool further, as shown in (d) and (e) of Fig. 1, until the whole lake again attains homothermy.

In the brief description of the observed features of stratification given above, two important points should be noted. The first is the transformation of a smooth, monotonically decreasing temperature distribution at the beginning of the warming season into a temperature distribution which exhibits a well-defined thermocline. The second is the continuous downward erosion of the thermocline into the deeper, colder layers of the lake. In our view, a satisfactory theory for the stratification cycle in a temperate lake must account for these important aspects. It is also our view that the basic phenomena that are responsible for the formation and the maintenance of the thermocline are the addition or loss of heat at the surface, turbulent transport of heat from the surface to greater depths and the striking interaction of the turbulence with the temperature gradients. Thus, it is essential to account for the variation of the turbulent transport properties with depth if a satisfactory theory of the thermocline is to be developed.*

Some authors[23] have used constant values for the eddy transport properties when solving for the thermal structure of lakes. The practice of assuming constant values for the eddy transport properties is especially prevalent in oceanic-thermocline theories, where it has been customary to interpret the thermocline, and the thermo-haline circulations related to it, in terms of Ekman's famous theory (see Sverdup,[24] et al) of wind-driven currents on a rotating globe. Ekman's original analysis, as well as most of the related analyses[25-28] that have been developed since, assumes a constant value for the eddy transport coefficients, invariant with depth. Therefore, these analyses predict a temperature distribution which decreases more or less uniformly downward from the surface. In particular, they do not predict a uniformly mixed upper layer with a well-defined lower boundary. Nevertheless, these results have been used to estimate the depth of the thermocline below the surface by artificially postulating it to be the depth at which the temperature has decayed to a value equal to e^{-1} times that at the surface.

The theory of the thermocline which is most satisfactory from a qualitative point of view, but unsatisfactory from a quantitative point of view, is due to Munk and Anderson.[29] The key feature of Munk and

---

* Some interesting qualitative features of "Motions in Thermoclines" have been pointed out by Mortimer, Verhandlungen Internationalen Vereinigung fur Theoretische und Angervandte Limnologie, Vol. 14, 1961, pp 79-83.

Anderson's theory is that it accounts for the decrease in eddy transport coefficients with increasing depth due to the stabilizing influence of temperature gradients. According to this theory, the sequence of events leading to the formation and maintenance of the thermocline are as follows: The heat from the topmost layers of a body of water are transferred to greater depths by the turbulence that is produced at the surface due to wind action. The turbulence that is produced at the surface gives rise to a certain vertical distribution of eddy transport coefficients within the top layers of the water body. However, these eddy transport coefficients are not independent of depth and, in fact, get progressively small with increasing depth due to the stabilizing influence of the temperature gradients.

The degree of inhibition of the turbulence by the stable temperature gradients is determined by the value of the Richardson number,[30] which is merely the ratio of the buoyancy and inertia forces.

Munk and Anderson[29] accounted for the interaction between the turbulence and the thermal stability by postulating the eddy transport coefficients to be certain physically meaningful functions of the gradient Richardson number. They introduced these functional relationships into the differential equations governing the temperature and current distributions and solved them simultaneously on a computer. They found that in general the Richardson number increases with increasing depth, and that at a critical depth turbulence is severely inhibited by the stabilizing influence of the buoyancy forces. Above the critical depth the water is kept well mixed and homogeneous by the dominant turbulent transport processes, while the layers below the critical depth are 'protected' from surface heating. Below the critical depth the temperature drops rapidly to a value appropriate to that at the bottom of the water body. Thus the fundamental reason for the existence of the thermocline is the inhibition of the turbulence by the stabilizing influence of buoyancy forces.

As Defant[31] (in his monumental two-volume treatise on oceanography) points out, Munk and Anderson's theory delves deeply into the fundamental reasons for the formation of the thermocline and throws much light into the

consequences of the nature of the interaction between turbulent transport processes and thermal stability. However, as pointed out earlier, Munk and Anderson's theory is unsatisfactory from a quantitative point of view and predicts depths of the thermocline which are much smaller than those actually observed. Moreover, since the theory is based on the assumption of the existence of a steady state, certain inconsistencies arise at large depths. The authors point out that "it appears that the distributions of current and temperature cannot both be stationary at the same time."[29]

Since the time of Munk and Anderson's original paper, a considerable amount of work has been done on the nature of the interaction between turbulence and thermal stability in connection with atmospheric-boundary-layer flows (see Refs. 32 and 33, for example), and these studies have enhanced our knowledge of the interaction considerably. One of the more important developments in connection with atmospheric turbulence has been the so-called "similarity theory" that was formulated by Monin and Obukhov.[34] These authors postulate that the influence of thermal stratification on the turbulence at any depth z, can be characterized by the parameter (z/L) alone where L is a length scale given by

$$L = \frac{\omega^{*3}}{k \alpha_v g \frac{q}{\rho C_p}} \qquad \text{(II. 1)}$$

In Eq. (II. 1) k is the von Karman constant (≈ 0.4) and C_p is the specific heat. The physical significance of the Monin-Obukhov length scale, L, is that it represents the depth at which the rate of production of turbulence by the Reynolds stress and that by the buoyancy flux are approximately the same. The significance of the Monin-Obukhov length in the stratification cycle of lakes, as well as its application to predicting the effects of thermal discharges have been discussed in detail by Sundaram et al.[16]

Thermocline theories based on mechanisms other than those described above have been put forth by Ertel,[35] Dake and Harleman[36] and Li.[37] The theories proposed by Ertel[35] and by Dake and Harleman[36] are based on the

assumption that the primary mechanism responsible for the formation of the thermocline is the differential absorption, at various depths, of the incoming solar radiation. It may be noted that Dake and Harleman[36] include the effects of turbulent diffusion in an indirect way. Li[37] has put forth a theory for the thermocline based on the so-called Burgers' equation, and his theory does not consider buoyancy effects at all. Li's theory essentially deals with the development of a turbulent layer in the upper regions of a body of water due to the onset of strong winds. The speed of downward propagation of the developing turbulent front is proportional to the wind speed, and the front disappears when the wind subsides.

It was mentioned earlier that actual observations indicate that the vertical temperature profile at the start of the stratification season in a temperate lake is fairly smooth, and that a thermocline forms only after a certain period beyond the time of maximum spring homothermy. However the thermocline forms well before the start of the cooling season, and a well-mixed upper layer already exists at the time the lake begins to lose heat to the atmosphere. None of the existing theories predict the above-noted features.

II. 3 Seasonal Stratification Cycle

In addition to the studies described above on thermocline formation, there are also some theories for the seasonal stratification cycle of temperate lakes. Some of these theories are based on the global (or integral) forms of the conservation relations in which the vertical temperature profiles are described in terms of a given number of characteristic parameters. The time evolution of each parameter is determined by using the conservation relations themselves as well as suitable moments of these equations.

The most important theory in this category is the one put forth by Kraus and Turner.[38] Kraus and Turner have included the effects of convection due to preferential heating below the surface or cooling at the surface as well as the effects of wind stirring. Their theory predicts the formation, immediately after maximum spring homothermy, of a thermolcine at great depths. As the heating season proceeds, the thermocline moves upwards,

and reaches its shallowest depth during summer solstice when the rate of surface heating is a maximum. The thermocline then begins its descent, and continues to do so till the time of fall homothermy.

Kraus and Turner's theory predicts many of the important observed features of stratification discussed earlier. However, as pointed out earlier, observations indicate that a thermocline does not form immediately following spring homothermy. While the depth over which surface influences are felt steadily decreases during the warming period,[16] a thermocline or a point of inflection does not form immediately following spring homothermy. As discussed by Sundaram et al,[16] the value of the Monin-Obukhov length, which is a measure of the depth of penetration of surface influence, decreases rapidly during the early parts of the warming season. However, a thermocline does not form till around the time when the Monin-Obukhov length reaches a minimum positive value.

Orlob[39,40] has developed a method of describing the thermal structure of deep lakes and reservoirs in which information derived from actual measurements is used in the analytical framework. He introduced the values of the eddy diffusivities deduced from measured vertical temperature profiles into a simple unsteady, one-dimensional heat conduction equation to solve for the seasonal changes in the thermal structure. While the eddy diffusivity was allowed to vary with depth and the experimentally determined values were fitted with empirical analytical expressions, the essential nonlinear dependence of the eddy diffusivity on the thermal structure itself was not included. Orlob has compared the predictions of the mathematical model with the measurements made in the specific body of water for which the model was constructed, and has found good agreement between the two.

II. 4 Thermal Discharges at or below the Level of the Thermocline

An important problem that arises in connection with thermal pollution is the effect of thermal discharges into a stratified body of water at or below the thermocline level. Discharges below the thermocline have been used extensively in connection with sewage disposal into marine environ-

ments.[41-44] The advantages of this mode of discharge have been described by Brooks.[45] The primary advantage is, of course, that because of sewage being heavier than the surface sea water, the sewage field can be held submerged below the thermocline thereby preventing contamination of the shore areas.

When considering the physical effects of thermal discharges into the hypolimnion of a stratified body of water, two specific problems have to be analyzed. The first is concerned with the behavior of the buoyant plume due to the discharge and the second is concerned with the effect of the discharge on the thermal structure of the entire body of water. While considerable knowledge exists on the first problem, practically nothing is known about the second.

When water that is withdrawn from the hypolimnion of a waterbody is returned to the hypolimnion after cycling through a power plant's condensors, it will tend to rise as a buoyant plume since it will be warmer than the surrounding hypolimnic water. As Rawn, Bowerman and Brooks[41] point out in connection with sewage disposal, three different types of plumes can be identified depending on the initial density and velocity of the effluent. In the first type, the effluent rises to the surface and spreads as a surface field (this was the most common type observed by Rawn et al). In the second type, the jet penetrates the thermocline and rises to the surface only to plunge down below the thermocline and spread as a thin submerged field. This type of plume occurs when the density of the plume is higher than that of the epilimnion and when the discharge velocity of the effluent is such that the plume has enough residual kinetic energy at the thermocline level to drive through it. In the third type, the plume rises to the thermocline level and spreads as a thin field below the epilimnion.

Rawn et al state the approximate condition for the submergence of the effluent field as

$$\frac{(S_T - 1)\,\rho_H + \rho_o}{S_T} > \rho_E \qquad \text{(II. 2)}$$

where S_T is the dilution factor at the point where the axis of the jet crosses the thermocline and ρ_H, ρ_E and ρ_o are the densities of the hypolimnion, epilimnion and discharge, respectively. Equation (II. 2), of course, does not account for the residual kinetic energy of the jet at the thermocline level.

Because of its importance to the location and design of submarine outfalls, jet discharges into fluids of a different density have been studied extensively both experimentally and theoretically. For example, as early as in 1929, Rawn and Palmer[46] had conducted an extensive (388 in number) set of experiments on the behavior of a fresh water jet in sea water. Among more recent works are those of Abraham,[47-49] Hart[42] and Fan and Brooks.[50,51] Recently, Fan[52] has also studied the behavior of a buoyant jet in a stagnant environment with a linear density stratification.

As pointed out earlier, almost nothing is known of the effects of thermal discharges at or below the level of the thermocline on the overall thermal structure of a large waterbody.

II. 5 Interfacial Mixing

Another question that has an important bearing on the problem of predicting the physical effects of thermal discharges is concerned with the magnitude of the frictional resistance at the interface between a warm layer and an underlying cooler pool of water. When water that is withdrawn from a river is circulated through a powerplant's condensers and then returned, with little momentum, to a point downstream of the intake, a wedge of warm water may be formed. This wedge moves upstream under the influence of the intake and, under certain conditions, recirculation of the heated water through the intake channel may occur.

Because of its obvious importance, the above problem has been studied by a number of authors.[8,53,54] As pointed out by Tichenor and Cawley,[10] one of the important quantities about which knowledge is required in order to solve the above problem is the magnitude of the friction at the interface between the warm and cold layers. At present, in most analysis, the interfacial friction is estimated by empirical means and a better definition of this quantity is needed.[10]

The magnitude of interfacial friction at the boundary between a warm layer and an underlying cooler body of water is strongly influenced by the stable density stratification at the interface. Indeed the stable density stratification tends to strongly inhibit the turbulent transfer of momentum, as well as of heat and mass, between the two layers. This phenomenon is not unlike that of the inhibition of the downward transfer of heat from the epilimnion to the hypolimnion of a stratified lake.

Transport across stably stratified interfaces is of interest in connection with a wide variety of environmental problems, the densimetric currents in lakes and reservoirs and the katabatic winds of the atmosphere being two important examples.[16] Because of the above reason, experimental studies of the nature of the mixing processes across a stably stratified interface have been carried out by a number of authors. For example, Keulegan[55] has studied, in a laboratory flume, the mixing processes at the interface of a fresh-water layer flowing over saline water. Keulegan[55] systematically varied the velocity of the upper layer and found that at low velocities the interface was quite stable, with very little mixing occurring across it. As the velocity was increased, internal waves started to appear at the interface. At even higher velocities, the crests of the internal waves began to break with the consequent slow mixing of the upper layer into the lower layer.

Experiments analogous to the one described above have also been conducted by Lofquist[56] and Ellison and Turner.[57] Lofquist considered the case when salt water flows turbulently under a pool of fresh water, while Ellison and Turner considered the case of a surface jet in a channel in which a layer of fresh water flows over a pool of salt water. Lofquist's experiments were primarily concerned with the internal waves at the stable boundary, while Ellison and Turner studied the nature of the turbulent entrainment process at the interface. These latter authors found that the entrainment coefficient depended on a bulk Richardson number[57] and decreased with increasing values of this number. At some critical value of the bulk Richardson number entrainment of the lower fluid into the upper layer ceased altogether.

Ellison and Turner[58, 59] have also studied the behavior of a layer of dense salt solution on the floor of a sloping rectangular pipe in which there is a turbulent flow. They measured both velocity and density profiles near the interface and correlated the turbulent transport coefficients for momentum and salt in terms of a local Richardson number.[59] They found that the ratio of turbulent transport coefficient for salt to that for momentum decreases with increasing values of the local Richardson number. However, because of experimental errors, and the influence of the shape of the pipe and the Reynolds number on the results, the results are not generally applicable.

Thus while some knowledge exists on the nature of the transfer processes at the interface between fresh and salt water, this knowledge is not directly relevant to the problem of the interfacial friction between a warm layer and underlying cooler water. Firstly, a complete analogy between the transfer of salt and heat has to be assumed in order for existing results to be usable. Secondly, accurate quantitative information on the interfacial friction is not available.

II. 6 Concluding Remarks

It can be seen from the above brief description that while some previous studies of the problems that are being considered here have been carried out, very few quantitative results exist. Thus while several theories of the thermocline have been advanced, none of these theories predict one of the most important observed features of stratification, namely, the change of a monotonically varying temperature distribution during the early parts of the warming season to one that displays a thermocline during the later parts of the warming season. Again, none of the existing theories have accounted for the important interactions between the wind-induced turbulence and the buoyancy gradients due to surface heating in an entirely satisfactory or consistent manner.

It should be emphasized that when considering the effects of thermal discharges on the stratification cycle, it is of paramount importance to account properly for the interaction between the turbulence and thermal

structures. As pointed out by Sundaram et al,[16] heated effluents not only influence the thermal structure directly, but they also influence it indirectly through their influence on the structure of the turbulence. Again, as pointed out by the above authors, if the effects of the thermal discharges on the mechanisms of mixing are altogether neglected (a step which cannot be justified), then the problem of predicting the effects of thermal discharges on the lake becomes relatively simple. There are no existing theories which account for the changes, due to the thermal discharges, in the eddy diffusivities in a stratified lake.

A theory for the formation of thermoclines in deep lakes and reservoirs is given in Section III. This theory includes a proper description of the interaction between wind-induced turbulence and buoyancy gradients due to surface heating. The analytical framework developed in Section III is extended to study the stratification cycle in Section IV and the effects of thermal discharges on the stratification cycle in Section V.

An experimental study of the interfacial mixing at a stable interface is described in Section VI.

III. THERMOCLINE FORMATION

III. 1 General Remarks

As pointed out in the last section, even though a number of theoretical models have been proposed to explain the characteristic thermal structure of temperate lakes, a satisfactory explanation for the formation and maintenance of thermoclines is still lacking. In the present section, it is shown that a satisfactory theory for the mechanism of formation and maintenance of thermoclines in a temperate lake has to take into account two essential aspects. Firstly, the mechanism of not only the formation but also the maintenance of a thermocline is an unsteady process even when conditions above the body of water under consideration are steady. Therefore, a satisfactory theory for the thermocline must include this basic aspect. Secondly, the formation of a thermocline is by the nonlinear interaction between the wind-generated turbulence and the stable buoyancy gradients in the body of water under consideration. This nonlinearity, while making the equations difficult to analyze, is an essential feature of the interaction between the turbulence and prevailing temperature structure and as such has to be retained.

III. 2 Basic Relations and Boundary Conditions

In a large, relatively deep lake, the transport of any property takes place much faster in the horizontal directions than in vertical ones, so that one can assume that horizontal homogeneity exists in planes parallel to the surface. It should be emphasized that the above assumption can be valid only in an approximate sense since, as pointed out by Wedderburn[60] a number of years ago, the existence of a current in the well-mixed upper layer, or the epilimnion, must necessarily involve an upward tilting of the isotherms toward the windward end of the lake. However, in the localized theoretical model being proposed here, the small horizontal nonhomogeneity due to the tilting of the isotherms is of no direct consequence since it does not influence the mechanisms of formation or maintenance of the thermocline. The implications of the assumption of horizontal homogeneity have been discussed at length by Sundaram et al.[16]

Under the assumption of horizontal homogeneity, the equation describing the vertical transport of heat is

$$\frac{\partial T}{\partial t} = \frac{\partial}{\partial \bar{z}} \left(K_H \frac{\partial T}{\partial \bar{z}} \right) \qquad \text{(III. 1)}$$

where T is the temperature, t is the time, $\bar{z}$ is the distance measured downward from the surface and K_H is the eddy diffusivity for the vertical transport of heat. Molecular thermal diffusivity is not explicitly accounted for in Eq. (III. 1) since it is in general smaller than the eddy diffusivity, and if necessary, it can be incorporated into the definition of K_H. It should be noted that Eq. (III. 1) is nonlinear since, in general, the diffusivity is a function of the thermal as well as current structure in the lake.

Before discussing the dependence of the eddy diffusivity on the thermal and current structures, it is appropriate to consider the initial and boundary conditions that have to be used in conjunction with Eq. (III. 1). In all of the calculations presented in the present section, the initial condition will be taken as that corresponding to the end of spring homothermy; that is, the initial condition will be taken as

$$T(\bar{z}, 0) = T_0 \qquad \text{(III. 2)}$$

where T_0 is the temperature of the lake at maximum spring homothermy. The boundary condition at the surface of the lake must describe the heat exchange between the lake and the atmosphere, and this can be written in the form,[7, 16]

$$q_s = -\rho C_p \left(K_H \frac{\partial T}{\partial \bar{z}} \right)_{\bar{z}=0} = K(T_E - T_S) \qquad \text{(III. 3)}$$

where q_s is the heat flux (taken positive when downward), K is a heat-exchange coefficient, T_S is the surface temperature and T_E is a fictitious surface temperature, called the equilibrium temperature, at which there would be no net heat transfer to or from the lake surface. The

equilibrium temperature and the heat-transfer coefficient are both functions of the environmental conditions above the lake and can be expressed as functions of the wind speed, air temperature and humidity and net incoming (sky and solar) radiation. Methods of evaluating T_E and K are described fully by Edinger and Geyer[7] and by Sundaram et al.[16]

It may be noted that Eq. (III. 3) is a statement of Newton's law of cooling. It should be pointed out that implicit in Eqs. (III. 1) and (III. 3) is the assumption that the bulk of the incoming solar radiation is absorbed within a small layer near the surface. This assumption is in general valid in most deep, turbid lakes. For example, as Ruttner[61] points out, the characteristic depth for absorption of the solar radiation in Seneca Lake, New York is considerably smaller than the depth of the well-mixed upper layer.

As mentioned earlier, theories of the thermocline based on the so-called "internal-radiation-absorption model" have been given by Ertel[35] and by Dake and Harleman.[36] These theories account for turbulent diffusion only in an indirect and empirical way, and they are based on the assumption that the primary mechanism responsible for the formation of a thermocline is the differential absorption, at various depths, of the incoming solar radiation. If necessary, the feature of the differential absorption of the incoming radiation can be easily incorporated into Eqs. (III. 1) and (III. 3). However, it is felt that the inclusion of this additional feature will not add significantly to the nature of the conclusions derived in the present paper.

III. 3 Forms of the Eddy Diffusivity

It was pointed out earlier that Eq. (III. 1) is nonlinear, since the eddy diffusivity, K_H, is a function of the thermal as well as the current structure in the lake. One of the primary objectives of the present study is to demonstrate that the nonlinearity of Eq. (III. 1) is an essential feature of the interaction between wind-induced turbulence and buoyancy gradients due to surface heating, and that, as such, it must be retained if a satisfactory theory for the thermal structure of a stratified lake is to be developed.

The interaction may be accounted for either explicity, or implicitly as in two-layer models[16] in which the upper and lower parts of the lake are described by different, but constant, eddy diffusivities. It should be emphasized that the interaction between the turbulence and thermal structures is crucial in determining the structure of each. It is this interaction that makes the problem of predicting the effects of heated discharges on the thermal structure of stratified lakes difficult, since the heated discharges not only influence the thermal structure directly, but they also influence it indirectly through their effect on the turbulence structure.[16]

The major mechanism by which turbulence is generated in the upper layers of a lake is the wind shear acting on the surface of the lake. Correspondingly, the buoyancy gradients are produced in the lake by the heat exchange, at the surface of the lake, between the environment and the lake. When the mean buoyancy field in the upper layers of a lake is statically stable, it tends to suppress the generation of wind-induced turbulence. Conversely, when the mean buoyancy field is statically unstable, it adds to the generation of wind-induced turbulence. The effects of the interaction between the turbulence and the buoyancy field on the structures of each other have been studied fairly extensively in connection with atmospheric and oceanic turbulence. Recent developments on the interaction between the turbulence and buoyancy fields in the lower atmosphere have been summarized by Lumley and Panofsky,[33] and those in the upper ocean have been summarized by Phillips[62] and Okubo.[63]

In general, the eddy diffusivity under arbitrary thermal stratification conditions can be written as the product of the eddy diffusivity under corresponding neutral stratification conditions and a function of an appropriate stability parameter characterizing the stratification. Thus, one can write

$$K_H = K_{H_o} f \text{ (stability parameter)} \qquad \text{(III. 4)}$$

where K_{H_o} is the eddy diffusivity under identical environmental conditions, but in the absence of stratification.

One of the more commonly used forms of the stability parameter is the gradient Richardson number,[30] R_i, which is defined as

$$R_i = -\alpha_v g \frac{\frac{\partial T}{\partial z}}{\left(\frac{\partial u}{\partial z}\right)^2} \qquad \text{(III. 5)}$$

where α_v is the coefficient of volumetric expansion of water, g is the acceleration due to gravity and u is the horizontal component of the current velocity. The denominator of the right-hand side of Eq. (III. 5) represents the rate of production of turbulence by Reynolds' stresses, while the numerator represents the rate of production or suppression of turbulence by the mean buoyancy field. The Richardson number is positive for a stable stratification, negative for an unstable stratification, and its absolute value increases with increasing stratification.

It was mentioned earlier that Eq. (III. 1) is, in general, coupled to the equation describing the velocity field. It can be seen now that the coupling occurs through Eqs. (III. 4) and (III. 5). The only existing theory of the thermocline which accounts for the interaction between turbulence and stratification, through a coupling between the velocity and temperature fields, is the theory of Munk and Anderson.[29]

As the wind blows over the surface of a lake, the turbulence in the upper layers of the lake are generated both by mean shear and by breaking of the waves. As Phillips[62] points out, while the momentum flux from the air to the waves is only a small fraction of the momentum flux transferred to the current, the energy flux to the waves is usually comparable to or greater than the energy flux to the current. Several Russian workers such as Dobrolonskii and Kitaigorodoskii (see Ichiye[64]) have indeed characterized the turbulence in the upper layers in terms of the predominant amplitudes, wavelengths, and periods of the surface waves.

Thus it is reasonable to suppose that the mechanical generation of turbulence in the upper layers of a lake can be characterized by the surface

conditions alone without an explicit consideration* of the current structure. In other words, the Richardson number characterizing the interaction between the mechanically generated turbulence and the thermal structure can be taken, instead of that defined in Eq. (III. 5), as

$$R_i = -\alpha_v g z^2 \frac{\frac{\partial T}{\partial z}}{\omega^{*2}} \qquad \text{(III. 6)}$$

where $\omega^* = \sqrt{\tau_s/\rho}$ is the friction velocity, τ_s is the surface shear stress induced by the wind and ρ is the density of water. Forms of the Richardson number similar to that given above have been used by Pritchard[65] in his analysis of the dispersion of contaminants in tidal estuaries and have also been used recently by Kato and Phillips.[66]

In the literature,[33, 63, 16] a number of different forms have been used for the function of f in Eq. (III. 4). Most of these relations are obtained by making various empirical assumptions; for example, some of the relations are extensions of Prandtl's mixing-length theory[67] to include the effects of stratification. Of the many existing relations, two have been chosen for the purposes of the present study as being typical ones. These relations are

$$K_H = K_{H_o} (1 + \sigma_1 R_i)^{-1} \qquad \text{(III. 7)}$$

and

$$K_H = K_{H_o} (1 - \sigma_2 R_i) \qquad \text{(III. 8)}$$

where σ_1 and σ_2 are empirical constants. The actual values of σ_1 and σ_2 are discussed in Appendix E.

---

* It will be seen later that an implicit accounting of the current structure is nevertheless necessary for a proper characterization of the turbulence structure over the entire depth of the lake.

The first of the above relations was deduced by Rossby and Montgomery[68] and the second relation was originally proposed by Holzman.[69] Kent and Pritchard[70] have tested Eqs. (III. 7) and (III. 8) with their observations in a coastal plane estuary, and their results seem to indicate that Eq. (III. 7) fits the experimental data better than Eq. (III. 8). However, within the scope of the accuracy of the measurements and the other unknowns involved, it is not possible to establish whether or not Eq. (III. 7) is a more suitable form than Eq. (III. 8).

In the present study both Eqs. (III. 7) and (III. 8) have been used, in conjunction with Eq. (III. 6), to express the eddy diffusivity K_H in Eq. (III. 1) in terms of the local temperature gradient.

III. 4 Turbulence in the Deeper Layers of a Lake

Equation (III. 6) describes the eddy diffusivity due to the turbulence generated by surface wind stress, and will not be valid for the deeper layers of a lake, since the mechanisms by which turbulence is generated in the deep layers are considerably different from those by which turbulence is generated in the upper layers. It has already been pointed out that the regions below the thermocline are little influenced by changes in surface conditions. It was also mentioned earlier that, while an explicit coupling between Eq. (III. 1) and the current structure was not retained in the present study, an implicit accounting has to be included.

When a lake is unstratified, the wind-induced current structure in it will be as shown in Fig. 2(a), with the entire lake being in circulation. However, when the lake is stratified, the wind-induced drift is confined to the upper layers with the maximum return current occurring near the thermocline as shown in Fig. 2(b). This characteristic current structure was first pointed out by Wedderburn[71] and has since then been verified by a number of others.[72, 12, 16] It immediately follows from the current structure that there is no mechanism by which the wind stress at the surface can directly create turbulence in the hypolimnion. This point needs to be emphasized since, in spite of all evidence to the contrary, some authors have assumed high values for the eddy diffusivity in the hypolimnion. The only mechanisms

by which turbulence can be created in the hypolimnion are indirect ones,[16] such as degradation of internal waves and currents produced by internal seiches,[73] and water withdrawal.[74] None of the above indirect mechanisms is explicitly accounted for either in the present study* or in any existing theory of the thermocline.

McEwen[75] has proposed a very simple method of demonstrating that the eddy diffusivities in the hypolimnion are small and nearly invariant with depth; he notes that the temperature distributions in the hypolimnia of most lakes can be well approximated by the relation

$$T - T_\infty = A e^{-az} \tag{III. 9}$$

where T_∞ is a constant, and the parameters A and a are independent of depth, but could be functions of time. If the assumption is made that the eddy diffusivity is constant in the hypolimnion, so that Eq. (III. 1) will be valid with a constant value ν in place of K_H, then Eq. (III. 9) leads to

$$\frac{\partial T}{\partial t} = \nu a^2 A e^{-az} \tag{III. 10}$$

If measurements, taken at various times, of the temperature profiles in the hypolimnion of a lake are available, and if $\log (T - T_\infty)$ and $\log \frac{\partial T}{\partial t}$ are plotted against the depth, z, then it is clear, that within the scope of the approximations made, two parallel straight lines must result. Conversely, the straightness and parallelism of the two lines together validate the assumptions that the eddy diffusivity is a constant and that Eq. (III. 9) represents the temperature distribution in the hypolimnion. The value of ν can be determined from the intercepts of the two curves on the $z = 0$ axis.

McEwen[75] used this method to evaluate the values of the eddy diffusivities in the hypolimnion of Lake Mendota, and the method has been used in various lakes by other authors.[12, 16] All these authors find that the eddy

* It should be noted, however, that in the present study the convective mixing due to water withdrawal from the hypolimnion by the power plant has been included explicitly. See Section V.

diffusivity is constant over an extended region of the hypolimnion (except close to the bottom of the lake), and that the values of $\tilde{\nu}$ are quite small, being only a few times larger than molecular diffusivity.

It is clear that Eqs. (III. 7) and (III. 8), which predict that the value of the eddy diffusivity will approach K_{H_o} at large depth, cannot be valid in the hypolimnion, because the value of K_{H_o} is typically two or three orders of magnitude greater than the molecular diffusivity. Moreover the dominant processes, such as seiches, by which turbulence is produced in the hypolimnion are not accounted for in the present study.

Since an explicit coupling between Eq. (III. 1) and the current structure has not been included in the present study, it is necessary to implicitly account for the observed change in the current structure with the onset of stratification and the different mechanisms of generation of turbulence in the epilimnion and hypolimnion. Of course, there are several implicit procedures possible, and a relatively simple procedure of accounting for the change in the current structure has been described by Sundaram and Rehm.[76] In the method used by these authors, Eq. (III. 1) was assumed to be valid over the entire lake with the eddy diffusivity being described by Eq. (III. 7) or (III. 8), so long as the minimum value of the eddy diffusivity was greater than some specified value, $\tilde{\nu}$. When the minimum value of the eddy diffusivity becomes equal to or less than $\tilde{\nu}$, Eq. (III. 7) or (III. 8) was assumed to be valid down to the point of minimum diffusivity and the eddy diffusivity was assumed to remain constant at the value $\tilde{\nu}$ below this point.

A somewhat more realistic procedure than the one described above can be formulated if it is recognized that the need for different methods of descriptions of the diffusivities in the upper and lower layers of the lake arises after the formation of the thermocline. Thus before the time of formation of the thermocline, when the temperature decreases monotonically with increasing depth, Eq. (III. 7) or (III. 8) can be used to describe the eddy diffusivity over the entire depth of the lake. After the thermocline forms, Eq. (III. 7) or (III. 8) can be an adequate representation for the eddy

diffusivity only in the epilimnion since the deeper layers are "protected" from direct wind effects by the stratification. Thus an appropriate procedure for the representation of the eddy diffusivity after the formation of the thermocline (that is, after the maximum value of the temperature gradient occurs at some point below the surface) is to assume that Eq. (III. 7) or (III. 8) is valid only in the region above the level at which the eddy diffusivity attains a minimum value. The value of the eddy diffusivity in the hypolimnion* is taken to be equal to the minimum value of the eddy diffusivity predicted by Eq. (III. 7) or (III. 8). This procedure, which yields a value of the hypolimnetic diffusivity which decreases continuously with the progress of the stratification, is more in accordance with observations[12, 16] than the time-independent value assumed by Sundaram and Rehm.[76] All the calculations on stratification described in the present report are based on the above implicit procedure for accounting for the change in the current structure with the onset of stratification.

III. 5 Numerical Integration of the Basic Equations

As pointed out earlier, the analysis of the thermocline can be divided for convenience into two phases, that of formation and that of the continuous downward migration of the thermocline into the deeper layers of the waterbody. Both of these phases are embodied in the solution of Eq. (III. 1) with the proper boundary conditions and an appropriately selected form of the thermal diffusivity. Quite general conditions relating the surface temperature and the heat flux have been given in Eqs. (III. 3) and (III. 4). However, to derive an understanding of the nonlinear and unsteady aspects of the interaction under simplest conditions, solutions for steady boundary conditions were obtained first. The formation process and the erosion of the thermocline into the hypolimnion were obtained with a constant temperature T_1 imposed at the surface or with a constant heat flux q_0 imposed

* It may be noted that the level of the plane of minimum eddy diffusivity is slightly different from that of the thermocline. However, this slight difference is of no consequence in the approximate implicit procedure being considered here.

at the surface. With the understanding gained from these examples, interpretation of solutions with the more general boundary conditions were simplified.

It has been emphasized earlier that the nonlinearity of Eq. (III. 1), which arises due to the coupling between the diffusivity and the temperature structure itself, is an essential feature and cannot be neglected. To investigate the effects of nonlinearity, Eq. (III. 1) was solved by a perturbation technique for the case when the effects of the nonlinearity are small. When the Richardson number is small, so that conditions are near neutral stability, the eddy diffusivity can be expanded (around its value for neutral stability) in increasing powers of R_i . The details of the perturbation procedure and the solution are described in Appendix A. The solution clearly displays a distortion of the temperature profile due to nonlinear effects. The reduction of the thermal diffusivity due to the increasing stability during the heating process tends to produce a thermocline, or an inflection point, in the temperature profiles. The solution is valid only at early times when the effects of the nonlinearity are small, and becomes invalid at later times when nonlinear effects become dominant.

Sundaram and Rehm[76] have investigated the effects of nonlinearity, for a rather general form of the eddy diffusivity, by using dimensional analysis. They found that both for the case of constant surface temperature and for the case of constant surface heat flux, a characteristic length scale and a characteristic time scale can be defined. The characteristic length scale determines the depth at which a thermocline first forms, and the characteristic time scale determines the time at which the thermocline forms.

Sundaram and Rehm[76] have also reported numerical solutions, in a nondimensional form, of Eq. (III. 1) for the forms of the eddy diffusivity given in Eqs. (III. 7) and (III. 8). The solutions display a nearly linear behavior at small times, but with increasing departures from the classical linear solutions at later times as the effects of nonlinearity become important. The solutions display clearly the formation of the thermocline and its

subsequent migration into the deeper layers of the lake. The characteristics of the solutions have been discussed in detail by Sundaram and Rehm, and they need not be repeated here. Here, some additional solutions will be described which include some improved features which are not included in the solutions reported by the above authors.

The solutions reported here differ from those reported by Sundaram and Rehm[76] in three specific features. First, as mentioned earlier, the manner of treating the coupling between the current and thermal structures is different in this report from the one used in Ref. 76. Second, in the present solutions the variations in the volumetric coefficient of expansion α_v of water, which were not included in Ref. 76, are included. (The changes in α_v during the early parts of the stratification process can have a significant influence on the details of stratification.) Third, the boundary condition that there be no heat flux through the bottom boundary (that is, the bottom mud) has been used in the present calculations.

Figures 3-5 show the results of a numerical integration for the form of the thermal diffusivity given in Eq. (III. 7) when the temperature is maintained at a constant value.* Note that unlike the results presented in Ref. 76, which were in nondimensional units, the results in Figs. 3-5 are presented in terms of dimensional quantities. The calculations are for the case in which the waterbody, whose depth is taken to be two-hundred feet, is assumed initially homothermal throughout at a temperature of about 3°C. At a given instant of time the temperature of the surface is suddenly raised to, and held constant at, about 10°C. The time evolution of the vertical distributions of the relevant quantities are then studied.

Figure 3 displays the temperature as a function of depth below the surface for various times. If the eddy diffusivity, K_H, in Eq. (III. 1) were assumed to be a constant, then all the temperature profiles in Fig. 3 would be self-similar. In particular, the temperature gradient would always decrease monotonically with increasing depth. The first and second profiles shown in Fig. 3, which respectively correspond to conditions one day and three days after the impulsive increase in surface temperature, do indeed

---

* The value of the semiempirical parameter σ_1, which is needed for performing the calculations, is discussed in Appendix E.

display temperature profiles which are nearly self-similar. It may be noted that during these early times conditions in the upper layers of the waterbody will actually be unstable, since the volumetric coefficient of water is negative below 4°C. In other words, for these conditions heating of the surface actually leads to an augmentation of the wind-induced turbulence in the upper layers of the waterbody so that the eddy diffusivities in these layers will be larger than those for neutral conditions. This phenomenon, which was not considered by Sundaram and Rehm,[76] is discussed in detail in Section IV.

By the third time (corresponding to ten days) shown in Fig. 3, the temperature throughout the waterbody is above 4°C and the stratification is stable everywhere. The nonlinear behavior is clearly evident in this plot which displays a point of inflection or the thermocline. The formation of the thermocline can also be seen clearly in Fig. 4 which shows a plot of the depth of the thermocline (that is, the depth at which the maximum temperature gradient occurs) against time. It can be seen from Fig. 5 that the eddy diffusivity is drastically reduced near the thermocline level.

The last two plots in Fig. 3, as well as Figs. 4 and 5, show the slow, continual progression of the thermocline to larger depths. Figures 3 and 4 clearly indicate the fact that the depth of the epilimnion increases even when surface conditions are held steady. It can be seen from Fig. 5 that the position at which the minimum diffusivity occurs (that is, the position at which the downward heat transfer is most inhibited), also propagates to greater depth. Also, the minimum value of the diffusivity decreases with increasing time.

Qualitatively similar results are also obtained for the case when the heat flux at the surface is suddenly increased and then held constant.

III. 6 Concluding Remarks

Some results are provided on the mechanisms by which thermoclines are formed and maintained in stratified lakes. It was pointed out that the thermocline is formed by the nonlinear interaction between the wind-induced turbulence and the buoyancy gradients created by surface heating. While

the nonlinear aspect of the interaction makes the problem difficult, the nonlinearity is an essential feature, and as such, has to be retained.

The influence on the eddy diffusivities of the interaction between the turbulence structure and the buoyancy gradients was included by using the techniques that have been successful in the study of atmospheric turbulence. That is, the eddy diffusivities were assumed to be given by the product of the eddy diffusivities under conditions of neutral stability and an appropriate function of a stratification parameter such as the gradient Richardson number. The nonlinear equations of the problem were then solved using an electronic computer.

It was demonstrated that, while the vertical temperature profile at the start of the stratification season in a temperate lake is fairly smooth, a sharp interface (the thermocline) develops because of the nonlinear interaction between the turbulence and the temperature structure. It was also shown that the continuous downward erosion of the thermocline into the deeper layers of the lake is a necessary part of its sustenance. The above conclusions were confirmed by considering the simple case of a semi-infinite region, initially at a uniform temperature, which is subjected to a sudden increase in surface temperature. In this case, the temperature distributions were initially similar to the error-function distribution for the linear case, but nonlinear effects soon came into play, and a thermocline was formed some distance below the surface. The thermocline also propagated steadily away from the surface.

The qualitative behavior of the solutions obtained here is in agreement with the experimental observations of Turner and Kraus[77] and Kato and Phillips.[66] The present solutions also confirm the features observed earlier by Sundaram and Rehm.[76]

IV. THE STRATIFICATION CYCLE

IV. 1 Effect of Changes in Surface Conditions on Thermocline Behavior

It was demonstrated in Section III that the mechanism responsible for the formation and maintenance of thermoclines in deep, temperate bodies of water is the nonlinear interaction between the wind-induced turbulence and the stable buoyancy gradients created by the heating of the surface layers by insulation. It was also shown that the thermocline propagates steadily away from the surface even when the surface temperature and the wind stirring are kept constant. That is, the unsteady behavior of the thermocline is inherent to the mechanism responsible for its formation and maintenance. It is now relevant to consider the effects on thermocline behavior of variations in the environmental conditions above the waterbody.

As a first step in studying the effects of varying surface conditions, a solution of Eqs. (III. 1), (III. 6) and (III. 7) was carried out for an imposed sinusoidal variation in surface conditions. The surface temperature was assumed to be well represented by the expression

$$T_s - T_{s_{av}} + \Delta T_s \sin \omega t \qquad \text{(IV. 1)}$$

where $T_{s_{av}}$ and ΔT_s are the average value and the amplitude of the variations. The quantity ω has units of reciprocal time and for an annual cycle is equal to $\frac{2\pi}{365}$ days $^{-1}$.

For the case of an imposed constant surface temperature, Sundaram and Rehm[76] have shown that a characteristic time for the formation of the thermocline can be formed from the difference $T_1 \quad T_o$ between the imposed and initial temperatures, the eddy diffusivity K_{H_o} and the quantity $\frac{\alpha_v g}{w^{*2}}$. For the present case, the characteristic time for thermocline formation can be written as

$$\tilde{\tau} = \frac{w^{*4}}{(\alpha_v \Delta T_s)^2 g^2 K_{H_o}} \qquad \text{(IV. 2)}$$

Clearly the nondimensional quantity $\omega\tilde{\tau}$, which represents the ratio of the time for formation of the thermocline to the characteristic time for variation of the imposed surface temperature, will have an important influence on the behavior of the thermocline. For example when this quantity is vanishingly small, so that the time for thermocline formation is negligible compared to the characteristic time for the changes in surface conditions, then a thermocline will form immediately following spring homothermy. As mentioned in Section II, the assumption that the above condition is valid is implicit in the theory proposed by Kraus and Turner.[38] According to the theory proposed by these authors, a thermocline and a completely homothermal epilimnion form immediately following spring homothermy. However, as pointed out earlier, most temperate lakes do not exhibit a thermocline, or a homothermal epilimnion until after several weeks beyond spring homothermy. In other words, in most lakes, the approximation that $\omega\tilde{\tau} \longrightarrow 0$ cannot lead to a proper representation of the thermal structure during the early parts of the stratification cycle.

The results for the time variations of the vertical temperature distributions for the early part of the stratification cycle, obtained from a solution of Eqs. (III. 1), (III. 6), (III. 7) and (IV. 1), are shown in Fig. 6. It can be seen that as in the case for the steady surface temperature, the temperature profiles are smooth at the initial times with a thermocline forming only at later times. It can also be seen from Fig. 6 that the thermocline propagates steadily downward into the deeper layers of the lake.

When considering the entire stratification cycle, it should be emphasized that the surface temperature is not specified a priori and that it has to be calculated as a part of the solution from the given environmental conditions above the lake. The primary purpose of the results presented in Fig. 6 is to demonstrate that the qualitative features of the formation and maintenance of a thermocline are the same for a gradually applied increase in surface temperature as they are for a suddenly applied increase in surface temperature or heat flux. Thus while changes in surface conditions undoubtedly influence the formation and maintenance of thermoclines, these

by themselves are not the primary reasons for the characteristic thermal structures of temperate lakes.

IV. 2 Seasonal Variations in Environmental Conditions above the Lake

It has been pointed out above that the seasonal variation of the surface temperature of a lake is not known, a priori, and that it has to be determined from the known variations in the environmental conditions above the lake. Thus when solving Eqs. (III. 1), (III. 6) and (III. 7) for the entire stratification cycle, the necessary boundary conditions at the surface have to be specified in terms of the known variations in the appropriate environmental conditions. It is intuitively obvious that one of the boundary conditions has to express the thermal energy exchange between the lake and the environment above it. It has also been long recognized by limnologists that the transfer of mechanical energy from the wind to the upper layers of the lake plays a very important role in determining the thermal structure.[61, 12] Birge was the first to compute the effect of the work done by the wind in distributing the heat that is received by the surface layers of the lake into the deeper layers.[77] In the present section the boundary conditions expressing the thermal and mechanical energy transfers to the surface layers of a lake are discussed.

The heat exchange across the surface of a body of water depends on a number of complex factors. A detailed discussion of the methods of computing the contributions to the heat exchange of a number of different mechanisms has been given by Edinger and Geyer[7] and Sundaram et al,[16] and it need not be repeated here. However, it is necessary to note that the heat exchange at the surface can be represented surprisingly accurately by the simple expression,

$$q_s = K (T_E - T_s) \qquad \text{(IV. 3)}$$

Both the equilibrium temperature, T_E, and the heat-exchange coefficient, K, are functions of the environmental conditions. Methods of determining T_E and K from the environmental conditions have been

described fully by Edinger and Geyer[7] and Sundaram et al.[16] The latter authors have also given various charts from which the values of T_E and K can be readily read off.

The physical significance of the equilibrium temperature is that it is the fictitious value of the surface temperature at which there will be no heat exchange between the lake and the surrounding. The equilibrium temperature is also the value to which the surface temperature of the lake would tend to, if the lake adjusted instantaneously to changes in environmental conditions. Thus the concept of equilibrium temperature is an extremely important one, and its significance will become apparent from the discussions to be presented in Sections IV. 3 and IV. 5.

The annual variation of the equilibrium temperature over most temperate lakes can be represented[16] by the simple sinusoidal relation,

$$T_E = \bar{T}_E + \delta T_E \sin(\omega t + \varphi) \qquad \text{(IV. 4)}$$

where $\bar{T}_E$ is the average value of the equilibrium temperature over one annual cycle, δT_E is one half of the annual variation and $\omega = \frac{2\pi}{365}$ days^{-1} The value of φ will depend upon the conditions from which the analysis is begun. The annual variations in the parameter K can also be represented in the same manner as in Eq. (IV. 4). However, in most cases the annual variation of K is small and it can be taken, to a sufficient accuracy, as a constant.

As mentioned earlier, in addition to boundary conditions associated with the exchange of thermal energy at the air-water interface, it is also necessary to specify the appropriate boundary conditions related to the transfer of mechanical energy across this interface due to wind stirring. The annual variations of the wind speed over a lake can have an important influence on the mixing processes within it, since the wind effect influences the eddy diffusivity, K_{H_o}, under neutral conditions as well as the Richardson number (through the friction velocity w^*). Semi-empirical relations between w^* and K_{H_o} and the wind conditions above the lake

are available and can be used to relate these quantities. For example, Munk and Anderson[29] have given a suitable semi-empirical relation between these quantities.

In the present study, the friction velocity has been allowed to be a cyclic function of time of the form,

$$\omega^* = B_1 + B_2 \sin(\omega t + \psi) \qquad \text{(IV. 5)}$$

where B_1, B_2 and ψ are constants to be determined from the known conditions above the lake, and ω is the angular frequency as before. A similar relation is assumed for the variation of K_{H_0} also.

IV. 3 Qualitative Considerations on the Seasonal Temperature Cycle

It has already been pointed out that the two important external conditions that have to be specified for a determination of the thermal structure of a lake are the degree of surface heating and the degree of wind mixing. The effects of these two conditions on the lake are closely coupled, of course, since the heat that can be received by the surface layers is dependent on the depth to which wind action can mix this heat, and conversely, the depth of wind mixing is itself a function of the degree of surface heating. The effect of wind mixing on the seasonal temperature cycle of a lake can be interpreted in terms of the changes in the values of either the Monin-Obukhov length or the over-all stability of the lake.[16] Both of these interpretations have been discussed in detail by Sundaram et al.[16] In the present section, some qualitative considerations on the effects of the variations in the equilibrium temperature on the seasonal temperature cycle will be given.

As mentioned earlier, the variation, over an annual cycle, of the equilibrium temperature over most lakes can be represented well by a sinusoidal function of the form given in Eq. (IV. 4). A schematic representation of this variation over one annual cycle, starting from the time when the heat content of the lake is a minimum, is shown in Fig. 7.* A schematic representation of the features of the variations in the surface temperature

* Some of the features noted on this figure have also been noted independently by Prof. K. B. Cady of Cornell University - private communication.

and the deep-water temperature that are observed[12, 16, 22, 61] in temperate lakes is also given in this figure. During winter, when the heat content of the lake is a minimum, the lake will also be completely homothermal due to the low over-all stability during this period. Since the heat flux at the surface of the lake has to change sign during the time of minimum heat content, it is clear from Eq. (IV. 3) that the surface temperature, the deep-water temperature and the equilibrium temperature will all coincide at this time.

During the spring months, the equilibrium temperature increases rapidly due to increasing insolation. While the surface temperature also increases during this period, it increases much more slowly than the equilibrium temperature, since the temperature of the surface layers depends not only on the rate of heating of these layers but also on the rate at which heat is removed, by turbulent mixing, from these layers to the deeper layers of the lake. During the early period, the lake remains nearly homothermal since, due to the low over-all stability, wind action is able to mix the surface heat into great depths. However, as the heating continues a thermocline forms, with the time of its formation usually coinciding with the time when the heat flux through the surface is a maximum. As the thermocline forms, the surface temperature begins to increase rapidly, since now the upper layers are heated preferentially in relation to the deeper layers (whose temperature increases only slightly).

After the formation of stratification, the surface temperature usually increases at a more rapid rate than the equilibrium temperature so that the heat flux into the lake begins to decrease. As the surface temperature continues to increase and the volume of the epilimnion increases, the lake begins to approach its maximum heat content. However in many lakes, the surface temperature begins to decrease before the maximum heat content is reached because of a decrease in over-all stability* of the lake and the

---

* The over-all stability of the lake is not to be confused with the static stability of the stratification. This point is discussed in detail by Sundaram et al.[16]

attendant rapid descent of the thermocline. As pointed out by Hutchinson,[12] the above behavior is exhibited by the Lunzer Untersee. It has also been found by Sundaram et al.[16] to be characteristic of Cayuga Lake.

The lake attains its maximum heat content as the equilibrium and surface temperatures once again coincide. Beyond this point the equilibrium temperature falls below the surface temperature, and the lake begins to lose heat. During this period, the stratification in the upper layers of the lake is statically unstable and the thermocline continues to descend rapidly into the deeper layers of the lake. When, in late fall, the thermocline descends to the bottom of the lake, the lake again attains homothermy and cools uniformly while losing heat. The minimum heat content (and the end of the cycle) is reached when the equilibrium temperature once more equals the surface temperature. The cycle is then repeated.

It is clear from the above discussion that the concept of the equilibrium temperature is an extremely useful one for studying the characteristic features of the stratification cycle of temperate lakes. The physical significance of the equilibrium temperature is that the redistribution of heat within a lake always tends to be in such a manner as to drive the surface temperature towards the equilibrium temperature. The relationship between the equilibrium temperature and the surface temperature is best illustrated by considering the linear form of Eq. (III. 1) in which the eddy diffusivity is assumed to be constant and equal to K_{H_o} . The solution to the linear equation, subject to the boundary conditions given by Eqs. (IV. 3) and (IV. 4) has been discussed in detail by Sundaram et al.[16] They found that the relationship between the surface temperature and the equilibrium temperature was governed by the nondimensional ratio of the rate of transfer of heat from the environment to the lake and the rate of transfer of heat from the surface layers to the deeper layers by turbulent diffusion. When this ratio is a large quantity, the surface temperature tends to follow the equilibrium temperature closely. In other words, for this case the conditions in the surface layers of the lake adjust immediately to changes in surface conditions. Conversely, when the above ratio is very small, the surface

temperature changes very little and conditions in the lake do not respond to changes in environmental conditions.

The qualitative considerations given above for the solution of the linearized problem will remain valid for the nonlinear case also. The primary purpose of the discussion given above is to emphasize that a successful model for the stratification cycle of a temperate lake should be capable of predicting the above characteristics.

IV. 4 Free Convection

The qualitative features of stratification that are displayed by most temperate lakes have been described above. Before proceeding to verify whether these features are predicted by the model being proposed here, one other point needs to be considered. This point is concerned with the change in character of the turbulence in the upper layers of the lake with the onset of the cooling season. Thus, during the cooling period, the representation given in Eq. (III. 7) for the eddy diffusivity is not an adequate one and has to be modified to take into account the change in the character of the turbulence.

During late summer, as the lake begins to lose heat to the environment, the stratification in the upper layers of the lake becomes statically unstable. In other words, in these layers the turbulence is augmented, rather than suppressed, by the buoyancy gradients. When the rate of cooling is relatively small, as in the early parts of the cooling season, the degree of augmentation of the wind-induced mechanical turbulence by the convective turbulence is still governed by the Richardson number. However when the rate of cooling becomes large, as in the later parts of the cooling period, the Richardson number no longer constitutes a meaningful parameter, since now the dominant transport mechanism in the upper layers is the convective turbulence and wind-induced turbulence has very little effect on the mixing processes. This does <u>not</u> mean that the quantity of mechanical energy transferred to the water by wind shear is small compared with the quantity of convective energy. Indeed, free convection is initiated when the above two energies are approximately equal. As Lumley and Panofsky[33] point out, the structures of mechanical and convective turbulences are quite

different, the latter being a far more efficient transporting agent. The mechanical eddies are usually quite small while the eddies produced by convection are relatively large, their size being of the order of the thickness of the unstable layer. Thus the latter provide larger correlations between the fluctuating quantities, and hence larger transport, than the former.

Formulae appropriate to free convection have been developed by various authors,[33,62] and these can be used to describe the transport processes during the cooling period. However, it should be pointed out that during the cooling parts of the stratification cycle both stable and unstable conditions will exist simultaneously, though at different levels, in the lake. Thus while the upper layers will be statically unstable, the lower layers, including the thermocline region, will exhibit a stable stratification. Therefore the appropriate procedure for representing the transport processes during the cooling period would be to use a suitable free-convection formula to represent the upper layers of the lake and to match this to Eq. (III. 7) at the level separating the unstable and stable regions. Clearly, this procedure will be quite complex, and it has not been adopted in the present study. Instead a relatively simple procedure for representing free convection has been chosen.

It can be seen from Eq. (III. 7) that, when the thermal stratification in the upper layers of a lake is unstable, the maximum value of the eddy diffusivity will occur at some depth below the surface. This depth represents the depth at which the rate of generation of turbulent energy by buoyancy forces is a maximum. In other words, convective eddies of the size of this critical depth provide the largest correlations between the fluctuating quantities. In the present study, whenever the stratification in the upper layers is unstable, the eddy diffusivity is assumed to be well represented by Eq. (III. 7) below the critical depth, while above this depth the eddy diffusivity is assumed to be constant everywhere and equal to the value at the critical depth. That is, the region above the critical depth is assumed to be kept well mixed by the convective turbulence.

While the above procedure for representing free convection is admittedly crude, it has been found to give a fairly accurate representation in practice. Other more sophisticated methods are, of course, possible.

For example, the convection velocity due to surface cooling can be included explicitly into Eq. (III. 1). However since, in the present study, the coupling between the velocity and thermal structures is included only implicitly, the effect of the free-convection velocity can also be included only implicitly.

Finally, it should be pointed out that in a temperate lake free convection can occur not only during the cooling season, but also during the early parts of the warming season when the temperature of the lake is below 4° C. The occurrence of free convection during the early parts of the warming season is automatically accounted for in the present study by including the effects of changes of temperature on the volumetric coefficient of expansion, α_v , of water.

IV. 5 Numerical Results and Discussion

When all the features described above are incorporated into the analytical model, calculations for the entire stratification cycle can be carried out. In the present program, calculations for complete annual cycles were carried out for a limited number of values of the various input parameters. The required input parameters have already been described in detail. These are:

i) The variation of the equilibrium temperature over the body of water under consideration.

The quantities $\overline{T_E}$, δT_E and φ in Eq. (IV. 4) have to be specified. The quantities depend on the environmental conditions above the waterbody, and methods of their determination have been discussed in detail by Sundaram et al.[16]

ii) The heat exchange coefficient, K .

The heat-exchange coefficient is also a function of the environmental conditions above the water, and the method for its determination has also been described by Sundaram et al.[16]

iii) The annual variation of the average wind speeds above the waterbody.

The known wind conditions above the waterbody can be used to determine the friction velocity, w^*, and the eddy diffusivity, K_{H_o}, for neutral conditions by utilizing an experimentally determined relation such as the one given by Munk and Andersen.[29]

The above three conditions are the only primary input conditions* required for the present analytical model. It should be noted that all three of these input conditions are concerned with the environmental conditions above the lake. Specifically, *no* knowledge of the temperature profiles within the lake, or eddy diffusivities derived from them, are needed. Some a priori knowledge of the thermal structure of the waterbody is a prerequisite in most of the existing models for the stratification cycle.[39,40]

The starting point for the calculations is from the time of the minimum surface temperature of the lake, and at this time the lake is assumed to be homothermal. However, it should be pointed out that the minimum temperature of the lake and the time at which the minimum temperature occurs are, a priori, not known. Nevertheless, because of the cyclic nature of the imposed boundary conditions, the solution will ultimately tend to a cyclic one (regardless of the initial conditions) provided that the computation is carried out over several cycles. On the other hand, if the initial conditions are chosen appropriately, the solution can be expected to return to the same conditions after just one cycle. Thus when information on the temperature of the lake is available for some period during spring homothermy, the calculations can be greatly simplified. This point will be illustrated later with a specific example.

In the present study a number of calculations, corresponding to different input conditions were carried out. The details of the numerical

* In addition to these conditions, a knowledge of the variation of the cross-sectional area of the waterbody with depth is also needed. This point will be discussed in detail later.

computational procedure are described in Appendix C. The computer program used had provisions for generating, automatically, plots of several key variables of interest. For each case, seven such computer-generated plots were produced. Three of these plots were concerned with the seasonal variations of the temperatures at different levels, the surface heat flux and the depth of the thermocline. The remaining four plots were for the vertical distributions, at various times during the stratification cycle, of temperature, heat flux, temperature gradient and eddy diffusivity.

Figures 8-14 show the above plots for a typical calculation. For this calculation the following input conditions were used:

$$T_E = 11 + 16 \sin\left(\frac{2\pi}{365} t + 0.531\right), \ ^\circ C$$

$$K = 180 \ BTU/ft^2 - day - ^\circ C$$

$$\omega^* = 0.1 + 0.025 \sin\left(\frac{2\pi}{365} t + 2.61\right)$$

$$K_{H_o} = 800 + 200 \sin\left(\frac{2\pi}{365} t + 2.61\right), \ ft^2/day$$

In addition to the above input conditions, the depth of the lake was assumed to be 200 ft and the minimum temperature during spring homothermy was assumed to be equal to 2.9°C. All the conditions given above correspond to conditions in Cayuga Lake, New York, which was chosen since extensive data on the thermal structure of this lake are available.[16]

The calculated seasonal variations in the thermal structure is shown in Fig. 8 which shows five temperatures, the equilibrium temperature (which is an input condition for the calculations), the surface temperature and the temperatures at depths of 50, 100 and 150 feet, as functions of time for approximately 1-1/4 cycles. As mentioned earlier, the imposed equilibrium temperature variation is sinusoidal with a mean of 11°C and an

amplitude of 16°C. A solution for and a discussion of the response when the problem is linearized (i. e., when the thermal diffusivity K_H is taken as constant) has been given in Section VII 5. 3 of Reference 16. According to this solution, for fixed values of the thermal diffusivity and of the heat transfer rate at the surface, the temperature variation at any depth would have a smaller amplitude and a phase shift with respect to the imposed equilibrium temperature variation; the amplitude would decrease and the phase shift increase with increasing depth. Figure 8 clearly displays the nonlinear behavior resulting from the interaction of the turbulence with the buoyancy field. Stratification in the lake can be seen to occur at around 60 days where the temperature plots at the greatest depths display severe deviation from the sinusoidal behavior predicted from a linearized model. As the thermocline descends, between 180 and 270 days, the temperature plots at depths below the surface again follow a sinusoidal curve after the thermocline has swept past that depth.

Some of the above features can be seen more clearly in Fig. 9 which displays temperature as a function of depth for various times during the annual cycle. Note that in all of the figures temperature is plotted in degrees centigrade, depth in feet and time in days. The lake was assumed to be homothermal at 2. 9°C initially, corresponding approximately to conditions in March. The first plot, at 30 days, displays a nearly homothermal profile at about 4°C resulting from the simultaneous heating at the surface and the complete wind mixing of the lake. The next plot, at 90 days and corresponding approximately to conditions which would be expected in June, clearly displays the thermocline. It may be noted that the qualitative features of the formation of the thermocline are analogous to those shown in Fig. 6 for a sinusoidally varying surface temperature. The third plot (at 180 days) in Fig. 9 displays the thermal structure of the lake as it starts into the cooling portion of the cycle. In this plot the thermocline is somewhat deeper than at 90 days and is much sharper due to the convective mixing which now supplements the wind-induced mixing in the surface (nearly homothermal) layer. The next three plots show the effects of progressive cooling and the enhanced mixing due to cooling upon the temperature structure.

At 240 days (corresponding approximately to November) the thermocline has descended beyond 100 feet showing a completely mixed upper layer and a characteristic temperature decay in the hypolimnion. At 300 days the mixed layer extends to the bottom of the lake (200 feet) and a slight temperature inversion exists. At 360 days the lake is once again homothermal at about 3°C. Two additional plots, at 420 and 500 days, display the heating part of a new cycle with the stratification again forming.

Figure 10 is a plot of the heat flux measured in Btu/ft^2 day at the surface as a function of time. The variation in this quantity deviates slightly from sinusoidal. Note that the heat flux changes sign (from the heating portion of the cycle to the cooling portion of the cycle) around 180 days. Well before this time, stratification, with the formation of the thermocline, has occurred. After this time, the wind-induced mixing in the epilimnion is supplemented by convective mixing due to cooling, and the depth of the thermocline rapidly increases. The corresponding vertical distributions of the local heat fluxes are shown in Fig. 11. It can be seen that at 30 days and at 90 days the maximum heat flux occurs at the surface and decreases monotonically with increasing depth. However, beyond summer solstice, the intermediate layers of the lake are heated relatively more rapidly than the surface layers. Thus at 180 days, the surface heat flux is zero while the downward heat flux at the layers close to the thermocline is relatively large. At 240 days the upper parts of the lake are cooling rapidly, but the region below about one-hundred feet continues to gain heat, the maximum downward heat flux again occurring close to the level of the thermocline. On the other hand, at 300 days, after the disappearance of stratification, the entire lake is losing heat to the atmosphere.

The vertical variation of the eddy diffusivity for various times during the stratification cycle are shown in Fig. 12. At 30 days, before the formation of the thermocline, the eddy diffusivity remains nearly invariant with depth. However as the thermocline forms, there is a drastic reduction in the values of the diffusivity in the lower layers as can be seen from the plots for 90, 180 and 240 days. In the plot for 240 days, the initiation of free convection (with the attendant increase in the value of the eddy diffusivity)

can be seen in the upper layers. By 300 days, a large part of the lake is dominated by free convection. At 360 days, the lake is again homothermal and the eddy diffusivity is nearly invariant with depth. The last two plots in Fig. 12, which are for the early parts of the second cycle, display the same general features as the plots for the first cycle.

Figure 13 is a plot of the vertical variation of the temperature gradients for the various times considered in Figs. 9, 11 and 12. It can be seen that at all times, the upper layers of the lake are nearly homothermal. On the other hand, relatively larger temperature gradients occur in the hypolimnion. In other words, the hypolimnion is always considerably less homothermal than the epilimnion.

Figure 14 is a plot of the depth of the thermocline versus time. The thermocline is seen to form at about 60 days. The depth of the thermocline is then seen to decrease to a minimum value of about 35 feet between 120 and 150 days. As noted above the depth of the thermocline increases rapidly beyond 180 days when the cooling part of the cycle begins. The thermocline reaches the bottom, and the lake attains homothermy, at about 270 days so that the length of the stratification period is about 210 days.

Clearly, the above results display all the observed characteristic features of the stratification cycle of temperate lakes that were discussed earlier. For example, in most temperate lakes the surface temperature begins to decrease before the lake has reached its period of maximum heat content.[12] It can be seen clearly from Fig. 8 that the maximum surface temperature of the lake is reached at about 150 days after the start of the calculations, while the maximum heat content of the lake does not occur till after thirty days later. The occurrence of this phenomenon in Cayuga Lake and the reasons for it have been discussed by Sundaram et al.[16] Again, in accordance with observations, the present model predicts the formation of the thermocline some time <u>after</u> the period of maximum spring homothermy (with an intermediate period of monotonically varying temperature distributions), but <u>before</u> the lake attains its maximum heat content and begins to lose heat to the atmosphere. On the other hand, some theories[38] predict

the formation of the thermocline immediately following maximum spring homothermy, and others[36] predict the formation of a well-mixed upper layer only after the start of the cooling season.

IV. 6 Cyclic Behavior of the Results

It has already been pointed out that the minimum temperature of the lake during spring homothermy is, in general, not necessary for a solution of the problem because of the cyclic nature of the solution. Thus, while an unique starting point for the calculations does not exist, the solution will always tend to a cyclic one, regardless of the starting conditions, provided the solution is carried out over several cycles. In the example considered in Section IV. 5, the calculation was started with the assumption that the minimum temperature during spring homothermy was 2. 9°C since this is known to be the case from actual observations in Cayuga Lake. Thus, for this example, it can be seen from Fig. 8 that the solution exhibits a cyclic behavior after just one cycle (with the temperature at the end of one cycle returning to the initial temperature), because of the proper choice of the initial condition. On the other hand, if the calculations had been started at some arbitrary temperature, say 4°C, then the solution will not become cyclic after the first cycle and the temperature at the end of one cycle will be different from 4°C (and also 2. 9°C). However, the temperature at the end of several cycles will automatically approach the correct temperature of 2. 9°C.

The above cyclic behavior of the solution has important implications for the practical applications of the theoretical model developed in the present study. As pointed out earlier, the necessary input conditions for the present analysis of the stratification cycle are the annual variations of the equilibrium temperature, the heat exchange coefficient and the wind speed above the lake. These quantities are the logical "external parameters" for specifying the thermal structure of the lake since these determine the exchange of thermal and mechanical energies between the lake and the atmosphere. Indeed, concepts such as the Monin-Obukhov length scale[16] are based on "external parameter" considerations. However, in many practical examples, a complete knowledge of the "external parameters" is

not available. For example, the equilibrium temperature over a waterbody depends on several complex factors such as the incoming (sky and solar) radiation, the temperature and humidity of the air over the waterbody and the wind speed. Complete and accurate information on all the above variables is often difficult to obtain.

The nonavailability of complete information on all of the external parameters over a lake does not mean that information on the thermal structure of the lake cannot be generated using the present theory. In fact, because of the requirement of cyclicity, the requirement of a complete specification of the "external parameters" can be relaxed if other compatible information on the thermal structure is available. For example, if some information on surface-temperature variation (such as the minimum temperature at spring homothermy and the maximum summer temperature) is available, then this information can be used instead of the equilibrium temperature.

Consider, the instance, the example given in Section IV. 5. Suppose that for the case considered, the minimum temperature at spring homothermy and the maximum summer temperature are known from measurements, but that no accurate information on the equilibrium temperature variation is available. Information on the other input quantities is assumed to be known. For such a case, all required information on the stratification cycle can be obtained using the present theory with a trial-and-error procedure. Figure 15 shows a calculation for the stratification cycle for the same condition given in Section IV. 5 except that now the equilibrium-temperature variation is taken to be given by

$$T_E = 14 + 13 \sin \left(\frac{2\pi}{365} t - 1.03 \right)^* \quad , ^\circ C$$

---

*Note that the phase difference, φ , has always to be chosen in such a manner that at $t = 0$, the equilibrium temperature equals the known initial temperature at spring homothermy.

The calculation is started at the known initial temperature at spring homothermy of 2.9°C, and the results for the first 420 days are shown in Fig. 15.

It can be seen from Fig. 15 that the solution does not display a cyclic behavior over the first year, and that the conditions after one year are considerably different from the starting conditions. Indeed, homothermy is not achieved till after 390 days and the temperature at homothermy is about 6°C. Thus, the assumed equilibrium temperature variation is clearly incompatible with the lake attaining homothermy at 2.9°C. On the other hand, it can be seen from Fig. 15 that the maximum predicted summer surface temperature for this case is not significantly different from that for the previous case.

In general it can be stated that, all other things being equal, the temperature at spring homothermy depends strongly on the minimum value of the equilibrium temperature and that the maximum surface temperature depends strongly on the maximum value of the equilibrium temperature. In the two examples considered above the maximum values of the equilibrium temperatures are the same and hence the maximum values of the surface temperature are not significantly different. On the other hand, the minimum values of equilibrium temperatures for the two cases are significantly different from each other, and hence the minimum temperatures at spring homothermy are different also. Thus a more accurate representation of the stratification cycle can be obtained by choosing an equilibrium-temperature variation in which the maximum value of T_E is the same as before but in which the minimum value of the equilibrium temperature is lower. A rough rule of thumb for choosing a new value for the minimum equilibrium temperature is that the difference between the new and the old values should be somewhat larger than the difference between the minimum surface temperature after one cycle and the initial temperature of spring homothermy By successive repetition of the iterative procedure described above, the correct choice for the equilibrium temperature, and the corresponding information on the other relevant quantities (such as the vertical distributions of temperature or the variation of the depth of the thermocline), can be arrived at fairly rapidly.

It should be emphasized that if the calculations for the above conditions were carried out over several cycles, the solution will ultimately tend to a cyclic behavior, but with the minimum and maximum temperatures being quite different from the specified values. This is because for a given set of 'external parameters' there is only one unique cyclic solution regardless of the initial starting conditions assumed. This is illustrated in Figs. 16-18 which show the results for nearly three years for the case when

$$T_E = 12 + 16 \sin\left(\frac{2\pi}{365} t - 0.642\right)$$

with all other conditions being the same as before. The calculations are started assuming an initial temperature of 2.9°C, as before, and it can be seen from Fig. 16 that the solution tends to a cyclic state at a higher value of the minimum homothermal temperature. The attainment of cyclicity is clearly evident from Figs. 17 and 18 which show the vertical distributions of temperature and eddy diffusivity for the same relative times during the three years. While noticeable differences can be seen between the distributions for the second and first years, the distributions for the third year are indistinguishable from those for the second year.

IV. 7 Comparison with Observations

As mentioned earlier, in the present program numerical calculations (using the analytical model) were performed only for a limited number of combinations of the various input parameters. Many of the calculations were designed to check the various aspects of the numerical program and some calculations were performed to check that the model was predicting the appropriate qualitative features. However, due to time limitations, neither a comprehensive parametric study of the behavior of the solution for various input conditions, nor calculations for conditions corresponding to specific waterbodies were carried out. It is hoped that these calculations can be performed in the near future.

For some of the calculations, the input parameters were chosen to correspond roughly to those of Cayuga Lake, since extensive information on the thermal structure of this lake is available.[16,22] However, it should

be emphasized that no attempt was made to duplicate exactly the "external parameters" for this lake. A detailed discussion of this specific example has already been given in Section IV. 5 and the results are presented in Figs. 8-14. Comparisons of the calculated and observed values for the temperature cycle, the temperature profiles and the thermocline depth are shown in Figs. 19-21. In all the figures, the measured values shown are the averages of the values for the years 1950, 1951, 1952 and 1968.

It can be seen from the figures that the agreement between the measured and computed values are very good both in a qualitative and in a quantitative sense. However, the quantitative agreement has to be viewed in the light of the fact that the "external parameters" used in the calculations represent the conditions over Cayuga Lake only in a rough manner. It may well be that, in this specific example, the mismatches in different "external parameters" produced opposing effects and that their net cancel lation is responsible for some of the good agreement found in Figs. 19-21 between the measured and computed values. It should also be pointed out that in a lake in which the area of cross section changes with depth, the assumption of horizontal homogeneity necessarily implies a distortion of the vertical scale. This fact was pointed out by Birge a number of years ago in connection with the calculation of the heat budget of a stratified lake.[12, 16] Thus a direct comparison (that is, without taking vertical distortion into effect) of the computed and measured values is not compatible with the assumption of horizontal homogeneity.

The points mentioned above have to be resolved by carrying out systematic calculations using the present model before definitive conclusions on the quantitative accuracy of the present scheme can be reached. Since such calculations have not yet been performed, it can only be stated here that the present scheme appears to give quite adequate quantitative accuracy. However it should be reiterated that the present scheme gives excellent qualitative agreement with all of the observed features of stratification in temperate lakes. Indeed, many of these features have never before been predicted analytically.

IV. 8 Concluding Remarks

In the present section, the theoretical concepts developed in Section III were used to generate an analytical model for the annual stratification cycle of a temperate lake. The analytical model essentially viewed the changes in the thermal structure of a waterbody in terms of certain "external parameters" characteristic of the environmental conditions over the waterbody. Specifically, the external parameters were used to characterize the transfer of thermal and mechanical energies at the air-water interface.

The results of the analytical model are in excellent agreement with the observed qualitative features of the stratification cycles of temperate lakes. In particular, the analytical model predicted accurately certain characteristic features which were never before predicted analytically. While because of the limited number of calculations that were carried out an assessment of the predictive accuracy of the model was not possible, comparisons of the calculations with observations in Cayuga Lake gave very good agreement.

V. EFFECTS OF THERMAL DISCHARGES

V. 1 General Remarks

In Section III it was shown that the mechanism responsible for the formation of thermoclines in stratified lakes is the nonlinear interaction between the wind-induced turbulence and the buoyancy gradients due to surface heating. In Section IV, the above concept was extended to study the entire stratification cycle. It is now relevant to enquire as to what the perturbing effects on this basic thermal structure will be when thermal discharges are introduced into the lake. Specifically, in this section we will consider the effects of thermal discharges from power plants for the case when the intake water is withdrawn from the hypolimnion, and the heated effluents are injected back into the hypolimnion in such a manner as to trap them below the thermocline during part of the stratified period.

When considering the effects of thermal discharges into the hypolimnion of a stratified waterbody, two specific problems have to be analyzed. The first is concerned with the behavior of the buoyant plume due to the discharges and the second is concerned with the effects of the discharges on the entire waterbody. These two problems have been termed the micro- and macro-scale problems by some authors.[10] As mentioned in Section II, the first problem (namely, the behavior of a buoyant jet in a density stratified environment) has been studied extensively in other connections. Therefore this problem is discussed only briefly in Section V. 2. On the other hand, very little is known about the effects of thermal discharges, at or below the level of the thermocline, on the entire waterbody. The latter problem is discussed in detail in Sections V. 3 and V. 4.

It should be emphasized that, as pointed out by Sundaram et al,[16] the primary difficulty of predicting the effects of heated effluents on the thermal structure of a stratified lake is that the discharges affect the thermal structure of the lake not only directly, but also indirectly by their influence on the turbulence structure in the lake. The effects of the thermal

discharges on the structure of the turbulence, and the resulting changes in the eddy diffusivities, are quite important since the manner in which the added heat is dispersed into the lake is controlled by the values of the eddy diffusivities. Thus one cannot assume, as has been done by some authors, that the thermal discharges do not affect the mechanisms of epilimnial mixing. This point is discussed in detail in Sections V. 3 and V. 4.

Finally, one additional point needs to be made here. When considering the effects of thermal discharges from a power plant with a hypolimnetic intake, it should be recognized that in addition to the effect associated with the discharge of heat there is also an effect associated with the transfer of large quantities of water from one level to another. This latter effect arises due to a change in the potential energy of the stratification and, as pointed out in Refs. 16 and 76, it can be viewed in terms of an equivalent change in wind conditions above the lake. This effect is discussed in detail in Section V. 4.

V. 2 The Buoyant Plume

When thermal discharges are injected into the hypolimnion of a stratified body of water, they will rise as a buoyant plume because of the positive buoyancy with respect to the surrounding cooler medium (see Fig. 21a). As the plume rises, it will entrain the cooler surrounding water into it. The entrainment will increase the volume of the plume and also reduce the temperature difference between the plume and the surroundings. In addition, the temperature difference between the plume and the ambient water also decreases due to the fact that the ambient temperature increases with increasing distance from the point of discharge. Even after the plume becomes neutrally buoyant, it will continue to rise because of its residual kinetic energy and will come to rest only when this energy is fully dissipated.

After this point the plume will spread rapidly in the horizontal direction as a relatively thin sheet. The initial horizontal spreading of the thermal plume will create a well-mixed layer which is nearly homothermal so that, due to the stable stratification at the (horizontal) boundaries of this

layer, vertical mixing will be inhibited. The assumption of horizontal homogeneity, which was used in Sections III and IV to study stratification, will continue to remain valid when considering the effects of the discharges on the entire waterbody. Indeed when considering the lake-wide effects of the discharges, it is appropriate to assume that the added heat is injected uniformly at the level at which the effluents spread.

Recently Baines and Turner[79] have studied, both experimentally and theoretically, the effects of continuous convection from a small source of buoyancy enclosed in a bounded region. They point out that conservation of mass requires that at any horizontal plane the upward volume flux in the plume be balanced by an equal downward flux in the surrounding region. Also, because of the stable stratification in the surrounding region, the fluid that is entrained into the plume at any level (including the intake level) can be assumed to come entirely from that level. In the present work, these concepts have been adapted to study the lake-wide effects of thermal discharges into the hypolimnion of a stratified lake. However, a detailed consideration of the behavior of the buoyant plume itself has not been included. Rather, the effluents have been assumed to be injected directly into the level at which the lake temperature is equal to the discharge temperature. It is planned to include the effects of dilution in future modifications of the present model using existing knowledge[79, 80] on the behaviors of buoyant plumes in density stratified environments.

V. 3 Effects of Discharge on Overall Thermal Structure

As mentioned earlier, there are two effects which must be included when modeling the influence of a power plant effluent upon the overall thermal structure of a body of water. Water withdrawn from lower, colder layers of a lake, heated and discharged into the lake again, adds thermal energy, and, by changing the vertical thermal structure of the lake, alters the potential energy of the lake. Therefore a power plant both adds heat and does work on the lake when using lake water for cooling. In the present section, terms will be added to Eq. (III. 1) which will explicitly include the far-field effects of heat added and of work done by the power plant.

As discussed earlier, detailed consideration of the buoyant plume created by the effluent will not be made. A proper accounting of interaction of the plume and the surrounding lake water would entail a model in which the current structure is explicitly treated, rather than implicitly treated as in the present model. The effects of dilution of the effluent by entrainment will not be considered either for the determination of depth at which the effluent begins its horizontal spread or for the determination of the volume of surrounding water entrained. Rather effluent water will be assumed to be discharged directly at the depth at which the lake temperature equals the effluent temperature, and this water will be considered to mix rapidly in the horizontal direction. If the temperature of the discharged water exceeds the temperature of the lake water at each depth, then the effluent will rise to the surface and spread. Both the intake and the outfall will be assumed not to affect the condition of horizontal homogeneity imposed by the basic model without the effects of discharges.

It should be noted that the limitations on the model imposed by neglecting dilution of the thermal plume will not change the qualitative behavior determined. All of the effects discussed in this section for thermal discharges into a stratified lake are qualitatively correct and are nearly quantitatively correct provided that the discharge temperature used in the calculations is chosen to be an effective discharge temperature. The major effect of the reduction of plume temperature due to dilution of the thermal effluents will be to change the level at which spreading of the discharge occurs. Depending upon the outfall configuration and the lake conditions, the quantity of lake water entrained into the discharge will generally be a small fraction of the volume of the water used for power-plant cooling. Therefore, the temperature at which the plume begins to spread will be somewhat lower than the actual temperature of the discharge at the outfall. The temperature at which the plume begins to spread, or the effective discharge temperature, can be taken to be somewhat (a few degrees) smaller than the actual discharge temperature to compensate for dilution within the plume. Throughout the subsequent considerations the temperature increase ΔT_p due to the power plant will be taken to be the difference between the water temperature at the intake level and an effective temperature at discharge.

V. 3. 1 Model When Discharge Remains Below the Lake Surface

In the present study, following Baines and Turner,[79] it has been assumed that the effluents spread instantaneously into a thin sheet at their level of neutral buoyancy, and the details of the actual horizontal spread have been ignored. This assumption is justified in view of the relatively long time scales involved in the consideration of the lake-wide effects of the discharges. In the present model, the effect of the intake will be equivalent to that of a uniformly distributed sink at the level of the intake, with the total strength of the sink corresponding to the volumetric flow rate through the power-plant condensors. There will be a corresponding uniformly distributed source of fluid at the effective level of injection of the discharge.

When considering the effects of thermal discharges from a power plant with a hypolimnetic intake, in addition to the effect associated with the discharge of heat there is also an effect associated with the transfer of large quantities of water from one level to another. This latter effect arises due to a change in the potential energy of the stratification and, as pointed out in Ref. 16, for a surface discharge it can be viewed in terms of an equivalent change in wind conditions above the lake. In the present model the effect of "pumping" water from a lower level to a higher one has been properly accounted for.

Although there are different ways in which the effects of heat and pumping work could be included, when the effluent is discharged below the surface, these effects will be added to Eq. (III. 1) through a single term $w_p \frac{\partial T}{\partial Z}$. Here w_p is the uniform, downward vertical velocity which is induced (between the level of the intake and the effective level of the discharge) by the power plant pumping; w_p can be assumed to be the volumetric flow rate Q_p through the power plant divided by the area A of the lake. With the addition of this term Eq. (III. 1) becomes

$$\frac{\partial T}{\partial t} = \frac{\partial}{\partial Z}\left(K_H \frac{\partial T}{\partial Z}\right) - w_p \frac{\partial T}{\partial Z} \quad , \qquad Z_i \geq Z \geq Z_a \qquad \text{(V. 1)}$$

If the level of the intake for water is fixed at Z_i and the effective level of

discharge of the heated effluent is at z_d (see Fig. 21a), then Eq. (V.1) is appropriate for $z_i \geq z \geq z_d$. Below the intake level, $z > z_i$, and above the discharge level $z < z_d$, the direct effects of the power-plant pumping are absent, and the governing equation is Eq. (III.1) again.

The meaning of the extra term in Eq. (V.1) can be understood simply by examining integrals of Eqs. (V.1). Integrating these equations from the surface of the lake, $z = 0$, to the bottom of the lake, $z = z_m$, we obtain

$$\frac{d}{dt}\int_0^{z_m} T\,dz = \left(K_H \frac{\partial T}{\partial z}\right)_{z=z_m} - \left(K_H \frac{\partial T}{\partial z}\right)_{z=0} - \omega_p \left[T(z_i) - T(z_d)\right] \quad (V.2)$$

Multiply by $\rho C_p A$ and note the boundary conditions that have been imposed at the bottom and at the surface of the lake.

The heat flux at the bottom of the lake is zero:

$$\rho C_p K_H \left.\frac{\partial T}{\partial z}\right|_{z=z_m} = 0$$

The heat flux at the surface of the lake:

$$-\rho C_p K_H \left.\frac{\partial T}{\partial z}\right|_{z=0} = K(T_E - T_S)$$

Then Eq. (V.2) can be rewritten

$$\frac{d}{dt}\int_0^{z_m} \rho C_p T A\,dz = AK(T_E - T_S) + Q_p \rho C_p \left[T(z_d) - T(z_i)\right] \quad (V.3)$$
$$\equiv A q_s + A q_p$$

Equation (V.3) is simply and directly interpretable. It states that the time rate of increase of thermal energy, integrated over the whole lake, is equal to the rate of heat addition through the surface Aq_s plus the rate of heat addition by the power plant Aq_p. Note that the rate of heat addition by the power plant is simply the water volumetric flow rate Q_p times the energy per unit volume required to heat water from the intake temperature $T(z_i)$ to the effective discharge temperature $T(z_d)$.

Taking the first moment of Eq. (V. 1) and integrating again from $z = 0$ to $z = z_m$, we find, after some manipulation,

$$\frac{d}{dt}\int_0^{z_m} z\,T\,dz = \int_0^{z_m}\left(-K_H\frac{\partial T}{\partial z}\right)dz - \omega_p z_d\left[T(z_d) - T(z_i)\right] + \omega_p\int_{z_d}^{z_i}\left[T(z) - T(z_i)\right]dz \tag{V. 4}$$

Equation (V. 4) can be interpreted in terms of the changes in the potential energy of stratification.

The potential energy of stratification of a lake can be written in the form

$$P = \rho\alpha_v g A\int_0^{z_m}(z - z_g)(T - \bar{T})\,dz \tag{V. 5}$$

where z_g is the depth of the center of gravity of the lake and $\bar{T}$ is the temperature the lake would attain at any given time if the wind energy were able to mix it completely. Note that the potential energy of stratification is always negative since wind energy is required to upset the stratification. Thus the stronger the stratification, the more negative will be the potential energy. The time rate of change of potential energy can be written as

$$\frac{dP}{dt} = \rho\alpha_v g A\frac{d}{dt}\int_0^{z_m} z\,T\,dz - \rho\alpha_v g A z_g\frac{d}{dt}\int_0^{z_m} T\,dz \tag{V. 6}$$

Equations (V. 6), (V. 3) and (V. 4) can be combined to yield

$$\frac{dP}{dt} = -\rho\alpha_v g A z_g\frac{q_p}{\rho C_p} + \rho\alpha_v g A\int_0^{z_m}\left(-K_H\frac{\partial T}{\partial z}\right)dz + \rho\alpha_v g A(z_d - z_g)\frac{q_p}{\rho C_p} + \rho\alpha_v g A\omega_p\int_{z_d}^{z_i}\left[T(z) - T(z_i)\right]dz \tag{V. 7}$$

The first term in the right-hand side of Eq. (V. 7) represents the change in the potential energy of stratification due to the surface heat flux, while the second term represents the change due to the heat flux in the deeper layers. Since the heat flux at the deeper layers arises out of the wind-induced mixing of the surface heat income, the second term can be identified with the effects

of wind mixing. The third term in Eq. (V.7) represents the change in potential energy of stratification due to the thermal discharges. Note that it depends only on the amount of heat added and the effective level of the discharge. The fourth term in Eq. (V.7) represents the effect of pumping and it depends on the pumping velocity ω_p.

V.3.2 Model When Discharge Surfaces

When the effective temperature at which the effluent is discharged is higher than the temperature at any depth within the lake, then the effluent will surface and spread horizontally. The model discussed above is no longer adequate since the term $\omega_p \frac{\partial T}{\partial z}$ in Eq. (V.1) requires the effluent and the ambient temperature at the discharge level to be equal. Under these conditions, then, heat in addition to that supplied to the lake by the term $\omega_p \frac{\partial T}{\partial z}$ must be explicitly introduced. If ΔT_p represents the effective temperature change produced in the intake water by the power plant, then the total heat added per unit time to the lake will be $Q_p \rho C_p \Delta T_p$, or the heat added q_p per unit area of the lake per unit time is $q_p = \frac{Q_p}{A} \rho C_p \Delta T_p = \omega_p \rho C_p \Delta T_p$. When the effluent surfaces, the surface temperature T_s is such that $T_s - T(z_i) < \Delta T_p$. The term $\omega_p \frac{\partial T}{\partial z}$ in Eq. (V.1) adds only $\omega_p \rho C_p \cdot [T_s - T(z_i)]$ heat per unit area per unit time. The additional heat per area per time, namely $\omega_p \rho C_p [T(z_i) + \Delta T_p - T_s]$, must be added explicitly into Eq. (V.1).

This heat is added by a source term in Eq. (V.1) of the form

$$S(z) = \frac{1}{\rho C_p} \frac{2 \rho C_p \omega_p [T(z_i) + \Delta T_p - T_s]}{a\sqrt{\pi}} e^{-\frac{(z - z_d)^2}{a^2}} \qquad \text{(V.8)}$$

where a is a length scale for the distribution of the source term. The factor $\frac{2}{\sqrt{\pi}}$ arises so that the integral of the source term over depth will approximately yield the total additional heat flux to be added. Therefore, when z_d reaches the surface, the explicit heat source term given by Eq. (V.6) is incorporated into Eq. (V.1). (Note that z_d is never allowed to become less than a in the numerical program).

$$\frac{\partial T}{\partial t} = \frac{\partial}{\partial z}\left(K_H \frac{\partial T}{\partial z}\right) - \omega_p \frac{\partial T}{\partial z} + S(z) \qquad 0 \le z \le z_i \qquad \text{(V.9a)}$$

$$\frac{\partial T}{\partial t} = \frac{\partial}{\partial z}\left(K_H \frac{\partial T}{\partial z}\right) + S(z) \qquad z_i < z \leq z_m \qquad \text{(V. 9b)}$$

An alternate method by which the additional heat flux $\omega_p \rho C_p [T(z_i) + \Delta T_p - T_s]$ can be added when the thermal discharge surfaces is by changing the boundary condition at the surface. In the present calculations the heat flux at the surface is given by Eq. (IV. 3), and, when the thermal plume surfaces, the additional heat due to the power plant is introduced by means of the source term in Eq. (V. 8). However, the additional heat flux $\omega_p \rho C_p [T(z_i) + \Delta T_p - T_s]$ could also be included in the calculation by increasing the heat flux q_s directly at the boundary. In future computations, this alternate procedure will be tried, and the results will be compared with those obtained by the present procedure.

V. 3. 3 Model with Pumping Only

In the preceding sections a model was introduced for calculating the effects on the overall thermal structure of a stratified lake of thermal effluents discharged at or below the level of the thermocline. In this model the effects of dilution of the effluent due to entrainment during the rise of the buoyant fluid have not been included. However, as noted before, the reduction in temperature of the effluent due to dilution by lake water entrained into the plume can be implicitly accounted for in the model by selecting an effective discharge temperature somewhat less than the actual discharge temperature.

In this section a model opposite, in a sense, to that discussed in the preceding sections is introduced to calculate the effects on the overall thermal structure of a stratified lake of pumping cold water from the hypolimnion and discharging it and mixing it into the epilimnion. In this model no heat is added to the water being pumped, and it is assumed that dilution and mixing of the cold effluent by the surface layers of lake water are complete. Dilution and mixing of the plume over a depth a (the length scale defined in the source term in Eq (V. 8)) can be accomplished practically by supplying a sufficient number of ports in a multiple-port diffuser at the outfall. This model is of interest when considering the effects on the thermal

structure of the lake of the work done when water is pumped from the hypolimnion to the surface.

In this model water is withdrawn at a depth z_i , pumped to the surface, discharged at temperature $T(z_i)$ and mixed with the water in the epilimnion. Such an example of pumping water from the hypolimnion into the epilimnion with no heating of the water, can be calculated as a special case of the model Eqs. (V. 9) and heat source term (V. 8). When pumping with no heating is simulated, the source term becomes negative, a sink. The heat absorbed by this sink must balance the heat added by the term $\omega_p \frac{\partial T}{\partial z}$. In an integral sense a balance will occur in Eqs. (V. 9) if ΔT_p is set to zero in the source term in Eq. (V. 8).

V.4 Numerical Results and Discussion

The numerical model for the effects of thermal discharges described in Section V.3 has been used to make several numerical integrations of Eqs. (V.1) and (V.9). The purpose of these calculations is to determine the effects on the overall thermal structure produced by discharging a heated effluent into the hypolimnion of a body of water. An additional objective of these calculations is to examine the effects on the thermal structure of pumping water from the hypolimnion to the epilimnion without heating the effluent. As discussed earlier, the thermal discharge of water into the hypolimnion of a lake produces two alterations: heat is added to the lake, and the potential energy of the thermal stratification is reduced by the pumping work. The latter effect is isolated by the calculations which model pumping alone, and for this reason calculations were performed with both thermal discharges and pumping alone.

The calculations presented in this subsection by no means represent a complete study of the effects of thermal discharges or of pumping upon the thermal structure of a body of water. Rather the results show some of the interesting features. A parametric study with this model of these effects would be very informative and highly desirable.

In this subsection the calculations performed to determine the effects of thermal discharges and of pumping alone are described. Comparison is made between these calculations and those describing the basic annual variation in a stratified lake. The comparison shows many important features which thermal discharge into the hypolimnion and pumping from the hypolimnion to the epilimnion can produce. Most of these features have never been discussed in quantitative terms before.

First, a discussion is given of the transient and periodic responses produced by a thermal discharge or by pumping alone. Then the general effects of a thermal discharge and of pumping are presented. Finally, comparison between the base calculation, the response with thermal discharge and the response with pumping alone is made.

V.4.1 Transient and Periodic Responses

As discussed in Section IV, the variation in the temperature or the thermal diffusivity within a lake will always be periodic because the surface conditions are periodic. If the initial conditions are chosen properly, these quantities will be periodic from the beginning of the calculation. In general, if arbitrary initial conditions are chosen, the solution will require a transient period before cyclic distributions of temperature are achieved.

To examine the effects of thermal discharges or of pumping alone, one must start with a periodic base calculation. In Section IV a detailed description was given of the procedure used to determine desired periodic conditions. Figures 8 through 14 are plots of the solution for the base calculation. With the parameters and the initial conditions chosen to be the same as for the base calculation the terms representing a thermal discharge can be introduced and the effects resulting from the discharge can be determined by numerical integration.

The base calculation represents the average annual distributions of temperature prevailing in an undisturbed temperate lake similar to Cayuga Lake. If a power plant were situated on this lake and if the waste heat discharged by the power plant were taken to be constant with time, then the response of the lake could be divided into a transient portion, during which the lake adjusted to the new heat budget and to the additional work done by pumping, and a periodic portion thereafter. The results presented in this subsection concentrate on the transient response. Although the periodic differences produced by a power plant are of great general interest, the practical limitations introduced by the length of the calculation and by the available time did not permit an adequate assessment of these differences.

V.4.2 Effects of Thermal Discharges

Since a power plant withdraws water, heats it and discharges it into the lake again, the water temperature at any time and at any level can be expected to be higher than the corresponding temperature without the discharge. The magnitude of this temperature increase can be estimated from the heating introduced by the power plant. It is convenient to consider the heat

added per unit time by the power plant divided by the surface area of the lake. This quantity, the heat flux added by the power plant, can be compared with the heat flux at the surface of the lake in the absence of the thermal discharge. In Fig. 10 the surface heat flux of the standard cycle has been shown, and the maximum value of the heat flux is seen to be about 2000 Btu/ft^2-day. The corresponding temperature variation at the surface of the lake is about 20°C (see Figure 8). For the calculations discussed in this subsection the heat flux attributed to the power plant was taken to be 280 Btu/ft^2-day. If this heat flux were added to that occurring naturally at the surface and if the mixing processes were taken to be unchanged, a maximum temperature increase of about 2-3°C would be expected from the power plant.

Heat can be discharged at a specified rate in a variety of ways, depending upon the flow rate of water used for cooling. As discussed before, the heat added per unit surface area of the lake per unit time is $q_{tp} = \frac{Q_p}{A} \rho C_p \Delta T_p$. For a fixed heat flux q_{tp} the temperature increase ΔT_p produced by the waste heat is inversely proportional to the volumetric flow rate Q_p of cooling water. Therefore, specification of the heat flux q_{tp} and of the volumetric flow rate or of the pumping velocity $w_p = Q_p/A$ within the lake determines the temperature increase. The temperature increase of the effluent water over that of intake water determines the level at which the discharge spreads horizontally within the lake and therefore the details of the change in the thermal structure produced by the power plant. Two flow-rate and temperature-increase combinations for the specified heat flux have been considered: in one case the pumping velocity was taken to be 1/4 ft/day with a temperature increase of 10° C at discharge and for the other case w_p = 1/6 ft/day and ΔT_p = 15°C.

In each case the temperature increase resulting from the power plant is small compared with the maximum natural variation of the temperature at the lake surface, and the qualitative features of the temperature variation with time at any depth will be the same as without the discharge. Therefore, differences in temperature produced by thermal discharges are of interest.

A comparison between temperature profiles without and with thermal discharge at three times during the year is shown in Fig. 22. The thermal

discharge has a pumping velocity of w_p = 1/4 ft/day and a discharge-temperature increase of ΔT_p = 10°C. The first set of plots, at 90 days, is chosen to show the temperature change after formation of the thermocline during the heating portion of the annual cycle. The curves show that the maximum temperature increase occurs at the surface and that smaller increases occur at greater depths. This behavior is to be expected for the following reason. The intake depth for this calculation has been placed at about 125 feet. At this depth the temperature has varied from its initial value of 2.9°C to around 6°C during the 90 days. With a discharge temperature 10°C above the temperature at the intake depth, the effluent is found to surface throughout the first 90 days. Consequently, the temperature increase produced by the discharge above the natural temperature will be expected to be greatest at the surface. At some time after 90 days the effluent will no longer surface, but will be trapped by buoyancy effects below the surface during part of the stratification period.

The second set of plots in Fig. 22, at 180 days, occurs just as the cooling portion of the annual cycle begins. The mixing above the thermocline is very complete both without and with the thermal discharge. In this region, above about 50 feet, the temperature increase produced by the thermal discharge is smaller than in a good portion of the hypolimnion, even though the discharge has again surfaced.

For this set of curves and for the curves representing 90 days, the thermocline is found to be at a somewhat greater depth with the thermal discharge than without. This result cannot be simply predicted a priori. The two changes produced by a thermal discharge, namely the heat added and the pumping work performed, have opposite effects on the thermocline. The additional heat tends to increase the temperature, temperature gradients and therefore the stability within the lake. On the other hand, the pumping work tends to enhance mixing within the lake. The former effect would, by itself, decrease the depth of the thermocline while the latter would increase its depth. A detailed discussion of these two competing effects and of their relationship to the Monin-Obukhov length has been given in Ref. 16. In the present case the thermocline is driven somewhat deeper between 90 and

180 days by the effects of the thermal discharge.

The last set of curves, for 300 days, occurs during the period of greatest cooling within the annual cycle. The cooling causes efficient convective mixing, which produces nearly uniform temperature distributions both without and with the thermal discharge. The temperature increase resulting from the thermal discharge is nearly $1.5^{\circ}C$.

The qualitative effects produced by the thermal discharge with ω_p = 1/6 ft/day and $\Delta T_p = 15^{\circ}C$ are the same as those described above, with one exception. A discharge-temperature increase of $15^{\circ}C$ above the temperature at the intake level forces the effluent to remain surfaced throughout the annual cycle.

The quantitative effects are summarized in Table 1. In this table the increases in temperature produced by the thermal discharge with ω_p = 1/4 ft/day are listed along with the increases produced when ω_p = 1/6 ft/day. The important feature common to both calculations is that the additional heat loads introduced by the thermal discharges are the same. The difference between the two results from the change in pumping work done. For the larger pumping velocity ω_p = 1/4 ft/day, more mixing work is introduced.

During the heating portion of the cycle the increased mixing produced with ω_p = 1/4 ft/day results in larger temperature increases in the deeper waters and correspondingly smaller temperature increases in the shallower waters. In each case a temperature increase over the naturally occurring temperature can be expected as a result of the heat added by the thermal discharge. However, for ω_p = 1/4 ft/day, heated waters near the surface are more effectively mixed into the deeper waters by the larger pumping velocity.

During the cooling portion of the cycle, when the lake is thoroughly mixed, the temperature increase throughout is larger for the case when ω_p = 1/4 ft/day. Once again the increased mixing resulting from the larger pumping rate explains this feature.

Table 1

TEMPERATURE DIFFERENCE PRODUCED BY THERMAL DISCHARGES WITH DIFFERENT DISCHARGE TEMPERATURES BUT THE SAME HEATING RATE

		ΔT_S		ΔT_{50}		ΔT_{100}		ΔT_{150}	
	DAYS	$w_p = 1/4$	$w_p = 1/6$	$w_p = 1/4$	$w_p = 1/6$	$w_p = 1/4$	$w_p = 1/6$	$w_p = 1/4$	$w_p = 1/6$
MAR	0	0.0	0.0	0.0	0.0	0.0	0.0	0.0	0.0
APR	30	0.41	0.41	0.34	0.34	0.28	0.28	0.24	0.24
MAY	60	0.82	0.84	0.76	0.75	0.46	0.45	0.29	0.28
JUN	90	1.06	1.22	1.22	1.13	0.54	0.46	0.22	0.20
JUL	120	0.58	0.84	1.65	1.46	1.07	0.80	0.31	0.24
AUG	150	0.50	0.67	1.63	1.70	1.75	1.31	0.55	0.41
SEP	180	0.64	0.84	1.05	1.25	2.30	1.77	0.87	0.65
OCT	210	1.10	1.17	1.16	1.22	2.68	2.05	1.23	0.91
NOV	240	1.62	1.51	1.62	1.52	1.67	1.54	1.30	0.93
DEC	270	1.42	1.25	1.46	1.30	1.47	1.30	1.39	1.22
JAN	300	1.52	1.38	1.45	1.31	1.39	1.26	1.36	1.23
FEB	330	1.50	1.39	1.43	1.33	1.37	1.27	1.33	1.23
MAR	365	1.35	1.28	1.38	1.31	1.39	1.31	1.39	1.31

The rate of heat added to the lake at any time is equal to the heat flux $K(T_E - T_s)$ at the lake surface times the surface area A of the lake plus the rate of heat added by the discharge. Under periodic conditions, i. e., when the lake has adjusted to the increased thermal load provided by the discharge, the integral over an annual cycle of the heat added at the surface plus the heat added by the discharge must be zero. Thus

$$K \oint (T_E - T_s) dt = - Q$$

where Q is the total heat added over a year by the thermal discharge and where K is the constant heat transfer coefficient at the lake surface. For both cases discussed above, the thermal discharge with ω_p = 1/4 ft/day and the discharge with ω_p = 1/6 ft/day, the total heat added is 280 AT , where A is the surface area of the lake and T is one year. Also, for both pumping rates the equilibrium temperature variation is the same. However, as discussed above, the larger pumping rate produces a lower surface temperature during the heating portion of the annual cycle. Therefore, since the integral of $\oint (T_E - T_s) dt$ is the same for both cases and since T_s is lower during stratification for the higher pumping rate, this temperature must be higher during the cooling portion of the cycle. During cooling, however, the lake is thoroughly mixed so that the surface temperature is very nearly the temperature throughout.

This argument describes the lake quantitatively only when the response has become periodic. However, it should still apply qualitatively also when the response is transient. Therefore, the temperature increases during the cooling portion of the annual cycle when ω_p = 1/4 ft/day are larger, as expected, than those increases when ω_p = 1/6 ft/day.

In this subsection a discussion of the effects of thermal discharges has been given and a detailed comparison between the thermal structures without and with thermal discharges has been made. In the next subsection the effects of pumping alone are presented.

V.4.3 Effects of Pumping Alone

When water is withdrawn from the hypolimnion of a lake and discharged and mixed at the surface, the thermal structure of the lake is changed. The pumping work done to change the potential energy of the lake results in an enhanced mixing within the lake. In this section the effects of pumping are discussed; no heat is added to the lake.

In general, as discussed in Section V.3.1, heating at the surface of a lake increases the absolute value of the potential energy of stratification, or stability,[16] of the lake whereas turbulent mixing tends to reduce it. Mixing of the heated surface waters into the deeper waters by pumping reduces the stability of the lake and produces temperature profiles for which the thermocline is lower than would occur naturally. Because of the increased volume of the epilimnion, its average temperature will be lower than that which occurs naturally. Because of the effective mixing within the epilimnion the temperature profiles will display a nearly uniform temperature throughout the increased volume. As a result, the maximum surface temperature of the lake is found to be lower than the corresponding natural maximum.

The pumping velocity for the plots shown in this section is w_p = 2 ft/day. The intake for water is situated at 125 ft, and the water is discharged and mixed at the surface. This pumping velocity should be compared with a typical velocity for descent of the thermocline of about 1 ft/day which occurs naturally in Cayuga Lake during the cooling portion of the annual cycle. For this pumping velocity the effects of the work done on the lake by pumping can be vividly demonstrated.

In Fig. 23 the annual temperature variation at the surface and at three levels, 50 feet, 100 feet and 150 feet, is shown when water is simply pumped. With reference back to the standard annual cycle shown in Fig. 8, one can see the features described above as consequences of pumping. For example, Fig. 23 shows that the maximum surface temperature with pumping included is approximately 18°C; Fig. 8 shows the natural maximum to be about 22°C. The temperature variations at 50 feet and 100 feet follow within a few degrees the temperature variation at the surface. This behavior is to

be contrasted with that shown in Fig. 8, where the temperature at 50 feet differs by several degrees from the surface temperature near its maximum. The temperature difference at 100 feet is even more pronounced, being about ten degrees for much of the stratification period.

The temperature plots at 50 feet and 100 feet are both for levels above that of the intake. On the other hand, the plot of temperature at 150 feet is for a depth below that of the intake, and this curve varies by as much as six degrees from the others. Therefore, as might be expected in this case, the mixing produced by the pumping between the levels of the intake and the discharge is quite complete, whereas the mixing induced below the intake is much smaller.

Another effect of pumping can be observed by a close comparison between Figs. 8 and 23. After a cycle, the temperature at homothermy is determined as the point at which the temperature curves for different depths cross. With pumping effects included, the temperature at homothermy is found to be somewhat less than a degree higher than that without pumping. As discussed in the previous subsection, this increase in temperature at homothermy results from the integrated change in surface heat flux induced by pumping.

Figure 24 shows the effect of pumping on the depth of the thermocline; this curve is to be compared with that shown in Fig. 14 for the seasonal variation of the thermocline with no thermal discharge or pumping effects introduced. The most dominant feature of Fig. 24 is the rapid descent of the thermocline to the intake level at 125 feet. As discussed above, this descent results from the rapid mixing between the intake and discharge levels produced by the pumping.

In Table 2 the temperature differences produced by different pumping rates, ω_p = 2 ft/day and ω_p = 1/4 ft/day, are compared. For both cases the intake level is at 125 feet and water is discharged and mixed at the surface. A temperature increase over the natural variation is a number greater than zero and a decrease is one less than zero. Both pumping rates show the qualitative features described above. During the heating portion of

Table 2

TEMPERATURE DIFFERENCES PRODUCED BY
DIFFERENT PUMPING RATES

		$\triangle T_S$		$\triangle T_{50}$		$\triangle T_{100}$		$\triangle T_{150}$	
	DAYS	$w_P = 1/4$	$w_P = 2$	$w_P = 1/4$	$w_p = 2$	$w_P = 1/4$	$w_P = 2$	$w_P = 1/4$	$w_P = 2$
MAR	0	0.0	0.0	0.0	0.0	0.0	0.0	0.0	0.0
APR	30	-0.005	-0.04	0.001	0.005	0.003	0.02	0.003	0.02
MAY	60	-0.03	-0.23	0.003	0.01	0.01	0.16	0.01	0.09
JUN	90	-0.32	-1.79	0.21	0.00	0.19	1.57	0.06	0.44
JUL	120	-0.95	-4.08	0.89	0.43	0.66	4.87	0.15	1.37
AUG	150	-0.98	-3.79	1.22	0.17	1.31	7.20	0.34	3.05
SEP	180	0.58	-1.76	0.10	-1.18	1.90	7.26	0.62	4.64
OCT	210	0.0	0.57	0.06	0.63	2.24	4.73	0.96	5.39
NOV	240	0.57	1.91	0.57	1.87	0.64	1.97	1.02	4.73
DEC	270	0.57	2.18	0.57	2.21	0.60	2.27	0.58	2.28
JAN	300	0.47	1.85	0.45	1.76	0.44	1.71	0.43	..69
FEB	330	0.34	1.37	0.34	1.33	0.34	1.29	0.33	1.28
MAR	365	0.19	0.86	0.23	0.99	0.26	0.99	0.26	1.02

the annual cycle, the temperatures in the upper levels of the lake in the presence of pumping are reduced below the natural ones while the temperatures in the deeper waters are increased. While the lake is cooling, on the other hand, the temperatures at all levels are increased above the values with no pumping. As expected this behavior is enhanced as the pumping rate, as expressed by the pumping velocity w_p , is increased.

V.4.4 Comparison Between the Effects of Thermal Discharge and the Effects of Pumping

The effects of thermal discharge and of pumping alone have been discussed in the previous two subsections. It is of interest now to compare these effects in a controlled fashion. In this subsection the results from the base calculation, a calculation with only a pumping velocity of 1/4 ft/day and a calculation with a thermal input of 280 Btu/ft^2-day and a pumping velocity of 1/4 ft/day are compared. In both cases, with a discharge and with pumping the intake level remains at 125 ft.

In Fig. 25 the temperature variations at the surface and at depths of 100 and 150 feet for all three cases are plotted. The seasonal variation of the temperature, chosen as the standard case, is shown as a dashed line. The temperature variations with the effects of a thermal discharge are shown as a solid line and the variations with pumping effects only are shown as a broken line. Throughout the cycle the thermal discharge is seen to increase the temperature above the natural variation at the surface, at 100 feet and at 150 feet. During the stratification period the effect of pumping at the same rate, but with no thermal input is to decrease the surface temperature below the natural variation. At depths of 100 and 150 feet the temperature is increased by pumping only but by an amount smaller than that produced by the thermal discharge. During the cooling portion of the cycle when mixing is complete, the temperatures at the surface and at 100 and 150 feet are always greatest when the effects of the thermal discharge are included. When pumping alone is included, the temperatures at all three positions are greater than the corresponding temperatures without pumping.

In Fig. 26 the thermocline depth for each case is plotted as a function of time. The depth of the thermocline is defined for the program as the position at which the magnitude of the temperature gradient is maximum. With the effects of the thermal discharge included a thermocline, according to this definition, immediately forms below the surface as a result of the heated effluent. The depth at which this thermocline forms depends upon the details of the heat-source term used to model the discharge; later, however, when a true thermocline forms, the thermocline depth no longer depends upon these details. The position of the thermocline discussed below will refer to the depth determined during this latter period.

With the effects of the thermal discharge included, the thermocline is found to occur at a greater depth than it does naturally for most of the stratification period. This result indicates that, during this time, the pumping work added to the lake by the discharge has a greater effect on the depth of the thermocline than does the discharge-heat added. With pumping alone, the thermocline occurs at still greater depths since work with no additional heat is introduced in this case. A close examination of these plots indicates that the stratification cycle is increased somewhat by the effects of pumping alone and somewhat more by the effects of thermal discharges.

In Fig. 27 the effects are shown of the thermal discharge and of pumping upon the thermal diffusivity. As discussed before, the thermal diffusivity at any point is a local measure of the ability of the water to disperse heat. It is determined by the local stability of the lake and by the competing effect of turbulent mixing. Pumping alone increases the dispersive capability of the lake. A thermal discharge introduces both of these competing effects: the pumping work performed by the discharge increases the mixing, while the additional heat introduced near the surface increases the stability

The first set of curves, at 90 days, display several differences between the effects produced by pumping and those produced by a thermal discharge. The thermal diffusivity calculated with pumping effects alone is

larger than either the natural diffusivity profile or the diffusivity with thermal discharge effects. Since mixing only is introduced by pumping, these results are expected. On the other hand, with increasing depth, the thermal diffusivity including the effects of thermal discharge is first somewhat larger and then smaller than the natural thermal diffusivity. This result shows that increased mixing is the dominant effect at smaller depths whereas increased stability due to the additional discharge heat dominates at greater depths.

The second set of curves is shown for 240 days. At this time convective turbulence due to cooling, as well as wind-induced turbulence, is producing mixing. The thermal diffusivity with the effects of thermal discharge and the diffusivity with the effects of pumping are very similar, and considerably larger than the natural diffusivity. At this time a very poor approximation to the diffusivity with thermal-discharge effects included is provided by the natural diffusivity.

The last set of curves shows the thermal diffusivities at 300 days. At this time the lake is mixed throughout. The thermal diffusivity with discharge effects is largest now. Both this diffusivity and the one with pumping effects included are somewhat larger than the natural diffusivity throughout the lake.

In this section the effects on the thermal structure of thermal discharges and of pumping water from deep levels to the surface have been discussed. The effect of the plume induced by the thermal discharge has been considered only in relation to its effects on overall thermal structure. A model, which includes mechanical work and thermal energy produced by a discharge, has been introduced to calculate the changes in thermal structure.

This theoretical model has been used specifically to study the effects of thermal discharges at or below the level of the thermocline on the seasonal stratification cycle of temperate lakes. The major advantage of a hypolimnetic discharge is that the effluents can be trapped below the thermocline at least during part of the stratification season, so that surface effects of the discharges can be expected to be minimized. The calculations presented in

this section show that the increases in temperatures, due to the thermal discharges, are indeed greater at deeper levels than at the surface. However, some increase in the average surface temperature of the lake is unavoidable, since such an increase is essential (once the lake attains a new thermal equilibrium) for the lake to dissipate the added power-plant heat to the atmosphere.[16]

Several other conclusions have been drawn from these calculations; the most important ones follow. A thermal discharge increases the temperature at any depth and at any time over the temperature occurring naturally. However, the relative magnitudes of the increases at various depths and times are dependent upon the specific mode of discharge. Pumping alone will increase the temperature in the hypolimnion and decrease it in the epilimnion during stratification. However, during the cooling portion of the cycle when the lake is well mixed, the temperature will be increased over the naturally occurring value. Pumping increases the depth of the thermocline over most of the stratification cycle. However, it may increase the stratification period. For the thermal discharge calculations performed, the depth of the thermocline was increased for most of the stratification cycle beyond the depth occurring naturally. The stratification period was found to increase with a thermal discharge.

VI. STUDY OF INTERFACIAL MIXING

VI. 1 Introduction

This section deals with a study of the flow of a layer of warm water over a body of colder water. The resulting interaction manifests itself by heat and momentum transfer between the two layers. In laminar, homogeneous flow, these processes are characterized by the thermal diffusivity κ and kinematic viscosity ν which are related through the properties of molecular motion. The resultant similarity of these processes is generally known as Reynolds analogy.[67] Flows in natural bodies of water are almost always turbulent, and the interaction of adjacent layers is then determined by eddies of various sizes. Such flows may be analyzed if κ and ν are replaced by appropriate eddy diffusivities for heat, K_{H_0}, and for momentum K_{M_0}, which may be several orders of magnitude larger than the corresponding molecular quantities.

If the density of the upper layer is less than that of the lower body of water, the stratification is stable, and buoyancy tends to inhibit the mixing process. Consequently, a rather marked interface appears across which heat and momentum transfer may be inhibited to different degrees. The Reynolds analogy is therefore not applicable to stratified flow.

The stability of a stratified flow is customarily expressed by a Richardson number Ri which may be formulated in different ways.[16] The overall or bulk Richardson number is essentially the ratio of the buoyancy to the inertia forces and is given by

$$\overline{Ri} = -\frac{\Delta\rho}{\rho}\,\frac{g h}{u^2} = \alpha_v \Delta T\,\frac{g h}{u^2} \qquad \text{(VI. 1)}$$

where ρ is the fluid density, $\Delta\rho$ the value of the (small) density difference between the upper layer and the lower body of water, h is the depth and u the average velocity of the upper layer, and g the gravitational acceleration.

If the density difference is expressed by the corresponding temperature difference ΔT, the second form is obtained where α_v is the coefficient of volumetric expansion.

In a stratified flow, the eddy diffusivities K_{H_o} and K_{M_o} of a flow of uniform temperature have to be modified to K_H and K_M which can be related to the Richardson number in the general form[16, 68]

$$K_H = K_{H_o} f(R_i) \tag{VI. 2}$$

$$K_M = K_{M_o} g(R_i) \tag{VI. 3}$$

where R_i is defined by Eq. (III. 5) and the functions $f(R_i)$ and $g(R_i)$ have the property that $f(0) = g(0) = 1$.

The purpose of the present study is to determine the values of K_H and K_M at the interface for different bulk Richardson numbers. At first, an analytical approach was considered, based on linearization of the Navier-Stokes equations, but a direct experimental approach seemed to be much more promising at the present time.

The experimental approach is related to that used by Ellison and Turner[57] who determined entrainment parameters rather than eddy diffusivities. They studied the spreading of a thin layer of low-density fluid flowing over a weir onto a channel of stagnant fluid of higher density. The duration of their experiments was limited to a few seconds, and velocity distributions were inferred from motion pictures of rising small plastic particles released from the bottom of the tank. A somewhat different approach to measure entrainment was used by Kato and Phillips[66] who used an annular tank at the surface of which a constant stress was applied by a slightly immersed ring rotated by an external drive. The shear stress was measured by the torque applied, and fluid motion was determined from motion pictures of the flow visualized by dye injection. Ellison and Turner found that entrainment

is substantially suppressed if the Richardson number exceeds approximately 0.8.* Since Ellison and Turner produced stratification by the use of salt solutions of various concentrations, no temperature measurements were involved in their experiments.

In the present study, stratification is produced by temperature gradients under conditions which allow observations over periods ranging from a few minutes to about one hour. The techniques and results obtained so far are discussed in the following sections.

VI.2 Theoretical Foundation for the Experimental Determination of K_M and K_H

The quantities K_M and K_H cannot be measured directly but must be computed from observable data on the basis of definitions and basic relationships.

Consider a horizontal channel of constant width in which a layer of warm water flows over initially cool water in the lower part of the channel. The only vertical velocities w in this system are produced by entrainment of the cool water by the warm water (see Refs. 57 and 66) and by effects of the end walls of the channel.

The determination of K_M involves solving the continuity and momentum equations for two-dimensional flow.[67]

Continuity:

$$\frac{\partial u}{\partial x} + \frac{\partial w}{\partial z} = 0 \qquad \text{(VI. 4)}$$

Horizontal (x) Momentum:

$$\frac{1}{\rho}\frac{\partial \sigma}{\partial x} + \frac{1}{\rho}\frac{\partial \tau}{\partial z} = \frac{1}{\rho}\frac{\partial p}{\partial x} + \frac{\partial u}{\partial t} + u\frac{\partial u}{\partial x} + w\frac{\partial u}{\partial z} \qquad \text{(VI. 5)}$$

*It should be noted that Ellison and Turner use a somewhat different definition of the Richardson number than the one used in the present study.

Vertical ($\mathcal{Z}$) Momentum:

$$\frac{\partial}{\partial \mathcal{Z}}\left(\frac{\mu}{\rho}\frac{\partial w}{\partial \mathcal{Z}} - \overline{w'^2}\right) + \frac{\partial}{\partial \chi}\left(\frac{\mu}{\rho}\frac{\partial w}{\partial \chi} - \overline{u'w'}\right) = \frac{1}{\rho}\frac{\partial p}{\partial \mathcal{Z}} + g + \frac{\partial w}{\partial t} + u\frac{\partial w}{\partial \chi} + w\frac{\partial w}{\partial \mathcal{Z}} \qquad \text{(VI. 6)}$$

K_M is defined by

$$\frac{\tau}{\rho} = K_M \frac{\partial u}{\partial \mathcal{Z}} = \frac{\mu}{\rho}\frac{\partial u}{\partial \mathcal{Z}} - \overline{u'w'} \qquad \text{(VI. 7)}$$

and $K_{M\chi}$ by

$$\frac{\sigma}{\rho} = K_{M\chi}\frac{\partial u}{\partial \chi} = \frac{\mu}{\rho}\frac{\partial u}{\partial \chi} - \overline{u'^2} \qquad \text{(VI. 8)}$$

where χ is the horizontal coordinate, positive in the direction of the warm water flow, $\mathcal{Z}$ is the vertical coordinate, measured positive upward from the tank bottom, u is the χ-component of velocity and w the $\mathcal{Z}$-component, u' and w' are the turbulent fluctuations of the velocity, p is pressure, ρ is density, t is time, τ is the shear stress, σ is the normal stress, and g is the acceleration due to gravity.

For the experimental system described in Section VI. 3 all terms in the vertical momentum equation (VI. 6) are small, except for the pressure gradient and the acceleration due to gravity because of the near horizontal homogeneity of the flow in the present experiment. Hence, (VI. 6) becomes

$$\frac{\partial p}{\partial \mathcal{Z}} = -\rho g \qquad \text{(VI. 9)}$$

In the horizontal momentum equation (VI. 5), σ for highly turbulent flows may be of the same magnitude as τ . However, $\frac{\partial \sigma}{\partial \chi}$ can be neglected compared with $\frac{\partial \tau}{\partial \mathcal{Z}}$. Hence (VI. 5) becomes

$$\frac{1}{\rho}\frac{\partial \tau}{\partial \mathcal{Z}} = \frac{1}{\rho}\frac{\partial p}{\partial \chi} + \frac{\partial u}{\partial t} + u\frac{\partial u}{\partial \chi} + w\frac{\partial u}{\partial \mathcal{Z}} \qquad \text{(VI. 10)}$$

The first step in the calculation of K_M is the determination of the vertical velocity ω. From equation (VI. 4), and the experimental velocity gradient $\frac{\partial u}{\partial x}$, ω can be calculated as a function of z with the boundary conditions that $\omega = 0$ at z 0, the tank bottom. From measured velocity profiles, the substantial derivative

$$\frac{Du}{Dt} = \frac{\partial u}{\partial t} + u \frac{\partial u}{\partial x} + \omega \frac{\partial u}{\partial z} \qquad \text{(VI. 11)}$$

can then be calculated. The pressure gradient $\frac{\partial p}{\partial x}$ is determined from the experimental data and equation (VI. 9) as discussed in Section VI. 5. Integration of equation (VI. 10) then yields the shear stress τ and use of equation (VI. 7) gives K_M.

The determination of the coefficient of thermal diffusivity K_H involves solution of the energy equation

$$\frac{1}{\rho c_p} \frac{\partial q}{\partial z} = \frac{\partial T}{\partial t} + u \frac{\partial T}{\partial x} + \omega \frac{\partial T}{\partial z} \qquad \text{(VI. 12)}$$

where q is the heat transfer rate and T the temperature. The various gradients and parameters can be calculated from the experimental data as a function of depth. The energy equation is then integrated from the tank bottom upward to give the heat transfer q at each depth and K_H is determined from the definition:

$$\frac{q}{\rho c_p} = K_H \frac{\partial T}{\partial z} \qquad \text{(VI. 13)}$$

The preceding analysis indicates that K_H and K_M can be evaluated if T and u are measured as functions of t, x and z. Practically, this requires suitable probes which allow the temperature and velocity to be measured as a function of time over the entire depth at several stations along the flow.

VI. 3 Design of the Flow System

An experimental setup is needed which can produce a substantially two-dimensional flow of a layer of warm water over a pool of cool water. This requirement can be met by a relatively long tank of rectangular cross section. The warm layer should be sufficiently deep to allow observations within the layer and its velocity high enough to make the flow turbulent. Flow in shallow water becomes turbulent if the Reynolds number based on the depth of the water exceeds about 300[11]. The Reynolds number of the layer of warm water is given by

$$Re = \frac{hu}{\nu} = \frac{Q}{b\nu} \qquad \text{(VI. 14)}$$

where Q is the volume flow rate and b the width of the tank. Thus, the depth of the layer can be varied without change of Reynolds number if the flow rate is kept constant.

An existing tank (210 cm long, 10 cm wide and 10 cm deep) with a transparent lucite front wall was adapted for the experiments, and Fig. 28 is a schematic layout of the flow system. Two partitions form the cool-water reservoir which is 170 cm long and 7 cm deep. The warm water enters into the right end section where a baffle insures uniform flow over the partition. After flowing over the left partition into the other end section, the water returns into a warm-water reservior. The flow rate can be controlled by valve No. 1 and measured by a rotameter. It was initially planned to control the depth of the layer by means of a gate at the left partition. When the gate turned out to be too difficult to adjust, the partition, as shown in the figure, was raised simply by attaching blocks of fixed height on top of it.

The warm-water reservoir (5 gallons) was kept well stirred by an electric stirrer and the temperature controlled by a thermostatically regulated electric immersion heater (450 watt). The water was circulated by a small

pump. An auxiliary return from the right end section to the reservoir was provided through valve No. 2. The purpose of this by-pass is to bring the water and pipes to the desired temperature without disturbing the cool water in the main tank. When all conditions are established, valve No. 2 is closed, and flow over the partition begins. The maximum flow rate that can be measured with the present rotameter is 60 cm^3/s corresponding to a maximum Reynolds number of 700.

The cool water was kept at approximately room temperature. In the course of an experiment, the cool water becomes partly mixed with warm water, and it would require several hours to let it cool down for another experiment. To reduce this waiting time, a supply of cool water was kept in a second tank where it was maintained at the desired temperature by means of a thermostatically controlled immersion heater, a cooling coil through which cold tap water flows and a stirrer. This reservoir and a second circulating pump were separated from the main tank by valves No. 3 and 4. Overflow pipes and an auxiliary container (not shown in the figure) prevented accidental spilling of the fluid.

The temperature of the warm water was measured by a thermometer upstream of the inlet partition and that in the main tank by a thermometer near the outlet.

VI. 4 Instrumentation

VI. 4.1 Velocity Measurements

Local flow velocities can be measured by means of tracers which can be observed photographically. Because of the density stratification, it is important that such tracers are neutrally buoyant regardless of their location in the fluid. A technique which seems particularly suitable for this purpose is based on the color change of an indicator solution if the hydrogen ion concentration (pH) is changed at a test point.

The technique used is an adaptation of a system described by Baker Consider an indicator solution which exhibits a marked color change at a p_H value that is characteristic for the indicator. If two electrodes connected to a battery are inserted into the fluid, the hydrogen ion concentration is reduced at the surface of the cathode corresponding to a local increase of p_H. Under properly selected conditions, the fluid adjacent to the surface of the cathode then changes color and subsequently moves with the rest of the fluid. Since nothing is added to the fluid, this tracer is always neutrally buoyant. Gradual diffusion increases the p_H value within the tracer fluid which, eventually, returns to its original color. A solution of the following composition was found to be satisfactory:

Distilled Water		1000 cm^3
Thymol Blue (1% solution)		10 cm^3
Hydrochloric Acid (0.1 normal)	approx.	1 cm^3

Before the acid is added, the thymol blue solution is deep blue. Acid is then added drop by drop under continuous stirring until the solution suddenly changes to a bright orange at a p_H value of about 8.

To produce as sharp a tracer line as possible, fine tungsten wire (about 25 μm diameter) is used as cathode. One end is cemented into a short piece of ceramic tubing (about 3 mm diameter and 5 mm long) which is pressed into a hole in the bottom of the tank. The other end of the wire is soldered to a thin rod held in an adjustable clamp above the surface of the water. In this manner, the wire can be stretched vertically from the bottom to the top of the water without disturbing the flow. The anode is formed by a stainless-steel wire running along an inside edge of the tank.

If a 90-volt battery is briefly connected to the two electrodes, a column of dark tracer fluid is formed on the surface of the tungsten wire (cathode) and subsequently moves with the fluid. To produce a well-defined tracer, the current pulse must be sufficiently short (about 1/3 second).

Furthermore, long pulses lead to considerable formation of gas bubbles by electrolysis; these are almost completely absent with short pulses. The motion of the tracer is recorded photographically as discussed below.

The probe wires had an unexpectedly short life which varied between a few weeks and a few days. They apparently corroded under the combined influence of the electric current and the slight alkalinity of the solution. The exact reason for their failure is not known. In the future, heavier wires or wires of a different material, such as platinum, will be used. Current pulses are produced by one cam of a multiple-cam switch (Industrial Timer Corp.). The cams are adjustable so that a microswitch is closed once during each revolution for a selected time. The speed of the cam can be adjusted in steps by a choice of gears between the drive motor and the cam shaft. By means of an auxiliary switch in the cam-drive circuit, it is possible to let the cam rotate continuously or for one revolution only. For continuous rotation, the selected interval between pulses is 2.67 seconds. This time is convenient to record the velocity in the warm upper layer of water, which is of the order of 1 cm/s. The velocity in the lower layers is about ten times smaller and would therefore require either many current pulses or a longer separation between pulses. Since many tracers on one photograph make the records difficult to evaluate, the following method was adopted. At the time t_1, one pulse was produced by a single revolution of the cam. About 30 seconds later, two more pulses were produced by two revolutions of the cam at the times t_2 and $t_3 = t_2 + 2.67$ where the interval $t_3 - t_1$ was measured with a stopwatch. The camera shutter was operated by a solenoid which has two switches in series in its power supply. One of these is another cam switch which was set so that it closes always at the instant when a flow visualization pulse is produced by the first cam. The other switch was closed manually after the time t_2 and before t_3. In this manner, the third pulse delineated the probe wire which otherwise would not be visible in the photographs. Thus, the low velocities in the lower layers of the water are determined by the displacement of the first tracer during the time $t_3 \quad t_1$ and the high velocities near the surface by the displacement of the second

tracer during the time $t_3 - t_2$.

Seven probes were installed along the centerline of the tank. Probe No. 1 was located about 5 cm downstream from the inlet partition and probe No. 7 about 25 cm upstream from the outlet partition. These probes served only to indicate the flow near the ends of the tank and were not photographed. Probes No. 2 to 6 were mounted 20 cm apart in the center of the tank.

An exploratory attempt was made to observe the vertical entrainment velocity by producing interrupted tracers. This was achieved by slipping a short piece of a finely drawn glass capillary (about 0.1 mm outside diameter) over one of the tungsten wires and annealing it on the wire with a fine flame. Although this probe indicated a vertical velocity, this configuration was not satisfactory for quantitative measurements.

To take photographs of the flow patterns, the tank was illuminated by two 500-watt photoflood lights. The camera was placed at the level of the center of the water at a distance of about 140 cm from the front of the tank and opposite the center probe. A Wollensak Raptar f/4.5 lens of 162 mm focal length was used. Photographs were taken on 4 in. by 5 in. sheets of Plux-X film (ASA 125) at f/5.6 and 1/50 s. The relevant portion of the photograph was enlarged for evaluation, and several such records are shown in Section VI. 5.

Taking photographs of an object under water when the camera is in air leads to a displacement of the object on the photograph because of the refraction of light at the air-water interface. Care must therefore be exercised in the evaluation of the photographs to avoid errors. Analysis of this problem is based on Fig. 29. The lucite front wall of the tank is sufficiently thin (6 mm) that its effect on the path of the light rays need not be considered.

Let the camera lens be located at C at the distance $L + \frac{t}{2}$ from the center of the tank O. If the line OC forms a right angle with the centerline of the tank, the point O is not displaced on the photograph, but a point P located at the distance X from O appears on the photograph as P' at an apparent distance X'. The angle of incidence of the ray PC is α on the side of the air and β on the side of the liquid. Let l be the distance of the point of incidence on the interface from the line OC. The law of refraction then yields

$$\frac{\sin \alpha}{\sin \beta} = N \qquad \text{(VI. 15)}$$

where N is the refractive index of the liquid. Elementary trigonometric relationships show that

$$X = L \tan \alpha + \frac{t}{2} \tan \beta \qquad \text{(VI. 16)}$$

$$X' = \left(L + \frac{t}{2}\right) \tan \alpha$$

These two equations may be combined to give the relative refraction error as

$$\frac{\Delta X}{X'} = \frac{X' - X}{X'} = \frac{1}{1 + 2\frac{L}{t}} \left(1 - \frac{\tan \beta}{\tan \alpha}\right) \qquad \text{(VI. 17)}$$

For any value of α, the corresponding value of β then follows from equation (VI. 15), the distance X' from the second of equations (VI. 16), and the refraction error from equation (VI. 17). Some results are shown in Fig. 30 for water ($N = 4/3$) and the present experimental conditions ($t = 10$ cm). For the magnitudes of the errors involved here, it is immaterial whether the refraction error is referred to X or to X'.

Figure 30 shows that a tracer located at 50 cm from the center of the tank appears displaced by about 0.5 cm (1%) if the photograph is taken from a distance of about 140 cm. It is therefore not permissible to assume that a photograph represents merely a size reduction in the ratio of the image distance to the object distance from the camera lens. Fortunately, the maximum distances from the center of the tank that are of interest here do not exceed about 50 cm, and within this range, the relative refraction error is practically independent of X if the camera lens is located 100 cm or more from the tank. The known distance between probe wires therefore may serve as a scale with which tracer motions can be measured on the photographs and which is already corrected for the refraction error. For this reason, it is important to have the probe wires outlined on the photograph, and this is achieved by synchronizing the camera shutter with the tracer pulses in the manner described in the foregoing.

If photographs of the five central probes are taken at various times during an experiment, both the velocity and its derivatives $\partial u/\partial t$ and $\partial u/\partial x$ can be obtained as functions of the depth below the water surface in accordance with the requirements indicated by the equations in Section VI. 2.

VI. 4.2 Temperature Measurements

The requirement that the temperature be measured at several stations over the entire depth of the flow can be satisfied by small probes which traverse the depth of the water at selected locations. The time dependence of the temperature distribution can then be obtained by repeating the traverses at regular intervals. A convenient method is to mount a small thermistor bead at the tip of a thin tube and record the resistance changes that result from temperature variations.

The temperature sensitive element of the probes is a bead thermistor (VECO No. 51A32) which has a diameter of about 0.3 mm.

The bridge circuit constructed to measure the resistance of the thermistor while it traverses the flow is shown in Fig. 31 . Two arms of the bridge are the probe resistance R and a load resistance R_L ; the other two arms are formed by R_1 and R_2 with the additional potentiometer R_3 to provide a zero adjustment. A conventional power supply, regulated by two Zener diodes, provides 6.2 volts to the bridge through the potentiometer circuit formed by R_4 , R_5 and R_6 . The setting of R_5 controls the actual bridge voltage and thus allows the sensitivity to be adjusted to a desired value. The purpose of the condenser across the recorder input is to eliminate high-frequency noise pickup by the probe circuit.

The variations of the thermistor resistance with temperature are highly nonlinear as indicated in the following table

T	R
°C	Ohms
0	330,000
25	100,000
50	35,000

A satisfactory linear response can be obtained by proper choice of the load resistance R_L . For three selected temperatures T_0 and $T_0 \pm \Delta T$, which cover the range of interest, let the corresponding values of the thermistor resistance be R_0 , R_+ and R_- . The fraction of the bridge voltage which is delivered to the recorder from the thermistor side of the bridge is given by $R_L /(R + R_L)$. Therefore, if R_L is chosen so that the condition

$$\frac{R_L}{R_+ + R_L} - \frac{R_L}{R_0 + R_L} = \frac{R_L}{R_0 + R_L} - \frac{R_L}{R_- + R_L}$$

is satisfied, the output voltages, which correspond to the temperatures T_0 and $T_0 \pm \Delta T$, are linearly related to these temperatures. If the entire range is sufficiently small, intermediate points are also close to the linear calibration. The exact value of R_L is not critical because a

small change merely places three other points on a straight line. As will be seen below, a value R_L = 100,000 ohms is satisfactory.

The short platinum-iridium leads to the thermistor are welded to thin copper wires which are then threaded through a ceramic tube of about 2 mm diameter. The bead is attached to the tip by Conap epoxy and is also given a thin coating of the same material to insulate it electrically when the probe is immersed in water. An enlarged photograph of the probe tip and a millimeter scale are shown in Fig. 32. It was found that water gradually penetrated through the walls of the ceramic tube. To prevent the resultant falsification of the thermistor resistance, the entire probe was coated with epoxy. For the last probe made, the ceramic tube was replaced by a glass tube of same size. This probe is more delicate than the others but does not require coating. Although the probes are electrically insulated from the water, the circuit resistance is sufficiently high to pick up noise signals which are eliminated by grounding of the water.

The design of the probes is shown in Fig. 33 . The ceramic tube referred to in the foregoing is about 12 cm long to reach from the bottom of the flow to a little distance above the surface of the water. The top end is cemented into a glass tube of about 4-mm diameter and 27-cm length. This tube can slide through a 10-cm long stainless steel bearing tube which is mounted vertically at the desired probe location several centimeters above the water surface. The wires from the thermistor are threaded to the top of the glass tube and are then connected to the described bridge circuit. By pulling at a string attached to the top of the glass tube, the probe can be raised or lowered. A metal rod is mounted horizontally above each probe, and the strings from all the probes can be brought close together by guiding them over these rods. A groove cut into the rods prevents side slipping. The rods are slightly staggered, as indicated in Fig. 33 , to prevent entangling of the strings. It is important that the length of the strings, which is different for each probe, remains constant and not be affected by humidity. A fine stainless-steel wire (about 0.1 mm) is therefore used except for a

short piece of soft nylon string for the part that slides over the guide rods; the steel wire turned out to be too stiff to follow the required bend without jerking. A small weight is attached to the top of each probe to keep the string under tension and insure a smooth motion.

A photograph of the drive mechanism is shown in Fig. 34 . The reversible, variable-speed motor (Gerald K. Heller Co., Model 2T60-6) drives a screw which is long enough for the required travel of the probes. The moving element is guided by two rigid brass rods. Two adjustable stops activate a reversing switch, so that the probes traverse the water tank up and down (at a rate of .3 cm/s) as long as the motor is kept running. One stop is adjusted to bring the probes to within about 2 mm from the bottom of the tank, and the other insures that they are out of the water at the highest point of their travel. All probe tips must touch the water surface at the same time, the necessary fine adjustment of the wire length is provided by attaching each wire to the drive mechanism by means of a screw which can be threaded in or out as needed. After the adjustment is made, the position is held by a locknut.

Six temperature probes are installed side by side with the velocity probes Nos. 1 to 6 (see preceding section). Each is connected to its own bridge circuit, and the outputs are recorded on a six-channel pen recorder (Brush-Clevite Mark 260). This instrument is also provided with four event markers which operate with an internal supply of -32 volts with respect to the chassis; closing of a contact produces a small deflection of an auxiliary pen. One of these markers is used in conjunction with the temperature records to indicate the instant when the probe tips touch the water and to provide reference marks that represent a known travel of the probes. Two more event markers are used to coordinate the temperature and velocity measurements (see Section VI. 4.3).

The instant of probe contact with the water is established by a special probe which is similar to the temperature probes except that the

stem with the thermistor tip is replaced by a steel needle. This probe is located at the position of the velocity probe No. 7. When the needle tip touches the water surface, the resistance between the needle and the grounded water is about 5000 ohms which is too high to operate the event marker. An electronic relay was therefore constructed based on the circuit shown in Fig. 35 where the values of the various components are indicated. The main element is the silicon controlled rectifier (SCR) 2N2323 which has a high resistance in the untriggered state. The current through the needle probe while it is immersed in the water is amplified by a simple transistor amplifier (2N697) and fed to the gate electrode of the SCR, the resistance of which then drops to a low value. As soon as the probe touches the surface of the water, the voltage on the condenser drops then suddenly from ground potential to approximately -32 volts. This pulse is transmitted to the recorder and produces a brief deflection of the event marker. As soon as the condenser is charged, the residual current through the 22,000 ohm resistance is smaller than the holding current of the SCR which then reverts to its untriggered state. If the gate current is still on the SCR triggers again momentarily, but the resultant oscillations are too small to operate the event marker. These oscillations stop when the probe tip leaves the water, and the initial conditions are restored. In this manner, the event marker indicates only the instance when the probe touches the water but not when it is withdrawn.

The moving element of the probe drive also operates a microswitch by two adjustable knobs visible in Fig. 34 . This switch is connected to the same event marker and thus indicates the instant when the knobs pass the switch. They are adjusted to produce marks on the record which represent a probe travel of 5 cm.

The probes were calibrated by immersing them in water of known temperature, and the results for one of them are shown in Fig. 36 for the range from 25°C to 35°C needed for the experiments. The calibration lines for the other probes are substantially similar. Each recording channel is 50 divisions wide (4 cm), and the slope of the calibration line varied between

5.3 and 5.5 div/°C for a recorder sensitivity setting of 2 mV/div. After this calibration was obtained, the calibration voltage for each probe (see Fig. 31) was adjusted with the help of a voltmeter to make all calibrations equal to 5.0 div/°C. The probe output is therefore 10 mV/°C, and a temperature range of 10°C corresponds to the full width of each channel.

Another probe characteristic of importance is the rate at which the thermistors can follow changes in temperature. This information was obtained by dipping the probes quickly into warm water and recording their response at the highest writing speed of the recorder (125 mm/s). The response of all probes is approximately exponential with a relaxation time (the time to reach 1-1/e of the total rise) that lies between 56 and 68 milliseconds. A discontinuous temperature would therefore be correctly indicated after about one-fifth of one second.

In view of the foregoing results, temperature traverses were made at about 0.3 cm/s with a writing speed of 125 mm/min. Under these conditions, errors caused by the lag of the thermistor response are negligible.

The probe drive exhibited some hysteresis in traversing the water in the upward and downward direction. Since the instant of contact with the water surface is recorded during the downward motion, all temperature records are evaluated only for this part of the traverse. Typical temperature recordings are shown in Section VI. 5.

VI. 4.3 Time Coordination of Temperature and Velocity Measurements

After starting the flow of the warm water, the experiment continued for many (up to 90) minutes. During this time several photographs and temperature traverses had to be taken. It was therefore important to record when each record was obtained. For this purpose, an electric clock was mounted over the water tank so that it appears on each photograph. The clock was started when the warm-water flow begins.

In addition, the paper of the temperature recorder was kept running during the entire experiment, and the instant of taking a photograph was marked by the second of the four event markers. To minimize the amount of recording paper to be handled, the writing speed was reduced to 25 mm/min between temperature traverses. A record of time was kept by means of a third event marker operated by a timer which closed the contact of this event marker briefly once every minute.

In the described manner, the time at which each temperature and velocity record was obtained can be easily identified.

VI. 4.4 Motion Picture of the Experiment

To demonstrate the instrumentation and to provide a vivid impression of the processes, a 16-mm color motion picture was taken. The movie camera was set at about the same place as the camera used for the flow visualization photographs. The movie was taken on Ektachrome film (ASA 125) at 24 frames per second at f/8.

The temperatures and velocities are about the same as for the experiment discussed in Section VI. 5.5. Several sequences were filmed, each lasting about 30 seconds with intervals of about 10 minutes between sequences. The gradual progress of the mixing process is clearly demonstrated. In addition, a temperature traverse was photographed to demonstrate the operation of the recorder.

VI. 5 Experimental Results

VI. 5.1 Velocity and Temperature Records

A selected portion of the data obtained during the experiments is presented in Figs. 37 and 38 for two values of the initial Richardson number $\overline{R}_{i_o} = 3.0$ and 0.1. The Richardson number $\overline{R}_i$ is defined in

equation (VI. 1) as

$$\overline{Ri} = \alpha_v \Delta T \, g \, \frac{h}{u^2} \qquad \text{(VI. 1)}$$

The initial value $\overline{Ri_o}$ is determined using the temperature difference ΔT, the hot water depth h and the flow velocity u at the inlet of the cold water tank. The local Richardson number at any point, $\overline{Ri_\ell}$, can be considerably different from $\overline{Ri_o}$, but $\overline{Ri_o}$ will be retained as a label to differentiate between the two sets of data. The values of the various parameters in the two experiments are given in Table 3.

TABLE 3

FLOW PARAMETERS

Initial Richardson number	3.0	0.1	- -
Temperature difference	8	2.7	°C
Hot water height at inlet	2.8	1.7	cm
Hot water flow rate	37	59	cc/sec
Flow velocity at inlet	1.3	3.4	cm/sec
Tank width	10.1	10.1	cm
Reynolds number	440	700	- -

Figures 37a and b consist of photographs taken at different times of the flow between station 2 and 6. Station 2 is 45 cm from the inlet and the others are spaced at 20-cm intervals. Time is measured from the moment the warm water begins to flow over the inlet weir. The neutrally buoyant pulses of dark thymol blue vividly trace the motion of the water. The time between pulses was 2.67 sec in the upper layer of warm water and 30 sec for the low-velocity reverse flow in the cool water. The velocity in the upper layer is slightly greater than 1 cm/sec while the reverse flow in the lower layer is about .05 cm/sec.

The refractive index of the warm water is different from that of the cold water, and hence the warm layer is visible in Fig. 37a as a slightly darker region. For the $\overline{Ri_o}$ = 3.0 tests, the layer of warm water penetrates very slowly into the cold water and at 90 minutes has reached halfway to the tank bottom. For comparison, the $\overline{Ri_o}$ = 0.1 photographs in Fig. 37b reveal that the warm water has penetrated more than halfway to the bottom by 5.7 minutes.

The temperature records given in Fig. 38 show the growth of the warm water region at the expense of the cool water at selected times and positions in the tank. The location of the surface and the 5-cm calibration marks discussed in Section VI. 4.2 are shown in the figure. Station 1 is 5 cm from the inlet weir. The rapid decay of the temperature gradient for the $\overline{Ri_o}$ = 0.1 tests compared with the $\overline{Ri_o}$ = 3.0 ones is striking. At 16.2 minutes, for $\overline{Ri_o}$ = 0.1 (Fig. 38b), the warm water extends uniformly to the bottom at station 1, whereas for $\overline{Ri_o}$ = 3.0 at 15 minutes (Fig. 38a) a sharp temperature gradient roughly 1 cm in depth distinctly separates the 4-cm deep layer of warm water flowing over the cool water.

The temperature extremes between the hot and cold water are plotted in Fig. 39 for the two experiments as a function of time. In both cases, the hot water temperature remained fairly constant. The temperature of the cold water at the tank bottom started to increase significantly at about 35 minutes for $\overline{Ri_o}$ = 3.0 at position 4 and 10 minutes for $\overline{Ri_o}$ = 0.1 at position 5. At later times, the increase in temperature of the water at the bottom indicates a significant heat transfer to the floor of the tank, and data reduction at these locations should therefore be restricted to earlier times.

VI. 5.2 Interface Location

The depth at which the maximum temperature gradient occurs is defined as the interface in the present report and corresponds with the boundary between the light and dark regions observed in Fig. 37a .

The location of the interface is plotted in Fig. 40a for $\overline{Ri}_o = 3.0$ and Fig. 40b for $\overline{Ri}_o = 0.1$. At the top of each figure, a schematic drawing of the cool-water tank gives the true slope of the interface relative to the flow. In the main portion of the figures, the vertical dimensions are exaggerated by a factor of ten compared with the horizontal dimension. The exit weir was made 1.9 cm higher than the inlet for the $\overline{Ri}_o = 3.0$ tests and 0.7 cm for $\overline{Ri}_o = 0.1$ to obtain the warm water heights at the inlet of 2.8 and 1.7 cm respectively.

As shown in Fig. 40 , the depth of the interface between the warm and cool water increases with time and distance downstream from the inlet weir up to about position 2. The rate of increase in interface depth for the $\overline{Ri}_o = 0.1$ experiment was about ten times that for the $\overline{Ri}_o = 3.0$ tests. By position 2, the interface depth, although still increasing with time, begins to decrease with increasing distance from the inlet. This is caused by the fact that the exit weir is considerably higher than the inlet. Consequently, the flow streamlines near the interface will be inclined upwards and the warm water at the top will accelerate to satisfy the equation of continuity.

A local Richardson number is defined as

$$\overline{Ri_\ell} = \alpha_v \, \Delta T_\ell \, \frac{g \, h_\ell}{u_\ell^2}$$

where the subscript ℓ denotes local values. Using values for h_ℓ from Fig. 40 , $\overline{Ri_\ell}$ was calculated as a function of distance from the inlet 3.4 minutes after the start of flow. The results given in Fig. 41 show that for the $\overline{Ri}_o = 3.0$ experiment, the local Richardson number $\overline{Ri_\ell}$ does not change much with distance because mixing is strongly inhibited by buoyancy. However, for $\overline{Ri}_o = 0.1$, mixing is so rapid that $\overline{Ri_\ell}$ at position 2 is greater than 3.0.

The implication of this result is that measurements at very low Richardson numbers require more closely spaced instrumentation much nearer to the inlet than in the present experimental setup. Measuring stations every 2.5 cm in the first 15 cm downstream of the inlet weir would

make it possible to study the details of the mixing process for local Richardson numbers varying from 0.1 or lower at the inlet to 1.0 at 15 cm. The existing apparatus is best suited for the study of flows with Richardson numbers greater than about one.

VI. 5.3 Flow Starting Process

The manner in which the warm water flow is initiated, coupled with the confining walls of the water tank, has a large effect on the velocity and temperature profiles at later times. Consideration must be given to these perturbations before interpretation and analysis of the data is possible. The starting process for $\overline{Ri}_o = 3.0$ can be visualized through use of the photographs in Fig. 42 . For this experiment, the cold water was replaced by a clear, slightly alkaline solution containing no thymol blue. The orange-colored warm water, containing thymol blue, turns dark blue, as shown in Fig. 42 , when it mixes with cold water.

The experiments were started by allowing the warm water to overflow the inlet weir (see Fig. 40a) at the volume flow rate Q which was determined by the 1.3 cm/sec velocity required at an inlet warm water height of 2.8 cm to give a Richardson number of 3.0. Because the height of the warm water was zero at time zero, the initial flow velocity was considerably higher. For example, in Fig. 42 , by 1/4 minute the dark region indicating the extent of the warm water has travelled slightly past position 3, or a distance of about 70 cm from the inlet. This corresponds to an average flow velocity of nearly 5 cm/sec. For the observed warm water height of 0.45 cm at 1/4 minute in Fig. 42 , the average Richardson number during the first 15 seconds of the experiment from equation (VI.1)was approximately 0.04. This very low value explains why the mixing region in Fig. 42 extends all the way to the tank bottom upstream of position 3 at 1/4 and 3/4 minutes.

As the level of the warm water rises, the forward velocity of the flow decreases. Between 1/4 and 3/4 minutes, the level in Fig. 42 increased from 0.45 to 1.15 cm, and the flow velocity dropped from 5 cm/sec to 1 cm/sec.

The resultant increase in average Richardson number from 0.04 to about 2.2 inhibits mixing between the warm and cold water, and the dark region between positions 3 and 5 does not penetrate as deeply into the tank, as shown in Fig. 42 . During this time, the cold water is displaced to the downstream end of the tank and its level rises as the warm water is added because the exit weir, Fig. 42a, is 1.9 cm higher than the inlet weir. At about 1 1/2 minutes, the water overflows the exit weir, and some cold water is lost before the warm water reaches the exit at approximately 2 minutes.

The initially large mixing near the inlet during starting coupled with the extra height of the exit weir and the rapid damping of the mixing as the water level rises produces a triangular wedge of cold water in the tank as shown in Fig. 42 . The vertical base of the triangle is along the exit weir and the apex at 3/4 minute is located at about position 2. This situation cannot persist because of buoyancy. The heavy cold water at the exit pushes upstream along the bottom displacing the hot water upward. This can be observed in Fig. 42 at 1 1/4 and 2 1/2 minutes as a propagation upstream of the light region with a corresponding decrease in depth of the dark region. In fact at 3 1/2 minutes, the movement of the cold water at the bottom from the exit to the inlet appears to have overshot the equilibrium level. There are indications that warm water has mixed with cold at quite large depths at station 6. This can also be observed in the velocity photographs, Fig. 37a at 3 minutes where the dark region at station 6 is quite a bit deeper than at station 3, demonstrating the reversal of warm water at the exit weir. By about 6 1/2 minutes, Fig. 42 , indicates that equilibrium between the warm and cold water has been reached, and the interface between the light and dark regions occurs at the depth at which the temperature in Fig. 38a first begins to rise above the cold-water value.

Large reverse flow velocities result from the upstream displacement of the cold water at the tank bottom as observed in the velocity photographs of Fig. 37a at 3 minutes. The peak reverse flow velocity at station 4 is plotted

in Fig. 43 as a function of time after the start of flow. Transient velocities of 0.4 cm/sec at 2 1/2 minutes die out to about .05 cm/sec by 5 minutes. This large circulation in the tank during starting is caused by the high exit weir and the low Richardson number during the first 15 sec of the experiment.

After the data had been obtained using the present experimental apparatus, trial tests were performed with the exit and inlet weirs at the same height and a reduced flow rate during the first few minutes. Reduction in the starting transient was observed and future tests will use this technique possibly with additional modification such as a flat plate mounted on top of the inlet weir. For low Richardson number tests, the significance of the starting effect will be considerably reduced since the Richardson number at which data are required can be made the same as that attained during starting. In addition, measurements probably can be made before the influence of the exit weir is felt.

VI. 5.4 End and Sidewall Effects

From the velocity photographs in Fig. 37a , it is clear that the warm water flow accelerates with distance from the inlet. The surface velocity in Fig. 44 was determined from records such as Fig. 37a and by timing surface floats over measured distances. An increase from 0.6 cm/sec at position 1 to 1.3 at position 6 was observed. However, below the surface the variation in velocity with distance from the inlet was not as large.

The flow accelerations can also be seen in Fig. 45 where the velocity-depth profiles are plotted for $\overline{Ri}_o = 3.0$ at positions 3, 4, and 5 at 30 minutes. The velocity increases with distance from the inlet in the upper layer and decreases slightly with distance in the lower portion of the shear layer. For an assumed constant-width channel, the equation of continuity from the water surface to the tank bottom is clearly not satisfied from positions 3 to 4 and 4 to 5 in Fig. 45 . On this basis, the conclusion was reached

that the sidewalls, which are only 10 cm apart, influenced the velocity profiles in the upper layer. Essentially, the velocity profile in a horizontal plane across the tank above the interface develops in a manner similar to that at the entrance of a pipe causing the apparent acceleration in flow at the top.

There will be an acceleration due to the exit weir being higher than the inlet. From the interface trajectories plotted in Fig. 40a , most of this acceleration occurs after position 6. The slight decrease in velocity with distance from the inlet at a fixed depth in the shear layer between positions 3 and 5 in Fig. 45 is a result of the upward motion of the interface induced by the exit weir. This decrease in mass flow would be balanced, to satisfy continuity, by a slight increase in velocity in the surface layer quite a bit smaller than that observed in Fig. 45 .

Because the velocity profiles in the surface layer are influenced by the sidewalls, the analysis of the data must rely on the velocity profiles below the interface where the assumption of two dimensional flow is valid since the velocities are low.

VI. 5.5 Analysis of the Data $\overline{Ri_o} = 3.0$

Based on the velocity profiles Fig. 37a , the temperature profiles Fig. 38a, 39a and the investigation of the starting process, the data obtained at position 4 and 30 minutes for $\overline{Ri_o} = 3.0$ appears to be the most suitable for the determination of the coefficients of thermal and momentum diffusivity. From Fig. 40a , the interface at position 4 and 30 minutes is located at a depth of 4.5 cm from the surface. The interface defined as the depth at maximum temperature gradient, corresponds with the boundary between the light and dark regions in the velocity photographs, Fig. 37a .

Velocity-depth profiles as a function of probe position are presented in Fig. 45 . As discussed previously, the profiles below the interface must

be used in the data analysis because the high velocities above are influenced by the sidewalls. The velocity at the interface at position 4 is about 0.3 cm/sec so that the assumption of two-dimensional flow below the interface is reasonable.

Temperature-depth profiles plotted from the data such as Fig. 38a are given in Fig. 46 for different positions. The maximum temperature gradient which locates the interface at 4.5 cm depth occurs at a temperature of about 27.6°C, only 2.5°C below the hot water value compared with an overall difference of 8°C. Below the interface, a gradual fall in temperature occurs to the cold-water value near the bottom. This spreading out of the temperature drop over a considerable depth is attributed to the initial mixing that occurs on starting.

Between the water surface and a depth of 5 cm, in Fig. 46 , the temperature of the water decreases slightly with distance from the tank inlet. However, below 5 cm, the temperature of the water increases with distance from the inlet. This occurrence, the significance of which will be made clear later, is caused by the starting process and by the reversal of warm-water flow at the high exit weir. Heat is transported to lower depths near the exit and then carried forward towards the inlet by the reverse flow.

The temperature-depth and velocity-depth profiles at position 4 are given in Fig. 47 at different times after the start of flow. The interface descends at the rate of about 1.5 cm per hour as the warm water erodes the body of cool water. Buoyancy inhibits the penetration of heat, and the temperature above the interface at a given depth increases slowly. Below the interface, the more rapid increase of temperature at times greater than 15 minutes in caused by the transport of heat by the reverse flow. The velocity profiles in the shear layer and reverse flow region show little change with time in Fig. 47.

The basic objective of the experiment is to use the data given in Figs. 45, 46 and 47 to determine the coefficients of momentum diffusivity K_M and thermal diffusivity K_H. As outlined in Section VI. 2, the first step in the calculation of K_M is the determination of the vertical velocity ω. At the interface where calculations were terminated, ω reached a value of 1.2×10^{-3} cm/sec.

As shown in Fig. 48, the substantial derivative Du/Dt (Eq. VI. 11), calculated from the velocity profiles is never greater than 0.2×10^{-3} cm/sec^2. For comparison, the minimum shear stress gradient $\left.\frac{\partial \tau}{\partial z}\right|_{min}$ which occurs for completely laminar flow can be calculated from the data, known values of viscosity μ for water and by using the equation

$$\left.\frac{1}{\rho}\frac{\partial \tau}{\partial z}\right|_{min} = \frac{\partial}{\partial z}\left(\frac{\mu}{\rho}\frac{\partial u}{\partial z}\right) \qquad \text{(VI. 19)}$$

In Fig. 48, $\left.\frac{\partial \tau}{\partial z}\right|_{min}$, whether positive or negative, is always considerably greater than Du/Dt. If the pressure gradient term $\frac{1}{\rho}\frac{\partial p}{\partial x}$ were negligible in the equation for the x-momentum, equation VI. 10, then

$$\frac{1}{\rho}\frac{\partial \tau}{\partial z} = \frac{Du}{Dt} \qquad \text{(VI. 20)}$$

However, the minimum possible value for $\partial \tau / \partial z$ is always about one order of magnitude larger than Du/Dt. Hence, the x-momentum equation cannot be balanced without including the pressure gradient term.

Integration of the z-momentum equation (VI. 9) with the surface pressure at $z = 10.1$ equal to atmospheric p_a gives

$$p_z - p_a = \int_z^{10.1} \rho g \, dz \qquad \text{(VI. 21)}$$

The density of the water varies with depth as a result of the variation in temperature. If the temperature at each depth were independent of the horizontal location x, the variation in pressure with horizontal position $\partial p/\partial x$ would be zero. However, referring to Fig. 46, the temperature is observed to vary with x. From position 4 to 5, the temperature above the interface drops typically about 0.1°C in 20 cm. The significance of this small temperature gradient can be estimated by noting that from equation (VI.21)

$$\frac{1}{\rho}\frac{\partial p}{\partial x} = \frac{g}{\rho}\int \frac{\partial \rho}{\partial x}\, dz = -\alpha_v g \int \frac{\partial T}{\partial x}\, dz \qquad \text{(VI.22)}$$

where $\frac{\partial \rho}{\partial T} = -\alpha_v \rho$, $\alpha_v = 2.4 \times 10^{-4}$/°C is the coefficient of volumetric expansion at the temperature of the water, and $g = 980$ cm/sec^2. For a constant $\frac{\partial T}{\partial x} = -\frac{.1°C}{20\ cm} = -5 \times 10^{-3}$ °C/cm and integrating from the surface to the interface at a depth of 4.5 cm gives $\frac{1}{\rho}\frac{\partial p}{\partial x} = 5.3 \times 10^{-3}$ cm/sec^2. The maximum value of the substantial derivative $\frac{Du}{Dt}$ below the interface is 0.2×10^{-3} cm/sec^2 which is insignificant compared with the pressure gradient term.

Use of equation (VI.22) with values for $\frac{\partial T}{\partial x}$ calculated at each depth determines $\frac{1}{\rho}\frac{\partial p}{\partial x}$ as a function of depth as shown in Fig. 48 by the curve labelled $\frac{1}{\rho}\frac{\partial p}{\partial x}\Big|_T$. A maximum value of $\frac{1}{\rho}\frac{\partial p}{\partial x}\Big|_T = 6.85 \times 10^{-3}$ cm/sec^2 is reached at a depth of about 5 cm followed by a drop to about 2.6×10^{-3} cm/sec^2 at the bottom. This decrease at depths greater than 5 cm results from the fact that at 5 cm, as shown in Fig. 46, the temperature gradient $\frac{\partial T}{\partial x}$ changes sign from negative to positive. Physically, above 5 cm depth, the water downstream is heavier than that upstream because it is colder and hence the pressure increases with distance. However, below 5 cm the water downstream is lighter than that upstream because it is warmer, but the heavier water above 5 cm relative to that upstream must be supported so that the pressure still increases with distance but at a rate that decreases with increasing depth.

Up to this point, the water surface has been assumed to be exactly horizontal. It would be anticipated that the surface slope $\frac{\partial H}{\partial x}$ would be zero or negative in the flow direction. The pressure gradient $\frac{\partial p}{\partial x}\Big|_s$ due to the slope would also be zero or negative and equal to $\rho g \frac{\partial H}{\partial x}$ independent of depth. In Fig. 48, the pressure gradient $\frac{\partial p}{\partial x}\Big|_T$ calculated from the temperature gradient is positive at all depths. However, above 7.6 cm $\frac{\partial \tau}{\partial z}\Big|_{min}$ is positive and between 7.6 cm and the tank bottom, it is negative. To satisfy the momentum equation (VI.10), $\frac{1}{\rho}\frac{\partial p}{\partial x}$ must also be negative in this region since the contribution from Du/Dt as shown in Fig. 48 is very small, and hence $\frac{1}{\rho}\frac{\partial p}{\partial x} = \frac{\partial \tau}{\partial z}$. At 7.6 cm depth $\frac{\partial p}{\partial x}\Big|_T = 3.5 \times 10^{-3}$ cm/sec^2 and decreases with increasing depth. Therefore, as a first approximation, if $\frac{\partial p}{\partial x}\Big|_s$ is taken equal to 3.5×10^{-3} cm/sec^2, the pressure gradient $\frac{\partial p}{\partial x} = \frac{\partial p}{\partial x}\Big|_T + \frac{\partial p}{\partial x}\Big|_s$ will change sign as required to balance the shear stress gradient at depths greater than 7.6 cm. Note that this corresponds with a surface slope $\frac{\partial H}{\partial x} = -3.5 \times 10^{-3}/g = -3.5 \times 10^{-6}$ cm/cm. For the 170-cm length of the water tank, the drop in the surface amounts to only 6×10^{-4} cm.

A more rigorous determination of the slope pressure gradient $\frac{\partial p}{\partial x}\Big|_s$ can be deduced by referring to the velocity-depth profile given in Fig. 48. At depths of 6.5 and 9.2 cm, the velocity goes through a local maximum, and hence the shear stress is zero at these points. The only forces acting on a control volume bounded by these two depths are those due to pressure since the convective terms are zero. The requirement that the pressure forces cancel between depths of 6.5 and 9.2 cm means that the shaded areas in Fig. 48 be equal which establishes the slope pressure gradient $\frac{\partial p}{\partial x}\Big|_s = -3.5 \times 10^{-3}$ cm/sec^2 in agreement with the first estimate. Since the shear stress at the surface is zero, an additional check is provided by the condition that the areas labelled A in Fig. 48 also must be equal. This condition is also satisfied.

In future experiments, the surface slope might be determined directly by noting on a high-speed recorder the instant that the temperature probes contact the water at several positions with and without flow. The no-flow case would locate the horizontal axis and the flow case would give the deviation from horizontal at each station from which the surface slope $\frac{\partial H}{\partial x}$ would be calculated.

With all of the forces acting on the water below the interface now determined, the momentum equation VI.10 was solved for the unknown shear stress τ . Integration was performed in steps from the zero shear stress point at 6.5 cm depth to the interface at 4.5 cm. The coefficient of momentum diffusivity K_M was then calculated using equation (VI.7). K_M increased from about 1.3×10^{-2} cm^2/sec in the low-speed reverse flow to about 2.6×10^{-2} at the interface compared with the dynamic viscosity for water of about 0.85×10^{-2}.

The coefficient of thermal diffusivity K_H was determined through the use of equations (VI. 12) and (VI. 13) as described in Section VI.2. The required gradients were calculated from the experimental data as a function of depth at position 4 for $\overline{Ri_o} = 3.0$. The thermal diffusivity K_H increased from the molecular value of 1.5×10^{-3} cm^2/sec at the tank bottom to about 2.1×10^{-3} in the low-speed reverse flow followed by a subsequent increase to 2.6×10^{-3} at the interface. Note that the turbulent Prandtl number $Pr = K_M/K_H$ in the low-speed reverse flow was unchanged from the laminar value of 6 since both K_M and K_H are about 40% greater than their respective laminar values. The Prandtl number at the interface was about 10 indicating that the transfer of heat is inhibited more by buoyancy than the transfer of momentum. For these tests, the local Richardson number was approximately 4.1 compared with an initial value at the inlet of 3.0.

VI.5.6 Effect of Richardson Number

With a view to determining values of K_M and K_H at a Richardson number lower than the 4.1 of the previous test, the data obtained for $\overline{Ri_o} = 0.1$

were examined. Based on Fig. 37b, and 38b, the optimum conditions for data reduction appear to be at position 5 at 5.7 minutes after the start of flow. As discussed in Section VI.5.2 and shown in Fig. 41, the Richardson number increases rapidly from a value of 0.1 at the inlet to 3.7 at the first measuring station, position 2. However, because the interface rises with distance from the inlet (Fig. 40) as a result of the starting process and the exit configuration of the tank, the local Richardson number $\overline{Ri}_\ell$ decreases to about 2.5 at position 5. This is sufficiently lower than the value 4.1 at which K_M and K_H have been determined to anticipate that there would be a change in K_M and K_H that would at least indicate the trend.

For the $\overline{Ri}_o = 0.1$ tests, temperature-depth and velocity-depth profiles are given at different times in Fig. 49 and at different positions in Fig. 50. Comparing these profiles with the corresponding ones at $\overline{Ri}_o$ 3.0 in Figs. 45, 46 and 47 shows the much more rapid penetration at low Richardson number of the warm water flow into the pool of cold water reaching very quickly into close proximity of the tank bottom.

The profiles for $\overline{Ri}_o = 0.1$ differ from those for $\overline{Ri}_o$ 3.0 in that there is no longer a slow flow at the bottom of the tank in the direction of the surface flow. In addition, as shown in Fig. 50, at all depths the temperature upstream of a given point is greater than or equal to that downstream and never falls below the temperature downstream as in the $\overline{Ri}_o = 3.0$ tests, Fig. 46. This means that, as given in Fig. 51, the pressure gradient $\frac{\partial p}{\partial x}\Big|_T$ resulting from the temperature gradient never decreases with increasing depth. Instead a plateau in $\frac{\partial p}{\partial x}\Big|_T$ is reached at a depth of 8 cm corresponding to the fact that $\partial T / \partial x$ in Fig. 50 goes to zero at about 8 cm.

The pressure gradient from the slope of the surface $\frac{\partial p}{\partial x}\Big|_S$, was calculated as in Section VI.5.5 except that for $\overline{Ri}_o = 0.1$ there are only two points of zero shear stress - at the surface and at a depth of 7.7 cm. For this

experiment as shown in Fig. 51, $\frac{\partial p}{\partial x}\Big|_s = -2 \times 10^{-3}$ cm/sec^2 compared with -3.5×10^{-3} for the $\overline{Ri}_o = 3.0$ experiment. The substantial derivative term $\frac{Du}{Dt}$ is quite large since the velocity profiles change rapidly with time t and the two positions coordinates x and z. The pressure gradient below the interface $\frac{\partial p}{\partial x} = \frac{\partial p}{\partial x}\Big|_T + \frac{\partial p}{\partial x}\Big|_s$ never goes negative corresponding to the fact that the gradient in shear stress $\frac{\partial \tau}{\partial z}$ is never negative because there is no forward flow at the bottom of the tank.

The vertical velocity ω and the coefficients of momentum diffusivity K_M and thermal diffusivity K_H were calculated as for the $\overline{Ri}_o = 3.0$ tests in Section VI.5.5. The results for both Richardson numbers are plotted in Fig. 52. Because of the necessity for a considerable amount of interpolation between rapidly varying parameters, the results for $\overline{Ri}_o = 0.1$ ($\overline{Ri}_\ell$ 2.5) are not considered to be as accurate as those for $\overline{Ri}_o = 3.0$ ($\overline{Ri}_\ell = 4.1$) . For $\overline{Ri}_\ell = 2.5$, the vertical velocity ω reaches a value of about 7×10^{-3} cm/sec at the interface compared with 1.2×10^{-3} for $\overline{Ri}_\ell = 4.1$. This should not be confused with an entrainment velocity since the flow is strongly influenced by the configuration of the exit weir.

The momentum diffusivity, the uncertainty of which is shown in Fig. 52 exhibits an interesting feature for $\overline{Ri}_\ell = 2.5$. K_M decreases from a value around 6.8×10^{-2} cm^2/sec in the reverse flow to about 5.0×10^{-2} at the interface. This is attributed to the fact that the velocity in the reverse flow is the same magnitude as that at the interface for $\overline{Ri}_\ell$ 2.5 . Consequently, the turbulent fluctuations in the flow below as well as above the interface are inhibited by buoyancy introduced by the stabilizing temperature gradient. The thermal diffusivity K_H for $\overline{Ri}_\ell = 2.5$ shows a similar although not as pronounced behavior with a value of about 6.2×10^{-3} cm^2/sec at the interface. The results for $\overline{Ri}_\ell = 4.1$ because of the much slower reverse flow and the stronger stability at the higher

Richardson number show a more conventional behavior of K_M and K_H equal to near molecular values at the bottom rising after a slight dip to 2.6×10^{-2} cm^2/sec and 2.6×10^{-3} cm^2/sec respectively at the interface.

The ratios at the interface of K_M and K_H to their corresponding molecular values are plotted in Fig. 53 against local Richardson number $\overline{Ri}_\ell$ with maximum observed values of 5.6 for $\frac{K_M}{\mu/\rho}$ and 4.1 for $\frac{K_H}{k/\rho c}$. Both ratios show the anticipated decrease with increasing Richardson number toward unity at high values of $\overline{Ri}_\ell$ as buoyancy completely inhibits turbulent mixing. Over the limited Richardson number range of the present experiments, thermal diffusivity is inhibited by buoyancy slightly more than momentum diffusivity. As a consequence, the turbulent Prandtl number $\frac{K_M}{K_H}$ of 10 at $\overline{Ri}_\ell$ 4.1 and 8.2 at $\overline{Ri}_\ell = 2.5$ are somewhat greater than the laminar value of 6 for water as shown in Fig. 54.

VI.6 Summary and Recommendations

Experimental techniques have been developed and successfully applied to the measurement of temperature and velocity profiles in the controlled flow of a layer of warm water over a pool of cool water. The measurements confirm the dominating influence of Richardson number for the inhibition of turbulent mixing by buoyancy. The rate at which the depth of the interface between the warm and cold water increases was about twenty times faster at an inlet Richardson number of 0.1 than at 3.0.

The present experiments were influenced, to varying degrees, by the starting process, the configuration of the exit weir , the location of the instrumentation, and the tank sidewalls and bottom, For these reasons, the existing apparatus was best suited for measurements at Richardson numbers greater than one. Under these conditions, the coefficients of momentum (K_M) and thermal (K_H) diffusivity at the interface and below were determined from the temperature and velocity profiles. At the interface, K_M increased from about 3 to 5.6 times the laminar value and K_H from 1.8 to 4.1 times as the Richardson number

decreased from 4.1 to 2.5. The turbulent Prandtl number varied from 10 to 8.2 compared with the laminar value of 6 for water.

In the low-speed reverse flow near the tank bottom for the highest Richardson number, the turbulent Prandtl number was equal to the laminar one with both K_M and K_H about 40% greater than their molecular values. At the tank bottom, K_H decreased to the molecular value.

Analysis of the experimental results revealed the strong influence on the low speed flow at high Richardson numbers of horizontal pressure gradients generated by temperature gradients and a slight slope of the water surface. The various reversals of flow direction unexplained in earlier work[56] because of insufficient data could be explained in the present experiment in terms of tank geometry and the interaction between the variable temperature-pressure gradient and the constant slope-pressure gradient.

Future work at low Richardson numbers (less than one) require modifications to the starting process and the exit weir, a wider, deeper and possibly longer tank and perhaps direct measurement of the surface slope and vertical velocity. The measuring probes will have to be located much nearer to the inlet and be more closely spaced. In addition, measurements will have to be taken at considerably shorter running times in order to determine the gradients in velocity and temperature required to calculate the coefficients of momentum and thermal diffusivity. The use of back lighting with both sidewalls transparent instead of front lighting would greatly improve the quality of the velocity photographs.

Most of the work has been devoted to the development of suitable experimental techniques, but the few data points that have already been obtained demonstrate that the approach merits further experiments. In addition to obtaining data for lower Richardson numbers, it should also be established whether the Richardson number uniquely determines the

effect of buoyancy on the mixing process or whether other parameters enter. In such experiments, the same Richardson number should be produced by different combinations of velocity, depth of the warm layer and temperature differences.

VII. CONCLUSIONS

The present study has been concerned with theoretical and experimental analyses of some problems on the physical aspects of thermal pollution. Specifically a theoretical study of the mechanisms of formation and maintenance of thermoclines in stratified lakes was carried out. The theoretical concepts developed in this study were then used to investigate the stratification cycle of temperate lakes and the effects of thermal discharges at or below the thermocline on the stratification cycle. An experimental study of the turbulent transport of heat and momentum across a stably stratified interface between a flowing layer of warm water and an underlying pool of cooler water was also carried out.

It was demonstrated that thermoclines are formed in temperate lakes by the nonlinear interaction between wind-induced turbulence and buoyancy gradients due to surface heating. While the nonlinear aspect of the interaction makes the problem difficult, the nonlinearity is an essential feature, and as such, has to be retained.

The influence on the eddy diffusivities of the interaction between the turbulence structure and the buoyancy gradients was included by using the techniques that have been successful in the study of atmospheric turbulence. That is, the eddy diffusivities were assumed to be given by the product of the eddy diffusivities under conditions of neutral stability and an appropriate function of a stratification parameter such as the gradient Richardson number. The nonlinear equations of the problem were then solved using an electronic computer.

It was demonstrated that, while the vertical temperature profile at the start of the stratification season in a temperate lake is fairly smooth, a sharp interface (the thermocline) develops because of the nonlinear interaction between the turbulence and the temperature structure. It was also shown that the continuous downward erosion of the thermocline into the deeper layers of the lake is a necessary part of its sustenance. The above conclusions were confirmed by considering the simple cases of a half-space,

initially at a uniform temperature, which is subjected to a sudden increase in surface temperature. It was shown that the temperature distributions were initially similar to the error-function distribution for the linear case. But nonlinear effects soon came into play, and a thermocline was formed some distance below the surface. The thermocline also propagated steadily away from the surface. In other words, the problem is inherently unsteady; the continuous downward movement of the thermocline is inherent to the mechanisms responsible for its formation, and will occur even when the surface conditions are held steady. It may be noted that previous attempts to treat the thermocline as a steady-state phenomenon have led to serious inconsistencies[29] in conditions at great depths.

The theoretical concepts developed were then applied to study the entire stratification cycle. It was shown that the seasonal stratification cycle of a temperate lake can be viewed as the response of the lake to certain imposed "external parameters" which specify the exchange of mechanical and thermal energies between the lake and the environment. Moreover, the stratification cycle can be described in terms of these "external parameters" alone without the need for specification of additional information on the thermal structure. In particular, no knowledge of arbitrarily defined "eddy diffusivities" peculiar to a given body of water is required.

The results of the theoretical model are in very good agreement with the observed qualitative features of the stratification cycle. For the one case in which quantitative comparison were made, good agreement with observations was obtained.

The effects on the stratification cycle of thermal discharges at or below the level of the thermocline were also assessed by using the analytical model. It was found that the effect of the thermal discharge was to increase the length of the stratification period as well as the temperature of epilimnion. It was shown that in addition to the effect due to addition of heat, there is also an important effect on the thermal cycle due to the transfer, by the power plant, of large quantities of water from one level to another.

An exploratory experimental study was also carried out of the interfacial friction between a flowing layer of warm water and an underlying pool of cooler water. It was found that the transfer of heat across the stable interface was inhibited more strongly than the transfer of momentum.

While the studies described here have yielded considerable amount of information directly relevant to the problem of thermal pollution, much needs to be done. A detailed parametric study of the effects of various environmental conditions on the thermal structure of a lake should be carried out by using the analytical model developed here. The model can also be used to assess the relative effects of various modes of discharge. The model proposed here can also be improved further by an explicit accounting of the coupling between the current and thermal structures and by a more accurate treatment of free convection.

In the experimental study, further systematic studies of the behavior of the transport processes at the interface for various values of the Richardson number have to be carried out.

APPENDIX A

PERTURBATION METHOD FOR THE STUDY OF THE NONLINEAR BEHAVIOR OF THE BASIC HEAT TRANSPORT EQUATION

It has been emphasized in Section III that while Eq. (III. 1) is nonlinear and as such difficult to solve, the nonlinearity is an essential part of the mechanism responsible for the formation of the thermocline and that therefore it cannot be neglected. Numerical integration of this equation was selected as the technique by which maximum information could be obtained about the solutions under general conditions, and these solutions have been reported in Sections III, IV and V. However, to gain an understanding of the basic nonlinear behavior of Eq. (III. 1) and to check the validity of the numerical solutions under limiting conditions, we analytically calculated solutions to Eq. (III. 1) when these solutions could be expected to deviate only little from the solution to the linear equation. Thus a perturbation technique was developed in which the difference between the solution to the linear equation and that for the full nonlinear equation was assumed to be small. In this appendix, a linearized equation for this perturbation is derived, and an analytical expression for the perturbation is obtained.

In the basic equation

$$\frac{\partial T}{\partial t} = \frac{\partial}{\partial Z}\left(K_H \frac{\partial T}{\partial Z}\right) \tag{A. 1}$$

it is assumed that the eddy diffusivity can be expressed in the form

$$K_H = K_{H_o} + \mu K_H^{(1)} \tag{A. 2}$$

where K_{H_o} is the eddy diffusivity under neutral conditions (corresponding to the linear problem), μ is a small perturbation parameter and $K_H^{(1)}$ is a function of the dependent variable T .

and the general solution is

$$T^{(1)}(\bar{z},t) = (T_1 - T_o)\ 1\ erf\ \frac{\bar{z}}{2\sqrt{K_{H_o} t}} \qquad \text{(A. 6)}$$

where $$erf(x) = \frac{2}{\sqrt{\pi}} \int_o^x e^{-\eta^2} d\eta$$

The initial and boundary conditions for Eq. (A. 5b) are

$$\begin{aligned} T^{(2)} &= 0 \quad \text{for} \quad t = 0 \quad \text{and} \quad \bar{z} \geq 0 \\ T^{(2)} &= 0 \quad \text{for} \quad \bar{z} = 0 \quad \text{and} \quad t \geq 0 \end{aligned} \qquad \text{(A. 7)}$$

The functional form for $K_H^{(1)}$ must now be selected in order to proceed with the solution. As discussed in Section III, a very reasonable form for K_H is

$$K_H = \left(1 + \mu \bar{z}^n \frac{\partial T}{\partial \bar{z}}\right) K_{H_o} \qquad \text{(A. 8a)}$$

This functional relation for the eddy diffusivity is similar to the form suggested by Holzman.[69] It can also be regarded as the relation obtained when any functional form suggested for the eddy diffusivity is linearized for small magnitudes of the nonlinear term.

For generality take

$$K_H^{(1)} = \bar{z}^n \frac{\partial T^{(1)}}{\partial \bar{z}} \qquad \text{(A. 8)}$$

where n is an arbitrary integer. Solutions for $T^{(2)}(\bar{z},t)$ will be given for $n = 0$, 1 and 2, and the meaning of the complete solution for $T(\bar{z},t)$ will be discussed briefly in each case.

The nonlinear behavior of Eq. (A. 1) enters through Eq. (A. 2). The solution for Eqs. (A. 1) and (A. 2) is sought in the region $Z \geq 0$ for $t \geq 0$ with the initial and boundary conditions that

$$\begin{aligned} T &= T_o \quad \text{at} \quad t = 0 \quad \text{for} \quad Z \geq 0 \\ T &= T_1 \quad \text{at} \quad Z = 0 \quad \text{for} \quad t \geq 0 \end{aligned} \tag{A. 3}$$

The solution for T is expanded in powers of the small parameter μ, as

$$T = T_o + \mu T^{(1)} + \mu^2 T^{(2)} + \cdots \tag{A. 4}$$

Equations (A. 2) and (A. 4) are substituted into (A. 1). All of the terms in Eq. (A. 1) can be grouped as coefficients of powers of μ. If each coefficient is separately equated to zero, the following sequence of equations is obtained:

$$\mu^1: \qquad \frac{\partial T^{(1)}}{\partial t} - K_{H_o} \frac{\partial^2 T^{(1)}}{\partial Z^2} = 0 \tag{A. 5a}$$

$$\mu^2: \qquad \frac{\partial T^{(2)}}{\partial t} - K_{H_o} \frac{\partial^2 T^{(2)}}{\partial Z^2} = \frac{\partial}{\partial Z}\left(K_H^{(1)} \frac{\partial T^{(1)}}{\partial Z}\right) \tag{A. 5b}$$

etc.

The initial and boundary conditions for Eq. (A. 5) can be derived from those given in Eq. (A. 3). For Eq. (A. 5) the initial and boundary conditions are

$$T^{(1)} = 0 \qquad \text{for} \quad t = 0 \quad \text{and} \quad Z \geq 0 ,$$

$$T^{(1)} = T_1 - T_o \quad \text{for} \quad Z = 0 \quad \text{and} \quad t \geq 0 ,$$

$n = 0$:

When $n = 0$, the solution for $T^{(2)}(Z, t)$ can be written, after some algebra, as

$$T^{(2)}(Z, t) = -\frac{(T_1 - T_0)^2}{\pi \sqrt{K_{H_0} t}} \frac{Z}{\sqrt{K_{H_0} t}} \int_0^1 \frac{d\chi}{\chi^{1/2} (2 - \chi)^{3/2}} \exp\left\{ - \frac{Z^2}{2 K_{H_0} t} \frac{1}{(2 - \chi)} \right\}$$

or (A. 9)

$$T^{(2)}(Z, t) = \frac{(T_1 - T_0)^2}{\sqrt{K_{H_0} t}} I^0 \left(\frac{Z}{\sqrt{K_{H_0} t}} \right)$$

where I^0 is obviously defined.

$n = 1$:

$$T^{(2)}(Z, t) = \frac{(T_1 - T_0)^2}{\pi \sqrt{\pi K_{H_0}}} \int_0^1 \exp\left[- \frac{Z^2}{2 K_{H_0} t} \frac{1}{2 - \chi} \right] \operatorname{erf}\left[\frac{Z}{2\sqrt{K_{H_0} t}} \frac{\chi}{(1 - \chi)(2 - \chi)} \right] \frac{d\chi}{\chi (1 - \chi)^{1/2}}$$

$$\cdot \left\{ \frac{1}{2} \sqrt{\frac{4 \pi K_{H_0} \chi (1 - \chi)}{2 - \chi}} - \frac{1}{2 K_{H_0} \chi} \left[\frac{4 K_{H_0} \chi (1 - \chi)}{2 - \chi} \right]^{3/2} \left\{ \sqrt{\pi} \left(\frac{1}{2} + \frac{Z^2}{4 K_{H_0} t} \frac{\chi}{(1 - \chi)(2 - \chi)} \right) \right.\right.$$

$$\left.\left. + \frac{Z}{2\sqrt{K_{H_0} t}} \sqrt{\frac{\chi}{(1 - \chi)(2 - \chi)}} \exp\left[- \frac{Z^2}{4 K_{H_0} t} \frac{\chi}{(1 - \chi)(2 - \chi)} \right] \Big/ \operatorname{erf} \frac{Z}{2\sqrt{K_{H_0} t}} \sqrt{\frac{\chi}{(1 \quad \chi)(2 - \chi)}} \right] \right\}$$

(A. 10)

or

$$T^{(2)}(Z, t) = (T_1 - T_0)^2 I' \left(\frac{Z}{\sqrt{K_{H_0} t}} \right)$$

where I' is defined by these relations

$n = 2$:

$$T^{(2)}(z,t) = \frac{2(T_1 - T_0)^2}{\pi} \sqrt{K_{H_0} t}\ \frac{z}{\sqrt{K_{H_0} t}} \left\{ \int_0^1 \exp\left[- \frac{z^2}{2 K_{H_0} t (2-\chi)} \right] d\chi \left[\frac{\sqrt{\chi}}{(2-\chi)^{3/2}} \right.\right.$$

$$\left.\left. - 3\ \frac{(1-\chi)\sqrt{\chi}}{(2-\chi)^{5/2}} \right] - \frac{z^2}{2 K_{H_0} t} \int_0^1 \exp\left[- \frac{z^2}{2 K_{H_0} t (2-\chi)} \right] d\chi\ \frac{\chi^{3/2}}{(2-\chi)^{7/2}} \right\}$$

(A. 11)

or

$$T^{(2)}(z,t) = (T_1 - T_0)^2 \sqrt{K_{H_0} t}\ I^2 \left(\frac{z}{\sqrt{K_{H_0} t}} \right)$$

Note from Eq. (A. 6) that $T^{(1)}(z,t)$ can be written as

$$T^{(1)}(z,t) = (T_1 - T_0) f\left(\frac{z}{\sqrt{K_{H_0} t}} \right)$$

Therefore, the solutions for T, through second order in μ, can be written

For $n = 0$

$$T = T_0 + \mu (T_1 - T_0) f\left(\frac{z}{\sqrt{K_{H_0} t}} \right) + \frac{\mu^2 (T_1 - T_0)^2}{\sqrt{K_{H_0} t}}\ I^0 \left(\frac{z}{\sqrt{K_{H_0} t}} \right)$$

For $n = 1$

$$T = T_0 + \mu (T_1 - T_0) f\left(\frac{z}{\sqrt{K_{H_0} t}} \right) + \mu^2 (T_1 - T_0)^2\ I^1 \left(\frac{z}{\sqrt{K_{H_0} t}} \right)$$

For $n = 2$

$$T = T_0 + \mu (T_1 - T_0) f\left(\frac{z}{\sqrt{K_{H_0} t}} \right) + \mu^2 (T_1 - T_0)^2 \sqrt{K_{H_0} t}\ I^2 \left(\frac{z}{\sqrt{K_{H_0} t}} \right)$$

The important feature to note from these solutions is the time dependence of the second-order terms. Both the zero and the first-order term can be regarded as functions of $Z/\sqrt{K_{H_0} t}$, the linear diffusion parameter. The step increase in temperature imposed at the surface $Z = 0$ at $t = 0$ will diffuse into the medium in a self-similar fashion as time increases. For $n = 0$, the second-order term is proportional to $1/\sqrt{K_{H_0} t}$ times a function of the similarity parameter $Z/\sqrt{K_{H_0} t}$. As time increases, therefore, the nonlinear effects, as embodied in the second-order term, will decrease relative to the zero and first-order terms. For $n = 1$, the second-order term is simply a function of the similarity parameter and will neither grow nor decay with increasing time. For $n = 2$ the second-order term is a product of $\sqrt{K_{H_0} t}$ and a function of the similarity parameter. Nonlinear effects can be expected to increase as time increases, and a perturbation solution will break down when the nonlinear term in (A. 8) becomes comparable to unity.

Direct numerical calculations of Eq. (A. 1) with initial and boundary conditions (A. 3) have verified the predictions made from the perturbation solution. In addition, temperature profiles calculated from the perturbation solution above have been used to check the details of the numerical calculations for this special case.

APPENDIX B

IMPLICIT METHOD OF CONSIDERING THE INTERACTION BETWEEN TURBULENCE AND BUOYANCY GRADIENTS

It was mentioned in Section III, that many of the characteristic features of stratification can be predicted by accounting for the interaction between turbulence and buoyancy gradients either explicitly or implicitly. The explicit procedure, described in Section III, involves accounting for the variability of the eddy diffusivity due to the interaction. In one form of the implicit procedure, which has also been discussed, the lake is divided into two or more layers described by different, but constant, values of the eddy diffusivity. In another form of the implicit procedure used by Moore et al[33] and by Kraus and Turner,[38] the vertical distribution of temperature in the lake is characterized by a given number of parameters; and the time evolution of these profile parameters is determined by using moments, over the entire depth of the lake, of Eq. (III. 1).

Integration of Eq. (III. 1) and its first moment yield

$$\rho C_p \frac{d}{dt}\int_0^{z_m} T(z,t)\, dz = q_s \tag{B. 1}$$

$$\alpha_v g \frac{d}{dt}\int_0^{z_m} z\, T(z,t)\, dz = \alpha_v g \int_0^{z_m} \frac{q}{\rho C_p}\, dz \tag{B. 2}$$

where z_m is the maximum depth of the lake. The right-hand side of Eq. (B. 2) can be expressed somewhat differently[38] by using the turbulent-energy balance, so that

$$\alpha_v g \frac{d}{dt}\int_0^{z_m} z\, T(z,t)\, dz = \frac{\omega^{*3}}{k} - D \tag{B. 3}$$

where the first term on the right-hand side represents the mechanical energy input from the wind, and the second term represents the dissipation of energy, over the entire depth of the lake by viscous forces.

Equation (B. 1) represents the conservation of heat, while Eq. (B. 3) represents the rate of decrease of the potential energy of stratification due to the net work done by the wind. The significance of various forms of Eq. (B. 3) has long been appreciated by limnologists,[12] who have computed the wind work required to distribute a given heat income at the surface.

Moore et al[33] have used Eq. (B. 1), along with the assumption that the depth of the epilimnion remains fixed, to solve for the seasonal variations in surface temperature. They have also used Eq. (B. 3) to derive a simple stratification criterion. Kraus and Turner[38] have used a two-parameter description of the vertical temperature profile, along with Eqs. (B. 1) and (B. 3), to solve for the seasonal variations of the temperature and of the depth of the upper, mixed layer.

It should be emphasized that implicit methods, because of their integral nature, cannot be used to predict the formation of a thermocline in the sense that was discussed in Section III. They can be used only to predict certain features of the maintenance of a thermocline. An assumption that is implicit in all integral methods is that the unsteady aspects of the problem arise primarily out of the unsteadiness in the boundary conditions at the surface. However, it was seen in Section II that unsteadiness is inherent to the mixing processes in the lake and that, when they are accounted for properly, the conditions in a lake will be unsteady even when conditions above it are steady.

Moreover, integral methods assume that the time scales for the mixing processes in a lake are very small compared to the time scale for the unsteadiness in the boundary conditions; that is, it is assumed that conditions in the lake adjust instantaneously to changes in surface boundary conditions. For example, in the method proposed by Kraus and Turner,[38] a steady heat flux applied to the surface will lead to the instantaneous formation of a mixed, upper layer whose depth is proportional to the Monin-Obukhov length scale.

In the present study, it is assumed that the vertical temperature profile can be represented by a mixed upper layer of temperature, T_s , and depth, h , with the temperature profile below the mixed layer being given by Eq. (III. 11). That is

$$T(z, t) = T_s \quad \text{for} \quad 0 < z \leq h$$
$$T(z, t) = T_\infty + Ae^{-az} \quad \text{for} \quad h < z < z_m \tag{B. 4}$$

The parameters A and a can be determined by requiring that the temperature and the heat flux be continuous at the bottom of the mixed layer. It was seen in Section III that Eq. (III. 11) is consistent with the assumption of a constant eddy diffusivity below the mixed layer.

If Eq. (B. 4) is introduced into Eqs. (B. 1) and (B. 3), one obtains, after some manipulation,

$$(h + \frac{1}{a}) \frac{dT_s}{dt} + (T_s - T_\infty) \frac{dh}{dt} - \frac{T_s - T_\infty}{a^2} \frac{da}{dt} = \frac{q_o}{\rho C_p} \tag{B. 5}$$

$$(\frac{h^2}{2} + \frac{h}{a} + \frac{1}{a^2}) \frac{dT_s}{dt} + (T_s - T_\infty)(h + \frac{1}{a}) \frac{dh}{dt}$$
$$- \frac{T_s - T_\infty}{a^2} (h + \frac{2}{a}) \frac{da}{dt} = \frac{w^{*3}}{k \alpha_v g} - D \tag{B. 6}$$

$$h \frac{dT_s}{dt} + (T_s - T_\infty) a w = \frac{q_o}{\rho C_p} \tag{B. 7}$$

where the last equation represents the criterion for the continuity of heat flux at the bottom of the mixed layer.

If appropriate initial and boundary conditions are specified, then Eqs. (B. 5) to (B. 7) can be used to solve for the time evolution of the quantities T_s , h and a . However, our objective here is to merely illustrate the behavior of the thermocline during the early phases of the stratification cycle.

Equations (B. 5) to (B. 7) can be used to derive the relation

$$\frac{h}{a}\frac{dh}{dt} = a\nu\left[\left(h + \frac{1}{a}\right)^2 - \frac{h^2}{2}\right] - \frac{1}{T_s\, T_\infty}\frac{q_o}{\rho C_p}\left[hL - \left(\frac{h^2}{2} - \frac{1}{a^2}\right)\right] \tag{B. 8}$$

where the dissipation D has been neglected and where L is the Monin-Obukhov length defined in Eq. (III. 8). Thus it can be seen that the movement of the thermocline is governed by the eddy diffusivity of the underlying layer as well as by the value of the Monin-Obukhov length. The first term on the right-hand side of Eq. (B. 8) is always positive, but the second term is negative since in general, $h > L$. Thus it is seen that the movement of the fully developed thermocline can be either upward or downward depending on the relative magnitude of the two terms on the right-hand side of Eq. (B. 8).

APPENDIX C

A DESCRIPTION OF THE NUMERICAL PROGRAM

The numerical program used for the calculations described in this report was modified extensively during this work. As a result the program has not been tested under all conditions which might be desired. However, the program has been found to perform simply and adequately under all conditions attempted.

Knowledge of the performance of the program has been gained by working with it, and this knowledge cannot be conveyed in a report. However, few warnings need to be given about operating the program. The program represents a satisfactory, working package for numerically integrating the basic heat transport equation.

In this appendix a description of the details of the program will be given. First the equations are presented. Then a discussion is given of all input quantities for the program. Next the algorithm is described for computing the temporal change in the temperature and thermal diffusivity profiles. Finally, the output plots and typical run times are discussed.

1. Equations

The program has been written to calculate, as a function of depth, thermal diffusivity and temperature profiles over a complete annual cycle. The equation integrated by the program is the model equation discussed in Sections III and V of the report

$$\frac{\partial T}{\partial t} = \frac{\partial}{\partial z}\left(K_H \frac{\partial T}{\partial z}\right) - \omega_p \frac{\partial T}{\partial z} + q_p \qquad \text{(C.1a)}$$

$$\text{for } z_i \geq z \geq z_d$$

$$\frac{\partial T}{\partial t} = \frac{\partial}{\partial z}\left(K_H \frac{\partial T}{\partial z}\right) + q_p \qquad \text{(C.1b)}$$

$$\text{for } z_m \geq z > z_i \quad \text{or} \quad z_d > z \geq 0$$

Note that Z_i is the specified intake depth, Z_d is the discharge depth which is found as described in Section V, ω_p is the specified pumping velocity and q_{tp} is the explicit thermal discharge or heat input term whose form is given in Section V.

When buoyancy effects and wind-induced turbulence dominate the diffusive mixing process, the thermal diffusivity K_H has the form given by Rossby and Montgomery.

$$K_H = K_{H_o} (1 + \sigma_1 R_i)^{-1} \tag{C.2}$$

where σ is a dimensionless constant and the Richardson R_i number has the form

$$R_i = -\left(\frac{g Z}{\omega^{*2}}\right)^{N-1} \alpha_v Z \frac{\partial T}{\partial Z} \tag{C.3}$$

The limitations of this form for the thermal diffusivity and the justification for the alterations to this form discussed below have been given in the body of this report. Note that this form of the thermal diffusivity can become infinitely large when the Richardson number becomes negative. During the cooling portion of the annual cycle, the Richardson number will become negative, and the form given by Eq. (C.2) for the thermal diffusivity is no longer valid (see Section IV). Under these conditions the thermal diffusivity is limited by a maximum value denoted as F_{max}. Similarly, from the form of K_H given by Eq. (C.2), the thermal diffusivity can become infinitesimally small as the Richardson number increases. During the heating portion of annual cycle the Richardson number can become very large, and the form (C.2) is no longer valid (see Section IV). Under these conditions the thermal diffusivity is limited by a minimum value F_{min}.

Equations (C.1) apply over the complete lake $Z = 0$ to $Z = Z_m$, where Z_m is the depth of the lake. Integration of these equations requires specification of initial conditions and boundary conditions. Initially the lake is always taken to be homothermal at temperature T_o. At the bottom of the lake the heat flux is taken to be zero, and this condition implies that

$$\left.\frac{\partial T}{\partial Z}\right|_{Z = Z_m} = 0 \tag{C.4}$$

At the surface of the lake one of three boundary conditions is applied: either (i) the surface temperature is specified

$$T_s = T(z\ 0) = A + B \sin(\Omega t + \phi) \tag{C.5a}$$

where A is a mean and B is an amplitude for the surface temperature variation, $\Omega = \frac{2\pi}{365}$ (day^{-1}) is the frequency of the variation and ϕ is a phase angle, (ii) the heat flux q at the surface is specified

$$q_s = q\Big|_{z=0} = -\left(K_H \rho C_p \frac{\partial T}{\partial z}\right)_{z=0} = A + B \sin(\Omega t + \phi) \tag{C.5b}$$

where A and B are now the mean and amplitude of the heat flux variation, (iii) the equilibrium temperature T_E is specified

$$-\left(\rho C_p K_H \frac{\partial T}{\partial z}\right)_{z=0} = K(T_E - T_s)$$

$$T_E = A + B \sin(\Omega t + \phi) \tag{C.5c}$$

2. Input Quantities

Since there does not appear to be a more efficient or understandable method for presenting details of a numerical program, reference to names of variables used in the Fortran program will be made. In particular to describe the input quantities for the program, we will list the Fortran names and give a brief description of the function of each of these quantities. Many input quantities are dimensional, and the dimensions of each will be given in square brackets after its description. If no dimensions appear, the input quantity is dimensionless. All input variables beginning with letters I, K, N or M are integer variables and all others are floating point, as is usual for Fortran programs.

Input variable	
NRUN	Run number
N	Exponent in the definition of the Richardson number given in Eq. (C.3)
K	Number of spatial or depth intervals
NDAYS	Time span of calculation [days]

NBC	Boundary condition indicator: NBC = 1, Surface temperature T_s is specified to be $A + B \sin(\Omega t + \phi)$, see Eq. (C.5a) NBC = 2, Heat flux q at surface is specified to be $A + B \sin(\Omega t + \phi)$ and the surface temperature is derived from Eq. (C.5b) NBC = 3, The equilibrium temperature T_E is specified to be $A + B \sin(\Omega t + \phi)$ and the surface temperature is derived from Eq. (C.5c)
IPLOT	Number of days at which spatial plots are desired. Spatial plots are always made on the final day.
MINUTS	Time in minutes allotted for the run
IPUMP	An indicator which is used in calculations involving thermal discharges. If IPUMP = 0, the thermal discharge is added in a normal fashion. If IPUMP ≠ 0, then the model includes the effect of pumping water from lower levels to the surface with no thermal input to pumped water.
NDAYPL	An array containing IPLOT elements that specify the days on which spatial plots are desired.
SIGMA	The constant σ which appears in the Rossby-Montgomery form for the thermal diffusivity, see Eq. (C.2)
FMAX	Maximum allowed value for the thermal diffusivity
FMIN	Minimum allowed value for the thermal diffusivity
A	Mean value of the surface temperature if NBC = 1 [°C], of the heat flux if NBC = 2 [Btu/ft^2-day], of the equilibrium temperature if NBC = 3 [°C].
B	Amplitude of the surface temperature if NBC = 1 [°C], of the heat flux if NBC = 2 [Btu/ft^2-day], of the equilibrium temperature if NBC = 3 [°C].
PHI	Phase angle in surface boundary condition
CON1, CON2	Constants C_1 and C_2 used in the definition of K_{H_o} in the expression for the thermal diffusivity given in Eq. (C.2)

$$K_{H_o} = (C_1 + C_2 Z)\, \omega^*$$

CON 1 has dimensions [ft] and CON 2 is dimensionless

B1, B2, PSI — Constants B_1, B_2 and ψ is the definition of ω^*

$$\omega^* = B_1 + B_2 \sin(\Omega t + \psi)$$

B1 and B2 have dimensions of [ft/sec] and ψ is dimensionless.

DELTAZ — Spatial mesh size Δz [ft]. The lake depth is the integer K times Δz, $z_m = K \Delta z$.

XK — The heat transfer coefficient K in Eq. (C.5c) [Btu/ft^2-day-°C]

TEMPO — The initial uniform temperature T_o [°C]

CTSTEP — A nondimensional constant C_t used in the determination of the time step size in the numerical integration. For stability $0 < \text{CTSTEP} < 0.5$.

WPP — Power plant pumping velocity ω_p used in Eq. (C.1a) [ft/day]

TEMPD — Temperature difference ΔT_p produced by the power plant [°C]

ZINTAK — Depth z_d of intake for power plant [ft]

ALEN — A length denoted a defining the thickness of the gaussian heat source q_p, see Section V [ft]

QPP — Heat q_p per unit area per time added by the power plant to the lake [Btu/ft^2-day]. Provided the discharged water remains below the surface,

$$q_p = \rho C_p \Delta T_p \omega_p$$

In addition to the input quantities described above certain constants are defined within the program. A list of these follows:

$\Omega = \frac{2\pi}{365}$ [days^{-1}] - the frequency of variation of the boundary condition at the surface,

$g = 32.2$ [ft/sec^2] - acceleration of gravity,

$\rho C_p = 112.32$ [Btu/°C - ft^3] - heat capacity per cubic ft of water,

$A_1 = 0.0$
$A_2 = 1.538 \times 10^{-5}$
$A_3 = -2.037 \times 10^{-7}$ - Constants which determine the quadratic expression that approximates the coefficient for volumetric expansion for water

$$\alpha_v = A_1 + A_2 (T - 4^\circ) + A_3 (T - 4^\circ)^2$$

3. Algorithm

Numerical integration of Eqs. (C.1) requires that these equations be replaced by a set of difference equations. These equations are parabolic and mathematically represent a diffusion process. Integration of the linear form of such parabolic equations has been studied extensively, and many finite difference equations have been used to obtain solutions for such equations (for example see Refs. 81 and 82). Integration of nonlinear forms of the diffusion equation by finite-difference methods has been widely used, but is much more poorly understood.

a. Difference Equation

In this program a straightforward explicit finite-difference scheme has been used. The total depth of the lake is divided into K equal increments each of length ΔZ. The time step is chosen at each time on the basis of stability considerations. The following notation is used:

$$\begin{aligned} \Delta t_k &= \text{the time increment chosen at the } k^{th} \text{ integration step,} \\ t_k &= \sum_{l=1}^{k} \Delta t_l \quad , \quad t_0 \quad 0 \, , \\ T_j^k &= T(j \Delta Z, t_k) = T(Z, t) \end{aligned} \tag{C.6}$$

The difference equation which replaces Eq. (C.1a) can be written

$$\begin{aligned} T_j^k = T_j^{k-1} &+ \frac{\Delta t_k}{(\Delta Z)^2} \left[(K_H \Delta T)_{j+\frac{1}{2}}^{k-1} - (K_H \Delta T)_{j-\frac{1}{2}}^{k-1} \right] \\ &+ \Delta t_k (q_{TP})_j^{k-1} - \frac{\Delta t_k}{2\Delta Z} \omega_p (T_{j+1}^{k-1} - T_{j+1}^{k-1}) \end{aligned} \tag{C.7}$$

where

$$(K_H \Delta T)_{j+\frac{1}{2}}^{k-1} = K_H \left[(j + \tfrac{1}{2}) \Delta Z, \; t_{k-1} \right] \left[T_{j+1}^{k-1} - T_j^{k-1} \right]$$

$$(K_H \Delta T)_{j-\frac{1}{2}}^{k-1} = K_H \left[(j - \tfrac{1}{2}) \Delta Z, \; t_{k-1} \right] \left[T_j^{k-1} - T_{j-1}^{k-1} \right]$$

A similar equation with the last term deleted arises from Eq. (C.1b). The meaning of the terms like $K_H\left[(j+\frac{1}{2})\Delta Z,\ t_{k-1}\right]$ is somewhat ambiguous because of the nonlinear form of K_H. If it is assumed for the moment that the thermal diffusivity K_H is specified at each depth by Eqs. (C.2) and (C.3) alone, then

$$K_H\left[(j+\tfrac{1}{2})\Delta Z,\ t_{k-1}\right] = K_{H_0}\left[(j+\tfrac{1}{2})\Delta Z\right]\left\{1+\sigma\left(\frac{g(j+\frac{1}{2})\Delta Z}{\omega^{*2}}\right)^{N-1}\right.$$

$$\left.\cdot\ \alpha_v\left[\tfrac{1}{2}\left(T_j^{k-1}+T_{j+1}^{k-1}\right)\right](j+\tfrac{1}{2})\Delta Z\ \frac{T_{j+1}^{k-1}-T_j^{k-1}}{\Delta Z}\right\} \qquad (C.8)$$

since $K_{H_0} = K_{H_0}(Z)$ and $\alpha_v = \alpha_v(T)$ However, the simple forms (C.2) and (C.3) are not always valid for the thermal diffusivity and therefore are not used at all spatial mesh points and at all times. The algorithm used in the computation to determine the diffusivity is discussed below.

b. The Thermal Diffusivity

Justification for the procedure for calculating the thermal diffusivity has been given in Section III and Section IV. Therefore only brief mention of the reasons for the procedures will be made here. At any time the form given by Eqs. (C.2) and (C.3) for the thermal diffusivity is calculated at each spatial mesh point. Denote this function by $\hat{K}_H$. It is on the basis of this function $\hat{K}_H$ that the value of the thermal diffusivity K_H at each point is chosen.

As discussed in Section III, the formation of the thermocline implies that wind-induced turbulence is suppressed at levels below the thermocline. Therefore, during the heating portion of the annual cycle once the thermocline has formed, the values of $\hat{K}_H$ below the thermocline do not represent the thermal diffusivity K_H. A cutoff procedure is used to eliminate this problem. Thermocline formation is defined by the condition that $\frac{\partial T}{\partial Z}$ reaches a minimum value which is not at the lake surface $Z = 0$. After thermocline formation the minimum value with respect to Z of $\hat{K}_H$ is determined. This value is denoted by $\hat{K}_{H_{min}}$ and the position at which

the minimum occurs is denoted by z_{min}. The thermal diffusivity K_H is chosen to be $\hat{K}_H$ for all $z \leq z_{min}$ and $\hat{K}_{H\,min}$ for all $z \geq z_{min}$. As discussed before the thermal diffusivity cannot decrease below a value determined by the molecular thermal diffusivity, and often this absolute minimum value will be somewhat larger than the molecular thermal diffusivity because of ambient turbulence within the hypolimnion. A value F_{min} is specified as input to each numerical calculation. If $\hat{K}_H$ becomes smaller than F_{min} at some depth, then for all z greater than this depth, $K_H = F_{min}$.

During the cooling portion of the annual cycle, again $\hat{K}_H$ becomes inappropriate in the upper layers of the lake. Because of cooling at the surface of the lake, convective mixing becomes important within the epilimnion. This mixing can be accounted for within the model by an increased value of the thermal diffusivity. Again a cutoff procedure is used to eliminate this problem. If $\hat{K}_H$ reaches a local maximum with respect to z during cooling, then the value of this maximum $\hat{K}_{H\,max}$ and the position z_{max} are determined. For $z \leq z_{max}$, the thermal diffusivity K_H is chosen to be $K_{H\,max}$, and it is chosen to be $\hat{K}_H$ for $z \geq z_{max}$. However, the thermal diffusivity is never allowed to exceed the value F_{max} specified for each calculation.

c. Time Step Determination

At any time t_k, the temperature profile is known, and from this profile the thermal diffusivity as a function of depth is determined in the manner described above. Then the maximum value $(K_H)_{max}$ of the thermal diffusivity is ascertained. From this value, the constant C_t specified for the calculation and the spatial mesh size Δz, the time step size Δt_{k+1} is computed

$$\Delta t_{k+1} = C_t \frac{(\Delta z)^2}{(K_H)_{max}} \qquad (C.9)$$

3. Output and Run Times

A very important feature of the numerical program is its ability to generate graphs directly from the computer. This feature has been found to

be very useful since much time and labor are saved when the plots are made by the computer. However, and even more important, these graphs provide immediate visualization and efficient understanding of the solutions.

Two types of graphs have been programmed, spatial and temporal graphs. Spatial graphs are those for which a dependent variable is plotted as a function of depth at a specified time. Temporal graphs are those for which a dependent variable is plotted as a function of time. Four spatial graphs and three temporal ones are generated for each numerical computation. On each spatial graph up to eleven plots can be made of the dependent variable; each plot is made for a specified day so that plots can be made at eleven different days. The temperature, the thermal diffusivity, the temperature gradient and the heat flux are the dependent variables which are graphed. Temporal graphs are made of temperature (surface temperature, temperature at three depths and the equilibrium temperature), depth of the thermocline and surface heat flux.

The calculations presented within this report were performed on an IBM 360/65 computer. The time required for each computation depended upon the number of days requested for the calculation. Typically a computation reported in Section IV or Section V ran for 400 days, or slightly over a complete yearly cycle. Such a run required 50,000-60,000 time steps and about 10-15 minutes of computer time. Calculations reported in Section III ran for 30-40 days requiring less than 4000 time steps and less than one minute of computer time. These times include the computer time required for performing the plots.

APPENDIX D

VERIFICATION OF THE ADEQUACY OF THE BASIC HEAT TRANSPORT EQUATION WHEN THE VARIABILITY OF THE VOLUMETRIC COEFFICIENT OF EXPANSION IS ACCOUNTED FOR

Throughout this report the equation

$$\frac{\partial T}{\partial t} = \frac{\partial}{\partial z}\left(K_H \frac{\partial T}{\partial z}\right) = -\frac{\partial}{\partial z}\left(\overline{w'T'}\right) \tag{D.1}$$

and its solution, for various boundary conditions, have been discussed at length.

There was some concern, however, that when a consistent account of the variation in the volumetric coefficient of expansion (α_v) was made, Eq. (D.1) would not be an adequate representation for the temperature field.

This uncertainty about the adequacy of Eq. (D.1) was primarily due to the fact that Phillips[62] has made extensive use of the buoyancy equation

$$\frac{\partial B}{\partial t} = \frac{\partial N}{\partial z} = -\frac{\partial}{\partial z}\left(\overline{w'b'}\right) \tag{D.2}$$

which is consistent with Eq. (D.1) only when α_v is a constant.

In Eq. (D.2), B is the mean buoyancy and b' is the fluctuation in buoyancy, with

$$b = B + b' = -g\,\frac{\rho - \rho_0}{\rho_0} \tag{D.3}$$

where ρ_0 is a reference density. Note that under the Boussinesq approximation[62]

$$b' = -g\,\frac{\rho'}{\rho_0} = \alpha_v\, g\, T' \tag{D.4}$$

and

$$\frac{\partial B}{\partial t} = \alpha_v\, g\, \frac{\partial T}{\partial t}$$

so that Eq. (D.2) becomes

$$\alpha_v \frac{\partial T}{\partial t} = -\frac{\partial}{\partial z}\left(\alpha_v\, \overline{w'T'}\right) \tag{D.5}$$

Thus, it is clear that Eq. (D.5) can be compatible with Eq. (D.1) only if α_v is a constant. It should be pointed out that Eq. (D.2) was obtained by Phillips from the mass-conservation (continuity) equation while Eq. (D.1) follows from the energy equation. However, since under the Boussinesq approximation both Eqs. (D.1) and (D.2) describe the temperature field, it is necessary to establish the reasons for the incompatibility between the two relations. After a detailed investigation it has been established that Eq. (D.2) is not an accurate representation of the mass-conservation relation when α_v is variable.

The continuity equation gives

$$\frac{\partial \rho}{\partial t} + div(\rho \vec{V}) = 0 \tag{D.6}$$

where $\vec{V}$ is the velocity vector. If $\rho = \bar{\rho} + \rho'$, $\omega = \bar{\omega} + \omega'$ etc., and if horizontal homogeneity is assumed to exist, then Eq. (D.6) gives

$$\frac{\partial \bar{\rho}}{\partial t} + \frac{\partial}{\partial z}(\overline{\rho'\omega'}) + \frac{\partial}{\partial z}(\bar{\rho}\,\bar{\omega}) = 0 \tag{D.7}$$

In the literature it has been customary to assume that, that under conditions of horizontal homogeneity, the last term in Eq. (D.7) is identically equal to zero. It should be emphasized that this assumption is not justified when α_v is a variable. Note that the same heat flux passing through two different horizontal planes a small distance apart will cause a relative motion between the two planes because of the different rates of expansion at the two locations. The last term in Eq. (D.7) indeed represents the mass flux into a fixed control volume (between two horizontal planes) due to the above differential expansion. This term can also be written in the form $-\frac{q}{\bar{\rho} C_p}\frac{\partial \alpha_v}{\partial z}$, so that Eq. (D.7) becomes

$$\frac{\partial \bar{\rho}}{\partial t} + \frac{\partial}{\partial z}(\overline{\rho'\omega'}) - \frac{q}{\rho C_p}\frac{\partial \alpha_v}{\partial z} = 0 \tag{D.8}$$

Thus the correct form of the buoyancy equation is

$$\frac{\partial B}{\partial t} = -\frac{\partial}{\partial z}(\overline{\omega' b'}) - g\frac{q}{\rho c_p}\frac{\partial \alpha_v}{\partial z} \qquad \text{(D.9)}$$

It can be easily verified that Eq. (D.9) reduces to Eq. (D.1) when Eqs. (D.4) are used to relate buoyancy to temperature. Thus under the approximation of horizontal homogeneity, Eq. (D.1) represents the correct description of the temperature field and this equation has been used throughout.

APPENDIX E

ON THE VALUE OF THE SEMIEMPIRICAL PARAMETER σ_1

In Section III, the form of the eddy diffusivity given by Equation (III. 7) was used to demonstrate that the thermocline is formed by the nonlinear interaction between wind-induced turbulence and buoyancy gradients due to surface heating. In Section IV, the same form of the eddy diffusivity was used to study the various features of the stratification cycle. Before the solutions given in these sections can be interpreted in a quantitative fashion, it is necessary to choose a numerical value for the parameter σ_1. In this context, it should be noted that in the present analysis the coupling between the current and thermal structures was included only implicitly. In other words, in Equation (III. 7) the form of the Richardson number given by Equation (III. 6), rather than that given by Equation (III. 5), was used. This point is quite important since almost all the values quoted in the literature for σ_1 are those associated with the form of the Richardson number given by Equation (III. 5).

In their theory of the thermocline, Munk and Anderson[29] used for the eddy diffusivity a relation of the form

$$K_H = K_{H_0} (1 + 3.33 R_i)^{-3/2} \qquad \text{(E-1)}$$

For small values of R_i, Equations (E-1) and (III-7) will be equivalent if the value of σ_1 were 5 and if the form of the Richardson number given in Equation (III-5) was used. It was pointed out in Section II that one of the more important developments since the time of Munk and Anderson's theory is the formulation of the so-called similarity theory of Monin and Obukhov.[34] Monin and Obukhov have proposed a relation for the eddy diffusivity of the form

$$K_H = K_{H_0} \left(1 + \beta \frac{z}{L}\right) \qquad \text{(E-2)}$$

where L is defined by Equation (II-1) and β is a semi-empirical parameter with a value of about 0.6.

If Equations (II-1) and (E-2) are combined with the relation

$$q = \rho C_p K_H \frac{\partial T}{\partial z} \tag{E-3}$$

one obtains, after some manipulation,

$$K_H = K_{H_o} \left(1 - \beta R_i \frac{k K_{H_o}}{\omega^* z}\right)^{-1} \tag{E-4}$$

where R_i is given by Equation (III-6). Since the eddy diffusivity under neutral flow conditions is given by the relation

$$K_{H_o} \sim k \omega^* z \tag{E-5}$$

Equations (E-4) and (III-7) would be identical if $\sigma_1 = k^2/\beta$ or, since the value of the von Karman constant k is approximately equal to 0.4, $\sigma_1 \simeq 0.1$. It may be pointed out that, in the literature, there is no unanimity of opinion as to the value of β. The theoretical analyses of Swinbank yield a value of 0.5 for β, while other authors have obtained values as high as 7.0 based on atmospheric data.[33]

Based on extensive measurements in the atmosphere, Elliot suggests a relation for the eddy diffusivity of the form,

$$K_H = K_{H_o} (1 + 7 R_i)^{-1/2} \tag{E-6}$$

with R_i given by Equation (III-5). The difficulty in comparing Equations (E-1) and (E-6) with (E-4) is indeed in the different forms of the Richardson number used in these relations. This difficulty would not have arisen if in the present analysis the coupling between the current and thermal structures had been included explicitly, rather than implicitly. If it is assumed that the velocity gradient is given by the relation[62]

$$\frac{\partial u}{\partial z} \simeq \frac{\omega^*}{k z} \tag{E-7}$$

then the value of σ_1 corresponding to Equation (E-6) would be 0.56.

In the present analysis the value of σ_1 has been taken as 0.1 since this value corresponds closely to Monin and Obukhov's original value as well as to Swinbank's theoretical result. However, this value has to be regarded as preliminary. When accurate and complete data on the thermal structure of a lake and the environmental conditions above it become available, a more accurate value for σ_1 can be determined. It should be noted that the parameter σ_1 appears only in the combination (σ_1/ω^{*2}). Thus a value of σ_1 is important only in its relationship to the representation of the wind conditions over a lake. The particular value of (σ_1/ω^{*2}) determines the quantitative behavior calculated, but does not influence the qualitative conclusions reached in the present study.

REFERENCES

1. Ingram, W. M. and Towne, W. W., "Stream Life below Industrial Outfalls," Public Health Repts. 74, 1059 (1959).

2. Hynes, H. B. N., The Biology of Polluted Waters, Liverpool University Press, 136, 1966.

3. Krenkel, P. A. and Parker, F. L., Biological Aspects of Thermal Pollution, Vanderbilt University Press, 1969.

4. Oglesby, R. T. and Allee, D. J. (editors), "Ecology of Cayuga Lake and the Proposed Bell Station," Publication No. 27, Water Resources and Marine Sciences Center, Cornell University, Ithaca, New York (1969).

5. Jensen, L. D., Davies, R. M., Brooks, A. S., and Meyers, C. D., "The Effects of Elevated Temperature upon Aquatic Invertebrates," EEI Publication No. 69-900, Edison Electric Institute, New York (1970).

6. "Aquatic Life Water Quality Criteria," Environmental Science and Technology 1, 888 (1967).

7. Edinger, J. E. and Geyer, J. C., "Heat Exchange in the Environment," Sanitary Eng. and Water Resources Rept., Johns Hopkins University (1967).

8. Parker, F. L. and Krenkel, P. A., Engineering Aspects of Thermal Pollution, Vanderbilt University Press, 1969. See also Parker, F. L. and Krenkel, P. A., "Thermal Pollution: Status of the Art," Rept. N03, Department of Environmental and Water Resources Engineering, Vanderbilt University (1969).

9. Christianson, A. G. and Tichenor, B. A., "Industrial Waste Guide on Thermal Pollution," Federal Water Pollution Control Administration Northwest Region, Pacific Northwest Water Laboratory (1968).

10. Tichenor, B. A. and Cawley, W. A., "Research Needs for Thermal Pollution Control," Paper presented at the National Symposium on Thermal Pollution, Vanderbilt University, Aug. 14-16, 1968. See also pp. 329-338 of Ref. 8.

11. Jeffreys, H., "The Flow of Water in an Inclined Channel of Rectangular Section," Phil. Mag. Ser. A 107, 189 (1925).

12. Hutchinson, G. E., A Treatise on Limnology, Vol. I - Geography, Physics and Chemistry, John Wiley & Son, 252, 1957.

13. Edinger, J. E. and Geyer, J. C., "Analyzing Steam Electric Power Plant Discharges," Paper presented at the National Symposium on Estuarine Pollution, ASCE, Stanford, 1967.

14. Edinger, J. E., Brady, D. K., and Graves, W. L., "The Variation of Water Temperatures Due to Steam Electric Cooling Operations," Paper presented at the 1967 WPCF Conference, New York, 1967.

15. Pannell, J. P. M., Johnson, A. E., and Raymont, J. E. G., "An Investigation into the Effects of Warmed Water from Marchwood Power Station into Southampton Water," Proc. Inst. Civil Engrs. 23, 35 (1962).

16. Sundaram, T. R., Easterbrook, C. C., Piech, K. R., and Rudinger, G., "An Investigation of the Physical Effects of Thermal Discharges into Cayuga Lake," Report VT-2616-O-2, Cornell Aeronautical Laboratory, Buffalo, N. Y. (Nov. 1969).

17. Zeller, R. W., "Cooling Water Discharge into Lake Monona," Ph. D. Thesis, University of Wisconsin (1967).

18. Zeller, R. W., Hoppes, J. A., Rohlich, G. A., "Heat Dissipation and Induced Circulations from Condenser Cooling Water Discharges into Lake Monona," Paper presented at ASCE Conference on Thermal Pollution, Massachusetts Institute of Technology, Aug. 1968.

19. Palmer, M. D., "Simulated Thermal Effluent into Lake Ontario," Proc. 12th Conference on Great Lakes Research, 1969.

20. Brooks, N. H., "Discussions from the Floor," on Ref. 10, p. 339 of Ref. 8.

21. Fairbridge, R. W. (editor), Encyclopedia of Oceanography, Reinhold Publishing Corp., New York, 911, 1966.

22. Henson, E. B., Bradshaw, A. S., and Chandler, D. C., "The Physical Limnology of Cayuga Lake, New York," Memoir 378, Agricultural Experimental Station, Cornell University, Ithaca, New York (1961).

23. Dutton, J. A. and Bryson, R. A., "Heat Flux in Lake Mendota," Limnol. Oceanog. 7, 1, 80, (Jan. 1962).

24. Sverdup, H. U., Johnson, M. W., and Fleming, H. W., The Oceans, Prentice-Hall Inc., New York, 1942.

25. Robinson, A. R., Stommel, H., and Welander, P., "The Oceanic Thermocline," Tellus 11, 295 (1959).

26. Robinson, A. R. and Welander, P., "Thermal Circulation on a Rotating Sphere, with Applications to the Oceanic Thermocline," J. Marine Res. 21, 25 (1963).

27. Eckart, C., Hydrodynamics of Oceans and Atmospheres, Pergamon Press, New York, 1960.

28. Stommel, H., "A Survey of Ocean Current Theory," Deep-Sea Res. 4, 149 (1957).

29. Munk, W. H. and Anderson, E. R., "Notes on the Theory of the Thermocline," J. Marine Res. 1, 276 (1948).

30. Richardson, L. F., "The Supply of Energy From and To Atmospheric Eddies," Proc. Roy. Soc. A 97, 354 (1920).

31. Defant, A., Physical Oceanography, Pergamon Press, New York, 1961.

32. Priestley, C. H. B., Turbulent Transfer in the Lower Atmosphere, The University of Chicago Press, 1959.

33. Lumley, J. L. and Panofsky, H. A., The Structure of Atmospheric Turbulence, Interscience Publishers, New York, 1964.

34. Monin, A. S. and Obukhov, A. M., "Basic Regularity in Turbulent Mixing in the Surface Layer of the Atmosphere," USSR Acad. Sci. Works of Geophys. Met. No. 24, 163 (1954).

35. Ertel, H. E., "Theories der Thermischen Sprungschicht in Seen," Acta Hydrophys. 1, 151 (1954).

36. Dake, J. M. K. and Harleman, D. R. F., "Thermal Stratification in Lakes: Analytical and Laboratory Studies," Water Resources Research 5, 2, 484-495 (April 1969).

37. Li, T. Y., "Formation of Thermocline in Great Lakes," Paper presented at the 13th Conference on Great Lakes Research, Buffalo, New York, March 31-April 3, 1970.

38. Kraus, E. B. and Turner, J. S., "A One-Dimensional Model for the Seasonal Thermocline. II. The General Theory and its Consequences," Tellus 19, 1, 98-105 (1967).

39. Orlob, G. T., "A Mathematical Model of Thermal Stratification in Deep Reservoirs," Paper presented at the Annual Meeting of the American Fisheries Society, Portland, Oregon, 1965.

40. Orlob, G. T. et. al., "Mathematical Models for the Prediction of Thermal Energy Changes in Impoundments," Water Resources Engineers, Inc. (Dec. 1969).

41. Rawn, A. M., Bowerman, F. R., and Brooks, N. H., "Diffusers for Disposal of Sewage in Sea Water," Trans. Am. Soc. Civil Engrs. 94, 1036 (1961).

42. Hart, W. E., "Jet Discharges into a Fluid with a Density Gradient," Trans. Am. Soc. Civil Engrs. 94, 171 (1961).

43. Pearson, E. A., "Submarine Waste Disposal Installations," Sixth International Conference on Coastal Engineering, University of Florida, Dec. 1957.

44. Camp, T. R., Water, and its Impurities, Reinhold Publishing Corp., New York, 332, 1963.

45. Brooks, N. H., "Controlling Ocean Pollution," Engineering and Science, Calif. Inst. of Tech., 13 (March 1966).

46. Rawn, A. M. and Palmer, H. K., "Pre-determining the Extent of Sewage Field in Sea Water," Trans. Am. Soc. Civil Engrs. 94, 1036 (1930).

47. Abraham, G., "Jet Diffusion in a Liquid of Greater Density," Trans. Am. Soc. Civil Engrs. 86, 1 (1960).

48. Abraham, G., "Horizontal Jets in Stagnant Fluid of Other Density," Proc. Am. Soc. Civil Engrs. 91, 38 (1965).

49. Abraham, G., "Entrainment Principle and its Restrictions to Solve Problems of Jets," J. Hyd. Res. 3, 1 (1965).

50. Fan, L. N. and Brooks, N. H., "Turbulent Mixing Phenomena of Ocean Outfalls," Proc. Am. Soc. Civil Engrs. 92, 296 (1966).

51. Fan, L. N. and Brooks, N. H., "Discussions of Horizontal Jets in a Stagnant Fluid of Other Density," Proc. Am. Soc. Civil Engrs. 92, 423 (1966).

52. Fan, L. N., "Turbulent Buoyant Jets into Stratified or Flowing Ambient Fluids," Calif. Inst. of Tech. Rept. No. KH-R-15 (June 1967).

53. Bata, Geza L., "Recirculation of Cooling Water in Rivers and Canals," J. of Hydraulics Div., Proc. Am. Soc. Civil Engrs., Paper 1265, HY3, 1957.

54. Harleman, D. R. F., "Mechanics of Condenser Water Discharge from Thermal Power Plants," 144, Ref. 8 (1969).

55. Keulegan, G. H., "Interfacial Instability and Mixing in Stratified Flows," J. Res. Nat. Bur. Std. 43, 487.

56. Lofquist, Karl, "Flow and Stress Near an Interface between Stratified Liquids," Phys. Fluids 3, 3, 158 (1960).

57. Ellison, T. H. and Turner, J. W., "Turbulent Entrainment in Stratified Flows," J. Fluid Mech. 6, 423, (1959).

58. Ellison, T. H. and Turner, J. S., "Mixing of a Dense Fluid in a Turbulent Pipe Flow. Part I. Overall Description of the Flow," J. Fluid Mech. 8, 514 (1960).

59. Ellison, T. H. and Turner, J. S., "Mixing of Dense Fluid in a Turbulent Pipe Flow. Part II. Dependence of Transfer Coefficients on Local Stability," J. Fluid Mech. 8, 529 (1960).

60. Wedderburn, E. M. and Watson, W., "Observations with a Current Meter in Loch Ness," Proc. Roy. Soc. Edinburgh 29, 617-647, 1908.

61. Ruttner, F., Fundamentals of Limnology, 3rd ed., University of Toronto Press, 7-56, 1966.

62. Phillips, O. M., The Dynamics of the Upper Ocean, Cambridge University Press, 198-243, 1966.

63. Okubo, A., "A Review of Theoretical Models for Turbulent Diffusion in the Sea," Journal of the Oceanographic Society of Japan, 20th Anniversary Volume, 286-318 (1962).

64. Ichiye, T., "Oceanic Turbulence (Review)," Tech. Paper No. 2, Oceanographic Institute, Florida State University (1963).

65. Pritchard, D. W., "The Movement and Mixing of Contaminants in Tidal Estuaries," Proc. of the First International Conference on Waste Disposed on the Marine Environment, edited by E. A. Pearson, Pergamon Press, 512-525, 1960.

66. Kato, H. and Phillips, O. M., "On the Penetration of a Turbulent Layer into a Stratified Fluid," J. Fluid Mech. 37, 4, 643-655 (1969).

67. Schlichting, H., Boundary Layer Theory, 2nd ed., McGraw-Hill Book Co., New York, 477-480, 1955.

67a. Baker, D. J., A Technique for the Precise Measurement of Small Fluid Velocities," J. Fluid Mech. 26, 573 (1966).

68. Rossby, C. C. and Montgomery, B. R., "The Layer of Frictional Influence in Wind and Ocean Currents," Pap. Phys. Oceanogr. 3, 3, 101 (1935).

69. Holzman, B., "The Influence of Stability on Evaporation," N. Y. Acad. Sci. 44, 13, (1943).

70. Kent, R. E. and Pritchard, S. W., "A Test of Mixing Length Theories in a Coastal Plain Estuary," J. Marine Res. 18, 62-72 (1959).

71. Wedderburn, E. M., "Current Observations in Loch Garry," Proc. of the Royal Society of Edinburgh, 30, 312-323, 1910.

72. Johnson, H., "Wind Currents in Lake Klammingen," Int. Assn. of Scientific Hydrology, Assembly, Oslo, 367-372, August 19-28, 1948.

73. Mortimer, C. H., "Water Movements in Lakes During Summer Stratification; Evidence from the Distribution of Temperature in Windermere," Phil. Trans. Roy. Soc. London, 236 B, 355-404 (1952).

74. Harleman, D. R. F., "Stratified Flow," Handbook of Fluid Dynamics (ed. V. L. Streeter), McGraw-Hill Book Company, New York, 26-1, 1961.

75. McEwen, G. F., "A Mathematical Theory of the Vertical Distribution of Temperature and Salinity in Water under the Action of Radiation Conduction, Evaporation and Mixing Due to the Resulting Convection -- Derivation of a General Theory and Illustrative Numerical Applications to a Tank, a Lake, and a Region of the North Pacific Ocean," Bull. Scripps Instn. Oceanogr. Tech. 2, 197 (1929).

76. Sundaram, T. R. and Rehm, R. G., "Formation and Maintenance of Thermoclines in Stratified Lakes Including the Effects of Power-Plant Thermal Discharges," AIAA Paper No. 70-238, American Institute of Aeronautics and Astronautics, New York (1970).

77. Turner, J. S. and Kraus, E. B., "A One-Dimensional Model of the Seasonal Thermocline. I. A Laboratory Experiment and its Interpretation," Tellus 19, 1, 88-97 (1967).

78. Birge, E. A., "The Work of the Wind in Warming a Lake," Trans. Wis. Acad. Sci. Arts Letters 18, 341 (1916).

79. Turner, J.S., "Buoyant Plumes and Thermals" Annual Reviews in Fluid Mechanics, Vol. I (ed: W. R. Sears and M. VanDyke) p. 29, Annual Reviews Inc. California, 1969.

80. Elliot, W. P., "A Comparison of Some Approaches to the Diobatic Wind Profile" Teane. Am. Geophy. Unia. 38, 21, 1957.

81. Crank, J., The Mathematics of Diffusion, Oxford University Press, London, 1956.

82. Richtmyer, R. D. and Morton, K. W., Difference Methods for Initial-Value Problems, Second Edition, Interscience Publishers, New York, 1967.

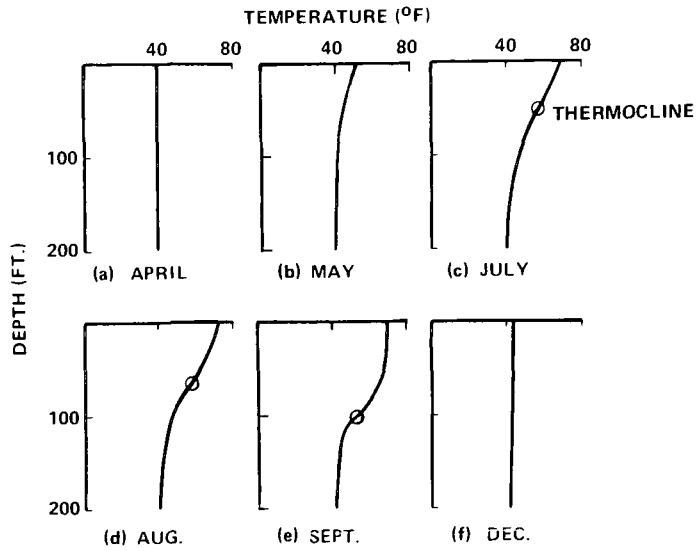

Figure 1 TEMPERATURE STRUCTURE OF CAYUGA LAKE, 1952
(AFTER HENSON, ET. AL. REF. 22)

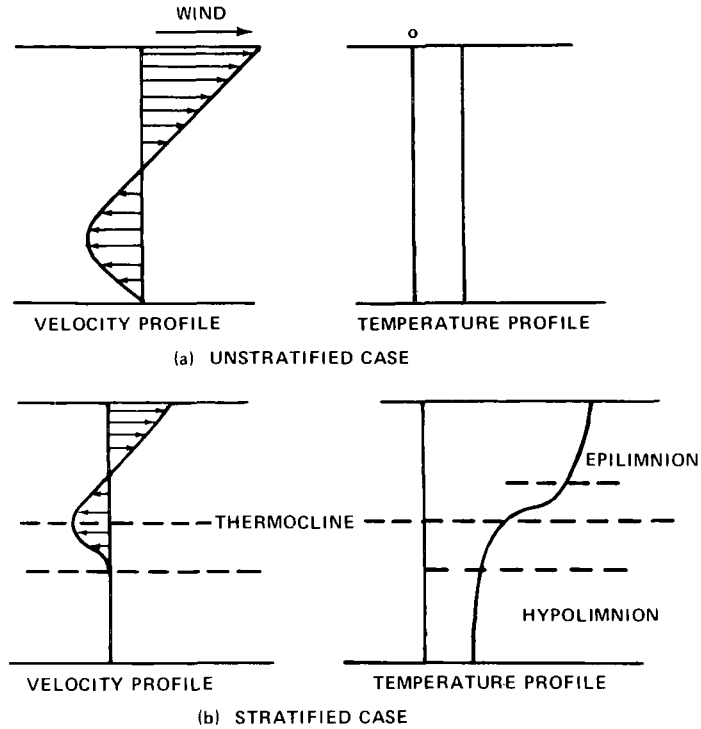

Figure 2 WIND-INDUCED CURRENTS IN A LAKE

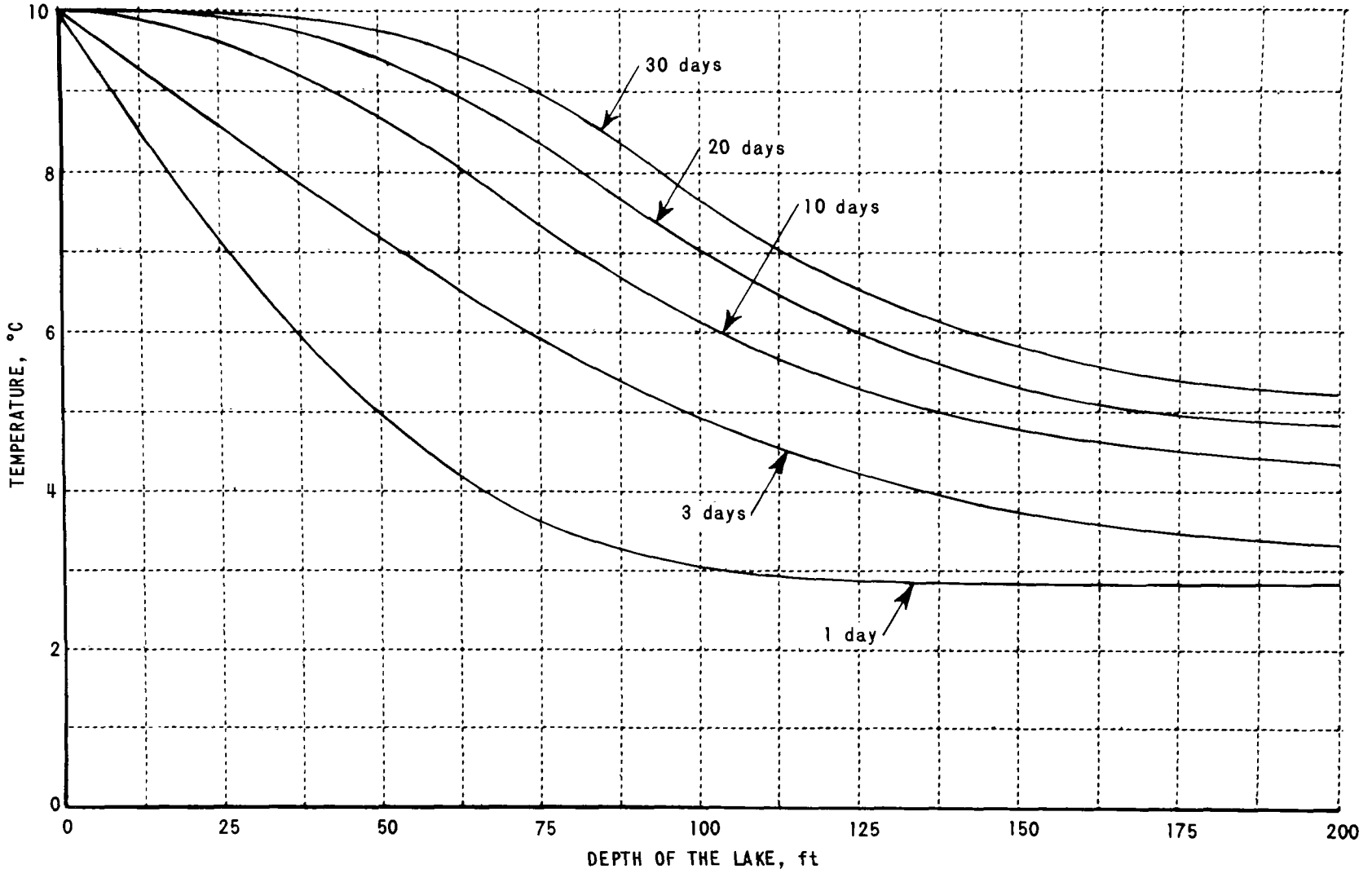

Figure 3 VERTICAL TEMPERATURE DISTRIBUTIONS FOR A CONSTANT SURFACE TEMPERATURE

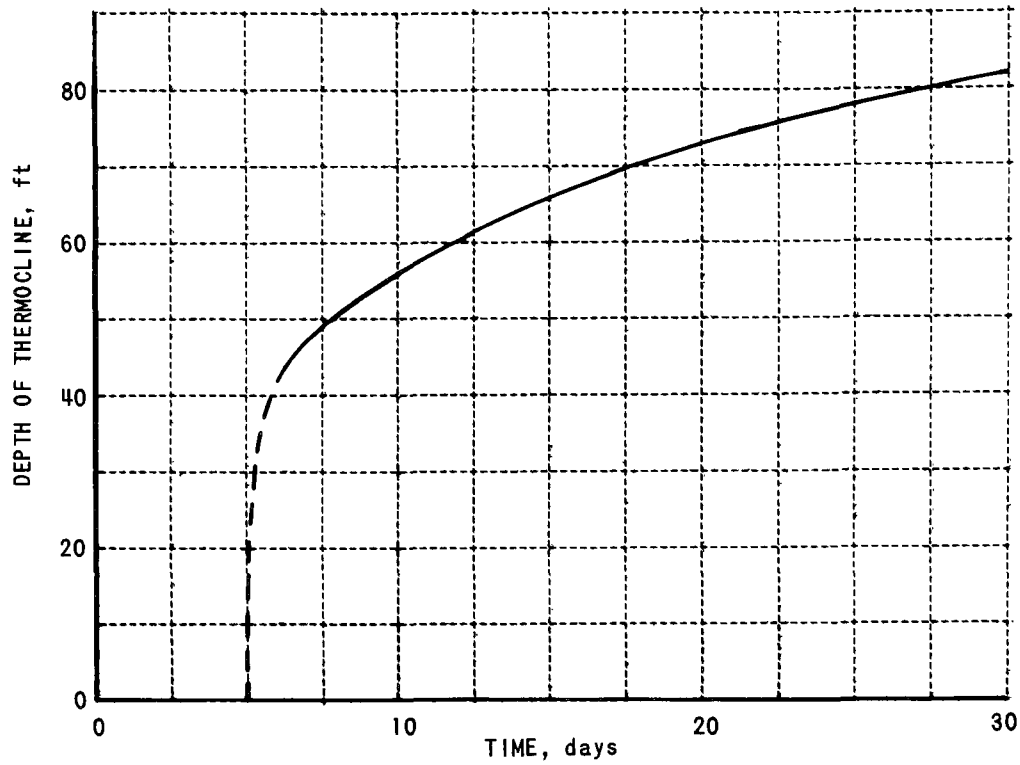

Figure 4 VARIATION OF THE DEPTH OF THE THERMOCLINE FOR A CONSTANT SURFACE TEMPERATURE

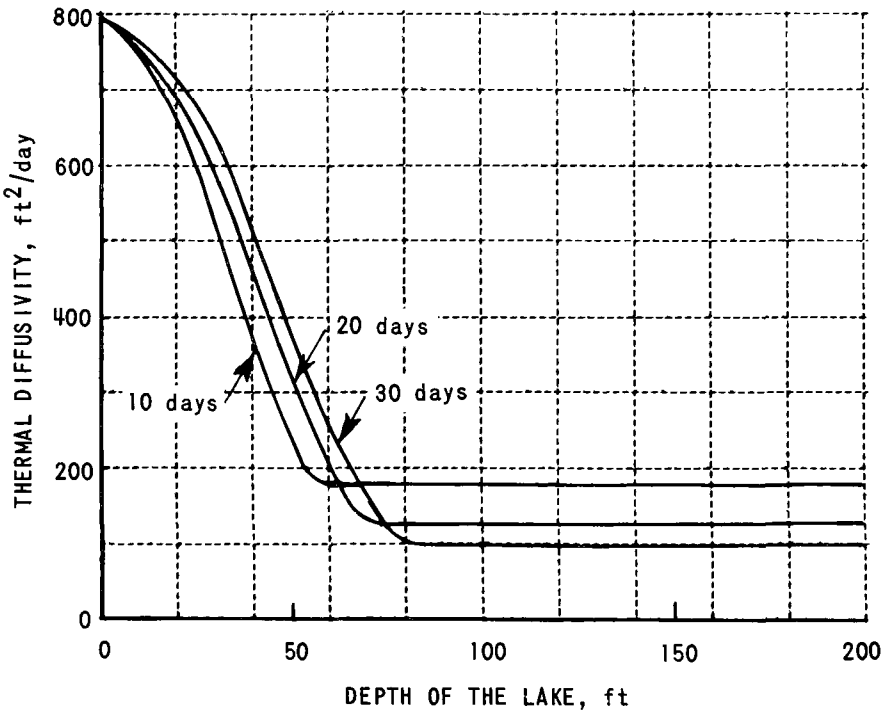

Figure 5 DISTRIBUTION OF THERMAL DIFFUSIVITY FOR A CONSTANT SURFACE TEMPERATURE

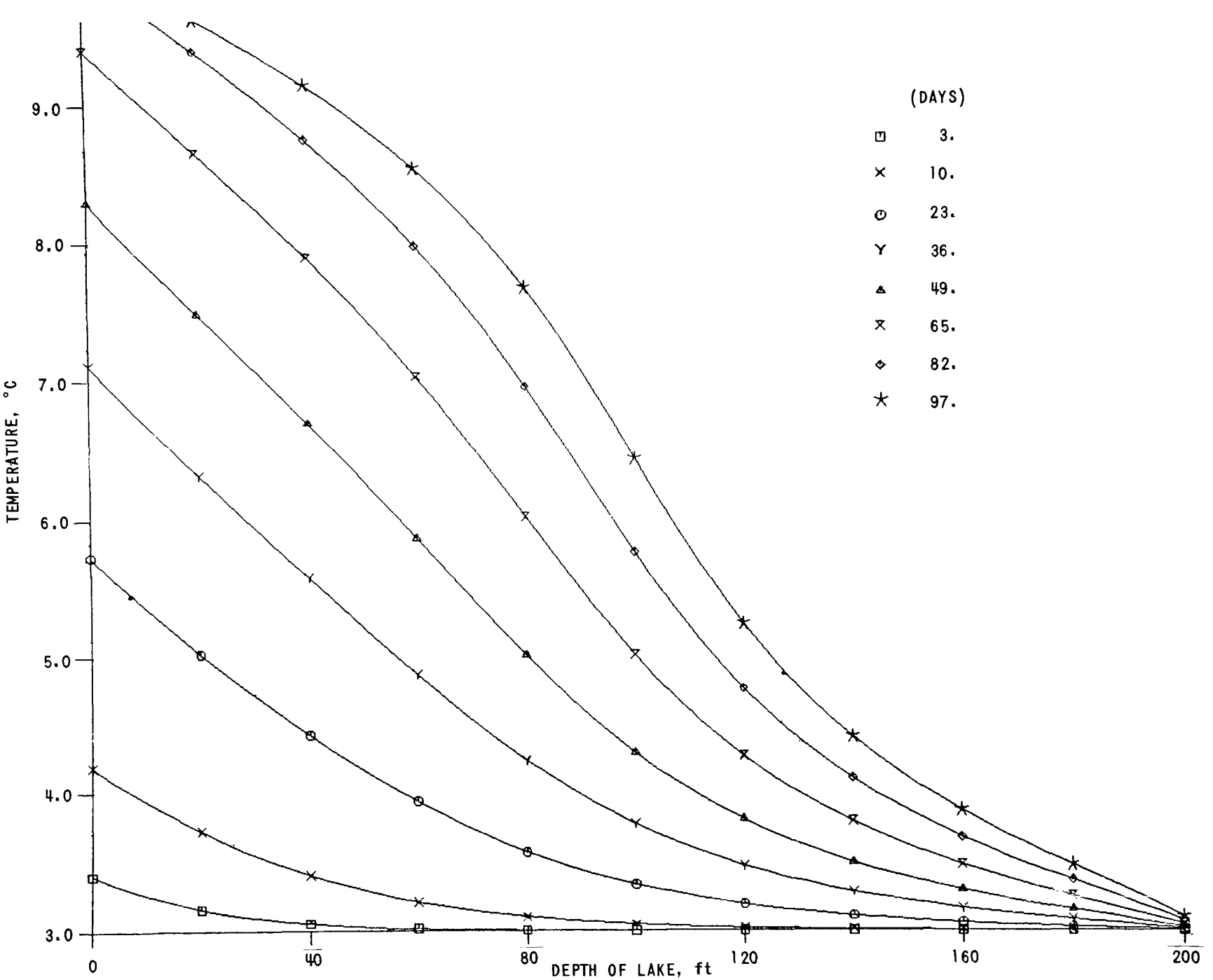

Figure 6 VERTICAL TEMPERATURE DISTRIBUTION FOR A SINUSOIDAL SURFACE TEMPERATURE

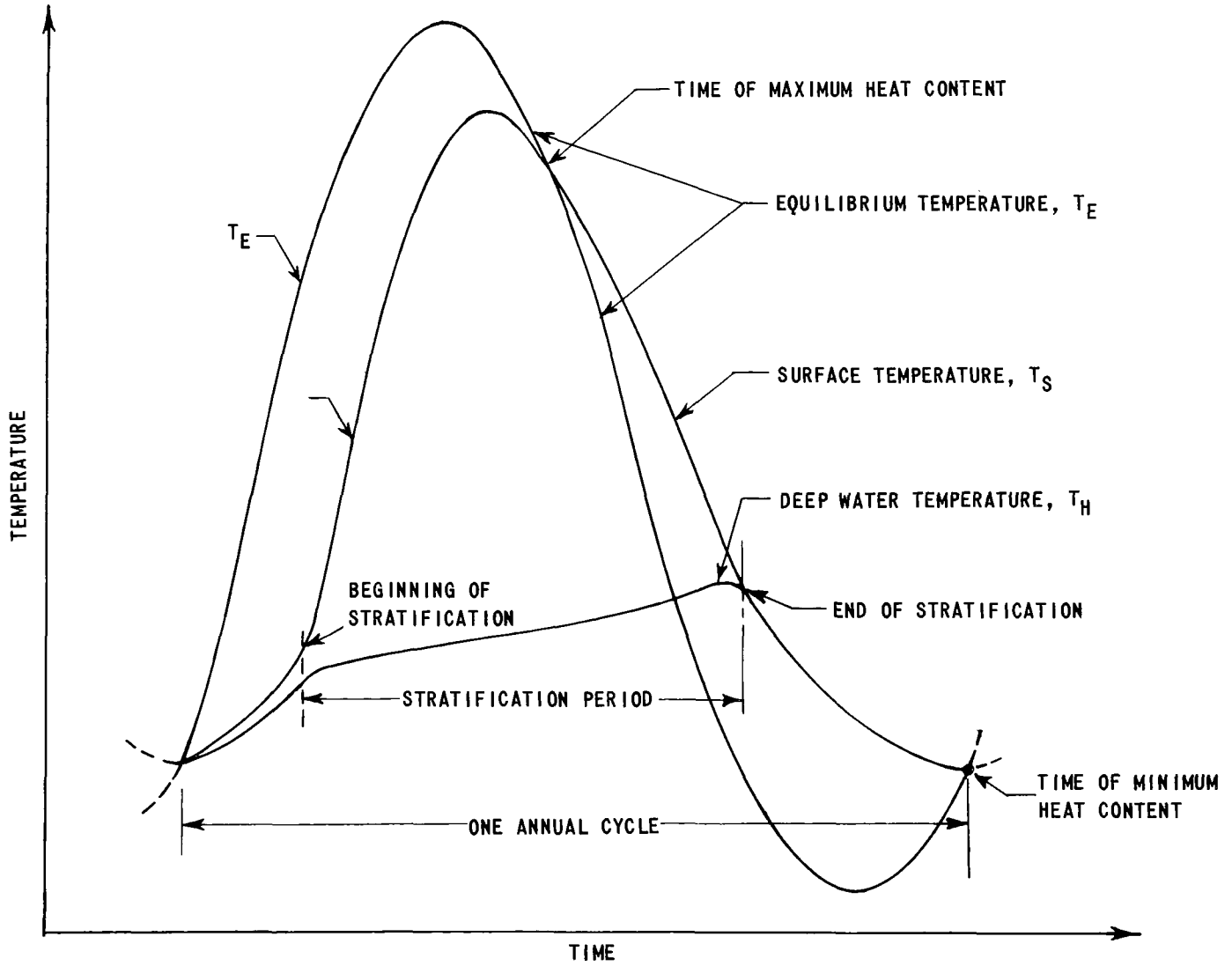

Figure 7 SCHEMATIC REPRESENTATION OF THE ANNUAL TEMPERATURE CYCLE

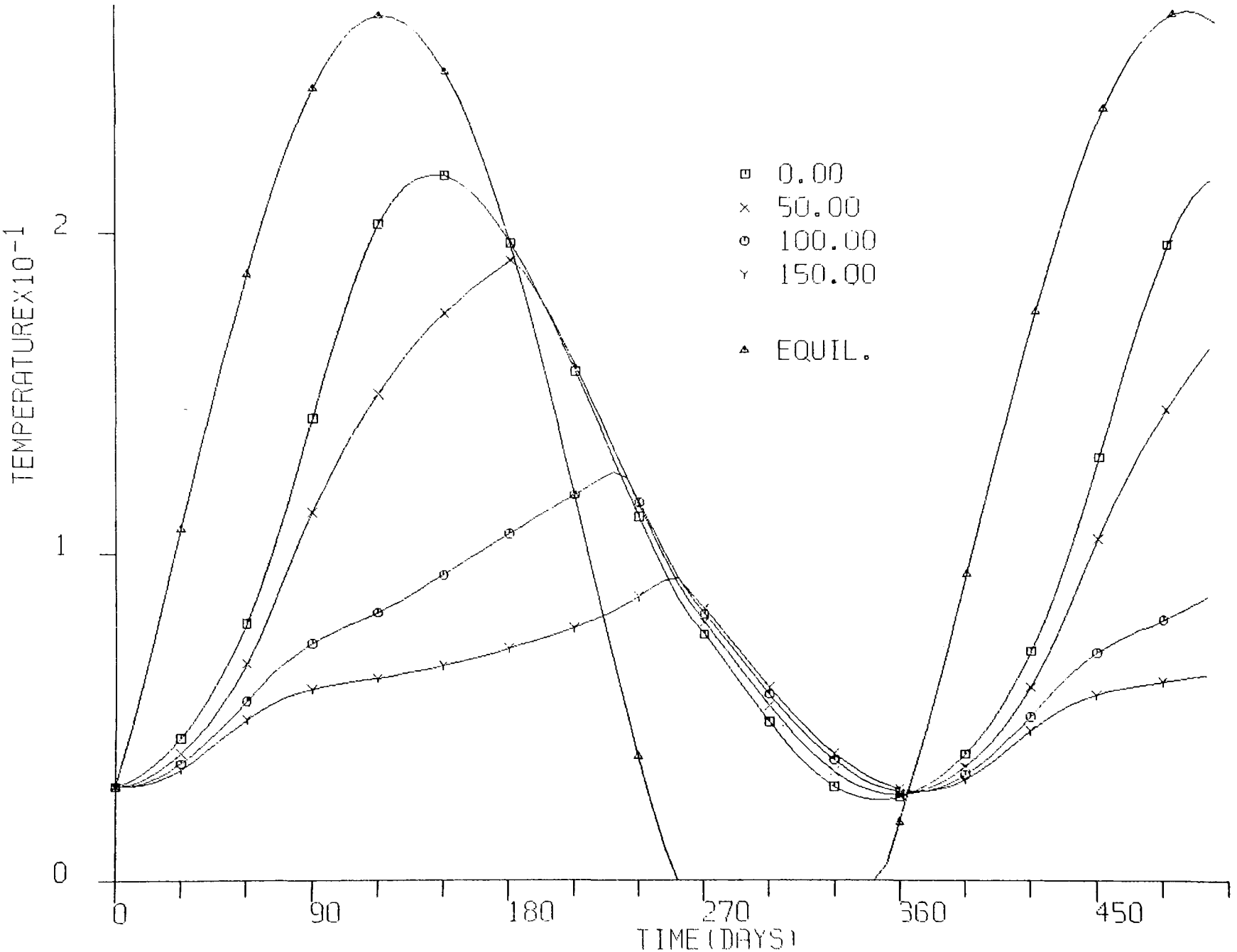

Figure 8 THE STRATIFICATION CYCLE

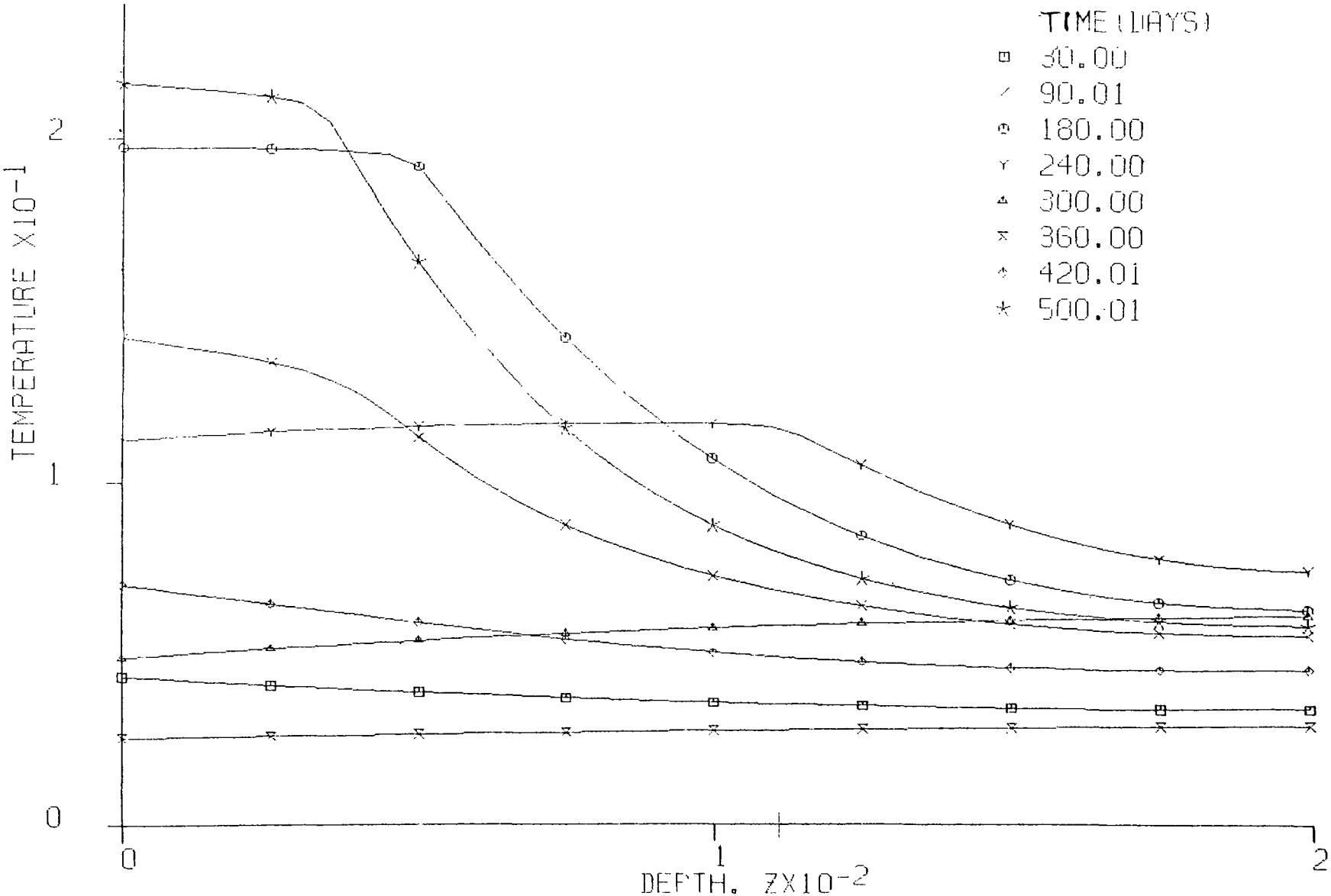

Figure 9 VERTICAL TEMPERATURE DISTRIBUTIONS

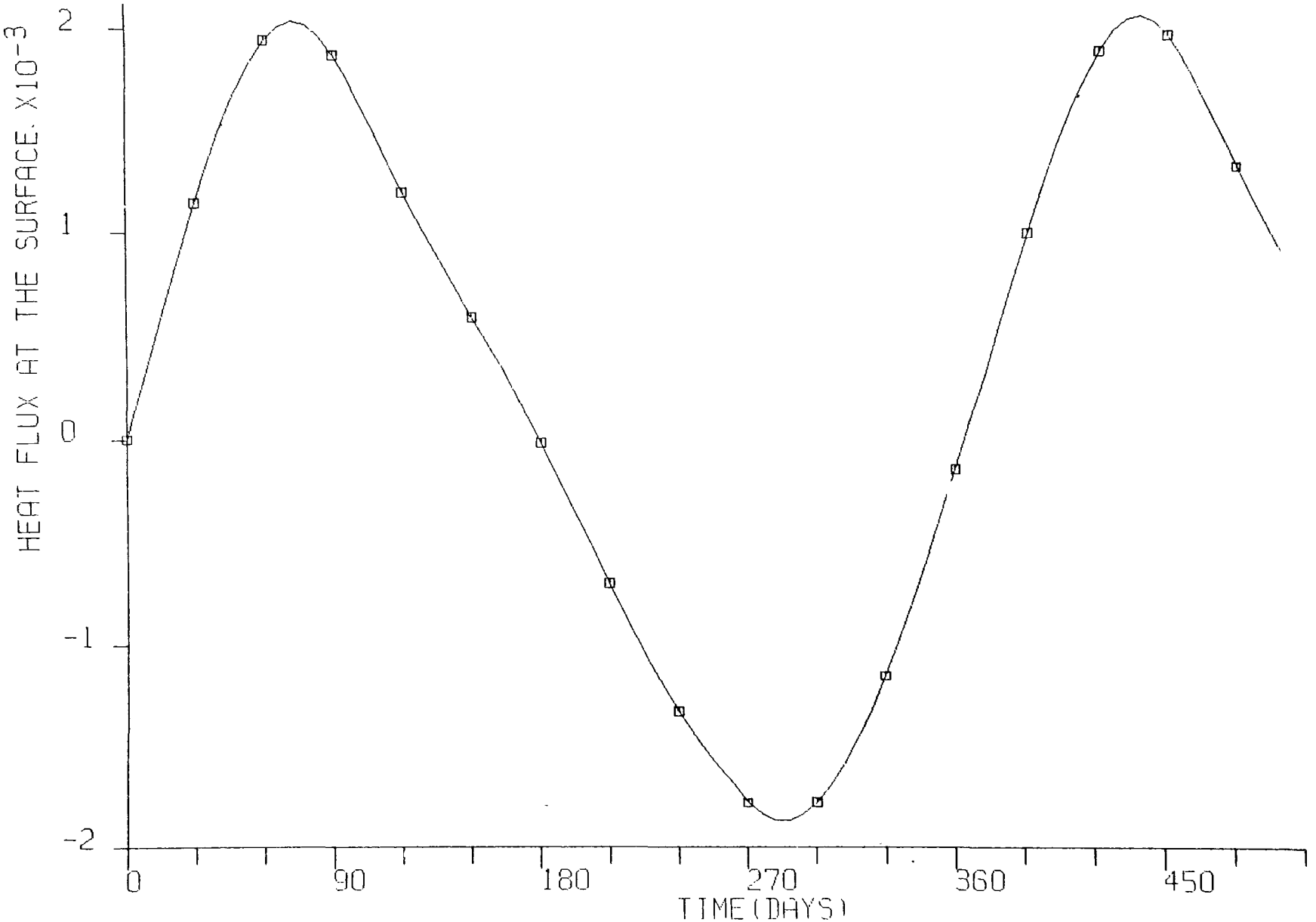

Figure 10 SEASONAL VARIATION OF SURFACE HEAT FLUX

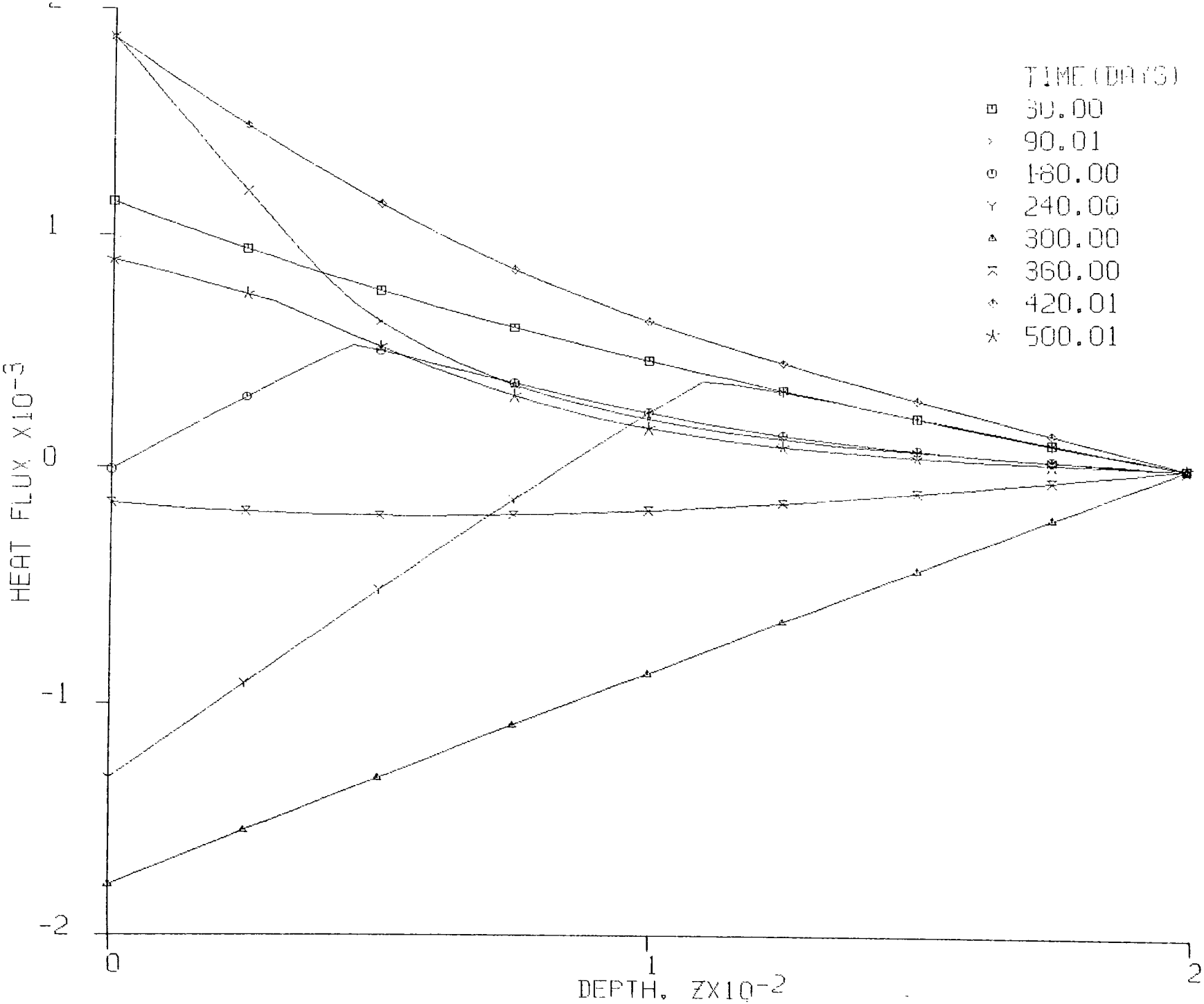

Figure 11 VERTICAL DISTRIBUTIONS OF HEAT FLUX

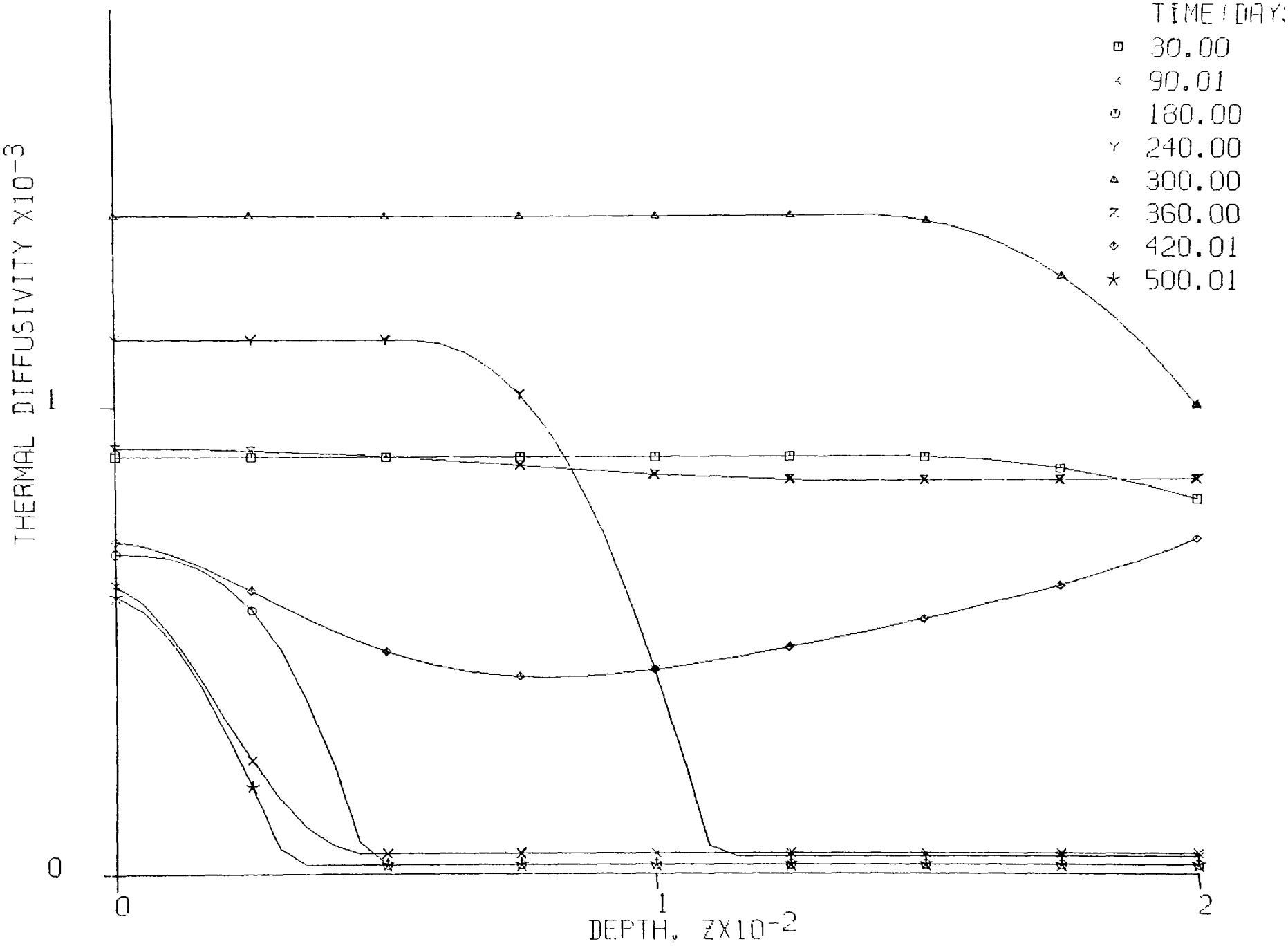

Figure 12 VERTICAL DISTRIBUTIONS OF THE THERMAL DIFFUSIVITIES

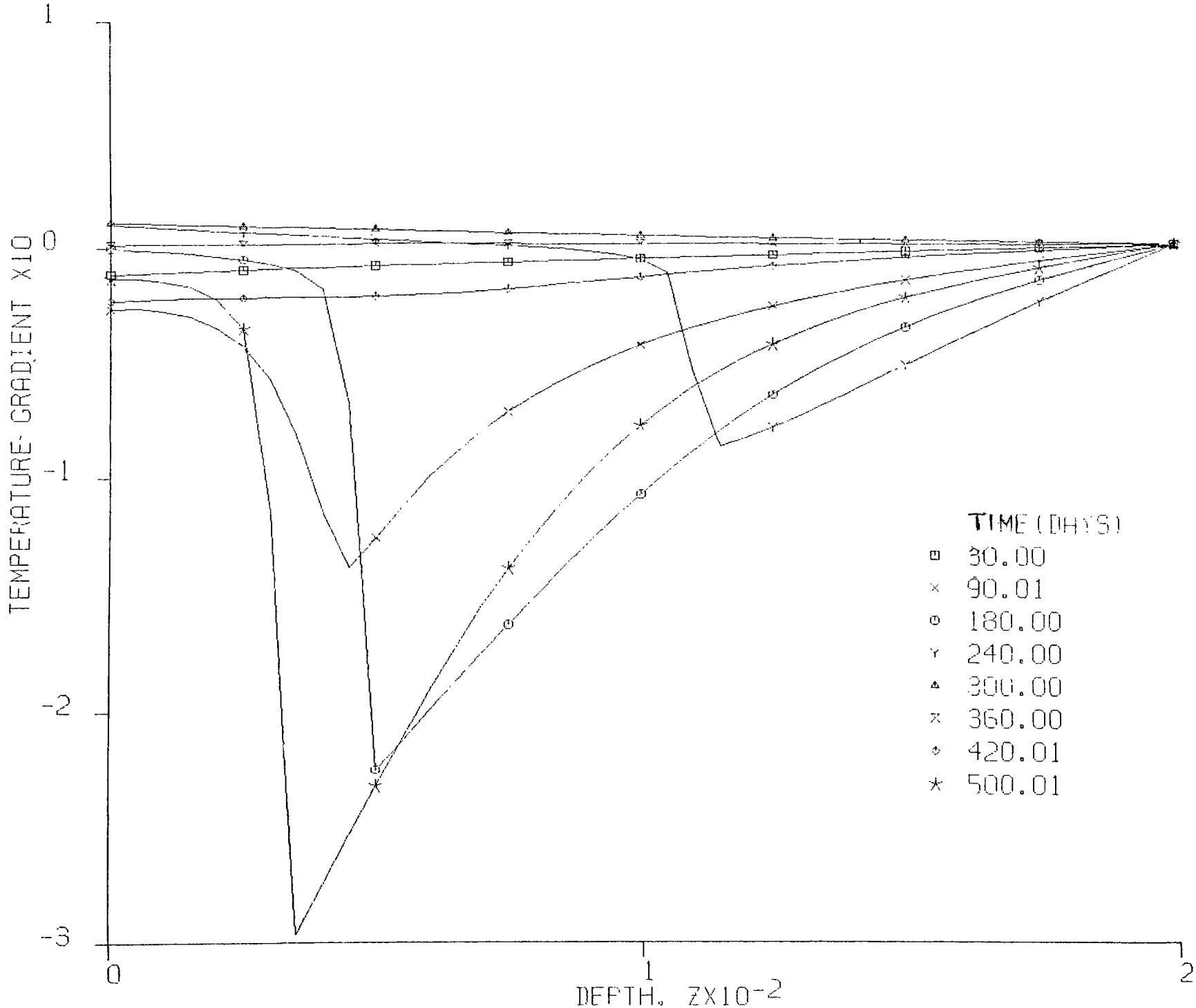

Figure 13 VERTICAL DISTRIBUTION OF TEMPERATURE GRADIENTS

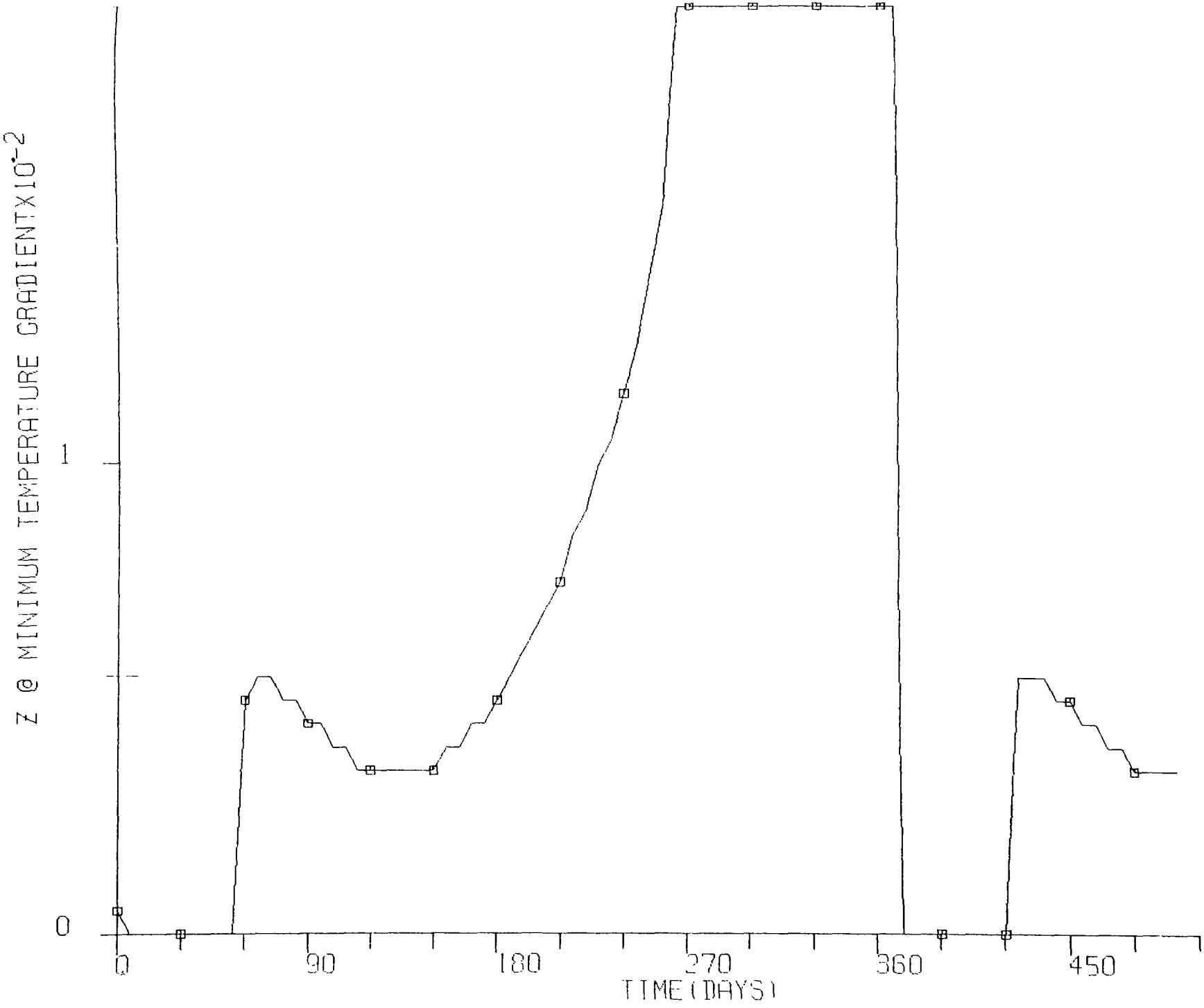

Figure 14 SEASONAL VARIATION OF THE THERMOCLINE DEPTH

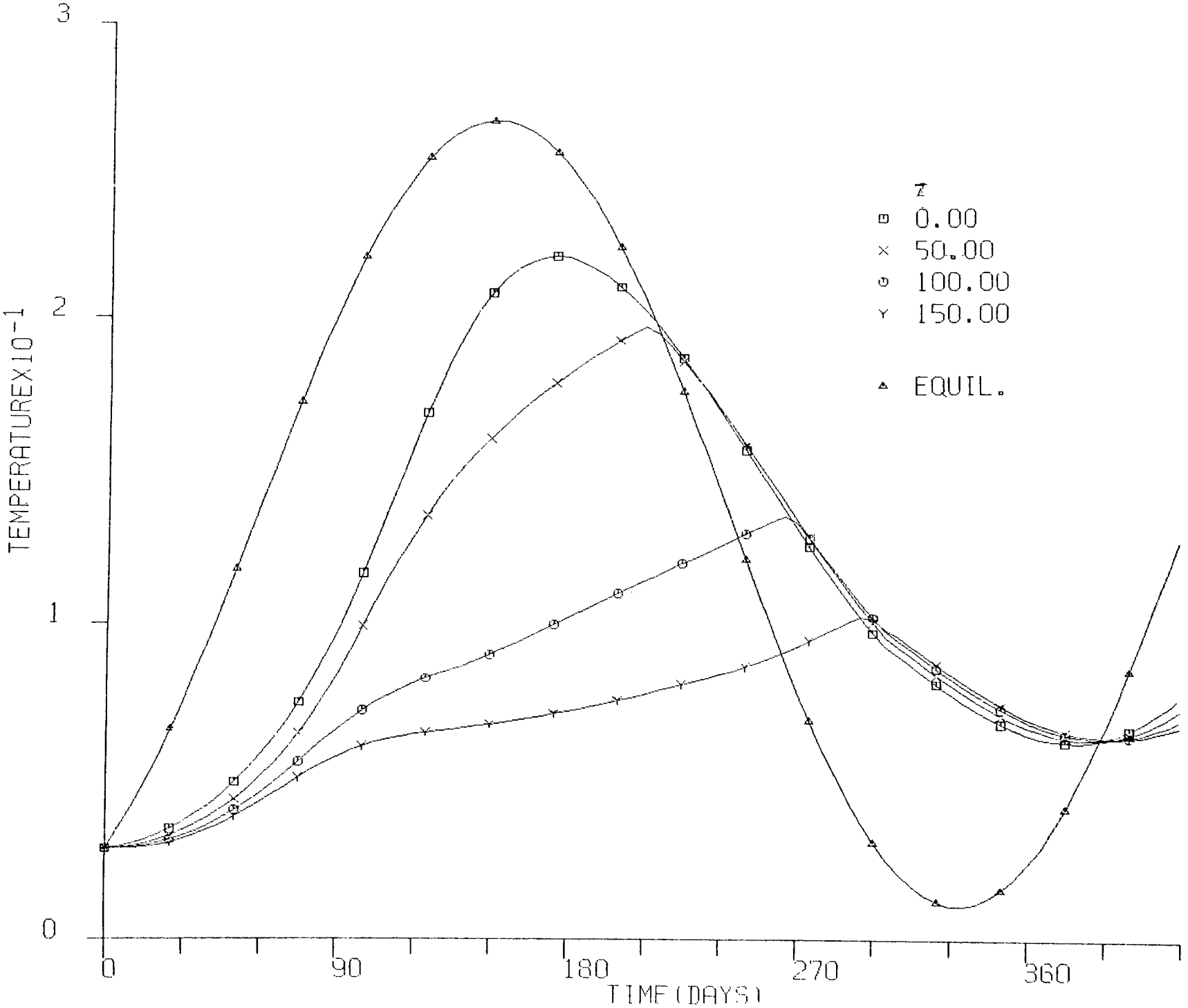

Figure 15 EFFECT OF IMPROPER INITIAL CONDITIONS

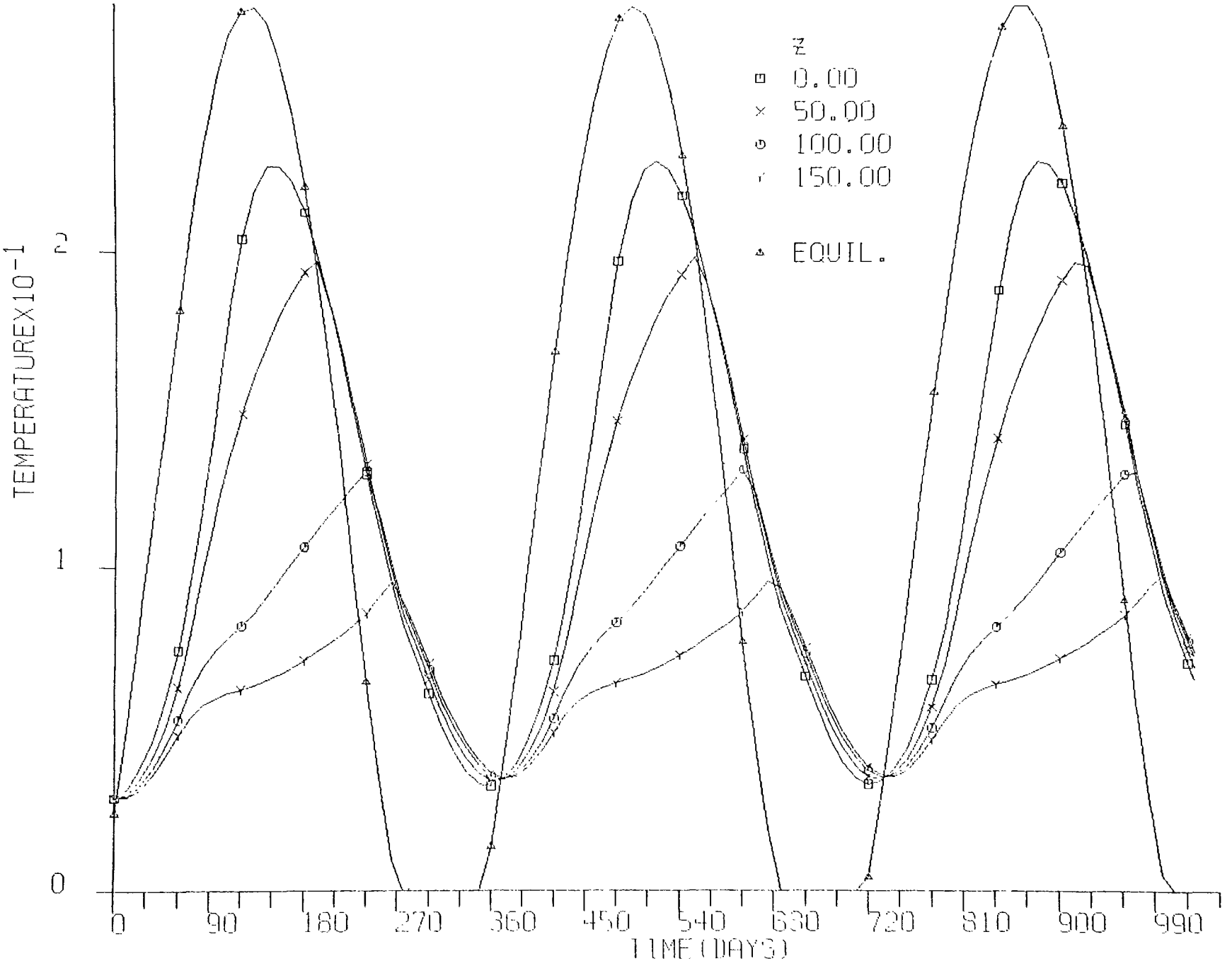

Figure 16 CYCLIC BEHAVIOR OF THE TEMPERATURE VARIATIONS

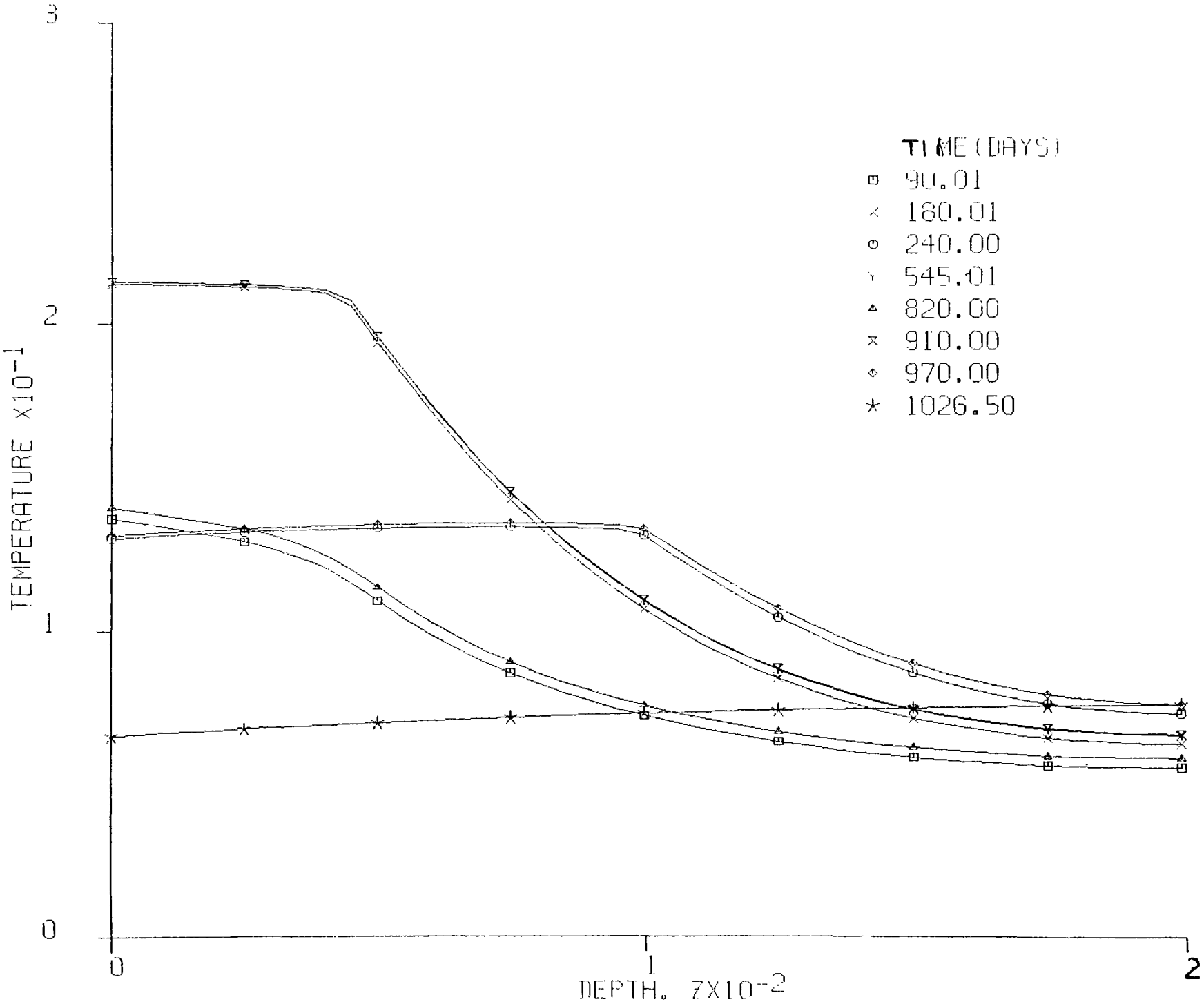

Figure 17 CYCLIC BEHAVIOR OF THE TEMPERATURE DISTRIBUTIONS

THERMAL DIFFUSIVITY X10-3
1
0
0
1
2
DEPTH, ZX10-2
TIME(DAYS)
90.01
180.01
240.00
545.01
820.00
910.00
970.00
1026.50

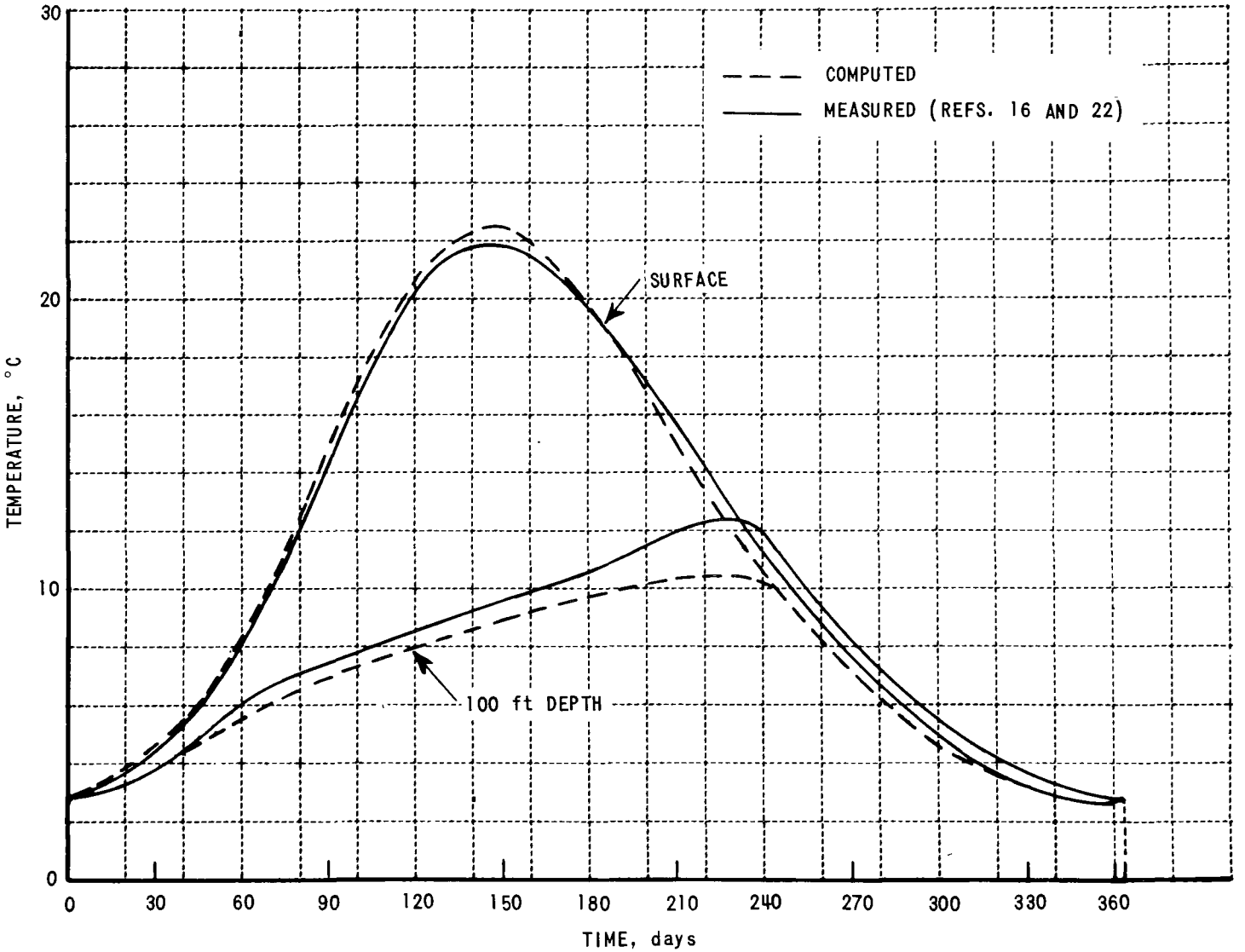

Figure 19 COMPARISON OF THE COMPUTED AND OBSERVED STRATIFICATION CYCLES OF CAYUGA LAKE, NEW YORK

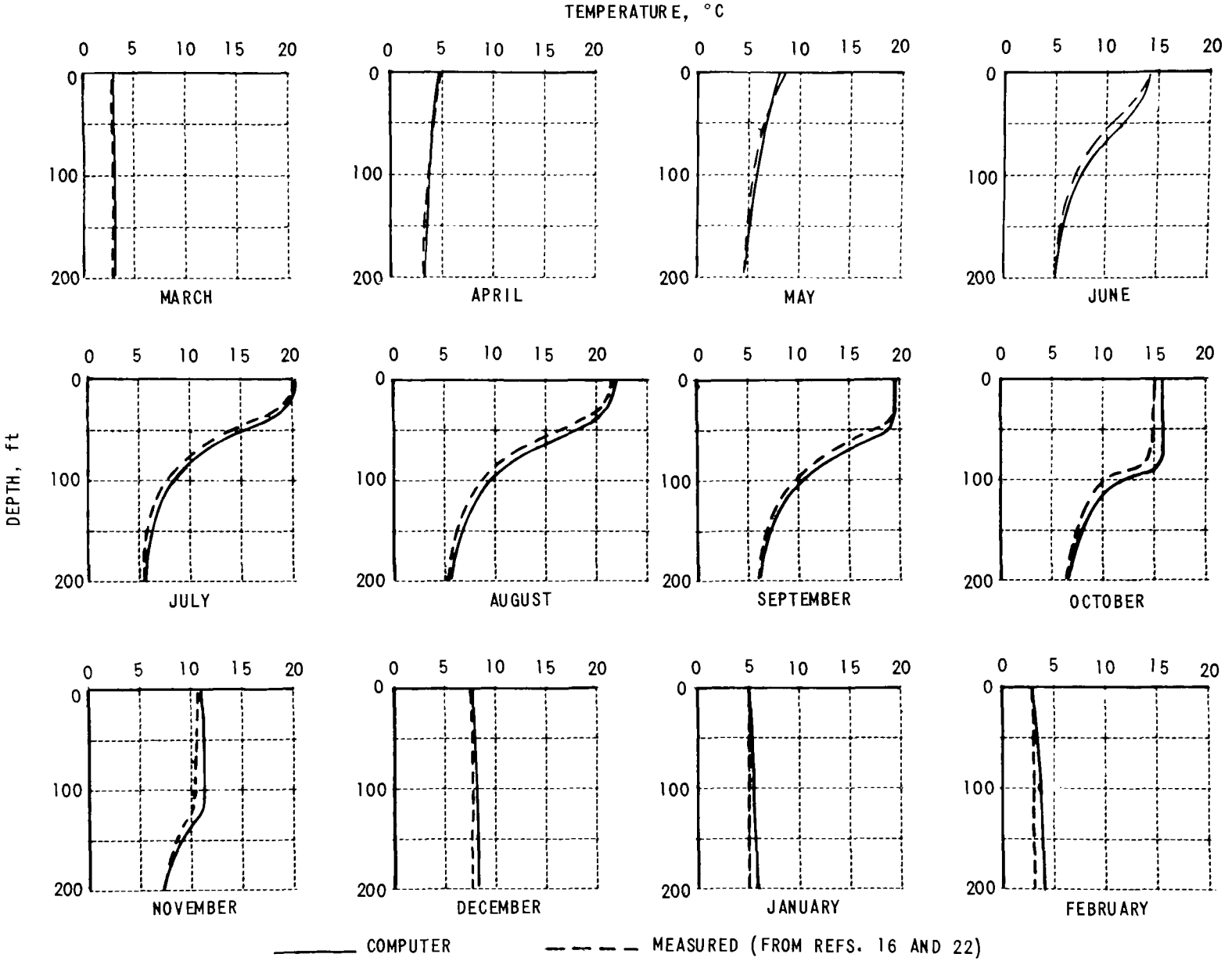

Figure 20 COMPARISON OF THE COMPUTED AND OBSERVED TEMPERATURE PROFILES FOR CAYUGA LAKE, NEW YORK

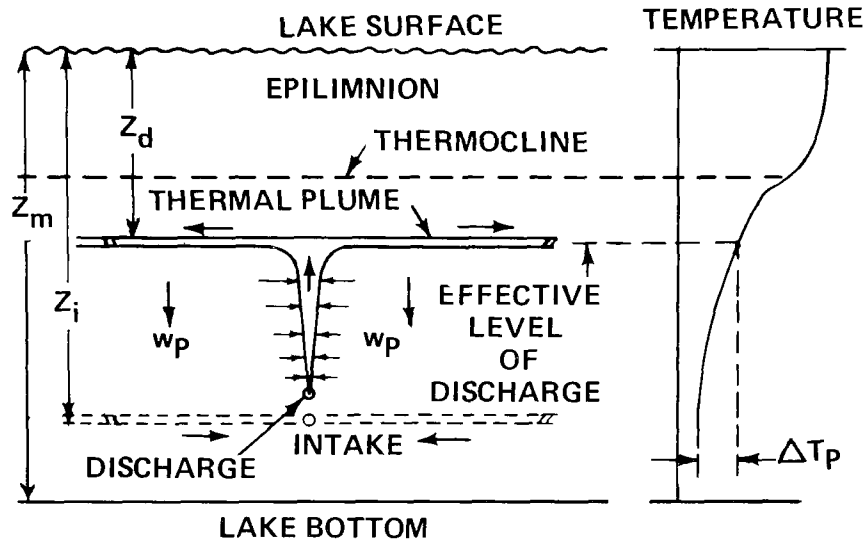

Figure 21a SCHEMATIC REPRESENTATION OF THE THERMAL PLUME

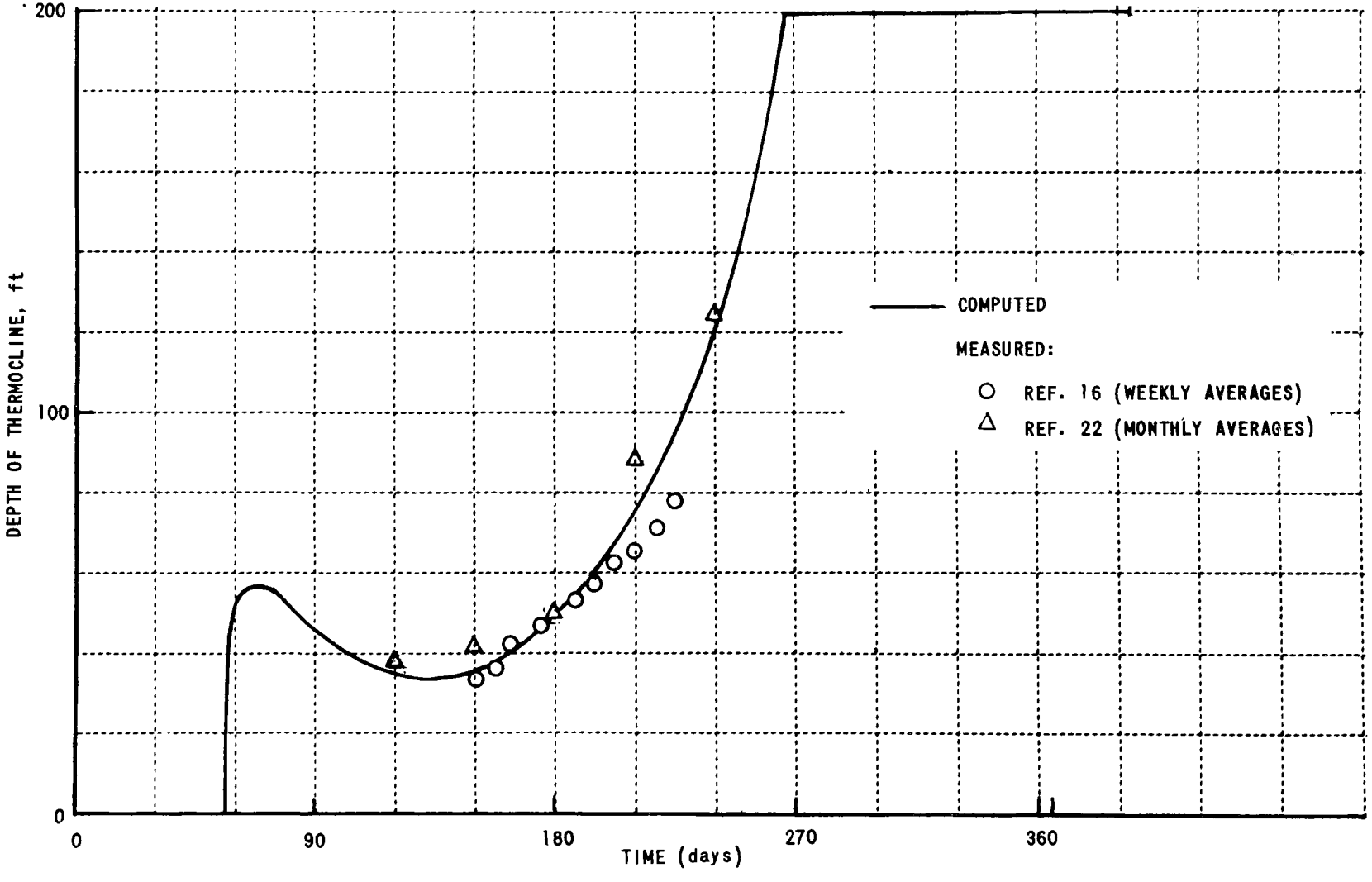

Figure 21b COMPARISON OF MEASURED AND OBSERVED THERMOCLINE DEPTHS FOR CAYUGA LAKE, NEW YORK

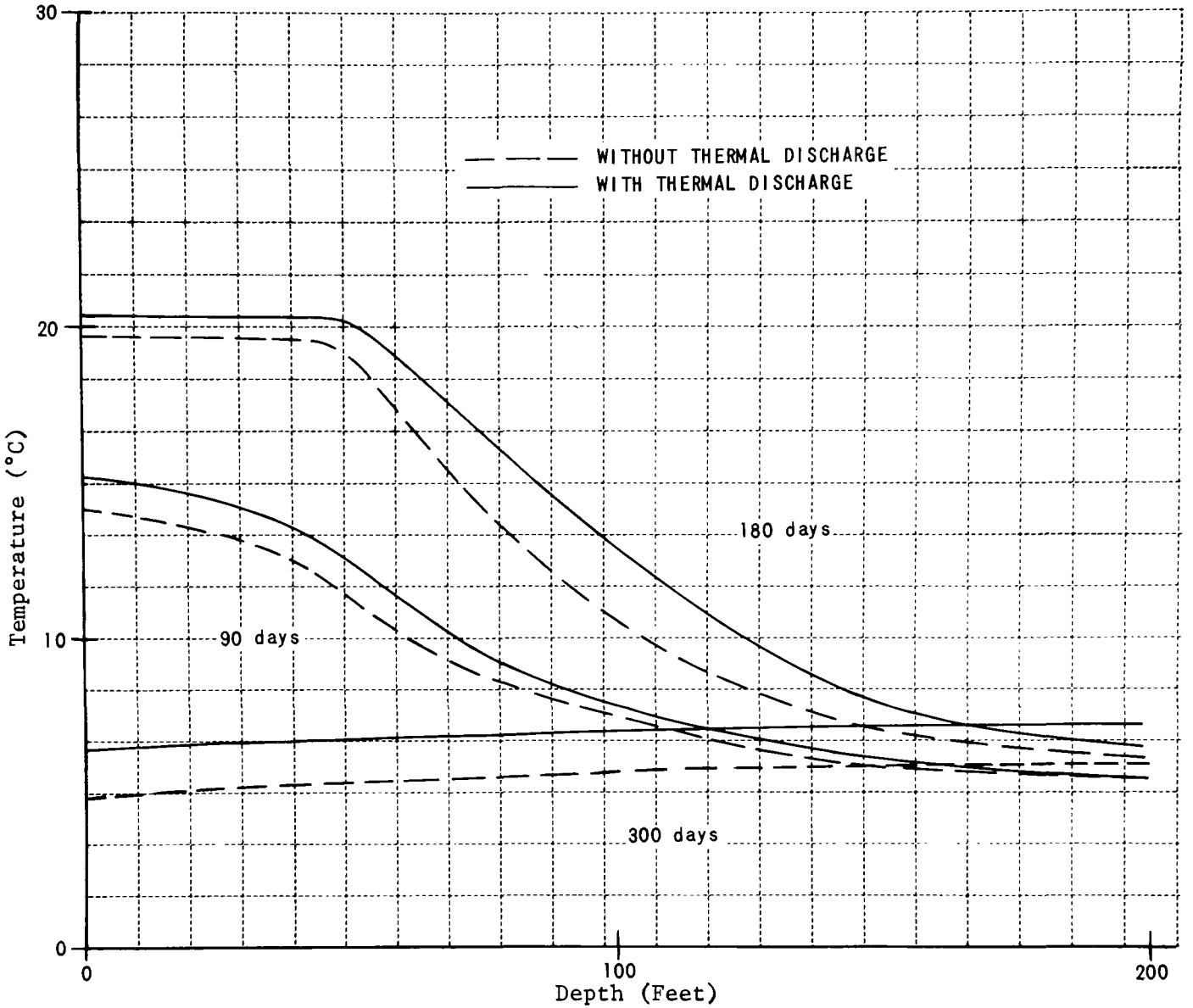

Figure 22 EFFECT OF THERMAL DISCHARGE ON VERTICAL TEMPERATURE DISTRIBUTION

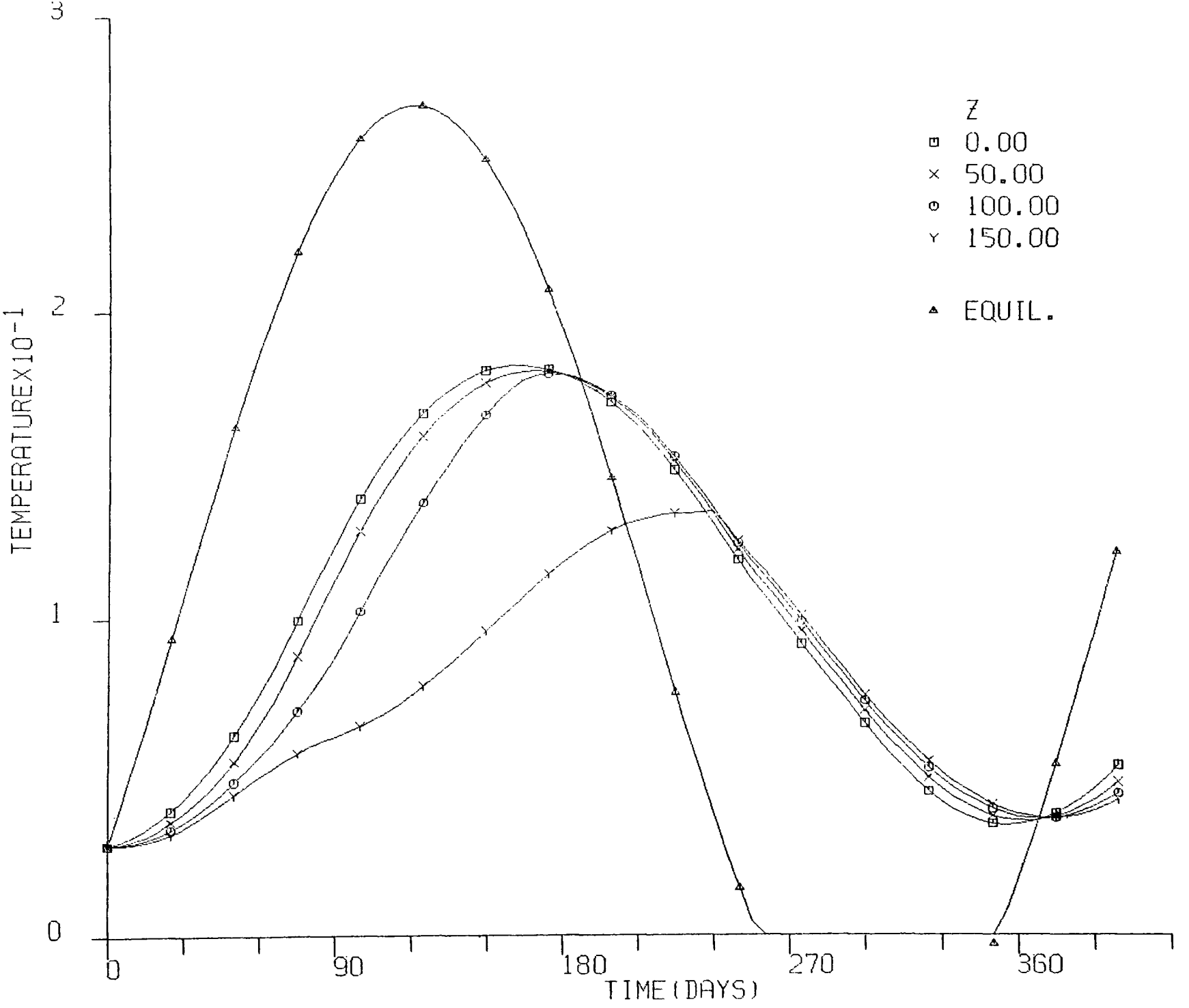

Figure 23 EFFECT OF PUMPING ON TEMPERATURE CYCLE

Z @ MINIMUM TEMPERATURE GRADIENTX10^{-2}
2
1
0
0
90
180
270
360
TIME(DAYS)

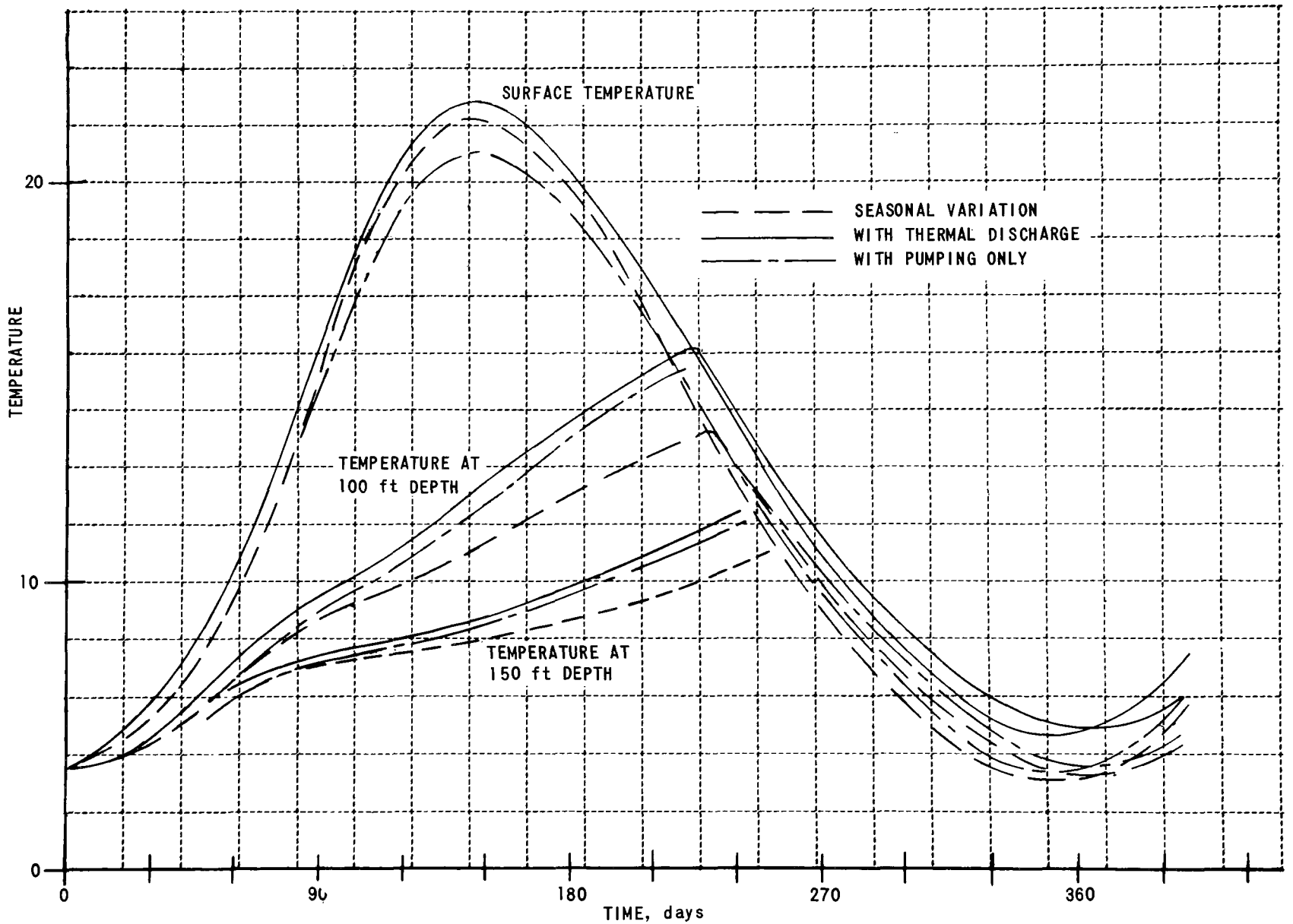

Figure 25 EFFECTS OF THERMAL DISCHARGE AND OF PUMPING ALONE ON STRATIFICATION CYCLE

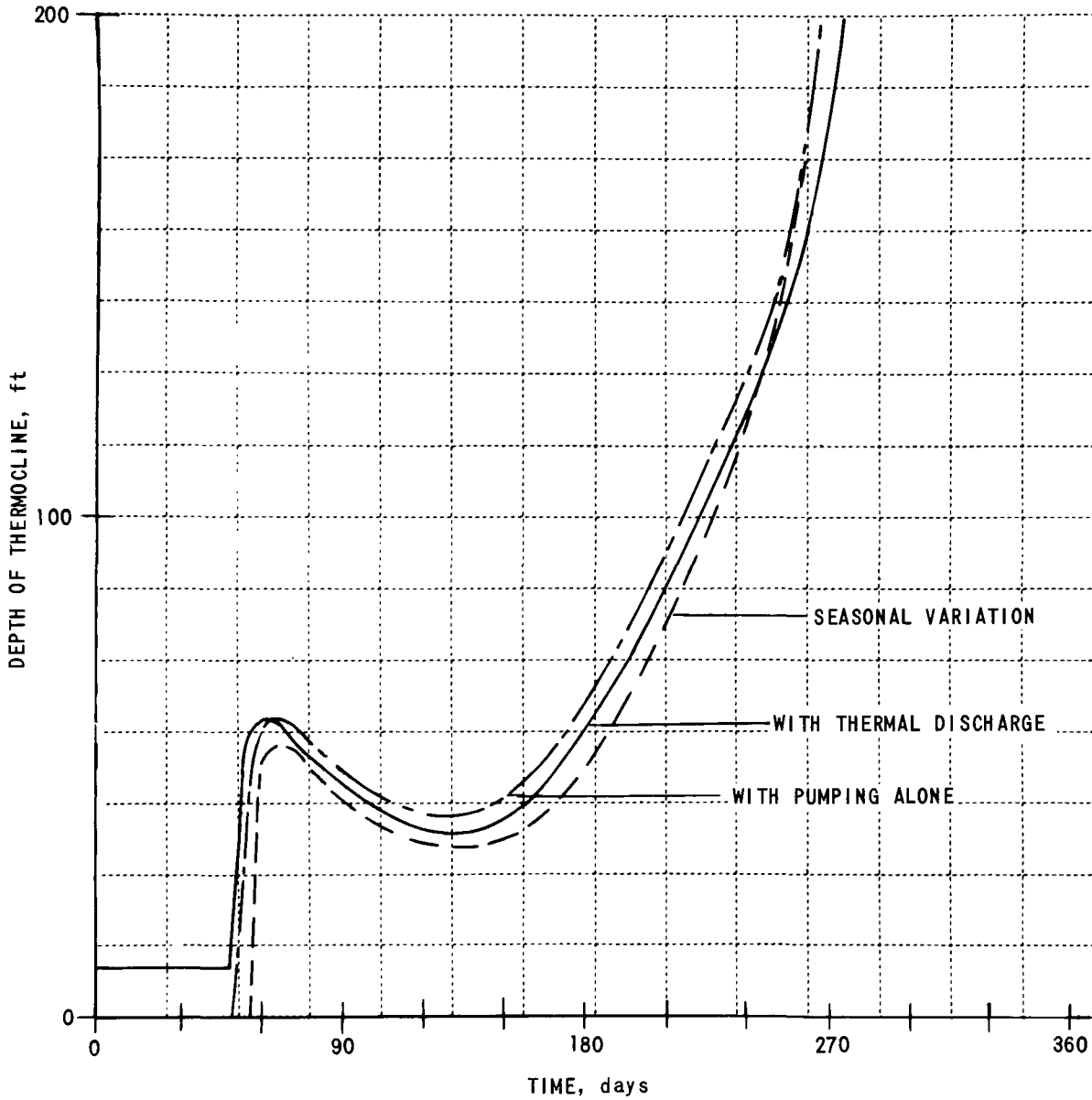

Figure 26 EFFECTS OF THERMAL DISCHARGE AND OF PUMPING ALONE ON DEPTH OF THERMOCLINE

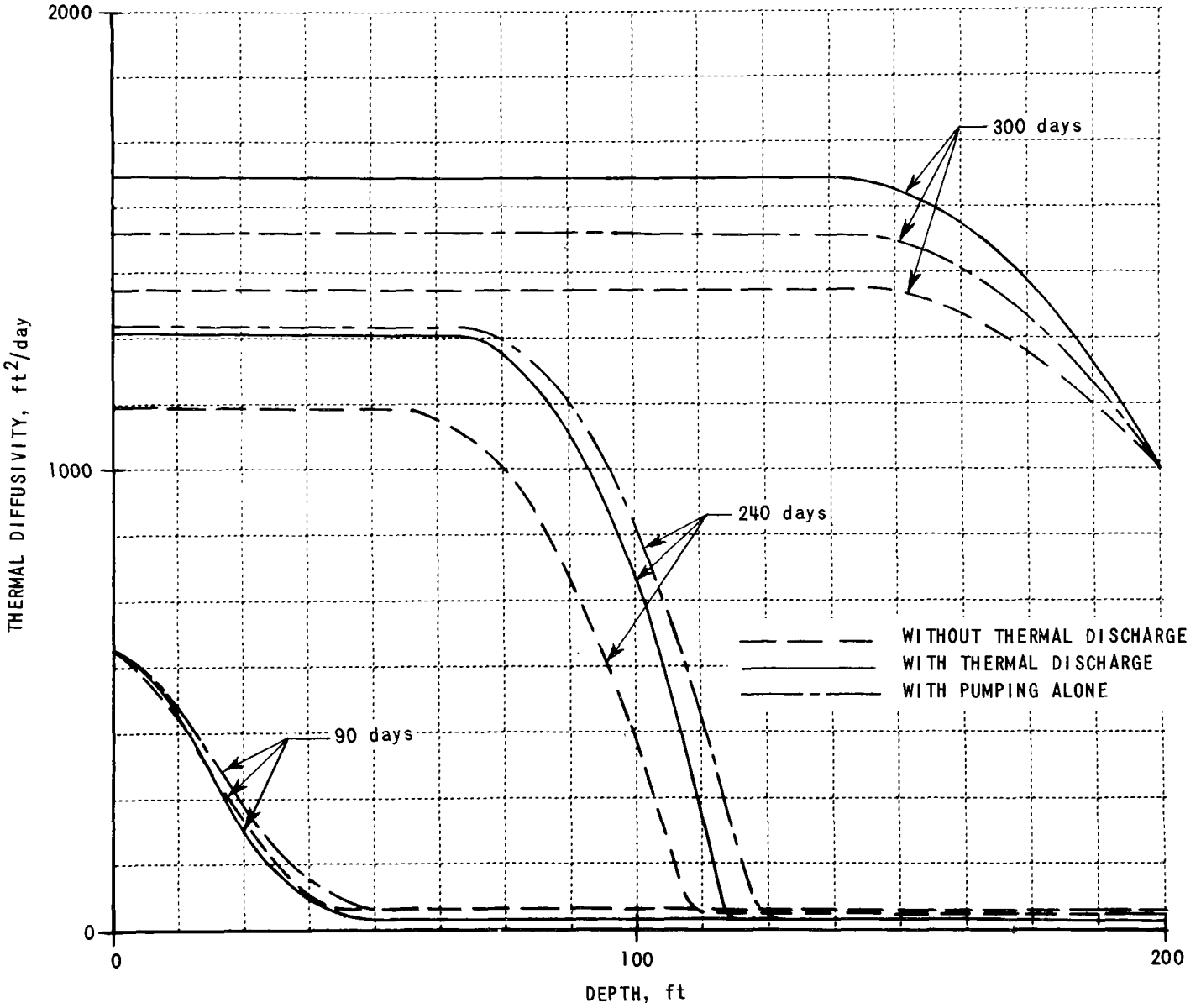

Figure 27 EFFECT OF THERMAL DISCHARGE AND PUMPING ON THERMAL DIFFUSIVITY

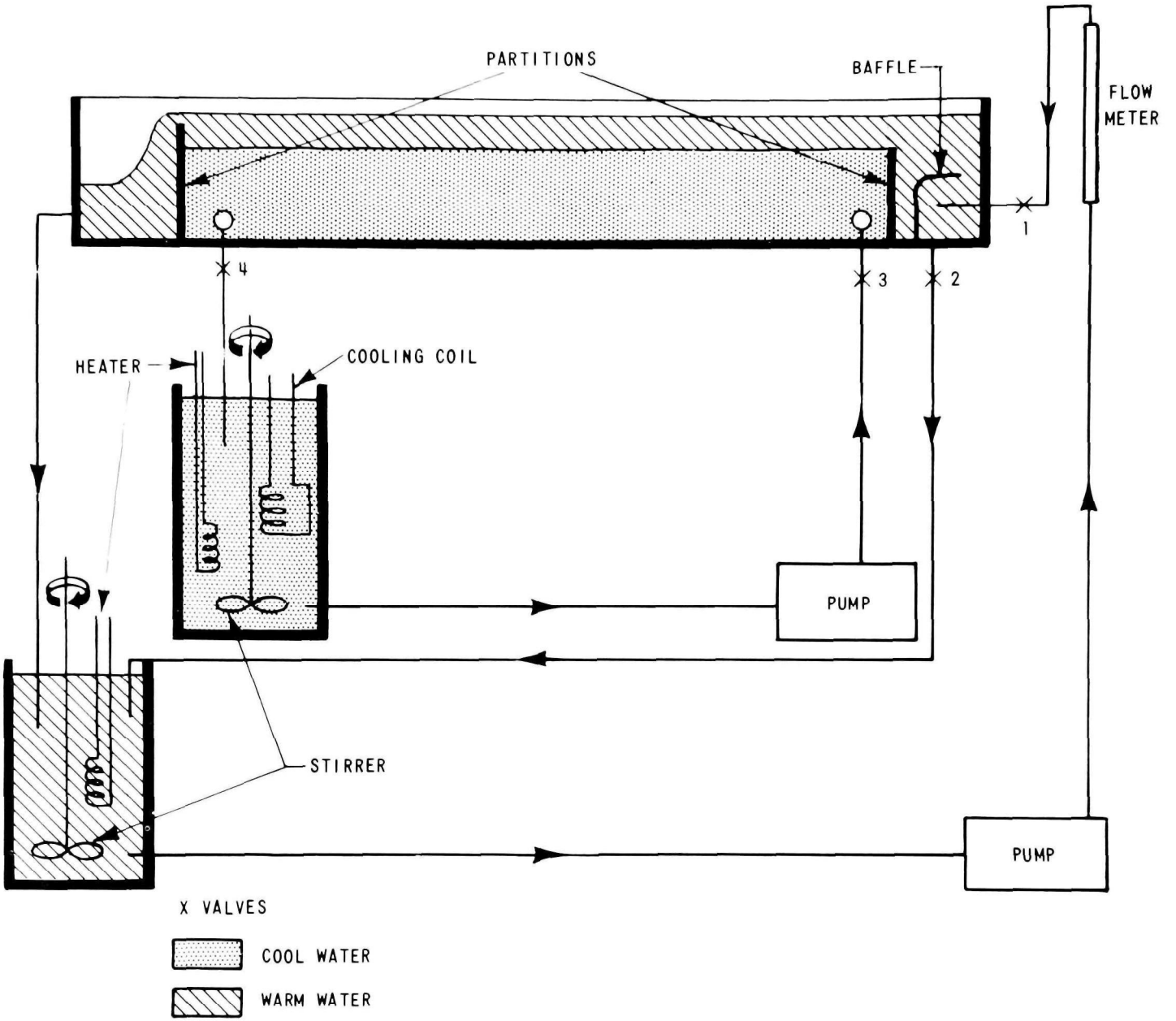

Figure 28 SCHEMATIC ARRANGEMENT OF FLOW SYSTEM

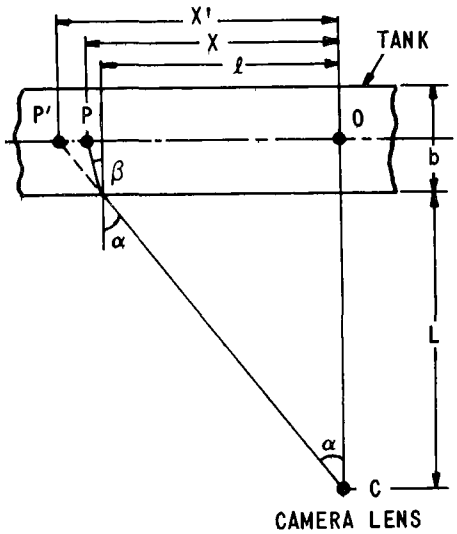

Figure 29 SKETCH FOR DERIVATION OF THE REFRACTION ERROR ON PHOTOGRAPHS OF FLOW TRACERS (PLAN VIEW)

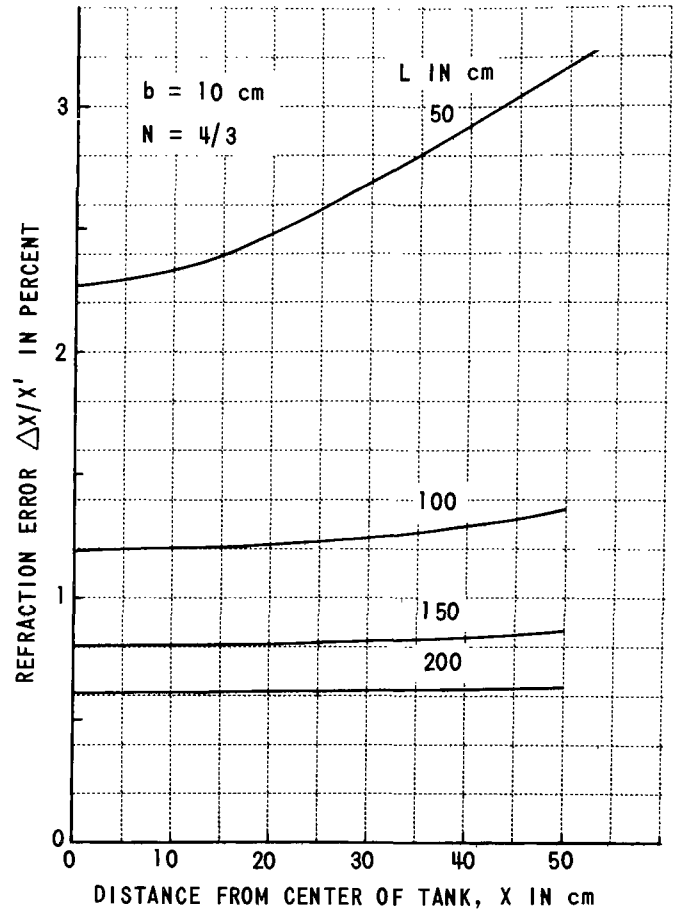

Figure 30 REFRACTION ERROR ON PHOTOGRAPHS OF FLOW TRACERS

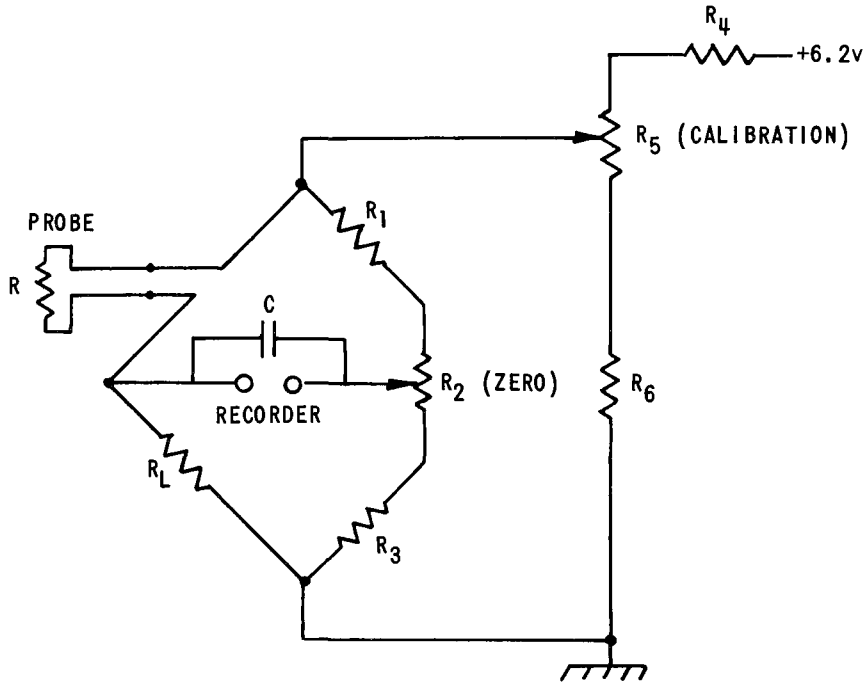

Figure 31 BRIDGE CIRCUIT TO MEASURE WATER TEMPERATURE
R = RESISTANCE OF THERMISTOR PROBE, $R_L = R_1 = R_3 = 0.1$ MΩ, $R_2 = 50$ kΩ, $R_4 = 5.1$ kΩ, $R_5 = R_6 = 1$ kΩ, $C = 0.33$ μF.

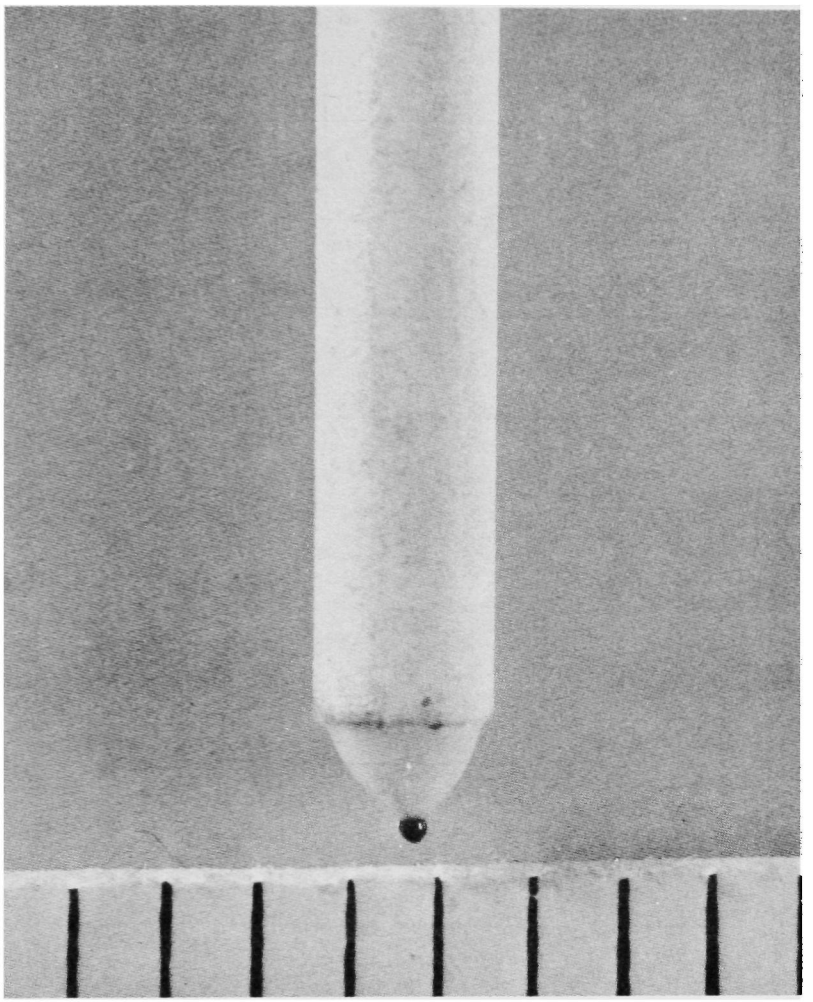

Figure 32 ENLARGED PHOTOGRAPH OF A THERMISTOR PROBE TIP - THE SCALE DIVISIONS ARE 1 mm APART

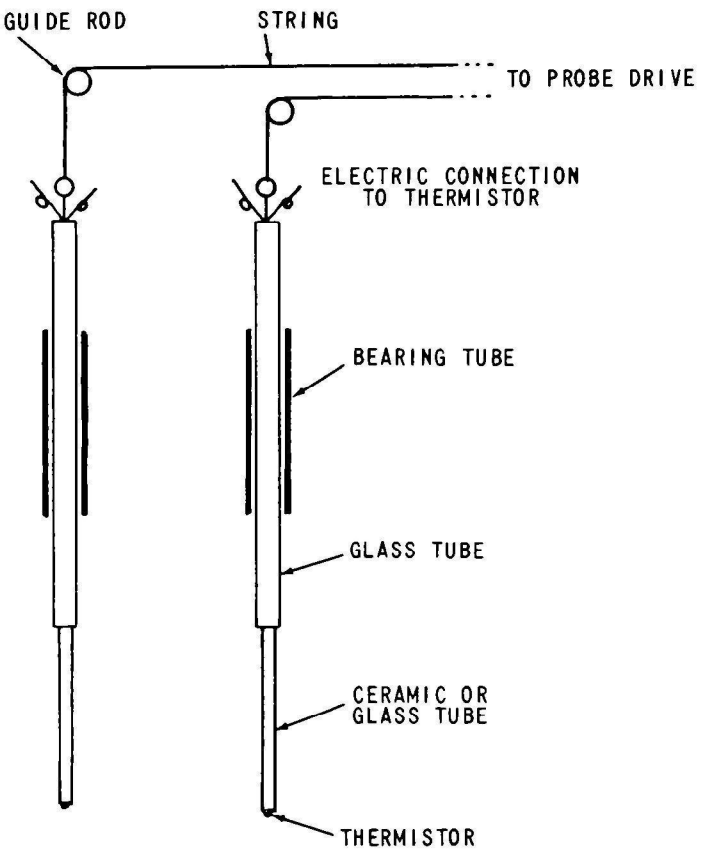

Figure 33 DESIGN OF TEMPERATURE PROBES NOT TO SCALE (ONLY TWO ARE SHOWN)

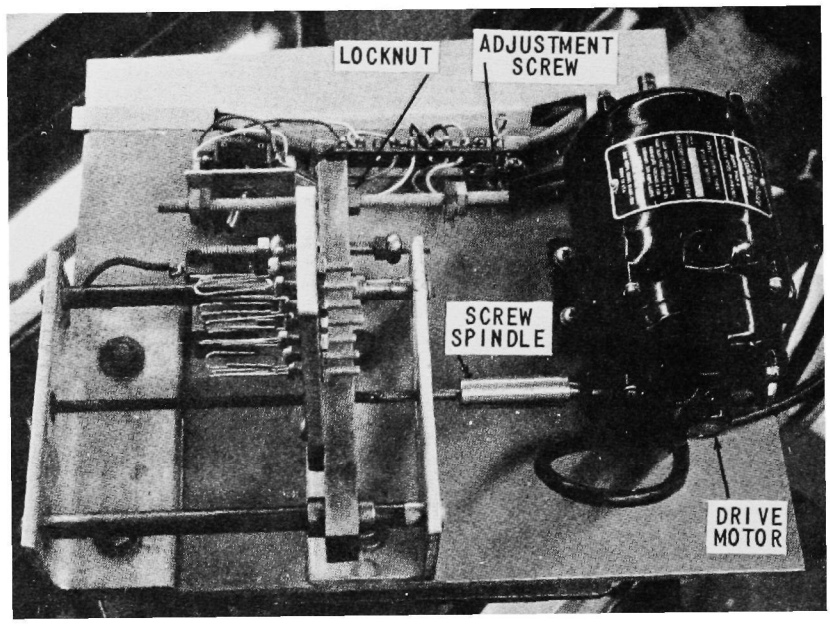

Figure 34 PHOTOGRAPH OF DRIVE MECHANISM FOR TEMPERATURE PROBES

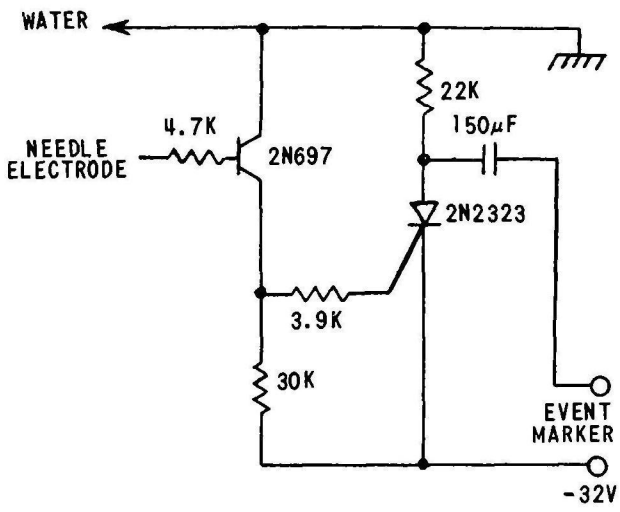

Figure 35 CIRCUIT OF ELECTRONIC RELAY FOR WATER CONTACT

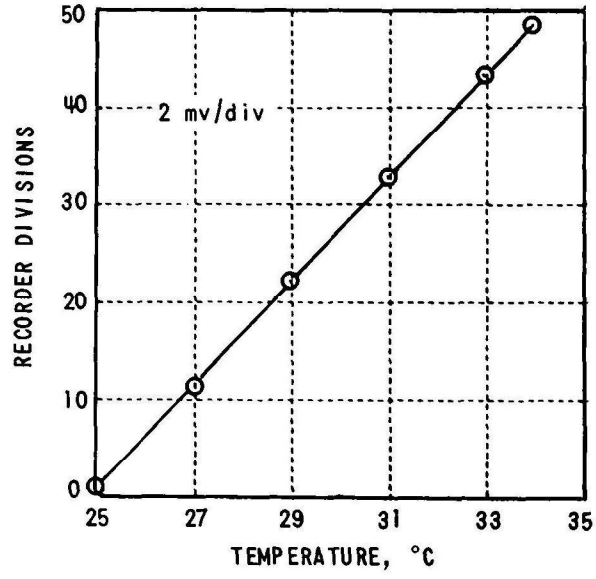

Figure 36 CALIBRATION OF ONE OF THE TEMPERATURE PROBES BETWEEN 25°C AND 35°C BEFORE ADJUSTMENT OF THE CALIBRATION VOLTAGE

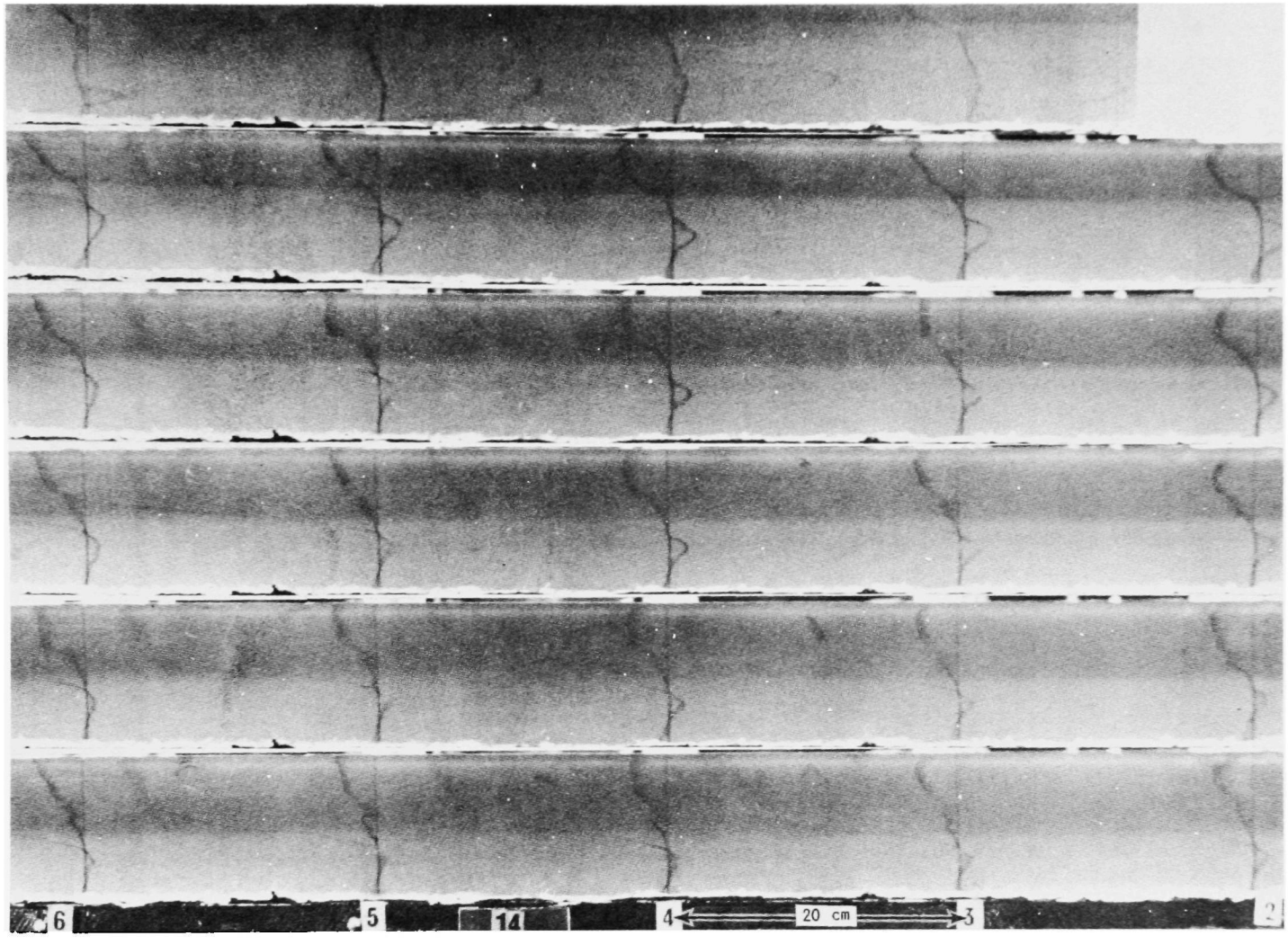

Figure 37a VELOCITY PROFILES $\overline{R}_{i_o}$ = 3.0 (UPPER TRACE 2.67 sec, LOWER 30 sec)

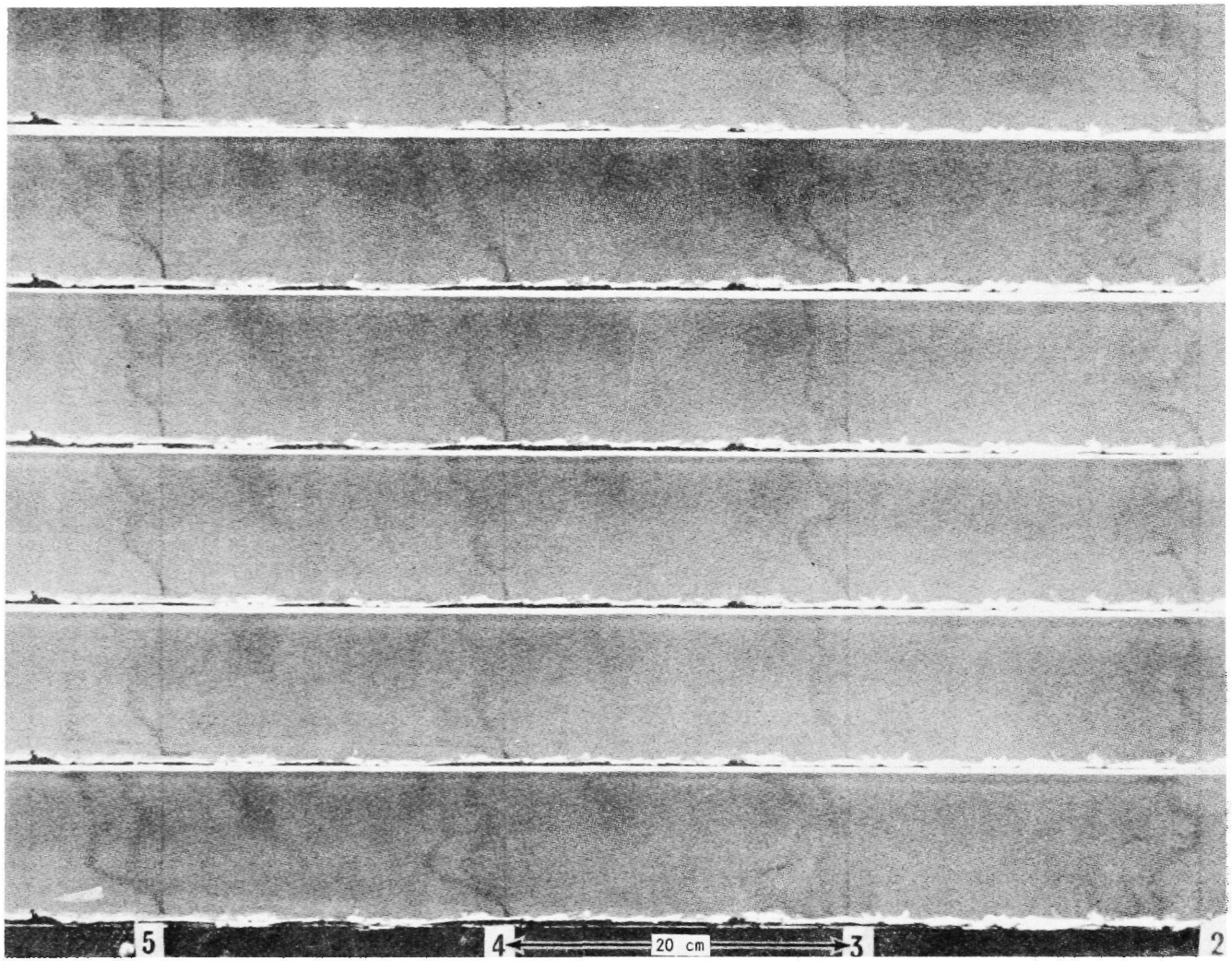

Figure 37b VELOCITY PROFILES $\bar{R}_{i_o}$ = 0.1 (ALL TRACES 2.67 sec)

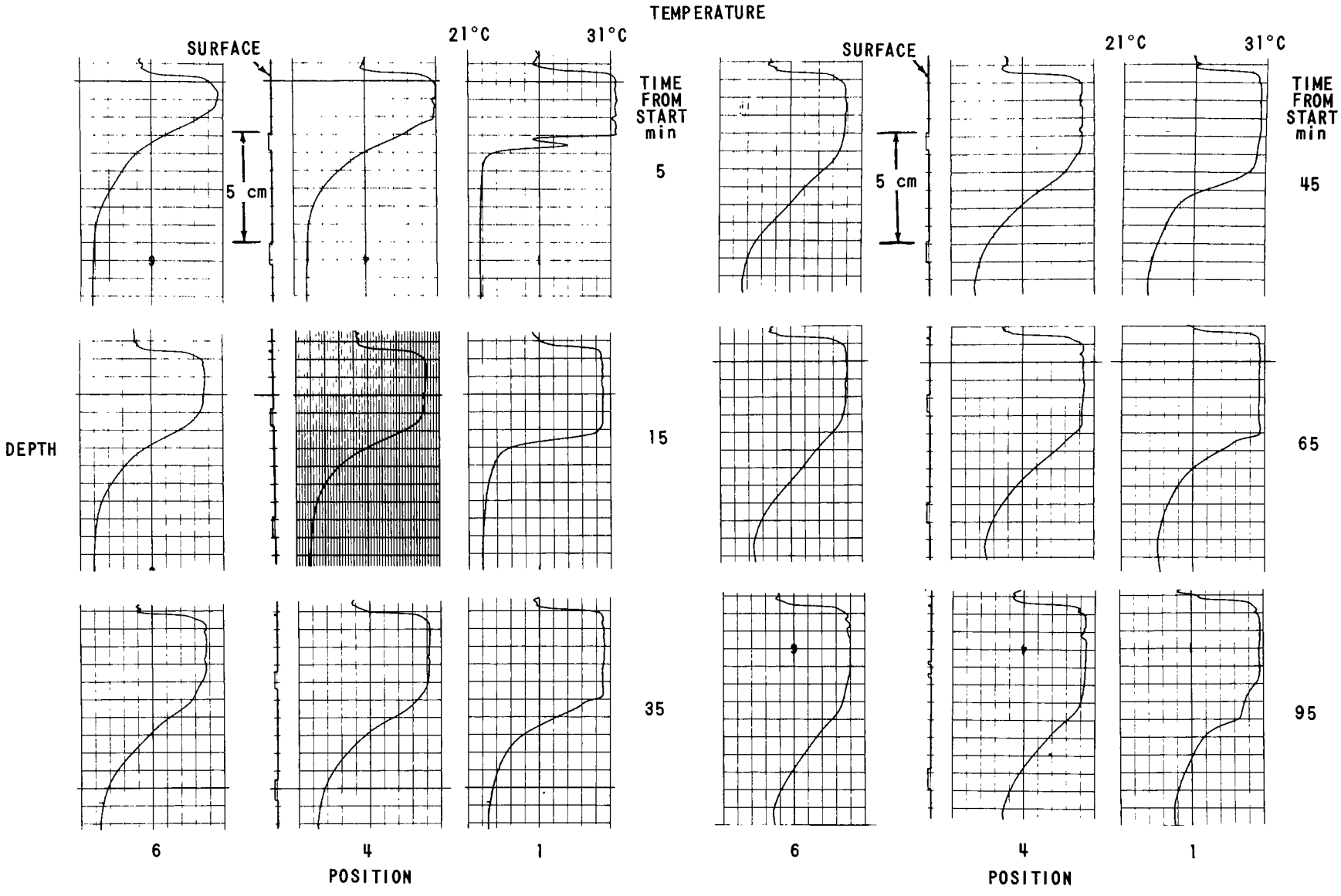

Figure 38a VERTICAL TEMPERATURE PROFILES $\bar{R}_{i_o} = 3.0$

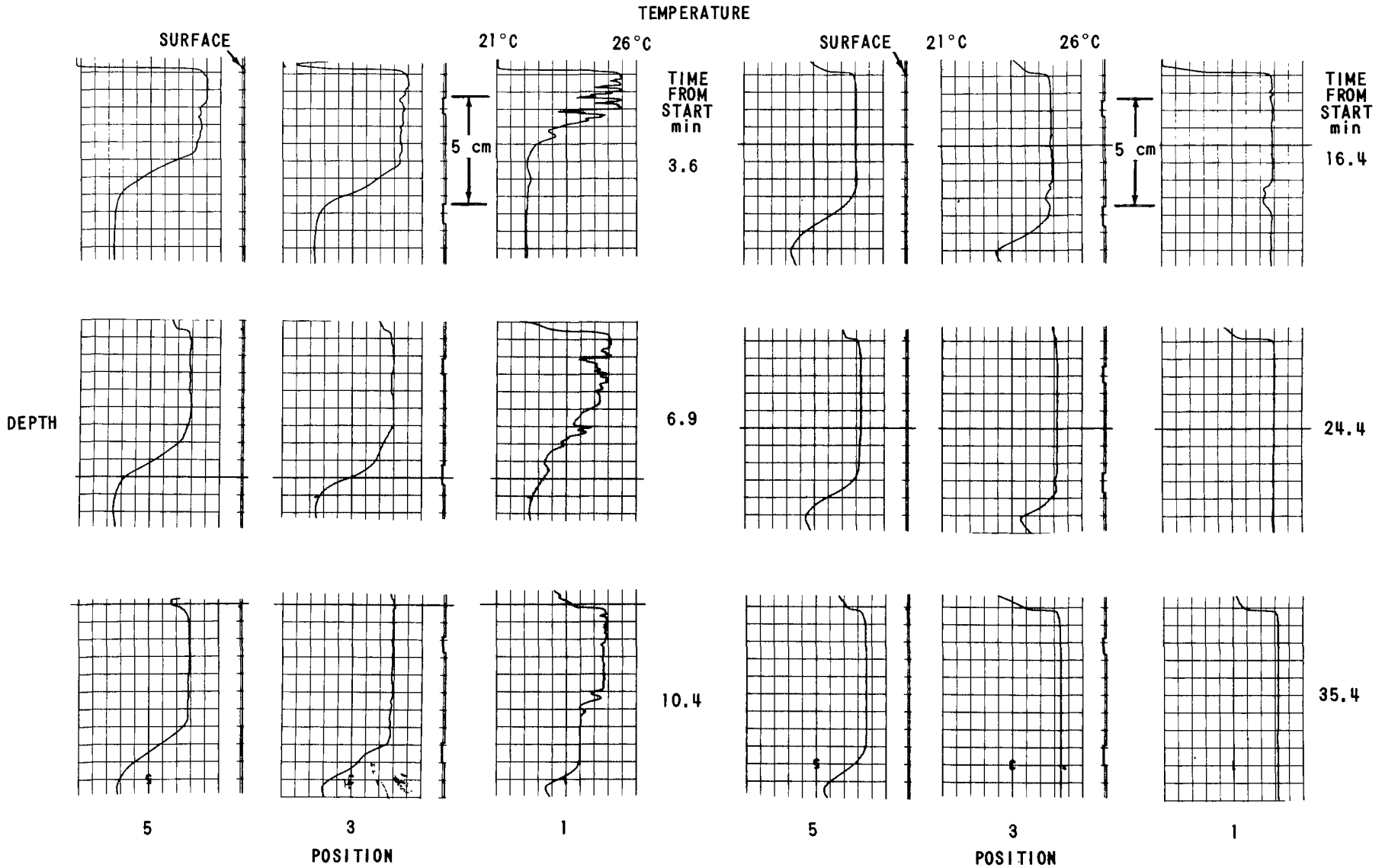

Figure 38b VERTICAL TEMPERATURE PROFILES $\bar{R}_{i_o} = 0.1$

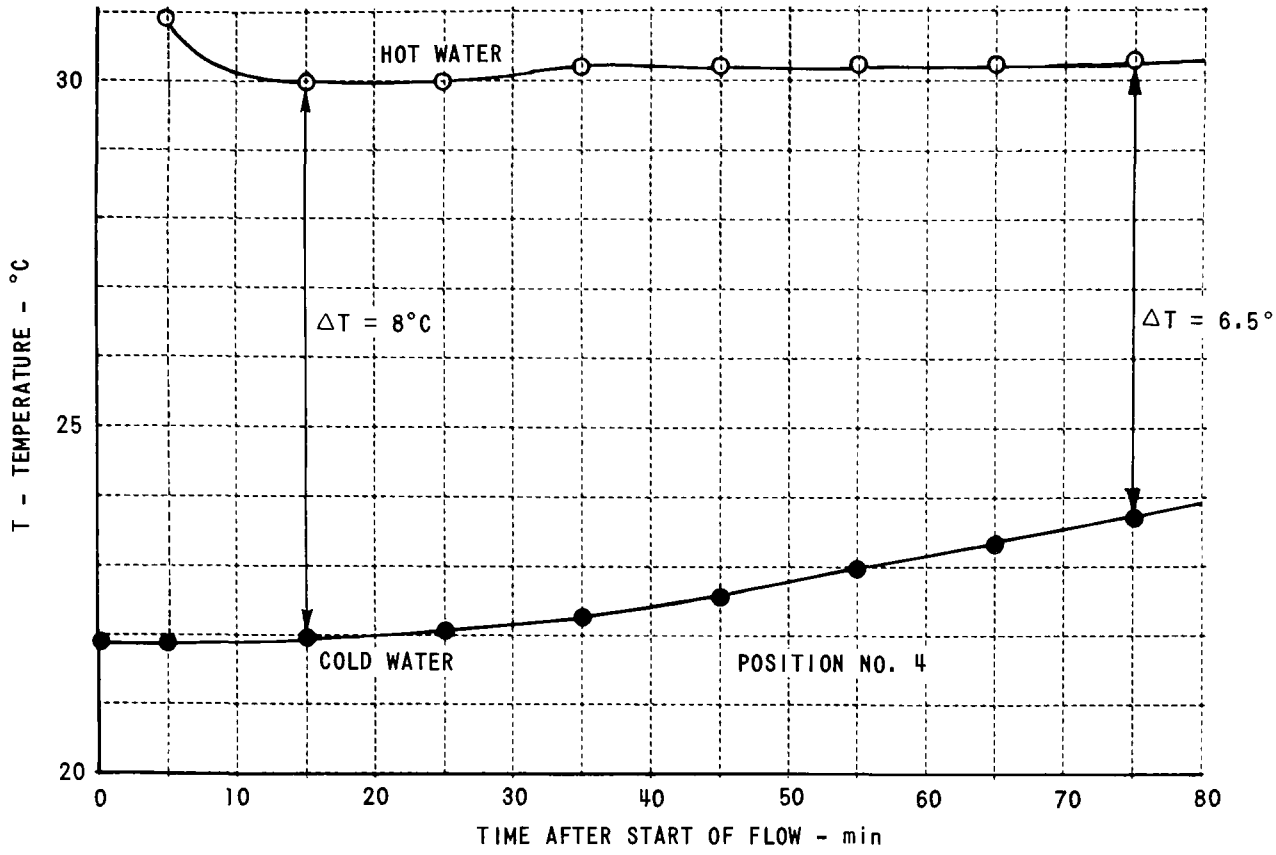

Figure 39a TEMPERATURE EXTREMES VS TIME $\bar{R}_{i_o} = 3.0$

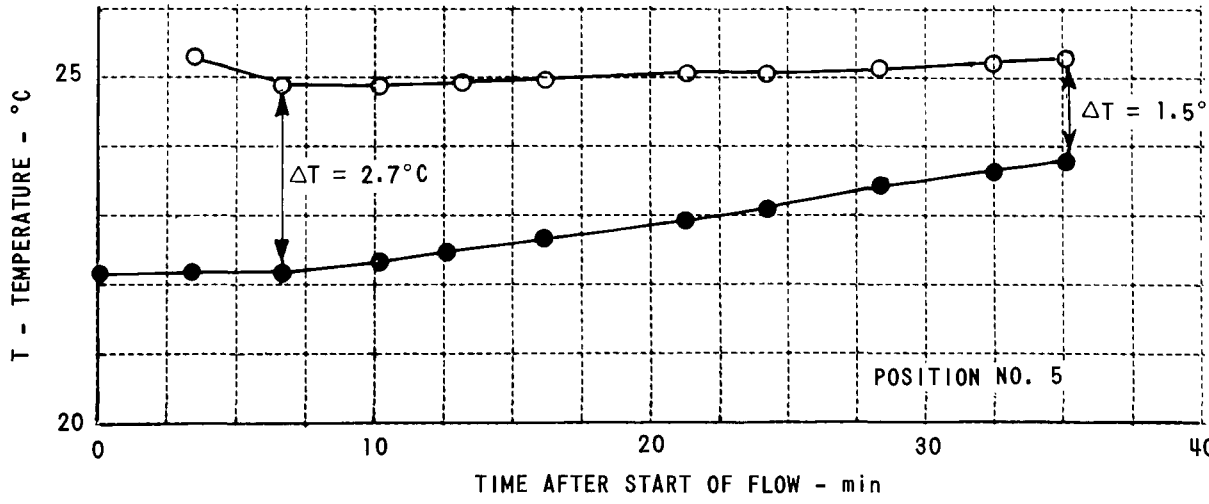

Figure 39b TEMPERATURE EXTREMES VS TIME $\bar{R}_{i_o} = 0.1$

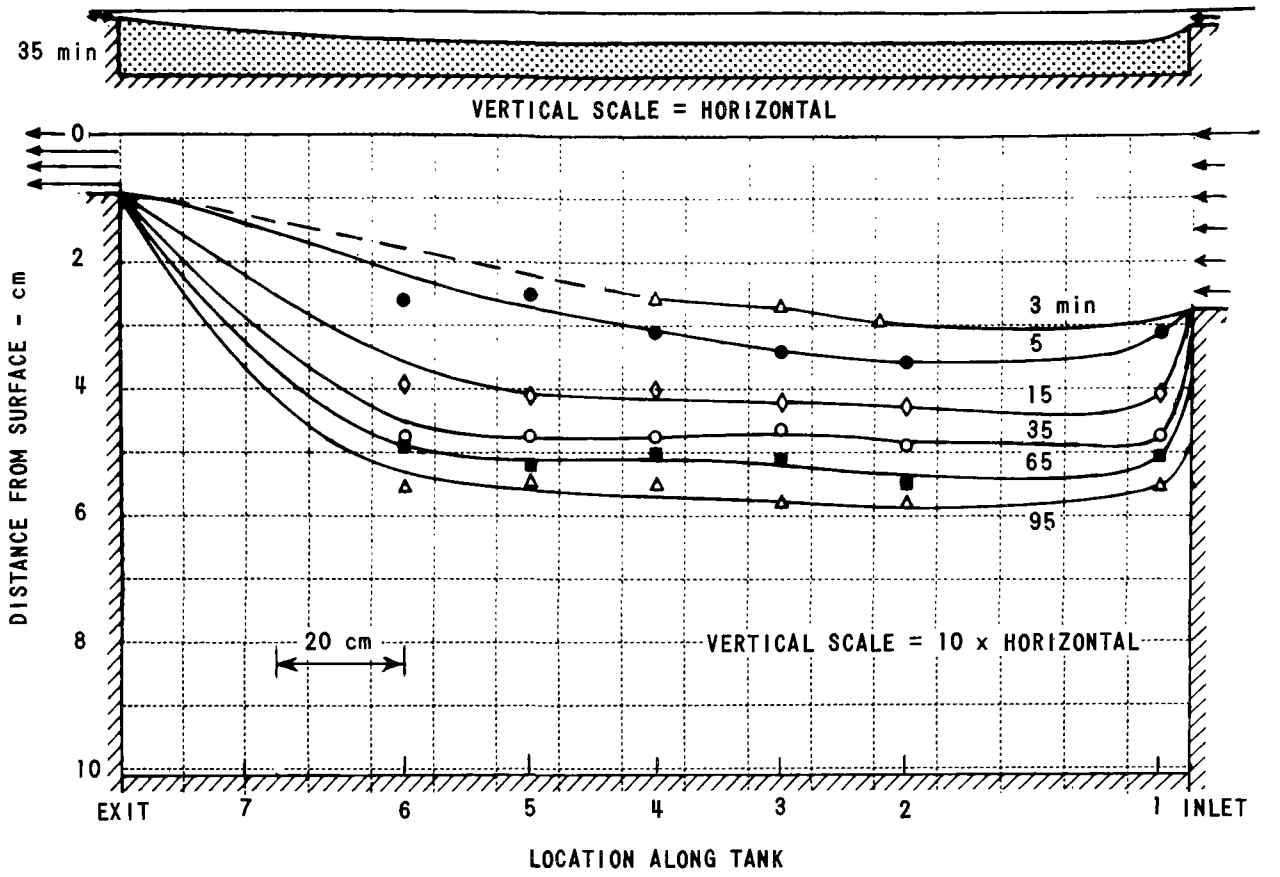

Figure 40a POSITION OF INTERFACE (max $\partial T/\partial Z$) $\bar{R}_{i_o}$ = 3.0

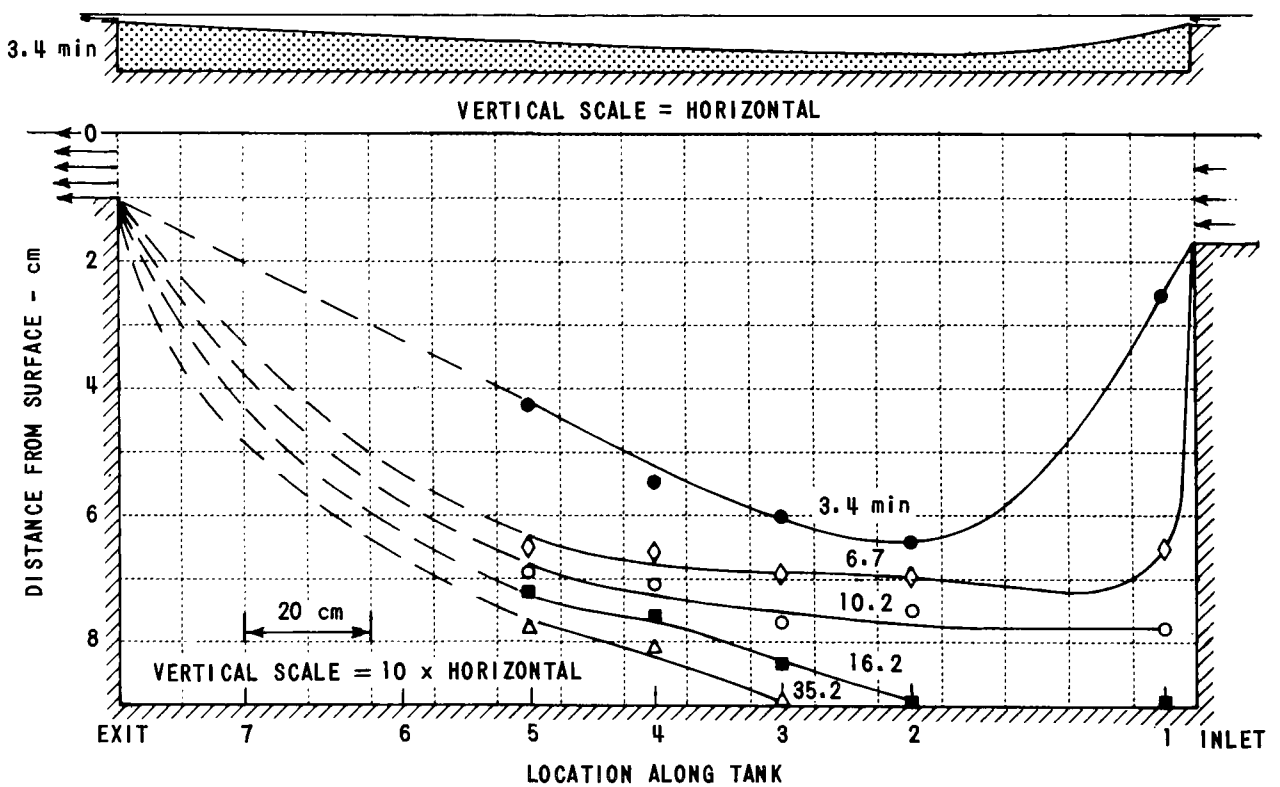

Figure 40b POSITION OF INTERFACE (max $\partial T/\partial Z$) $\bar{R}_{i_o}$ = 0.1

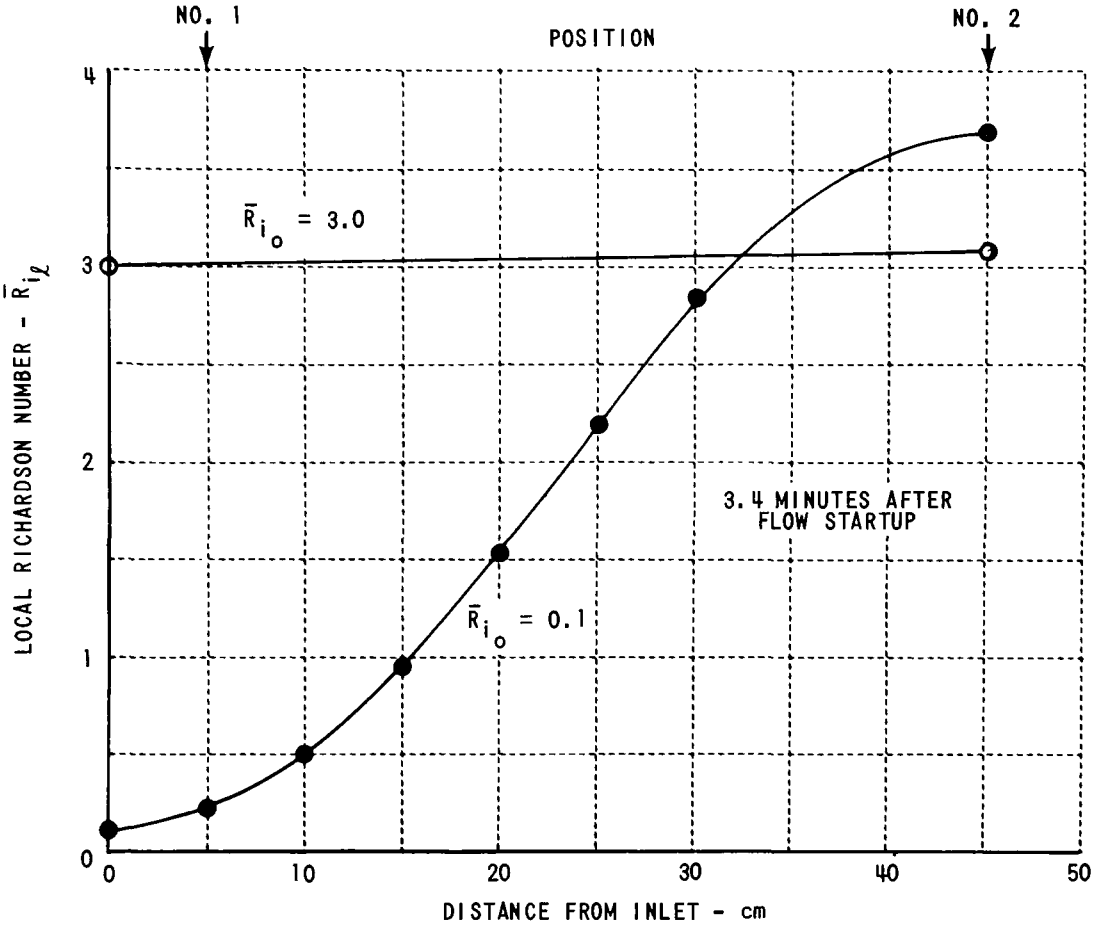

Figure 41 VARIATION OF LOCAL RICHARDSON NUMBER, $\bar{R}_{i_\ell}$, WITH DISTANCE

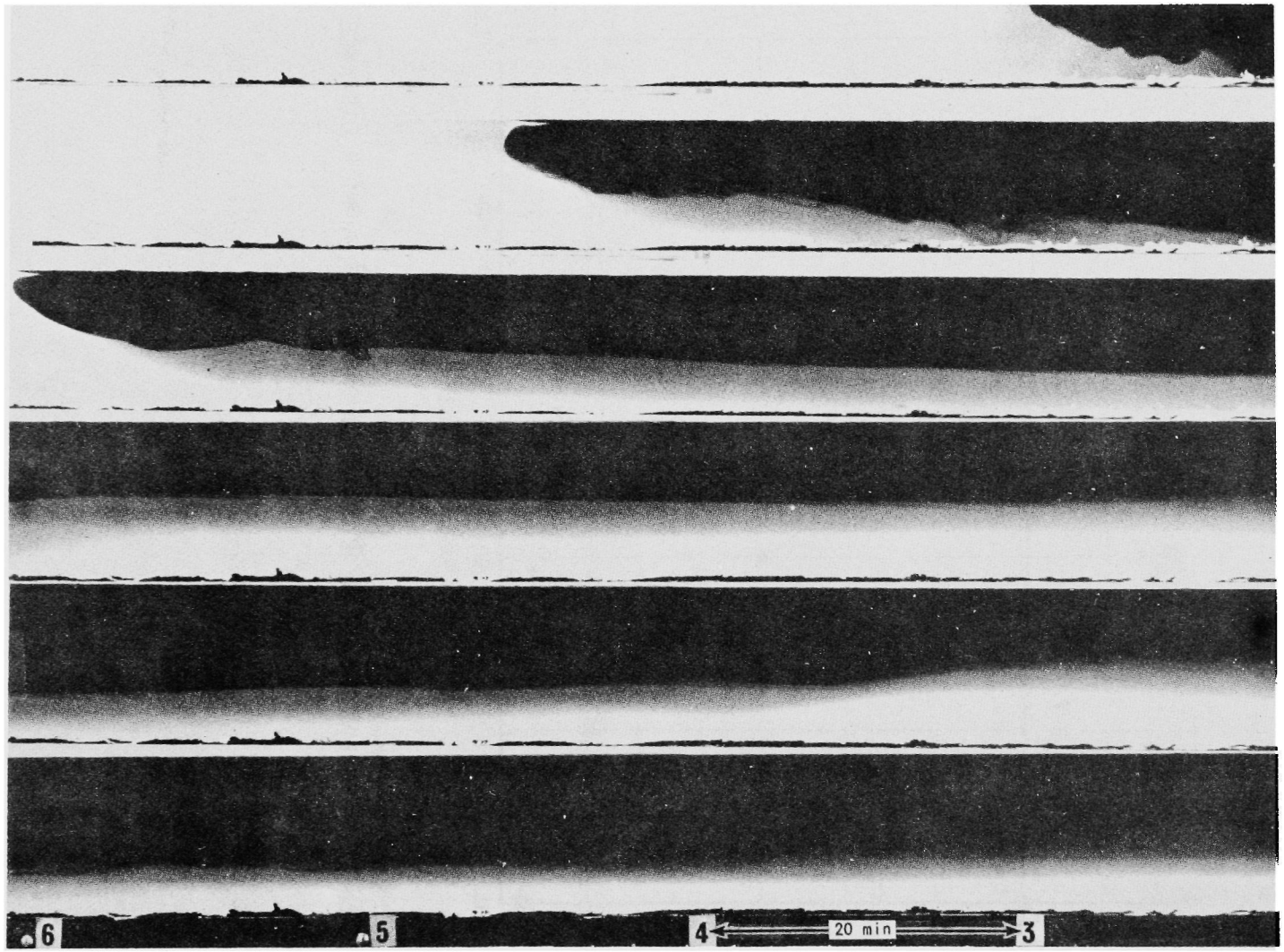

Figure 42 STARTING PROCESS $\overline{R}_{i_o}$ = 3.0 WARM WATER-THYMOL BLUE, COLD WATER-SODIUM HYDROXIDE, (DARK REGION INDICATES MIXING OF TWO FLUIDS) h_o = DEPTH OF WARM WATER AT INLET

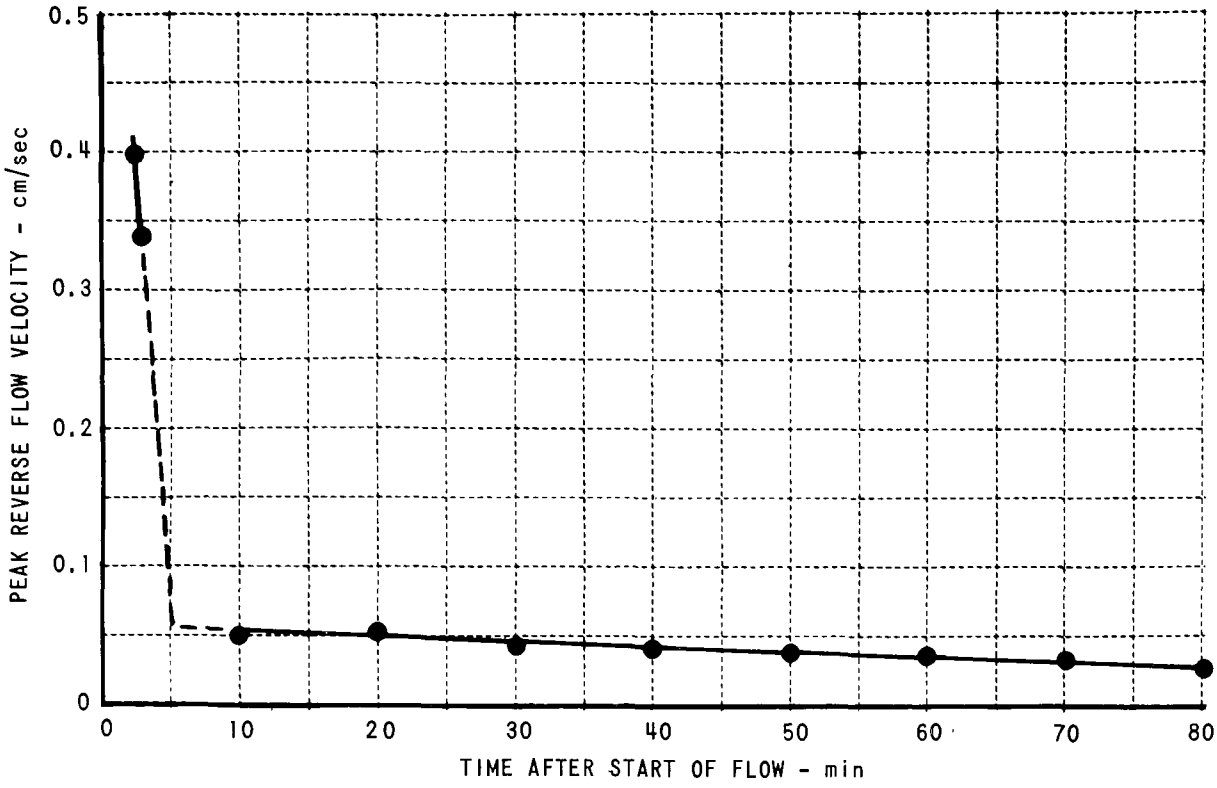

Figure 43 PEAK REVERSE FLOW VELOCITY $\bar{R}_{i_o} = 3.0$

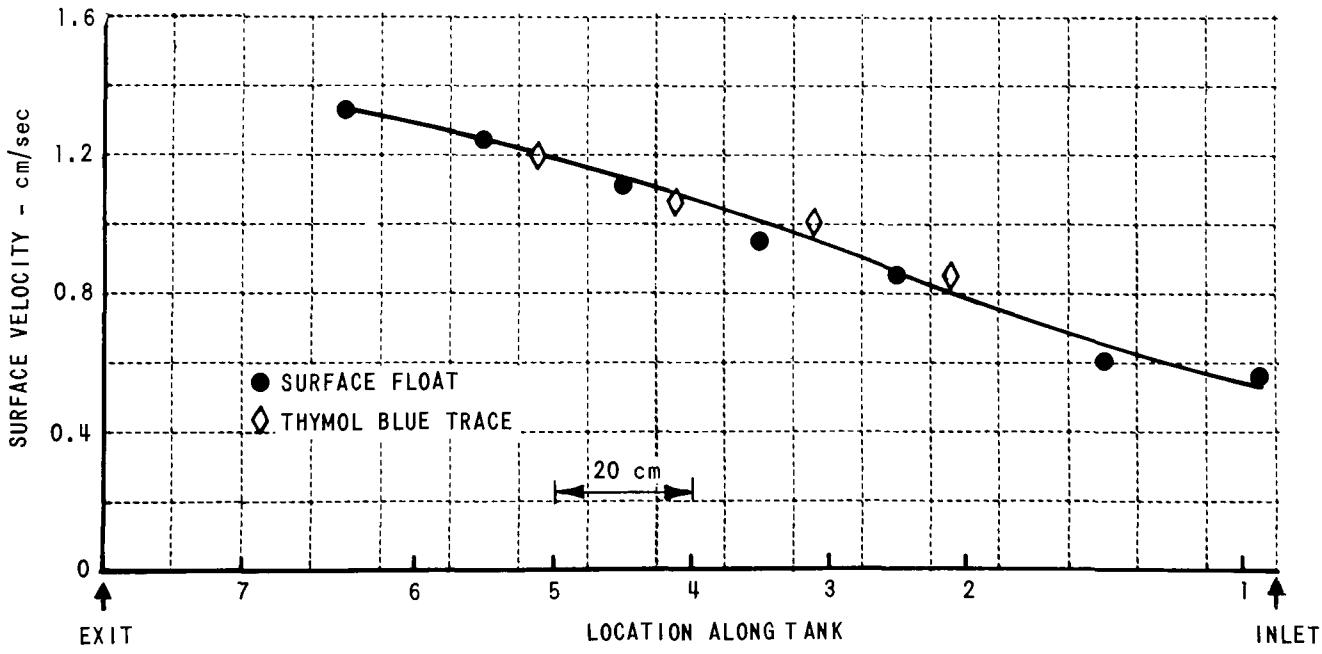

Figure 44 VELOCITY AT SURFACE $\bar{R}_{i_o} = 3.0$

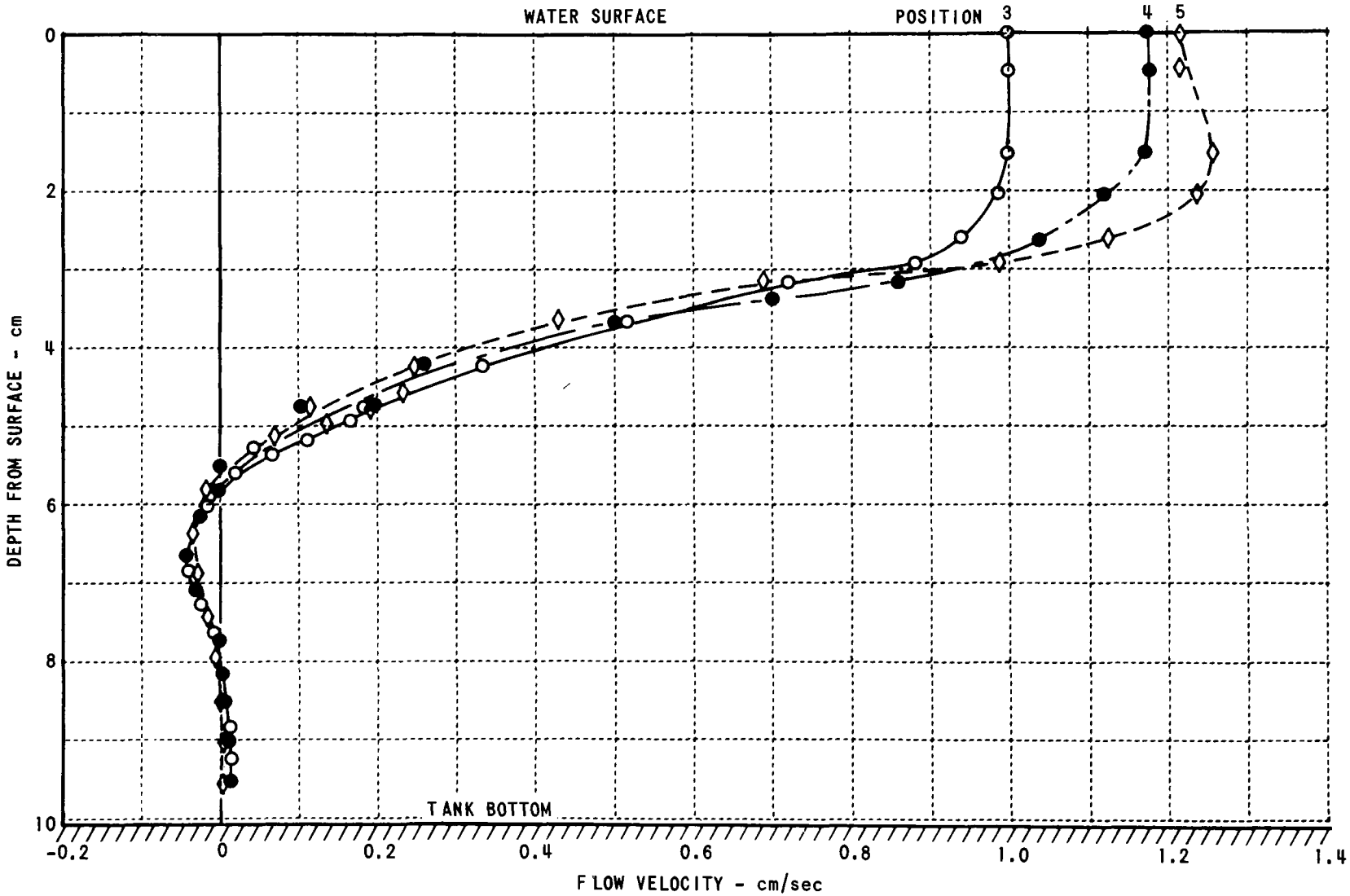

Figure 45 FLOW VELOCITY VS DEPTH AND POSITION $\bar{R}i_o$ = 3.0, 30 min

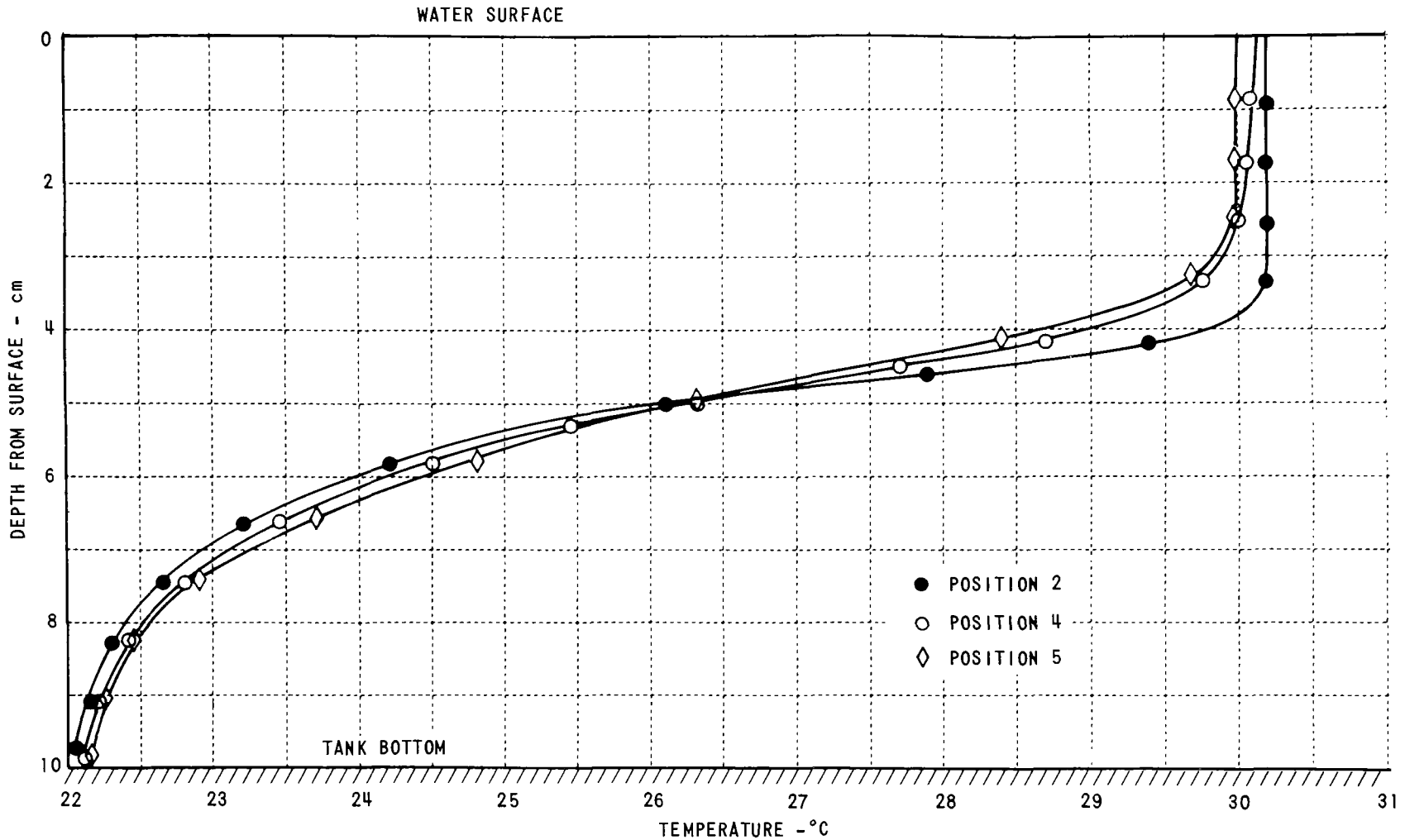

Figure 46 TEMPERATURE VS DEPTH AND POSITION $\bar{R}_{i_o}$ = 3.0, 25 min

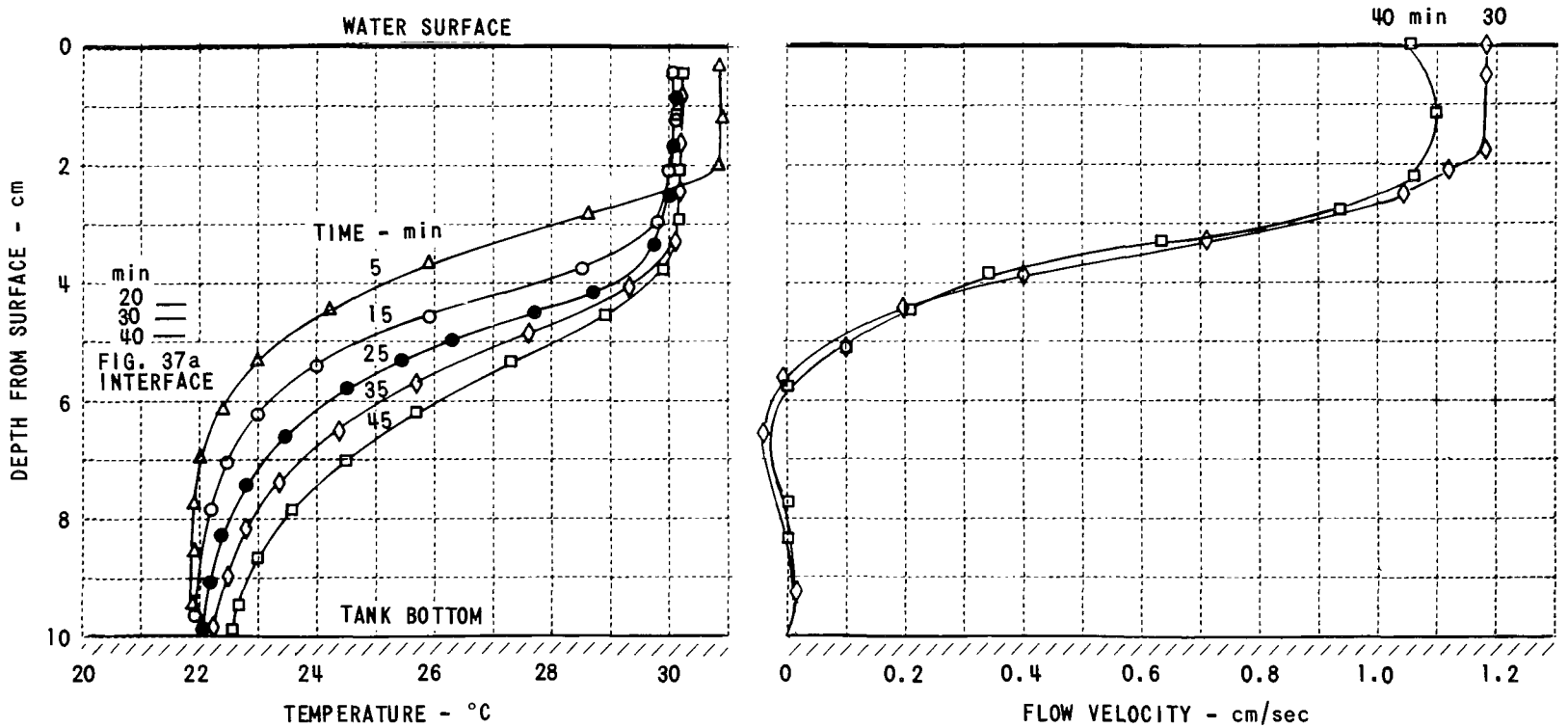

Figure 47 TEMPERATURE, FLOW VELOCITY VS DEPTH AND TIME, $\bar{R}_{i_o}$ = 3.0, POSITION 4

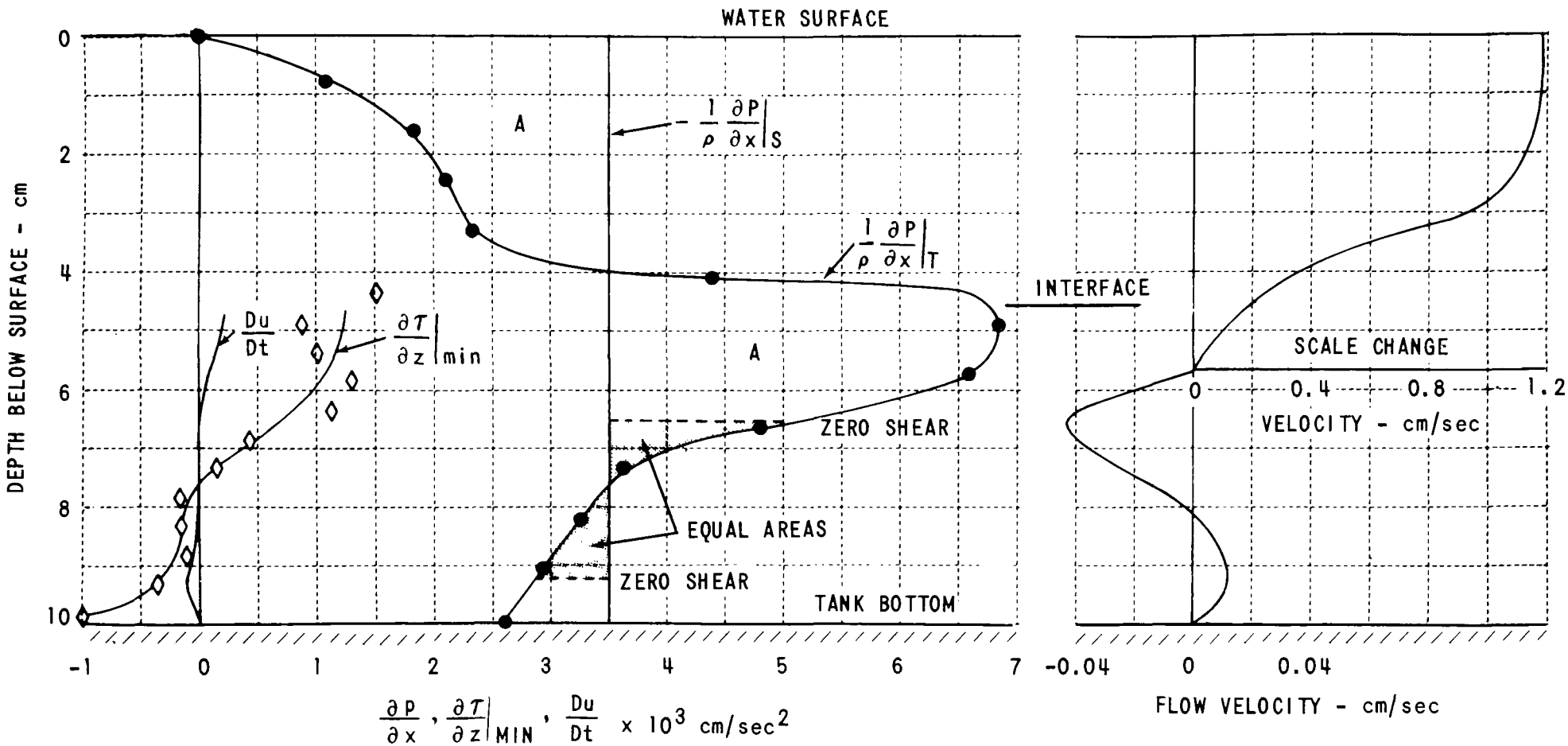

Figure 48 SOLUTION OF MOMENTUM EQUATION $\bar{R}_{i_o} = 3.0$, POSITION 4, 30 min, $\bar{R}_{i_\ell} = 4.1$

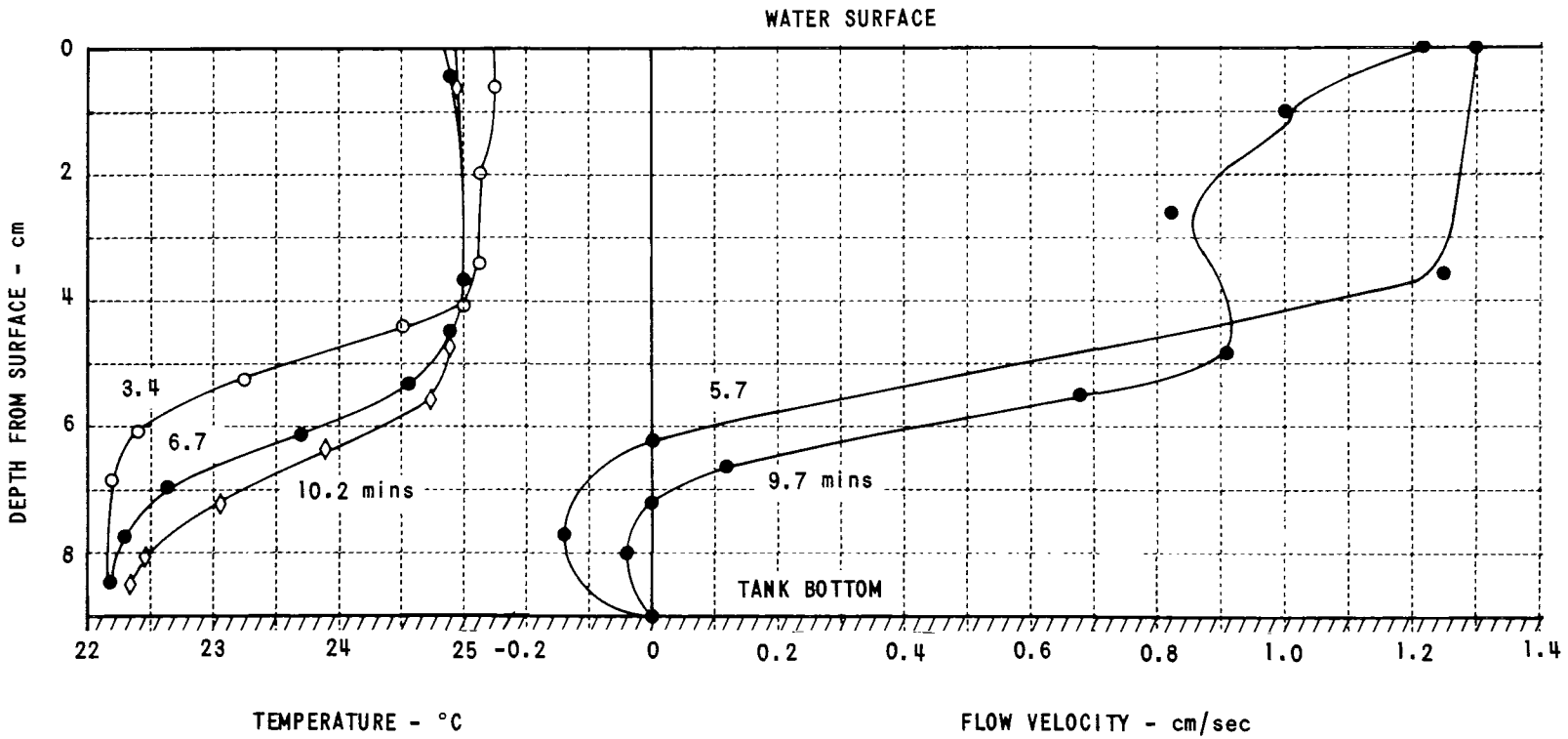

Figure 49 TEMPERATURE, VELOCITY VS DEPTH AND TIME $\bar{R}_{i_o}$ = 0.1, POSITION NO. 5

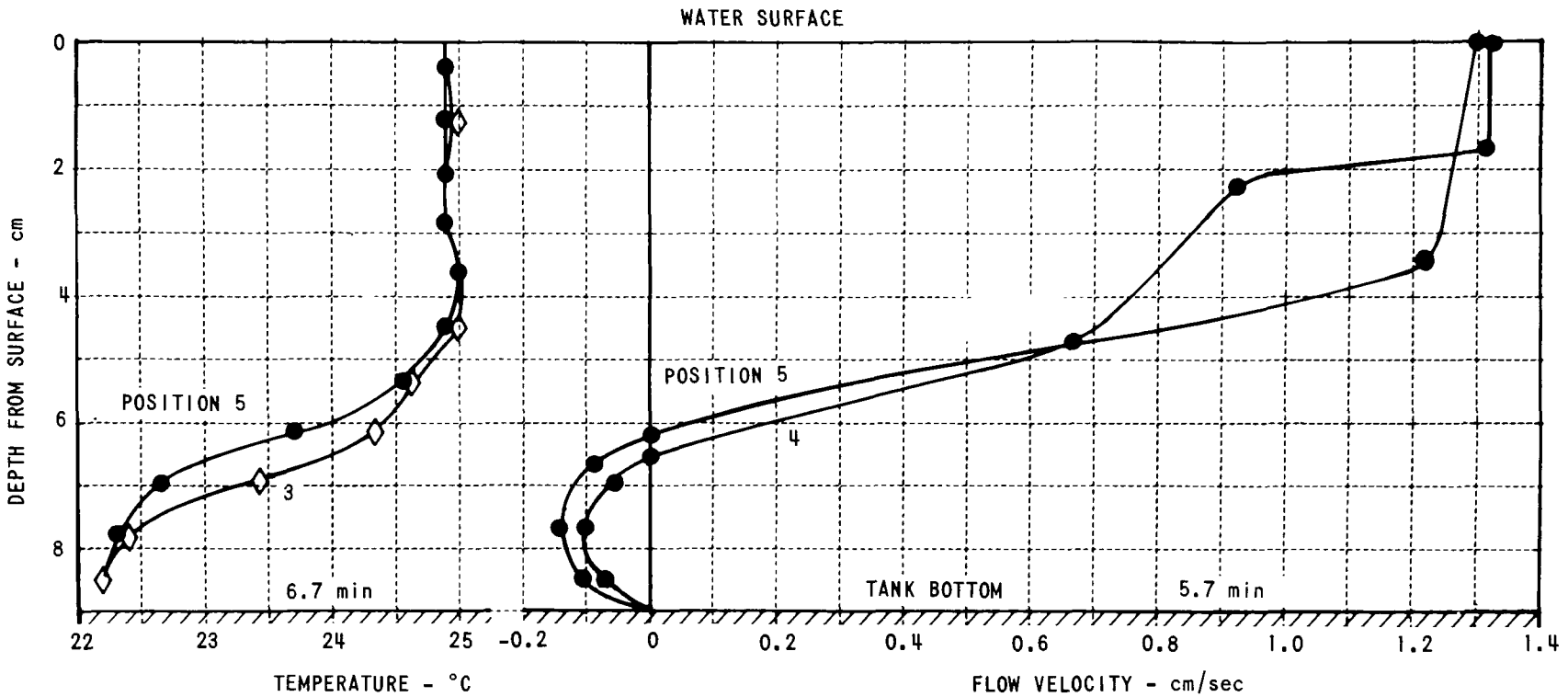

Figure 50 TEMPERATURE, VELOCITY VS DEPTH AND POSITION $\bar{R}_{i_o}$ = 0.1, 5.7 AND 6.7 min

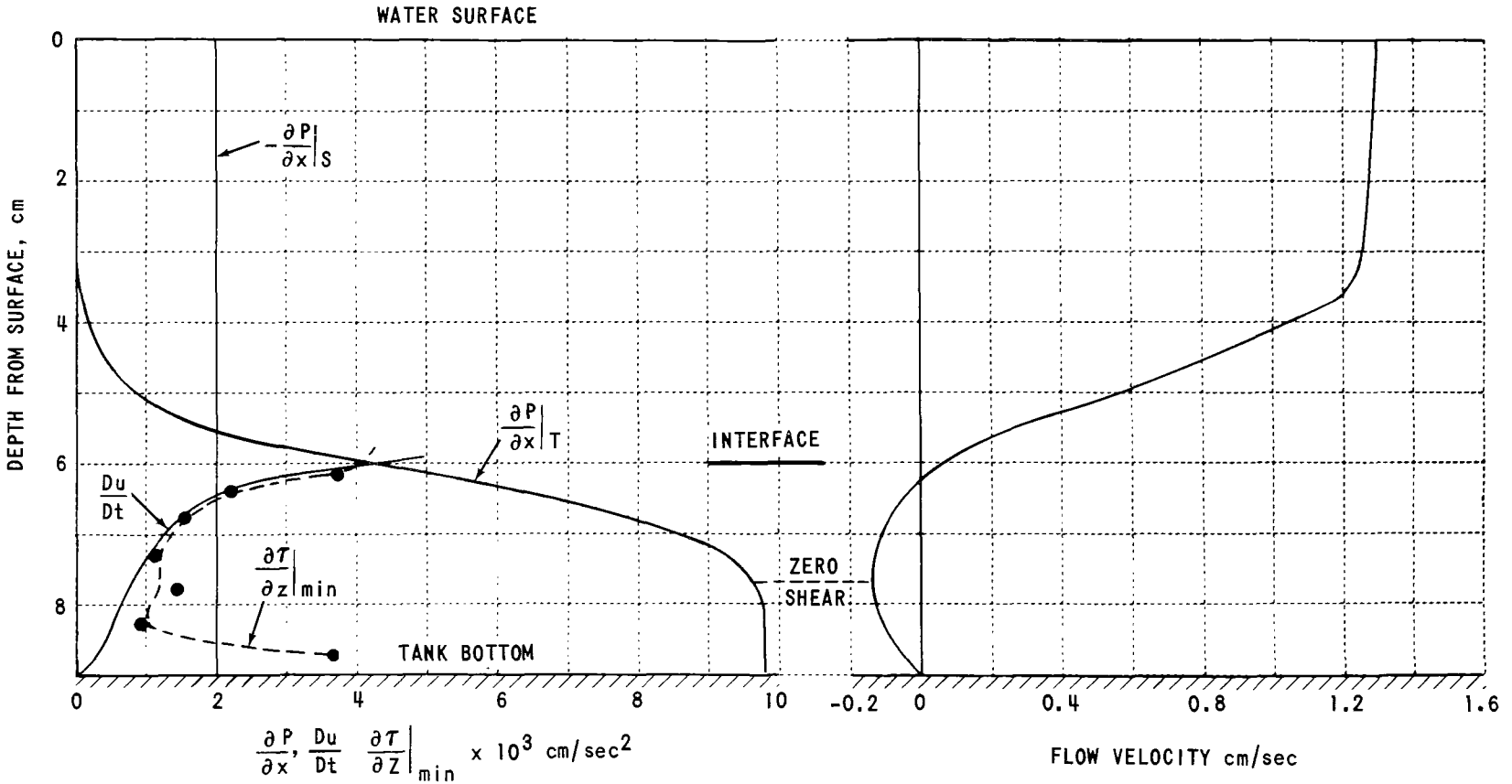

Figure 51 SOLUTION OF MOMENTUM EQUATION $\bar{R}_{i_o}$ = 0.1, POSITION 5, 5.7 min, $\bar{R}_{i_\ell}$ = 2.5

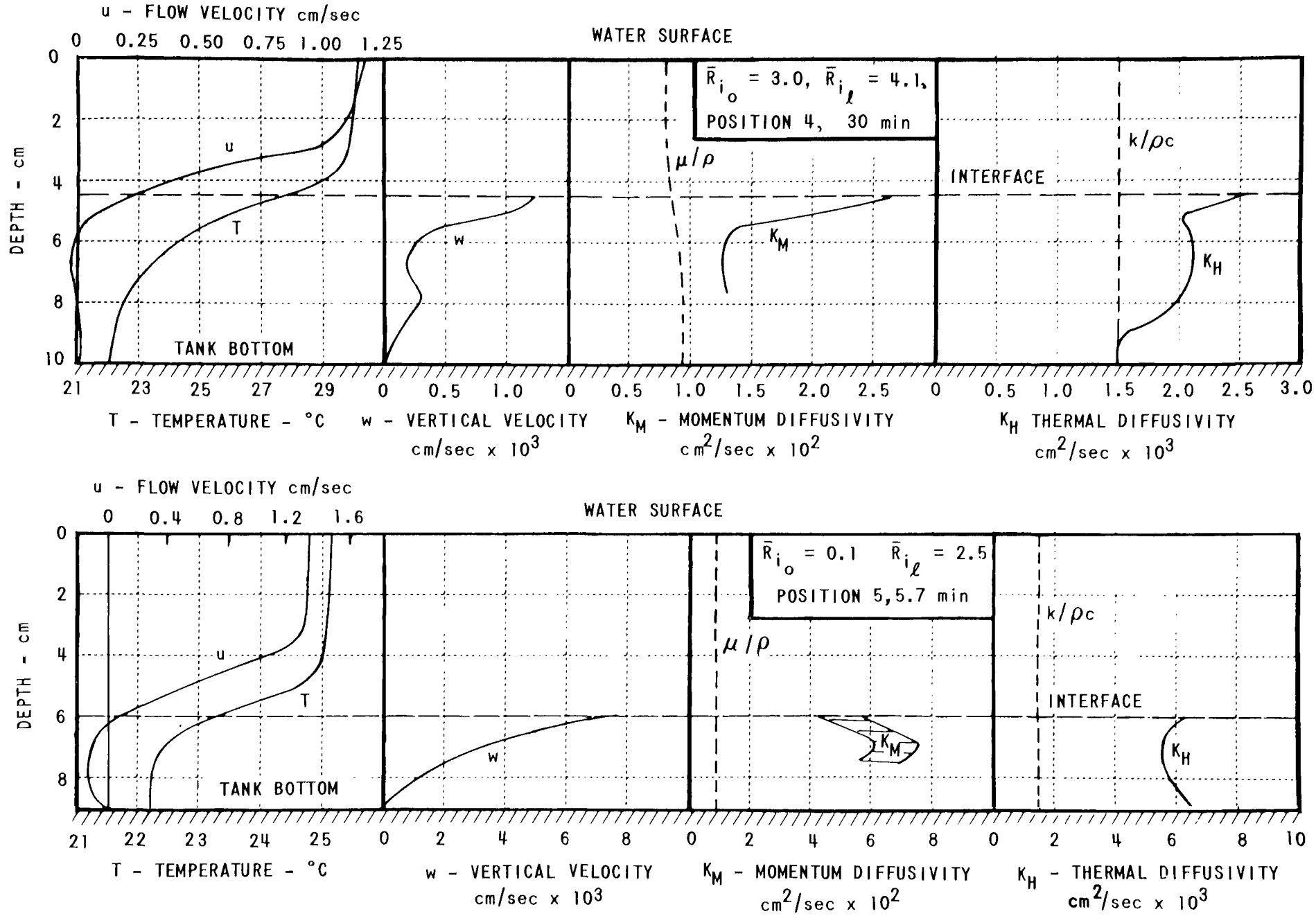

Figure 52 VERTICAL VELOCITY, MOMENTUM AND THERMAL DIFFUSIVITY COEFFICIENTS

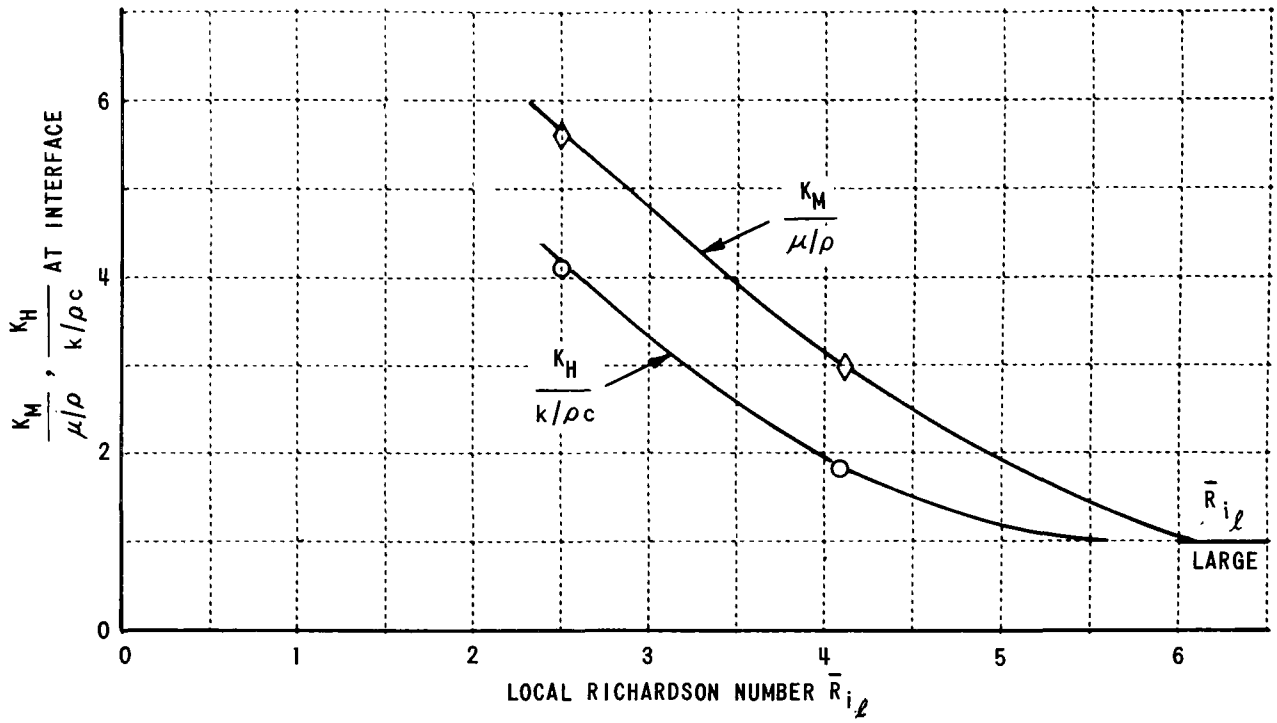

Figure 53 $\frac{K_M}{\mu/\rho}$, $\frac{K_H}{k/\rho c}$ AT INTERFACE VS RICHARDSON NUMBER

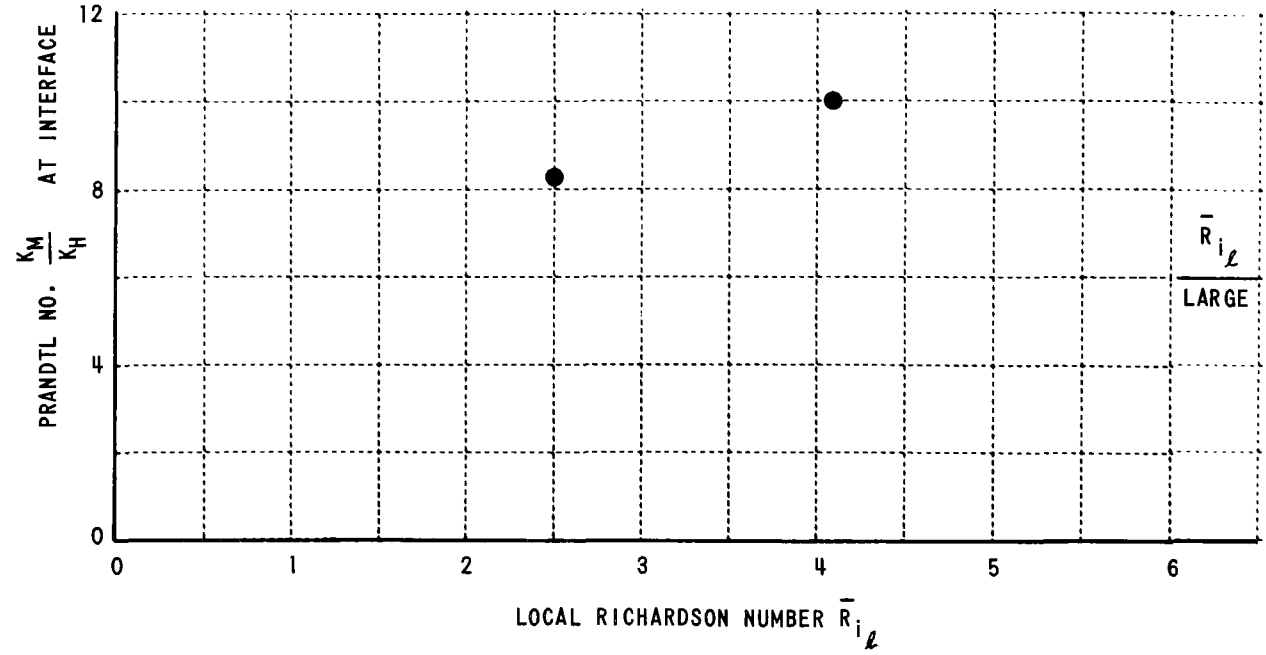

Figure 54 PRANDTL NUMBER AT INTERFACE VS RICHARDSON NUMBER

1 Accession Number	2 Subject Field & Group	SELECTED WATER RESOURCES ABSTRACTS INPUT TRANSACTION FORM
	Ø2H, Ø5B	

5 Organization

Cornell Aeronautical Laboratory

6 Title

RESEARCH ON THE PHYSICAL ASPECTS OF THERMAL POLLUTION

10 Author(s)

Sundaram, T. R.
Rehm, R. G.
Rudinger, G.
Merritt, G. E.

16 Project Designation

FWQA Contract #14-12-526

21 Note

22 Citation

Water Pollution Control Research Series, Report Number 16130DPU02/71, Water Quality Office, Environmental Protection Agency

23 Descriptors (Starred First)

*Stratification, *Path of pollutants, *Thermal pollution, Lakes, Reservoirs, Water temperature, Mathematical models, Thermocline, Hydrodynamics, Diffusion, Laboratory tests, Thermal power plants

25 Identifiers (Starred First)

*Temperature prediction, Warm water wedge, Interfacial mixing.

27 Abstract

The mechanisms of formation and maintenance of the characteristic thermal structure of deep, temperate lakes are investigated along with the effects on the thermal structure of discharges of waste heat from electric generating plants. It is shown that a thermocline is formed by the nonlinear interaction between the wind-induced turbulence and stable buoyance gradients due to surface heating.

A theoretical description of the stratification cycle of temperate lakes is given in which the interaction between wind-induced turbulence and buoyancy gradients is included explicitly. The theoretical model predicts all the observed features of stratification accurately. It is shown that thermal discharges increase the temperature of the epilimnion and also the temperature during spring homothermy. A lengthening of the stratification period also occurs. In addition, the attendant transfer of large quantities of water from one level to another has a significant effect.

An exploratory experimental study is described on the nature of the interfacial mixing between a flowing layer of warm water and an underlying cooler pool of water. It is shown that the downward transfer of both momentum and heat are severely inhibited at the interface by the stable buoyancy gradients; momentum to a lesser degree.

This report was submitted in fulfillment of Contract Number 14-12-526 under the sponsorship of the Federal Water Quality Administration.

Abstractor T. R. Sundaram | Institution Cornell Aeronautical Laboratory

WR:102 (REV. JULY 1969)
WRSIC

SEND TO: WATER RESOURCES SCIENTIFIC INFORMATION CENTER
U.S. DEPARTMENT OF THE INTERIOR
WASHINGTON, D. C. 20240

* GPO: 1969—359-339